Light with a twist : ray aspects in singular wave and quantum optics

Habraken, S.J.M.

Light with a Twist

Ray Aspects in Singular Wave and Quantum Optics

Steven J. M. Habraken

The pictures on the front cover respectively show the phase and the intensity patterns of one of the long-lived modes of a rotating two-mirror cavity with general astigmatism. The background shows a detail of original handwritten notes.

Light with a Twist

Ray Aspects in Singular Wave and Quantum Optics

PROEFSCHRIFT

ter verkrijging van
de graad van Doctor aan de Universiteit Leiden,
op gezag van Rector Magnificus prof. mr. P. F. van der Heijden,
volgens besluit van het College voor Promoties
te verdedigen op dinsdag 16 februari 2010
klokke 13:45 uur

door

Steven Johannes Martinus Habraken

geboren te Eindhoven
in 1980

Promotiecommissie:

Promotor:	Prof. dr. G. Nienhuis	Universiteit Leiden
Leden:	Prof. dr. T. D. Visser	Technische Universiteit Delft / Vrije Universiteit Amsterdam
	Prof. dr. C. W. J. Beenakker	Universiteit Leiden
	Prof. dr. M. W. Beijersbergen	cosine B. V. / Universiteit Leiden
	Dr. E. R. Eliel	Universiteit Leiden
	Prof. dr. D. Bouwmeester	Universiteit Leiden / University of California, Santa Barbara (USA)
	Prof. dr. J. M. van Ruitenbeek	Universiteit Leiden

ISBN 978-90-815060-1-4

aan mijn ouders
en aan Astrid

Contents

1 Twisted light

1.1 Introduction

In this thesis we theoretically investigate optical modes with a highly non-trivial spatial, and in some cases also spectral, structure. We introduce an algebraic method to obtain explicit expressions of the modes to all orders inside a two-mirror cavity with twisted boundary conditions and apply these to study some of their physical properties. We generalize the concept of a cavity mode to the case of a two-mirror cavity that is put into uniform rotation about its optical axis and focus on the special case of a rotating astigmatic two-mirror cavity. We extend our algebraic method to account for time-dependent mirror settings and study some optical and opto-dynamical properties of this simple, but surprisingly rich, set-up. We discuss a complete and general characterization of the parameter space underlying basis sets of paraxial optical modes and study the geometric phase shift that arises from it. This phase shift constitutes the ultimate generalization of the Gouy phase in paraxial wave optics. We show that, in free space, the concept of a rotating mode of the radiation field can be generalized beyond the paraxial regime and show that the field can be quantized in an orthonormal, but otherwise arbitrary, basis of rotating modes, thereby constructing the first exact quantum theory of rotating light.

In this first, introductory, chapter we put the material discussed in the rest of the thesis in a somewhat broader context. Twisted and rotating boundary conditions are a natural source of orbital angular momentum and vorticity in optical fields. In the next section we give a brief historical introduction to these topics and discuss some applications in various branches

of modern quantum optics. The mathematical method that we develop and apply to characterize the dynamics of, mostly classical, wave fields generalizes well-established operator techniques from quantum mechanics. It is exact up to leading order of the (time-dependent) paraxial approximation and hinges upon the tight connection between wave and ray optics. Throughout the thesis we shall mostly use it in its canonical operator representation. However, both the analogy with quantum mechanics and the connection with ray optics are more conveniently discussed in the equivalent integral representation, which is the optical analogue of the path-integral formulation of quantum mechanics. This is worked out explicitly in sections 1.3 and 1.4. In the final section of this chapter, we give a detailed outline of this thesis.

1.2 Optical angular momentum

The ability of light to exert torques and forces on a material object was first recognized by Kepler. In his book *De cometis libelli tres* [1], published in 1619, he proposed that the empirical fact that a comet's tail always points away from the sun, is due to a radiative force exerted by the sun light. Initially, this proposal attracted quite some attention, especially in the context of the then ongoing debate whether light is composed of particles or should be considered a wave phenomenon. However, since various attempts to experimentally observe mechanical forces of light failed, the interest slowly dwindled [2].

When in the early 1860's Maxwell was the first to realize that light is a manifestation of the electromagnetic field [3], it became possible to study the mechanical properties of light, such as its energy, momentum and angular momentum, within the framework of classical electrodynamics. By studying the exchange of energy between a set of charged particles and the electric and magnetic fields, Poynting showed in 1884 that the energy density associated with the electromagnetic field in vacuum can be expressed as $\left(\epsilon_0|\mathbf{E}|^2 + \mu_0^{-1}|\mathbf{B}|^2\right)/2$, where $\mathbf{E}$ and $\mathbf{B}$ are respectively the electric and the magnetic field, and ϵ_0 and μ_0 are the permittivity and the permeability of vacuum [4]. From similar considerations, one may deduce that the momentum density of the electromagnetic field in vacuum can be expressed as $\mathcal{P} = \epsilon_0 \mathbf{E} \times \mathbf{B}$ so that the angular momentum associated with the electromagnetic field is given by [4]

$$\mathbf{J} = \int d_3\mathbf{r} \left(\mathbf{r} \times \mathcal{P}\right) = \epsilon_0 \int d_3\mathbf{r} \left(\mathbf{r} \times (\mathbf{E} \times \mathbf{B})\right). \tag{1.1}$$

By Helmholtz's theorem, the electric and magnetic field can be decomposed into the transverse radiation field and the longitudinal Coulomb field such that $\mathbf{E} = \mathbf{E}_{\parallel} + \mathbf{E}_{\perp}$, with $\nabla \cdot \mathbf{E}_{\perp} = 0$ and $\nabla \times \mathbf{E}_{\parallel} = 0$. From Maxwell's equations it follows that the longitudinal contribution to the magnetic field vanishes so that the angular momentum arising from the radiation field can be obtained from equation (1.1) by replacing the electric field by the transverse electric field $\mathbf{E}_{\perp}$. In general, it is convenient to introduce a scalar potential Φ and a vector potential $\mathbf{A}$ such that $\mathbf{E} = -\nabla\Phi - \dot{\mathbf{A}}$ and $\mathbf{B} = \nabla \times \mathbf{A}$ [4]. The scalar potential does not contribute to the radiation field so that $\mathbf{E}_{\perp} = -\dot{\mathbf{A}}_{\perp}$. Substitution of $\mathbf{E}_{\perp} = -\dot{\mathbf{A}}_{\perp}$ and $\mathbf{B} = \nabla \times \mathbf{A}$ in the expression of the

angular momentum of the radiation field in vacuum yields after partial integration [5]

$$\mathbf{J}_{\text{rad}} = \mathbf{L}_{\text{rad}} + \mathbf{S}_{\text{rad}} \,, \tag{1.2}$$

with

$$\mathbf{L}_{\text{rad}} = \epsilon_0 \sum_i \int d_3\mathbf{r}\, \left(\dot{\mathbf{E}}_\perp\right)_i \left(\mathbf{r} \times \nabla\right) \mathbf{A}_i \qquad \text{and} \qquad \mathbf{S}_{\text{rad}} = \epsilon_0 \sum_i \int d_3\mathbf{r}\, \dot{\mathbf{E}}_\perp \times \mathbf{A} \,, \tag{1.3}$$

where the index i runs over the vector components of the field. The first contribution in equation (1.3) is extrinsic in that it depends on the origin of the coordinate system used. By a proper choice of the origin, it can be made to vanish. As such, it may be viewed as the wave-optical analogue of the orbital angular momentum associated with the center-of-mass motion of two bodies, one of which orbits around the other [6]. The second contribution in equation (1.3), on the other hand, is obviously intrinsic and has the flavor of spin. However, although it may be shown that it indeed takes the form of the expectation value of the spin of a spin-1 particle, its interpretation as a spin is not without severe and fundamental difficulties [5]. These difficulties originate from the fact that the photon travels at the speed of light and, therefore, by special relativity, must have zero rest mass. The spin of a massive particle may be defined as its total angular momentum in a co-moving frame but, since the photon travels at the speed of light, its co-moving frame is non-existent. As a result, its spin is ill-defined [7]. This is illustrated by the fact that, in a quantized description of the radiation field, the operators corresponding to the components of $\mathbf{S}_{\text{rad}}$ do not obey the proper commutation rules [8, 6].

Physically speaking, the intrinsic (or spin) contribution to the angular momentum of the radiation field arises from its vector nature. In a circularly polarized beam it amounts to $\hbar$ per photon. Since a linearly polarized beam contains equal contributions of the two opposite circular polarizations, it bears no net spin angular momentum. Already in 1936, it has been demonstrated experimentally that the exchange of spin angular momentum between a circularly polarized beam of light and a birefringent crystal through which it propagates, gives rise to a torque on the crystal [9]. The extrinsic (or orbital) contribution to the angular momentum, on the other hand, arises from the phase structure of the field. Although optical forces arising from transverse phase gradients had been observed in optical tweezers [10], it was not before 1992 that it was realized that optical beams bearing orbital angular momentum can easily be produced and manipulated in experimental set-ups with laser beams [11]. In the standard case of a Laguerre-Gaussian beam [12], the orbital angular momentum arises from an optical vortex on the beam axis. Optical vortices are point singularities of the phase of the radiation field and give rise to helical wave fronts, which characterize a circular rather than a linear distribution of the transverse momentum [13]. During the past decades, the physics of optical vortices has been studied widely in the field of singular optics [14, 15]. In addition to vorticity, also general astigmatism contributes to the orbital angular momentum in optical fields [16, 17]. General astigmatism arises when the transverse intensity and phase distributions of an optical beam are anisotropic and non-aligned [18]. It gives rise to tumbling of

the beam under free propagation [17]. The orbital angular momentum per photon in optical beams with vortices and/or general astigmatism can be significantly larger than the spin angular momentum per photon in a circularly polarized beam. Under realistic experimental conditions, values of $10\hbar$ per photon can be achieved easily. Perhaps the most natural source of optical orbital angular momentum is physical rotation of a transverse field pattern [19, 20]. However, under typical circumstances, this rotational contribution is very small compared to the orbital angular momentum due to the transverse structure of a beam.

In the eighteen years that have passed since the first experiments were performed, optical orbital angular momentum has played a central role in various branches of modern quantum optics [21]. As opposed to the space of polarization states, which is inherently two-dimensional, the space of optical orbital angular momentum states is infinite-dimensional. Since in 2001, quantum entanglement in the orbital angular momentum of photons was first demonstrated experimentally [22], this infinite-dimensional nature has offered a whole range of interesting possibilities and challenges see, for instance, reference [23]. Also in the field of optical tweezers, the orbital angular momentum has been used to manipulate small particles [24]. Recently, it has been shown theoretically that the orbital angular momentum in a Laguerre-Gaussian beam can be sufficiently large to trap and cool the rotational degree of freedom of a mirror [25]. This suggests possible application of optical orbital angular momentum in the rapidly developing field of (cavity) opto-mechanics.

1.3 Classical optics and quantum mechanics

Long before the days of Maxwell, and even before the debate whether light consists of particles or should be considered a wave was settled in favor of the wave description by Young's famous double-slit experiments in 1801, the propagation and diffraction of waves was pretty well-understood. In 1678, Huygens first formulated his principle that every point on a wave front acts as a source of spherical waves. The wave front at a distant location is the envelope of these spherical waves. It took until 1690 before Huygens published the principle in his book *Traité de la lumière* [26]. Between 1815 and 1819, the wave theory of light was significantly refined by Fresnel, who, in the spirit of Young's double-slit experiment, added the notion of interference to what is nowadays called the Huygens-Fresnel principle. For monochromatic complex scalar waves $E(\mathbf{r}, t) = E(\mathbf{r}) \exp(-i\omega t)$ it can be expressed as [27]

$$E(\rho, z) = \frac{2\pi k}{i} \int d_2\rho_0 \, \frac{\exp\left(ik|\mathbf{r} - \mathbf{r}_0|\right)}{|\mathbf{r} - \mathbf{r}_0|} E(\rho_0, z_0) \cos\theta \,, \tag{1.4}$$

where $\rho = (x, y)^{\mathrm{T}}$ is the transverse position vector, $k = \omega/c$ is the wave number and θ is the angle between the position vector $\mathbf{r}$ and the normal to the wave front in the z_0 plane. The Huygens-Fresnel integral (1.4) characterizes the complex spatial field $E(\rho, z)$ in some transverse plane z as a coherent superposition of spherical waves emanating from point sources in the plane z_0. The amplitudes and relative phases of the spherical waves are given by the transverse field distribution $E(\rho_0, z_0)$ in the plane z_0. The additional obliquity factor $\cos\theta$ is

related to the fact that only spherical waves that propagate away from the sources are taken into consideration [28]. It gives the spherical waves an angular profile. In its original form, the Huygens principle explains reflection and refraction of light at an interface. The modified Huygens-Fresnel principle as described by equation (1.4) also describes phenomena arising from interference and diffraction. At the time it was formulated, the Huygens principle was more of brilliant but somewhat qualitative guess rather than a formal and mathematically rigorous statement. However, in 1882 Kirchhoff derived the Huygens-Fresnel integral directly from Maxwell's equations [4]. In hindsight, the Huygens-Fresnel integral (1.4) may be considered as the first example of a path integral in physics.

The fundamental principle that underlies the ray-optical description of light is the principle of least time, first formulated by Fermat in 1662. This principle states that a ray of light optimizes the optical path length between two points in space and plays a role analogous to that of the principle of least action in classical mechanics. Since the speed of light is determined by the optical density of the medium, as characterized by the refractive index $n(x, y, z)$, the velocity of a ray of light is not an independent dynamical variable. It follows that a ray of light can be fully characterized by its three spatial coordinates as a function of some parameter, which we choose to be the z coordinate. In that case, the optical path length of a ray can be expressed as

$$L = \int_{z_1}^{z_2} dz\, n(x, y, z) \sqrt{1 + x'^2 + y'^2}\,, \tag{1.5}$$

where z_1 and z_2 are the z coordinates of the begin and end points of the ray and where $x' = \partial x/\partial z$ and $y' = \partial y/\partial z$. Since the path length plays the role of the action, the argument of the integral in equation (1.5) is the Lagrangian $\mathcal{L}$ that describes the propagation of optical rays through a medium characterized by the refractive index $n(x, y, z)$. With the corresponding momenta, which are defined as $\partial\mathcal{L}/\partial x'$ and $\partial\mathcal{L}/\partial y'$, this naturally leads to a canonical formulation of geometric optics [29].

In many optical set-ups, the light propagates along a well-defined direction so that paraxial approximations (from the Ancient Greek $\pi\alpha\rho\alpha$, which literally means alongside of) are justified. In mathematical terms, the assumption that the light mainly propagates along the z axis implies that $x', y' << 1$. In case of paraxial propagation through vacuum ($n = 1$), the Lagrangian arising from the path length (1.5) can be approximated by

$$\mathcal{L} = 1 + \frac{1}{2}\left(x'^2 + y'^2\right). \tag{1.6}$$

The corresponding momenta are given by $\vartheta_x = \partial\mathcal{L}/\partial x' = x'$ and $\vartheta_y = \partial\mathcal{L}/\partial y' = y'$ and correspond to direction angles measured with respect to the z axis. Following the standard construction of the Feynman path integral [30], $\hbar$ being replaced by $\lambda\!\!\!^{-} = \lambda/2\pi = 1/k$, the path integral corresponding to the Lagrangian in equation (1.6) can be expressed as

$$E(\rho, z) = \frac{2\pi k e^{ik(z-z_0)}}{i(z - z_0)} \int d_2\rho_0\ \exp\left(\frac{ik\left((x - x_0)^2 + (y - y_0)^2\right)}{2(z - z_0)}\right) E(\rho_0, z_0)\,, \tag{1.7}$$

which clearly is a paraxial approximation of the Huygens-Fresnel integral (1.4) [12]. If we write the field as the product $E(\rho, z) = u(\rho, z)\exp(ikz)$ of a spatial profile $u(\rho, z)$ and a carrier wave $\exp(ikz)$, it follows that (1.7) corresponds to the general solution of the paraxial wave equation

$$\left(\nabla_\rho^2 + 2ik\frac{\partial}{\partial z}\right)u(\rho, z) = 0\,, \tag{1.8}$$

where $\nabla_\rho^2 = \partial^2/\partial x^2 + \partial^2/\partial y^2$ is the transverse Laplacian. The paraxial wave equation (1.8) takes the form of the Schrödinger equation for a free particle in two dimensions, $\lambda\!\!\!^{-} = 1/k$ playing the role of $\hbar/m$ with m the mass of the particle. It describes the spatial evolution of the profile $u(\rho, z)$ of a paraxial beam, which characterizes its large-scale spatial structure, and plays a central role in this thesis.

It is noteworthy that, in the present context of monochromatic scalar waves, the paraxial approximation plays a role similar to that of the non-relativistic approximation in quantum mechanics [31]. In the optical case, the exact wave equation reduces to the paraxial wave equation for fields that mainly propagate along a well-defined direction while in quantum mechanics, the Klein-Gordon equation, which describes a massive scalar field, reduces to the ordinary Schrödinger equation for fields that only contain mainly time-like components.

1.4 First-order optics

An interesting property of the paraxial Lagrangian (1.6) is that the evolution of the transverse coordinates $\rho = (x, y)^{\mathrm{T}}$ and the corresponding momenta $\theta = (\vartheta_x, \vartheta_x)^{\mathrm{T}} = \partial\rho/\partial z$, which are conveniently combined in a four-dimensional ray vector $\mathscr{r}^{\mathrm{T}} = (\rho^{\mathrm{T}}, \theta^{\mathrm{T}})$, is linear. The solution of the Euler-Lagrange equation deriving from the Lagrangian (1.6) can be expressed as

$$\mathscr{r}(z) = \begin{pmatrix} 1 & 1z \\ 0 & 1 \end{pmatrix}\mathscr{r}(0)\,, \tag{1.9}$$

where 0 and 1 are the 2×2 zero and unit matrices. The fact that this transformation can be represented by a 4×4 matrix is not a unique property of paraxial propagation through vacuum. It is well-known that, in leading order of the paraxial approximation, the transformations due to various lossless optical elements such as thin lenses and mirrors can also be represented by real 4×4 matrices acting on a ray vector $\mathscr{r}$ [12]. In the special case of isotropic elements, all four 2×2 submatrices of the 4×4 ray matrix are proportional to the 2×2 unit matrix. It follows that the transformation of the two transverse components $(x, \vartheta_x)^{\mathrm{T}}$ and $(y, \vartheta_y)^{\mathrm{T}}$ of a ray $\mathscr{r}$ can be described by the same reduced 2×2 ray matrix. Such 2×2 ray matrices are called *ABCD* matrices [12]. Free propagation as described by equation (1.9) is obviously isotropic. It is an example of a transformation that can be described by an *ABCD* matrix. A ray that lies in a plane through the optical axis of the element through which it passes can be characterized by its distance to the optical axis $R = |\rho|$ and the corresponding direction angle $\vartheta = \partial\rho/\partial z$. One may show easily that also in this case the transformation due to an isotropic

optical element can be represented by an $ABCD$ matrix. If the two-dimensional vector that characterizes such a ray is denoted $\mathfrak{r} = (R, \vartheta)^{\mathrm{T}}$, this transformation can be expressed as

$$\mathfrak{r}_{\mathrm{out}} = \begin{pmatrix} A & B \\ C & D \end{pmatrix} \mathfrak{r}_{\mathrm{in}} \,, \tag{1.10}$$

with $A, B, C, D \in \mathbb{R}$. The transverse position R and the propagation direction ϑ constitute a pair of canonically conjugate variables. From the fact that this canonical structure is preserved under the lossless transformation in equation (1.10), it follows that a physical $ABCD$ matrix must have a unit determinant so that $AD - BC = 1$. The transformation of a sequence of optical elements can be constructed as the product of the ray matrices describing each of the elements and, since the determinant of a matrix product equals the product of the determinants of the matrices, it follows that the determinant of any $ABCD$ matrix that describes a lossless isotropic optical set-up is equal to 1.

The optical path length between a point R_1 in the input plane and a point R_2 in the output plane of an isotropic optical set-up that is described by an $ABCD$ matrix can be expressed as [12]

$$L(R_1, R_2) = L_0 + \frac{1}{2B}\left(AR_1^2 - 2R_1R_2 + DR_2^2\right) \,, \tag{1.11}$$

where L_0 is the path length along the optical axis of the set-up. The corresponding path integral, with $\lambda\!\!\!^{-} = 1/k$ again playing the role of $\hbar$, takes the following form [32, 12]

$$E(\rho_2, z_2) = \frac{2\pi k e^{ikL_0}}{iB} \int d_2\rho_1 \; \exp\left(\frac{ik\left(AR_1^2 - 2R_1R_2 + DR_2^2\right)}{2B}\right) E(\rho_1, z_1) \,. \tag{1.12}$$

This obviously reduces to equation (1.7) in case of free propagation $A = D = 1$ and $B = L_0 = z_2 - z_1$. The expression in equation (1.7) shows explicitly that the propagation of a wave through an optical set-up is fully determined by the geometric-optical characteristics of the optical set-up. This description of wave propagation is geometric in that it derives from the Fermat principle, which has a clear geometric significance.

It is well-known from textbook quantum mechanics that the path-integral description is exact in the case of first-order systems, the non-relativistic free particle and the harmonic oscillator being the simplest examples [30]. Since Gaussian integrals can be solved exactly, it follows that the evolution of Gaussian wave packets under the integral transformation for a first-order system can be calculated analytically. Less well-known is that the path-integral description is also exact for infinitely many complete sets of excited states, which, analogous to the case of the harmonic oscillator, can be obtained from pairs of bosonic ladder operators. In the optical context, such excited states have the significance of higher-order transverse modes [33]. Two very well-known examples are the Hermite-Gaussian and Laguerre-Gaussian modes, which are of crucial importance in experiments with laser beams [12].

1.5 Thesis outline

In this thesis, we study the spatial structure and physical properties of higher-order optical modes that have a twisted nature due to the presence of astigmatism and optical vortices. Our characterization of such twisted states of light involves pairs of bosonic ladder operators that generate a basis set of optical modes. Although the ladder operators act in the wave-optical domain, we shall demonstrate that their transformation under paraxial propagation and optical elements can be expressed in terms of the ray matrix that also describes the transformation of a ray. The ladder operators generate a complete set of higher-order mode patterns that exactly solve the Huygens-Fresnel integral (1.12) for an arbitrary first-order system. In regions of free propagation, the modes obey the paraxial wave equation (1.8). As opposed to the Huygens-Fresnel integral, which cannot easily be generalized to the case of set-ups with non-isotropic optical elements, the ladder operator-method allows for direct generalization to the case of transverse modes with astigmatism. Although the method keeps its elegance and simplicity, the spatial patterns of astigmatic higher-order modes display a very rich structure that gives rise to vorticity and orbital angular momentum. In the first two chapters, we apply the ladder-operator method to study the mode structure and the physical properties that arise from it in the presence of twisted and rotating boundary conditions.

- In chapter 2 we show that the paraxial modes of a geometrically stable two-mirror cavity with general astigmatism, i.e., a cavity that consists of two non-aligned astigmatic mirrors, can be obtained from pairs of bosonic ladder operators. From the transformation property of the ladder operators it follows that the ladder operators that generate the cavity modes can be constructed from the eigenvectors of the round-trip ray matrix that describes the transformation of a ray after one round trip through the cavity. The eigenvalues determine the frequency spectrum of the cavity. As a result of the twisted nature of the astigmatic boundary conditions, the spatial structure of the cavity modes becomes twisted as well. This twist induces vorticity and orbital angular momentum in the cavity modes.

- In chapter 3 we generalize the concept of an optical cavity mode to the case of a cavity in uniform rotation. We generalize the ladder-operator method developed in the second chapter to account for the time dependence of a rotating cavity and obtain explicit expressions of the rotating cavity modes. These are applied to study some of their physical properties including the rotationally induced orbital angular momentum.

Although relatively simple in terms of the number of degrees of freedom involved, a rotating astigmatic two-mirror cavity turns out to be a surprisingly rich dynamical system. Chapters 4 and 5 are devoted to specific dynamical properties of a rotating cavity and its modes.

- In chapter 4 we show that rotation affects the focusing properties of the mirrors of an astigmatic two-mirror cavity in such a way that the cavity can both be stabilized and

destabilized by rotation. As such it bears some similarity with both the Paul trap and the gyroscope. We study the rotationally induced transition from a stable to an unstable geometry and vice versa in terms of the structure of and the orbital angular momentum in the rotating cavity modes.

- In chapter 5 we show that optical vortices appear in the modes of an astigmatic two-mirror cavity when it is put into rotation about its optical axis. We study some physical properties of the emerging vortex pattern. We make a comparison with rotationally induced vortices in material systems and discuss explicit results for a specific case. In section 5.5, we discuss limitations of possible experimental realizations of an optical set-up that captures the essential features of the rotating astigmatic cavities that we study in chapters 3, 4 and 5.

Since the transformations of the ladder operators can be expressed in terms of a ray matrix, which has a clear geometric significance, it follows that also the ladder-operator method is geometric in that it relates to the principle of Fermat.

- In chapter 6 we focus on such geometrical aspects. We study the geometry of the parameter space underlying the pairs of bosonic ladder operators and the geometric phase shifts that it gives rise to. Such phase shifts constitute the ultimate generalization of the Gouy phase in paraxial wave optics. We recover both the ordinary Gouy phase shift and the geometric phase that arises from cyclic transformations of optical beams bearing orbital angular momentum as limiting cases. We discuss an analogy with the Aharonov-Bohm effect in quantum eletrodynamics that reveals some deep insights in the nature and origin of this geometric phase.

Finally, the last chapter completes the discussion of rotating light.

- In chapter 7 we show that the exact wave equation, which derives without approximations from Maxwell's equations, allows for solutions that are monochromatic in a rotating frame. Since, in complex notation, monochromatic fields are separable in space and time, it follows that these solutions are stationary in a rotating frame. As a result, both the polarization and the spatial patterns of the vector components of the corresponding fields rotate uniformly in a stationary frame. We discuss the quantization of the radiation field in an orthonormal but otherwise arbitrary basis of such rotating modes. We derive the equations of motion for light in a rotating frame and show that quantization in the rotating frame is consistent with quantization in the stationary frame. We discuss the paraxial counterpart of the exact theory and indicate how a quantum-optical description of the rotating cavity modes, as introduced in chapter 3, can be obtained.

Several chapters in this thesis are based on material that has been (or will be) published elsewhere. Although all of them have been rewritten, I have tried to keep them independently

readable. As a result, there is some overlap, in particular between the three chapters on rotating cavities. Physics-oriented readers may at first read chapters 4 and 5, in which the emphasis is on the physical phenomena rather than on the mathematical method used, and go back to the relatively heavy mathematics in chapter 2 and 3 at a later stage. Mathematically oriented readers, on the other hand, may consider first reading chapter 6, in which the mathematics underlying the ladder-operator method that is crucial to this thesis is discussed in its most general and, as a result, abstract form.

The notation used in this thesis has been harmonized as much as possible without sacrificing intuition. Generally speaking, vectors in three-dimensional space are set in a bold font while vectors in the transverse plane are denoted with small Greek letters. Both two and four-dimensional ray vectors are denoted in a script font while vectors in other (parameter) spaces are denoted with arrows above the symbol. The bra-ket notation of quantum mechanics is used to denote vectors in the Hilbert space of transverse states of classical light. Quantum states of the radiation field are indicated with bra and ket vectors with round brackets. All operators are denoted with a hat above the symbol. Matrices acting on the transverse spatial coordinates (or momenta) are set in a sans serif font while ray matrices, which act on either two- or four-dimensional rays are set in the standard roman font. These and other notational conventions used in this thesis are listed in table 1.1.

Symbol	Meaning
Coordinates	
(x, y, z)	Cartesian coordinates
$(R\cos\phi, R\sin\phi, z)$	Cylindrical coordinates
$(r\sin\vartheta\cos\varphi, r\sin\vartheta\sin\varphi, r\cos\vartheta)$	Spherical coordinates
Vectors	
$\mathbf{r} = (x, y, z)^{\mathrm{T}}$	Position in three dimensions
$\mathbf{k} = (k_x, k_y, k_z)^{\mathrm{T}}$	Wave vector in three dimensions
$\rho = (x, y)^{\mathrm{T}}$	Transverse position
$\theta = (\vartheta_x, \vartheta_y)^{\mathrm{T}}$	Transverse propagation direction
$\epsilon = (\epsilon_x, \epsilon_y)^{\mathrm{T}}$	Transverse polarization
$\mathscr{r}, \mathscr{s} = (\rho, \theta)^{\mathrm{T}}$	Two- and four-dimensional real ray vectors
μ, ν	Normalized complex (eigen)rays
$\vec{A}, \vec{R}$	Vectors in a parameter space
$\lvert u\rangle, \lvert v\rangle$	Transverse states of classical light
$\lvert ...\rangle$	Quantum state of light
Fields	
$\mathbf{E}, \mathbf{B}$	Electric and magnetic fields
$\mathbf{A}$	Vector potential
$\mathbf{C}$	Vector potential in a rotating frame
$\mathbf{F}, \mathbf{G}$	Vectorial mode functions
$\mathbf{V}$	Vectorial mode function in a rotating frame
Operators	
$\hat{a}^{(\dagger)}_{1,2}, \hat{b}^{(\dagger)}_{x,y}$	Raising and lowering operators
$\hat{a}^{(\dagger)}_{\lambda}, \hat{c}^{(\dagger)}_{\mu}, \hat{v}^{(\dagger)}_{\nu}$	Creation and annihilation operators (chapter 7)
Generalized beam parameters	
$r_{1,2}$ and $t_{1,2}$	Scalar coefficients of a ladder operator
R and T	2×2 coefficient matrices of a vector of ladder operators
$\mathsf{S} = \mathsf{V}^{-1}$	2×2 matrices that characterize the astigmatism
$\chi_{1,2}$	Generalized Gouy phases
η, ξ	Spinors on the Hermite-Laguerre sphere
Beam profiles	
u, v	Transverse profile of a paraxial beam
$\tilde{u}$	Transverse Fourier transform of u

Table 1.1: List of Symbols

2

Twisted cavity modes

2.1 Introduction

A typical optical cavity consists of two spherical mirrors facing each other. The modes of such a cavity are transverse field distributions that are reproduced after each round trip, bouncing back and forth between the mirrors [12]. The usual approach to the problem of finding the modes of an optical cavity is by considering the free propagation of light from one mirror to the other (in integral or differential form) and imposing the proper boundary conditions. In the paraxial limit the propagation through free space can be described by the paraxial wave equation, which has the Huygens-Fresnel integral equation as its integral form. The boundary condition is that the electric field vanishes at the surface of the mirrors, which implies that the mirror surfaces match a nodal plane of the standing wave that is formed by a bouncing traveling wave. Conversely, a Gaussian paraxial beam, which has spherical wave fronts, can be trapped between two spherical mirrors that coincide with a wave front, as indicated in figure 2.1. This imposes a condition on the curvatures and the spacing L of the mirrors. When the radii of curvature are R_1 and R_2, the condition is simply [12]

$$0 \leq g_1 g_2 \leq 1 \ , \tag{2.1}$$

where the parameters $g_1$and g_2 are defined by

$$g_i = 1 - \frac{L}{R_i} \tag{2.2}$$

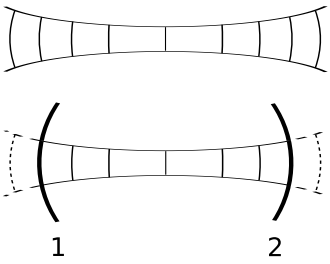

Figure 2.1: A freely propagating Gaussian beam can be trapped by mirrors that coincide with its wave fronts. Its wave fronts are then turned into nodal planes of the standing-wave pattern inside the cavity.

for $i = 1, 2$. This is precisely the stability condition of the cavity. A stable cavity is a periodic focusing system for which the round-trip magnification is equal to 1 so that it supports stable ray patterns. Such a cavity has a complete set of Hermite-Gaussian modes, with a simple Gaussian fundamental mode. For a two-mirror cavity with radii of curvature R_i and a spacing L obeying the stability condition (2.1), the modes are characterized by the Rayleigh range z_R and the round-trip Gouy phase χ that are given by [12]

$$\frac{z_\mathrm{R}^2}{L^2} = \frac{g_1 g_2 (1 - g_1 g_2)}{(g_1 + g_2 - 2 g_1 g_2)^2} \qquad \text{and} \qquad \cos\left(\frac{\chi}{2}\right) = \pm\sqrt{g_1 g_2}\,. \tag{2.3}$$

The plus sign is taken if both g_1 and g_2 are positive whereas the minus sign is taken when both are negative. The wave numbers of the Hermite-Gaussian modes HG_{nm} with transverse mode numbers n and m are determined by the requirement that the phase of the field changes over a round trip by a multiple of 2π. This gives the resonance condition

$$2kL - (n + m + 1)\chi = 2\pi q \tag{2.4}$$

for the wave number k, with a longitudinal mode index $q \in \mathbb{Z}$.

It is a simple matter to generalize this method to the case of astigmatic mirrors, provided that the mirror axes are parallel. Each mirror i can be described by two radii of curvature $R_{i\xi}$ and $R_{i\eta}$, corresponding to the curvatures along the two axes. In this case of simple, or orthogonal, astigmatism the paraxial field distribution separates into a product of two contributions, corresponding to the two transverse dimensions. Stability requires that each of the two dimensions obey the stability condition (2.1) for the parameters $g_{i\xi}$ and $g_{i\eta}$, and each dimension has its own Rayleigh range and Gouy phase. The resonance condition for a cavity with simple astigmatism takes the modified form

$$2kL - \left(n + \frac{1}{2}\right)\chi_\xi - \left(m + \frac{1}{2}\right)\chi_\eta = 2\pi q\,, \tag{2.5}$$

where χ_ξ and χ_η are the Gouy phases for the ξ and η direction respectively.

The situation is considerably more complex when the axes of the two astigmatic mirrors are non-aligned. In this case of twisted cavity, the light bouncing back and forth between the mirrors becomes twisted as well and the cavity modes display general, or non-orthogonal, astigmatism, which is characterized by the absence of transverse symmetry directions. Also in this case the stability condition and the structure of the cavity modes is, in principle, determined by the requirement that the mirror surfaces match a wave front of a traveling beam. It is, however, not simple to derive the mode structure and the resonance frequencies of the cavity from this condition. The stability of a twisted cavity or lens guide as well as the propagation of the Gaussian fundamental mode, which is characterized by its elliptical intensity distribution and its elliptical or hyperbolic wave fronts, has been studied by several authors using analytical techniques [18, 34, 35, 36, 37]. Also higher-order modes have received some attention [38].

A few years ago, a general description has been given of freely propagating paraxial modes of arbitrary order with general astigmatism [17]. The method is based on the use of bosonic ladder operators in the spirit of the quantum-mechanical description of the harmonic oscillator [33] and has a simple algebraic structure. Here, we generalize this approach to study the modes to all orders of geometrically stable twisted cavities. In this case, the basis set of modes is fixed by the geometric properties of the cavity, i.e., the radii of curvature that characterize the astigmatic mirrors, their (relative) orientation and their separation. Rather than using the condition that the wave fronts match the mirror surfaces, our method is entirely based on the eigenvalues and eigenvectors of the four-dimensional ray matrix that describes the transformation of a ray after one round trip through the cavity. This matrix generalizes the *ABCD* matrix, which describes the propagation of a ray through an isotropic optical set-up [12]. We discuss the relevant (group-theoretical) properties of this ray matrix in section 2.2. After a brief discussion of paraxial wave optics in an astigmatic cavity in section 2.3, we give in section 2.4 an operator description of fundamental Gaussian modes and higher-order modes. Here we demonstrate that the cavity modes can be directly expressed in terms of the properties of the ray matrix. In section 2.5, we discuss some physical properties of the modes including the orbital angular momentum that is due to their twisted nature and their vorticity. Explicit results for a specific case are briefly discussed in section 2.6.

2.2 Paraxial ray optics

2.2.1 One transverse dimension

In geometric optics, a light beam in vacuum is assumed to consist of a pencil of rays [29]. In each transverse plane a ray is characterized by its transverse position x and its propagation direction $\vartheta = \partial x/\partial z$, where z is the longitudinal coordinate. The angle ϑ gives the propagation direction of the ray with respect to the optical axis of the set-up through which it propagates. Both the transverse position x and the propagation direction ϑ of a ray transform under free propagation and optical elements. In lowest order of the paraxial approximation ($\vartheta << 1$)

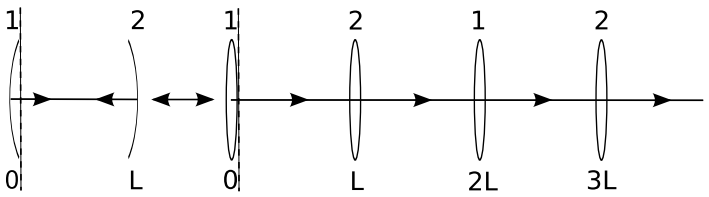

Figure 2.2: Unfolding a two-mirror cavity into an equivalent periodic lens guide; the mirrors are replaced by lenses with the same focal lengths and the reference plane is indicated by the dashed line.

this transformation is linear and can be represented by a 2×2 ray matrix acting on a ray vector $\mathbf{r} = (x, \vartheta)^{\mathrm{T}}$

$$\begin{pmatrix} x_{\mathrm{out}} \\ \vartheta_{\mathrm{out}} \end{pmatrix} = M \begin{pmatrix} x_{\mathrm{in}} \\ \vartheta_{\mathrm{in}} \end{pmatrix} . \tag{2.6}$$

Here M is a ray matrix that transforms the input beam of the optical system into the output beam. The matrices that represent various optical elements can be found in any textbook on optics, see, for instance, reference [12]. The ray matrix for propagation through free space over a distance z is given by

$$M_{\mathrm{f}}(z) = \begin{pmatrix} 1 & z \\ 0 & 1 \end{pmatrix} . \tag{2.7}$$

The trajectory that corresponds to this transformation is a straight line with the direction angle ϑ, where the transverse position $x' = x + \vartheta z$ changes linearly with the distance z. The transformation of a ray through a paraxial thin lens can be expressed as

$$M_{\mathrm{l}}(f) = \begin{pmatrix} 1 & 0 \\ -1/f & 1 \end{pmatrix} , \tag{2.8}$$

where f is the focal length of the lens which is taken positive for a converging lens. The transverse position is invariant under this transformation. The angle ϑ, which specifies the propagation direction, changes abruptly at the location of the lens. It can be easily shown that this transformation reproduces the thin-lens equation.

The transformation matrix of a sequence of first-order optical elements can be constructed by multiplying the matrices that correspond to the various elements in the correct order. Closed optical systems such as a cavity can be unfolded into an equivalent periodic lens guide, as indicated in figure 2.2. The mirrors are replaced by thin lenses with the same focal lengths. One period of the lens guide is equivalent to a single round trip through the cavity. When we choose the transverse reference plane just right of mirror 1 (or lens 1), we can construct the ray matrix that describes the transformation of a single round trip in the form

$$M_{\mathrm{rt}} = M_{\mathrm{l}}(f_1) M_{\mathrm{f}}(L) M_{\mathrm{l}}(f_2) M_{\mathrm{f}}(L) . \tag{2.9}$$

Here L is the distance between the two mirrors of the cavity, and $f_{1,2}$ are the focal lengths of the mirrors that are related to the radii of curvature by $f_{1,2} = R_{1,2}/2$.

The ray matrices that correspond to lossless optical elements are real and have a unit determinant. Since the product of real matrices yields a real matrix whose determinant is equal to the product of the determinants, it follows that this is also true for the ray matrix that describes the transformation of any composite lossless system. In case of one transverse dimension these are the defining properties of a physical ray matrix so that the reverse of the above statement is also true: any real 2×2 matrix that has a unit determinant corresponds to the transformation of a lossless optical set-up that can be constructed from first-order optical elements. Mathematically speaking, physical ray matrices constitute the group $SL(2, \mathbb{R})$ under matrix multiplication.

An important characteristic of an optical cavity is whether it is geometrically stable or not. In many cases a cavity will support only rapidly diverging or converging ray paths. Only in specific cases does a cavity support a stable ray pattern. Usually the stability criterion of an optical cavity is formulated in terms of the parameters that characterize the geometry, i.e., the radii $R_{1,2}$ of curvature of the mirrors and the distance L between them. For our purposes, however, it is more convenient to relate the stability of a cavity to the eigenvalues λ_1 and λ_2 of the round-trip ray matrix M_{rt}. Since $\det M_{\mathrm{rt}} = 1$, it follows that $\lambda_1 \lambda_2 = 1$. If we assume that these eigenvalues are non-degenerate, i.e., $\lambda_1 \neq \lambda_2$, the corresponding eigenvectors μ_1 and μ_2 are linearly independent, so that an arbitrary input ray $\mathscr{r}_0$ can be written as

$$\mathscr{r}_0 = a_1 \mu_1 + a_2 \mu_2 \ . \tag{2.10}$$

After n round trips through the cavity this ray transforms to

$$\mathscr{r}_n = M_{\mathrm{rt}}^n \mathscr{r}_0 = a_1 \lambda_1^n \mu_1 + a_2 \lambda_2^n \mu_2 \ . \tag{2.11}$$

From this transformation of a ray through the cavity it is clear that the absolute values of the eigenvalues determine the magnification of the ray. It follows that a cavity is stable only if the absolute value of both eigenvalues is equal to 1. In case of a non-degenerate round-trip ray matrix M_{rt} this condition requires that the eigenvalues, and therefore the eigenvectors, are complex. Since M_{rt} is a real matrix, its eigenvectors as well as its eigenvalues must be each other's complex conjugates, so that

$$\mu_1 = \mu_2^* = \mu \qquad \text{and} \qquad \lambda_1 = \lambda_2^* = e^{i\chi} = \lambda \ . \tag{2.12}$$

The phase χ is the round-trip Gouy phase of the cavity, which determines its spectrum according to equation (2.4). For a real incident ray $\mathscr{r}_0$, equation (2.10) takes the form

$$\mathscr{r}_0 = 2\mathrm{Re}\,(a\mu) \ , \tag{2.13}$$

where $a = a_1 = a_2^*$. With equation (2.11) this leads to the expression

$$\mathscr{r}_n = 2\mathrm{Re}\left(a\mu e^{in\chi}\right) \ , \tag{2.14}$$

for the transformed ray after n round trips. This shows that both the position and the propagation direction of the ray at successive passages of the reference plane display a discrete oscillatory behavior. An interesting case arises when the Gouy phase χ is a rational fraction of 2π, i.e., if

$$\chi = \frac{2\pi K}{N} , \tag{2.15}$$

where K and N are integers. Then the two eigenvalues of M_{rt}^N are both equal to 1, so that $M_{\mathrm{rt}}^N = 1$. Inside a cavity this means that the trajectory of a ray will form a closed path after N round trips.

For a different choice of the reference plane, the round-trip ray matrix M_{rt} takes a different form. The two forms are related by a transformation determined by the ray matrix from one reference plane to the other. The same transformation also couples the eigenvectors. The eigenvalues, and therefore the notion of stability, are independent of the choice of the reference plane.

2.2.2 Two transverse dimensions

The description that we have discussed in the previous subsection can be generalized to optical set-ups with two independent transverse dimensions. In this case both the transverse position and the propagation direction of a ray become two-dimensional vectors. The transverse coordinates are denoted $\rho = (x, y)^{\mathrm{T}}$, and $\theta = (\vartheta_x, \vartheta_y)^{\mathrm{T}}$ are the angles that specify the propagation direction in the xz and yz planes. Likewise, the transformation from the input plane of an optical set-up to its output plane is represented by a 4×4 ray matrix, in the form

$$\begin{pmatrix} \rho_{\mathrm{out}} \\ \theta_{\mathrm{out}} \end{pmatrix} = M \begin{pmatrix} \rho_{\mathrm{in}} \\ \theta_{\mathrm{in}} \end{pmatrix} . \tag{2.16}$$

For an isotropic (non-astigmatic) optical element the 4×4 matrix is obtained by multiplying the four elements of the 2×2 ray matrix with a 2×2 unit matrix $\mathsf{1}$. For instance, the transformation for propagation through free space over a distance z can be expressed as

$$M_{\mathrm{f}}(z) = \begin{pmatrix} \mathsf{1} & z\mathsf{1} \\ \mathsf{0} & \mathsf{1} \end{pmatrix} , \tag{2.17}$$

where $\mathsf{0}$ is the 2×2 zero matrix. In case of an astigmatic optical element, at least some part of the ray matrix is not proportional to the identity matrix. For our present purposes, the most relevant example is that of an astigmatic thin lens. The ray matrix that describes its transformation can be written as

$$M_{\mathrm{l}}(\mathsf{F}) = \begin{pmatrix} \mathsf{1} & \mathsf{0} \\ -\mathsf{F}^{-1} & \mathsf{1} \end{pmatrix} , \tag{2.18}$$

where F is a real and symmetric 2×2 matrix. Its eigenvalues are the focal lengths of the lens, while the corresponding, mutually perpendicular, real eigenvectors fix the orientation of the lens in the transverse plane.

Again, the ray matrix that describes a composite optical system can be constructed by multiplying the ray matrices that describe the optical elements in the right order. In particular, the ray matrix that describes the transformation of a round trip through an astigmatic cavity can be obtained by unfolding the cavity into the corresponding lens guide and multiplying the matrices that represent the transformations of the different elements in the correct order

$$M_{\mathrm{rt}} = M_{\mathrm{l}}(\mathsf{F}_1) M_{\mathrm{f}}(L) M_{\mathrm{l}}(\mathsf{F}_2) M_{\mathrm{f}}(L) \; . \tag{2.19}$$

Here L is again the distance between the two mirrors and $\mathsf{F}_{1,2}$ are the matrices that describe the mirrors. If both mirrors have two equal focal lengths, i.e., if they are spherical, the cavity has cylinder symmetry. If one of the mirrors has two different focal lengths, i.e., is astigmatic, while the other is spherical or if both mirrors are astigmatic but with the same orientation, the cavity has two transverse symmetry directions and is said to have simple (or orthogonal) astigmatism. If this is not the case, i.e., if both mirrors are astigmatic and if they are in non-parallel alignment there are no transverse symmetry directions and the cavity has general (or non-orthogonal) astigmatism [18].

A typical ray matrix M is real, but not symmetric, so that its eigenvectors cannot be expected to be orthogonal. However, it is easy to check that the ray matrices (2.17) and (2.18) obey the identity

$$M^{\mathrm{T}} G M = G \tag{2.20}$$

where G is the anti-symmetric 4×4 matrix

$$G = \begin{pmatrix} 0 & 1 \\ -1 & 0 \end{pmatrix} . \tag{2.21}$$

The same identity must hold for a composite optical set-up, in particular for the round-trip ray matrix M_{rt} (2.19). This is the defining property of a physical ray matrix that describes a lossless first-order optical system. It generalizes the defining properties of a 2×2 ray matrix to the astigmatic case. In mathematical terms, the above identity defines a symplectic group under matrix multiplication [39]. Physical ray matrices must be in the real symplectic group of 4×4 matrices, denoted as $Sp(4, \mathbb{R})$. The determinant of physical 4×4 ray matrices is equal to 1. It is noteworthy that the 2×2 analogue of equation (2.20) defines $Sp(2, \mathbb{R}) \cong SL(2, \mathbb{R})$.

From the general property (2.20) of the ray matrix (2.19) we can derive some important properties of its eigenvalues and eigenvectors. The eigenvalue relation is generally written as

$$M_{\mathrm{rt}} \mu_i = \lambda_i \mu_i \tag{2.22}$$

where μ_i are the four eigenvectors and λ_i are the corresponding eigenvalues. By taking matrix elements of the identity (2.20) between the eigenvectors, we find

$$\lambda_i \lambda_j \mu_i^{\mathrm{T}} G \mu_j = \mu_i^{\mathrm{T}} G \mu_j \; . \tag{2.23}$$

The matrix element $\mu_i^{\mathrm{T}} G \mu_i$ vanishes, so this relation gives no information on the eigenvalue for $i = j$. For different eigenvectors $\mu_i \neq \mu_j$, we conclude that either $\lambda_i \lambda_j = 1$, or $\mu_i^{\mathrm{T}} G \mu_j = 0$.

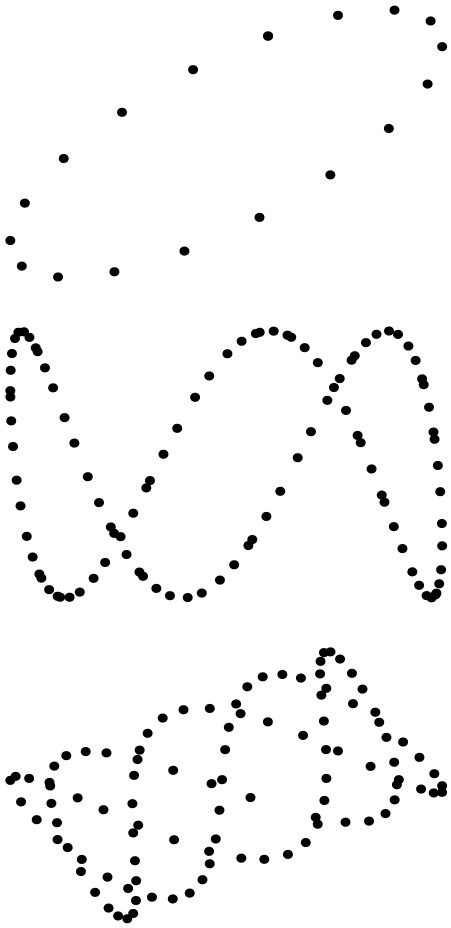

Figure 2.3: Hit points at a mirror of a ray in a cavity with degeneracy. The cavity has no astigmatism (above), simple astigmatism (middle) or general astigmatism (below). The cavity without astigmatism consists of two spherical mirrors with focal lengths $\simeq 1.08L$ and $\simeq 2.16L$. The cavity with simple astigmatism consists of two identical aligned astigmatic mirrors with focal lengths $\simeq 1.47L$ and $\simeq 2.94L$. The cavity with general astigmatism consists of two identical mirrors with focal lengths $\simeq 1.075L$ and $\simeq 2.15L$ which are rotated over an angle $\phi = \pi/3$ with respect to each other. In all cases the incoming ray is given by $r_0 = (1,\ 1.8,\ 3,\ 0.02)$.

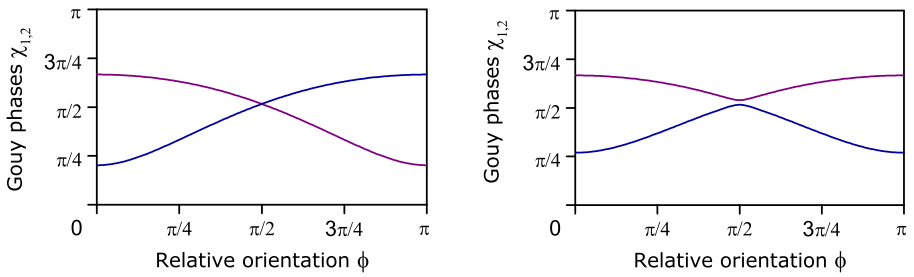

Figure 2.4: The dependence of the two Gouy phases on the relative orientation of two identical (left) and two slightly different (right) astigmatic mirrors. In the left window the mirrors are identical with focal lengths $f_\xi = L$ and $f_\eta = 10L$, with ξ and η indicating the principal axes of the mirrors. In the right figure the second mirror has focal lengths $f_\xi = L$ and $f_\eta = 4L$. Rotation angle $\phi = 0$ corresponds to the orientation for which the mirrors are aligned.

Since $M_{\rm rt}$ is real, when an eigenvalue λ_i is complex, the same is true for the eigenvector μ_i. Moreover, μ_i^* is an eigenvector of $M_{\rm rt}$ with eigenvalue λ_i^*. Provided that the matrix element $\mu_i^\dagger G \mu_i \neq 0$, the eigenvalue must then obey the relation $\lambda_i^* \lambda_i = 1$, so that the complex eigenvalue λ_i has absolute value 1. Just as in the case of one transverse dimension, stability requires that all eigenvalues have absolute value 1. Apart from accidental degeneracies, we conclude that a stable astigmatic cavity has two complex conjugate pairs of eigenvectors μ_1, μ_1^*, and μ_2, μ_2^* with eigenvalues λ_1, λ_1^*, and λ_2, λ_2^*, that can be written as

$$\lambda_1 = e^{i\chi_1} \qquad \text{and} \qquad \lambda_2 = e^{i\chi_2} \ . \tag{2.24}$$

Hence the eigenvalues now specify two different round-trip Gouy phases, and the complex eigenvectors obey the identities $\mu_1^{\rm T} G \mu_2 = 0$ and $\mu_1^\dagger G \mu_2 = 0$. On the other hand, the matrix elements $\mu_1^\dagger G \mu_1$ and $\mu_2^\dagger G \mu_2$ are usually nonzero. These matrix elements are purely imaginary, and without loss of generality we may assume that they are equal to the imaginary unit i times a positive real number. This can always be realized, when needed by interchanging μ_1 and μ_1^* (or μ_2 and μ_2^*), which is equivalent to a sign change of the matrix element. It is practical to normalize the eigenvectors, so that

$$\mu_1^\dagger G \mu_1 = \mu_2^\dagger G \mu_2 = 2i \ . \tag{2.25}$$

An arbitrary ray in the reference plane characterized by the real four-dimensional vector

$$\mathbf{z}_0 = \begin{pmatrix} \rho \\ \theta \end{pmatrix} \tag{2.26}$$

can be expanded in the four complex basis vectors as

$$\mathbf{z}_0 = 2\mathrm{Re}\left(a_1 \mu_1 + a_2 \mu_2\right) \ , \tag{2.27}$$

in terms of two complex coefficients a_1 and a_2. These coefficients can be obtained from a given ray vector r_0 by the identities

$$a_1 = \frac{\mu_1^\dagger G \, r_0}{2i} \qquad \text{and} \qquad a_2 = \frac{\mu_2^\dagger G \, r_0}{2i} \; . \tag{2.28}$$

This is obvious when one substitutes the expansion (2.27) in the right-hand sides of (2.28). After n round trips, the input ray (2.27) is transformed into the ray

$$r_n = M^n \, r_0 = 2\mathrm{Re}\left(a_1 \mu_1 e^{in\chi_1} + a_2 \mu_2 e^{in\chi_2}\right) \; . \tag{2.29}$$

This is a linear superposition of two oscillating terms that pick up a phase χ_1 and χ_2 respectively after each passage of the reference plane. When the two Gouy phases are rational fractions of 2π with a common denominator N, the ray path will be closed after N round trips. Then the cavity can be called degenerate. In this case the hit points of the ray on the mirrors (or in any transverse plane) lie on a well-defined closed curve. For a cavity that has no astigmatism this curve is an ellipse [12]. The transverse position and the propagation direction of the incoming ray determine the shape of the ellipse. In special (degenerate) cases it can reduce into a straight line or a circle. In case of a degenerate cavity with simple astigmatism the hit points lie on Lissajous curves [40, 41]. The ratio of the Gouy phases is equal to the ratio of the numbers of extrema of the curve in the two directions, while the incoming ray and the actual values of the Gouy phases determine its specific shape. The presence of general astigmatism gives rise to skew Lissajous curves, which are Lissajous curves in non-orthogonal coordinates. These properties are illustrated in figure 2.3.

The two round-trip Gouy phases of a cavity with two astigmatic mirrors depend on the relative orientation of the mirrors ϕ. When the cavity consists of two identical mirrors that are in parallel alignment, i.e., $\phi = 0$, it has simple astigmatism and the plane halfway between the mirrors is the focal plane for both components. Simple astigmatism also occurs for the anti-aligned configuration $\phi = \pi/2$, when the axis with the larger curvature of one mirror and the axis with the smaller curvature of the other one lie in a single plane through the optical axis. In this case both components necessarily have the same Gouy phase, and their foci lie symmetrically placed on opposite sides of the transverse plane halfway between the mirrors. The two Gouy phases attain extreme values for the aligned and the anti-aligned configuration. For intermediate orientations the cavity has general astigmatism, with Gouy phases varying between these extreme values. A crossing occurs in the anti-aligned geometry. The crossing is avoided when the mirrors are slightly different. The behavior of the Gouy phases as a function of the relative orientation ϕ is sketched in figure 2.4.

2.3 Paraxial wave optics

We describe the spatial structure of the modes in an astigmatic cavity in the same lens-guide picture that we used for the rays. The longitudinal coordinate in the lens guide is indicated by z, and $\rho = (x, y)^{\mathrm{T}}$ denotes the two-dimensional transverse position. A monochromatic

beam of light with uniform polarization in the paraxial approximation is characterized by the expression

$$\mathbf{E}(\mathbf{r}, t) = \mathrm{Re}\left\{E_0 \epsilon u(\rho, z) e^{ikz - i\omega t}\right\} \tag{2.30}$$

for the transverse part of the electric field. It contains a carrier wave with wave number k and frequency $\omega = ck$, a normalized complex polarization vector ϵ and an amplitude E_0. The magnetic field is given by the analogous expression

$$\mathbf{B}(\mathbf{r}, t) = \frac{1}{c}\mathrm{Re}\left\{E_0(\mathbf{e}_z \times \epsilon) u(\rho, z) e^{ikz - i\omega t}\right\} , \tag{2.31}$$

where $\mathbf{e}_z$ is a unit vector along the propagation direction z. The transverse spatial structure of the beam for each transverse plane is determined by the normalized profile $u(\rho, z)$. During propagation in free space, the z dependence of the profile is governed by the paraxial wave equation

$$\left(\nabla_\rho^2 + 2ik\frac{\partial}{\partial z}\right) u(\rho, z) = 0 . \tag{2.32}$$

In a region of free propagation, the transverse profile $u(\rho, z)$ varies negligibly with z over a wavelength. On the other hand, u changes abruptly at the position of a thin lens. The effect of an astigmatic lens is given by the input-output relation for the beam profile [27]

$$u_{\mathrm{out}}(\rho) = \exp\left(-\frac{ik\rho^{\mathrm{T}}\mathsf{F}^{-1}\rho}{2}\right) u_{\mathrm{in}}(\rho) , \tag{2.33}$$

where the real symmetric matrix F specifies the orientation and the focal lengths of the lens. Again, an astigmatic lens in the lens guide models an equivalent astigmatic mirror in the cavity.

The paraxial wave equation (2.32) has the form of the Schrödinger equation for a free particle in two dimensions, where the longitudinal coordinate z plays the role of time. This analogy suggest to adopt the Dirac notation of quantum mechanics to describe the dynamics of classical light fields [42]. The beam profile is analogous to the particle wave function and we associate a profile state vector $|u(z)\rangle$ to it, so that

$$u(\rho, z) = \langle \rho | u(z) \rangle , \tag{2.34}$$

where $|\rho\rangle$ is an eigenstate of the transverse position operator $\hat{\rho} = (\hat{x}, \hat{y})^{\mathrm{T}}$. The canonically conjugate momentum operator is given by $k\hat{\theta} = -i\,(\partial/\partial x, \partial/\partial y)^{\mathrm{T}}$. The average (or expectation) value of this operator corresponds to the transverse momentum per photon in units of $\hbar$ [43]. The longitudinal momentum per photon equals $\hbar k$ and it follows that the operator $\hat{\theta}$ represents the ratio of the transverse and longitudinal momentum. Therefore, it corresponds to the local propagation direction in a beam and is the wave-optical analogue of the propagation direction θ of a ray. The components of $\hat{\rho}$ and $\hat{\theta}$ satisfy the canonical commutation relations

$$[\hat{x}, \hat{\vartheta}_x] = [\hat{y}, \hat{\vartheta}_y] = i\lambda\!\!\!^{-} , \tag{2.35}$$

where $\lambda\!\!\!^{-} = 1/k$. The effect of free propagation and of astigmatic lenses can be represented by unitary operators acting on the state vectors $|u\rangle$ in the Hilbert space of transverse modes. The paraxial wave equation (2.32) can be represented in operator notation as

$$\frac{d}{dz}|u(z)\rangle = -\frac{ik}{2}\hat{\theta}^2|u(z)\rangle \ . \tag{2.36}$$

Hence free propagation over a distance z has the effect

$$|u(z_0 + z)\rangle = \hat{U}_\mathrm{f}(z)|u(z_0)\rangle \tag{2.37}$$

with

$$\hat{U}_\mathrm{f}(z) = \exp\left(-\frac{ikz}{2}\hat{\theta}^2\right) , \tag{2.38}$$

while the effect of an astigmatic lens can be expressed as

$$|u_\mathrm{out}\rangle = \hat{U}_\mathrm{l}(\mathsf{F})|u_\mathrm{in}\rangle \tag{2.39}$$

with

$$\hat{U}_\mathrm{l}(\mathsf{F}) = \exp\left(-\frac{ik\hat{\rho}^\mathrm{T}\mathsf{F}^{-1}\hat{\rho}}{2}\right) . \tag{2.40}$$

The unitary transformation of an optical system can be constructed by multiplying the operators representing the elements in the proper order. Therefore, the unitary transformation describing a single round trip through the astigmatic cavity can be written as

$$\hat{U}_\mathrm{rt} = \hat{U}_\mathrm{l}(\mathsf{F}_1)\hat{U}_\mathrm{f}(L)\hat{U}_\mathrm{l}(\mathsf{F}_2)\hat{U}_\mathrm{f}(L) \ , \tag{2.41}$$

where the reference plane is the same as sketched in figure 2.2. It is clear that other unitary round-trip operators can be constructed for different reference planes. For different choices the operators are related by unitary transformations.

The variation of the position $\rho(z)$ and the direction $\theta(z)$ of a ray during propagation must be reproduced by the variation of the average value of $\hat{\rho}$ and $\hat{\theta}$ over the beam profile. Since the variation of this profile during propagation is governed by the evolution operator $\hat{U}(z)$, the propagation of a ray in geometric optics should be reproduced by the expectation value of $\hat{U}^\dagger\hat{\rho}\hat{U}$ and $\hat{U}^\dagger\hat{\theta}\hat{U}$, in analogy to the Heisenberg picture of quantum mechanics. Therefore, the wave-optical propagation operator $\hat{U}$ and the ray matrix M must be related by

$$\hat{U}^\dagger\begin{pmatrix}\hat{\rho}\\ \hat{\theta}\end{pmatrix}U = M\begin{pmatrix}\hat{\rho}\\ \hat{\theta}\end{pmatrix} . \tag{2.42}$$

One may check explicitly that this relation holds in the case of free propagation (described by $\hat{U}_\mathrm{f}$ and M_f) and for astigmatic lenses (described by $\hat{U}_\mathrm{l}$ and M_l). From this one verifies that the relation (2.42) must hold generally for any optical system that is composed of regions of free propagation, interrupted by astigmatic lenses (or mirrors).

It is noteworthy that the general property (2.20) of transfer matrices M can be reproduced by using this relation (2.42), combined with the fact that the Heisenberg-transformed operators $\hat{U}^\dagger\hat{\rho}\hat{U}$ and $\hat{U}^\dagger\hat{\theta}\hat{U}$ obey the canonical commutation rules (2.35).

2.4 Operator description of Gaussian modes

A characteristic of the paraxial wave equation is that a transverse beam profile with a Gaussian shape retains its Gaussian structure under propagation through free space. The same is true when the beam passes a thin lens (or a mirror) as described by the transformation of equation (2.40). The Gaussian shape is the general structure of a fundamental paraxial mode. The standard set of higher-order modes have the form of the same complex Gaussian multiplied by a Hermite polynomial in each of the transverse coordinates [12]. This provides the basis of Hermite-Gaussian modes, which can be rearranged to yield the basis of Laguerre-Gaussian modes. There is a clear similarity between these bases of paraxial optical modes and the stationary states of the isotropic quantum-mechanical harmonic oscillator in two dimensions. In analogy to the algebraic description of the harmonic oscillator, isotropic paraxial optical modes of different order can be connected by bosonic ladder operators [33]. In reference [17], it has been shown that the algebraic description of freely propagating paraxial modes can be generalized to account for general astigmatism.

Here, we show that the complete set of modes of a geometrically stable two-mirror cavity can be obtained from two pairs of bosonic ladder operators. These ladder operators are linear combinations of the position operator $\hat{\rho}$ and the propagation-direction operator $\hat{\theta}$ and can be expressed in terms of the eigenvectors of the round-trip ray matrix M_{rt}.

2.4.1 Gaussian modes in one transverse dimension

For simplicity, we first consider a single period of the lens guide that represents the cavity described in section 2.2, with one transverse dimension. In this case, the higher-order modes are obtained by repeated application of a raising operator $\hat{a}^{\dagger}$, acting on the fundamental mode. The raising operator is the Hermitian conjugate of the lowering operator, which can be expressed as

$$\hat{a}(z) = \sqrt{\frac{k}{2}}\left(r\hat{\vartheta} - t\hat{x}\right) , \tag{2.43}$$

where k is the wave number, and the z dependence of the ladder operators is determined only by the variation of the complex parameters r and t as a function of the longitudinal coordinate z. These parameters also determine the z dependent profile of the fundamental mode

$$u_0(x,z) = \left(\frac{k}{r^2\pi}\right)^{1/4} \exp\left(\frac{iktx^2}{2r}\right) \equiv \left(\frac{k}{r^2\pi}\right)^{1/4} \exp\left(-\frac{ksx^2}{2}\right) , \tag{2.44}$$

where $s = -it/r$. The parameters r, t and s have been defined such that they have a purely geometric significance, in that they are fully determined by the geometric properties of the cavity, the length L, and the focal lengths $f_{1,2}$, independent of k. They determine the transverse beam width and the radius of curvature of the wave front according to $w = \sqrt{2/(ks_{\mathrm{r}})}$ and $R = 1/s_{\mathrm{i}}$, where s_{r} and s_{i} are respectively the real and imaginary parts of s.

For each value of z, the ladder operators $\hat{a}$ and $\hat{a}^\dagger$ must obey the bosonic commutation rule

$$[\hat{a}(z), \hat{a}^\dagger(z)] = 1 \,, \tag{2.45}$$

which requires that r and t obey the normalization identity

$$r^* t - t^* r = 2i \,. \tag{2.46}$$

With this condition, the fundamental mode profile (2.44) is normalized, in the sense that $\int dx |u(x,z)|^2 = 1$ for all values of z. Moreover, the lowering operator (2.43) gives zero when acting on the fundamental mode (2.44), so that $\hat{a}(z)|u_0(z)\rangle = 0$.

The z dependent propagation operator $\hat{U}(z)$ is defined to transform the beam profile in the reference plane at $z = 0$ of the lens guide into the profile in another transverse plane at position z. Then $|u(z)\rangle = \hat{U}(z)|u(0)\rangle$ describes a light beam propagating through the optical system. This means that in the regions of free propagation between the lenses, $|u(z)\rangle$ solves the paraxial wave equation (2.32), while it picks up the appropriate phase factor when passing through a lens. The z dependence of the parameters r and t must be chosen in such a way that the ladder operators $\hat{a}(z)$ and $\hat{a}^\dagger(z)$ acting on a z dependent mode $|u(z)\rangle$ create another mode that solves the wave equation. This condition can be summarized as

$$\hat{a}(z)|u(z)\rangle = \hat{U}(z)\hat{a}(0)|u(0)\rangle \,, \tag{2.47}$$

which, in view of the unitarity of the propagation operator, is equivalent to the operator identity

$$\hat{a}(z) = \hat{U}(z)\hat{a}(0)\hat{U}^\dagger(z) \,. \tag{2.48}$$

When this is the case, a complete orthogonal set of higher-order modes is obtained in terms of the raising operator and the fundamental mode, in the well-known form

$$|u_n(z)\rangle = \frac{1}{\sqrt{n!}}\left(\hat{a}^\dagger(z)\right)^n |u_0(z)\rangle \,. \tag{2.49}$$

In reference [33], it has been shown that the transformation (2.48) of the lowering operator (2.43) under free propagation, as described by the transformation in equation (2.38), implies that the parameter t is constant in a region of free propagation, while r has the derivative $dr/dz = t$. Upon passage through a lens with focal length f, as described by the transformation in equation (2.40), r does not change, whereas t modifies according to the relation $t_{\text{out}} = t_{\text{in}} - r/f$. This z dependence of the parameters can be summarized by the statement that the transformation of the two-dimensional vector $(r,t)^{\mathrm{T}}$ during propagation is identical to the transformation of a ray $(x,\vartheta)^{\mathrm{T}}$. This transformation is described by the ray matrix $M(z)$ that corresponds to $\hat{U}(z)$ in accordance with equation (2.42), so that

$$\begin{pmatrix} r(z) \\ t(z) \end{pmatrix} = M(z) \begin{pmatrix} r(0) \\ t(0) \end{pmatrix} \,. \tag{2.50}$$

Now it is straightforward to obtain the modes and the eigenfrequencies of the cavity. The condition for a mode is that the mode profile $u(x, z)$ reproduces after a round trip, up to a phase factor. This is accomplished when the two-dimensional vector $(r(0), t(0))^{\mathrm{T}} = \mu$ is an eigenvector of the round-trip ray matrix $M_{\mathrm{rt}} = M(2L)$, after proper normalization of μ to ensure that r and t obey the identity (2.46). (In the case that $r^*t - t^*r$ turns out to be a negative imaginary number, we just take the other eigenvector μ^* instead of μ.) With this choice, the fundamental mode obeys the relation $|u_0(2L)\rangle = \exp(-i\chi/2)|u_0(0)\rangle$, and the lowering operator transforms after a round trip as $\hat{a}(2L) = \exp(i\chi)\hat{a}(0)$, with χ the round-trip Gouy phase. The n^{th}-order mode (2.49) then obeys the well-known relation

$$|u_n(2L)\rangle = e^{-i(n+1/2)\chi}|u_n(0)\rangle \,. \tag{2.51}$$

As indicated in equation (2.30), the complex electric field, which should reproduce exactly after a round trip, is proportional to $u_n(x, z)\exp(ikz)$, so that the resonance condition reads

$$2kL - \left(n + \frac{1}{2}\right)\chi = 2\pi q \,, \tag{2.52}$$

where $q \in \mathbb{Z}$ plays the role of the longitudinal mode number. This relation defines the frequencies of the cavity modes $\omega = ck$.

In conclusion, we have shown that the cavity modes are determined by the values of the parameters r and t, such that in the reference plane the vector $(r(0), t(0))^{\mathrm{T}}$ is equal to the normalized eigenvector μ of the round-trip ray matrix M_{rt}. The z dependence of the parameters $r(z)$ and $t(z)$ is governed by the ray matrix that connects the reference plane $z = 0$ in the lens guide to another transverse plane z. This is equivalent to the statement that the vector $(r(z), t(z))^{\mathrm{T}}$ coincides with the eigenvector of the ray matrix for a round trip starting in the transverse plane z. Different modes of the cavity take a different form and have different wave numbers k, but they are all characterized by the same complex parameters r and t.

Before turning to the case of two transverse dimensions, it is illuminating to relate the z dependence of the ladder operators to their structure in terms of the matrix G. In the present case of one transverse dimension, this matrix as defined in (2.21) is two-dimensional, just as the vectors $(r, t)^{\mathrm{T}}$ and $(x, \vartheta)^{\mathrm{T}}$. Then the property (2.20) of M_{rt} is just equivalent to the statement that $\det M_{\mathrm{rt}} = 1$. Also for a single transverse dimension the ray matrix M_{rt} is linked to the propagation operator $\hat{U}_{\mathrm{rt}}$ by the identity (2.42). We can rewrite the expression (2.43) for the lowering operator as

$$\hat{a}(z) = \sqrt{\frac{k}{2}}(r(z), t(z))G\begin{pmatrix} \hat{x} \\ \hat{\vartheta} \end{pmatrix} \,. \tag{2.53}$$

When we substitute this expression in the transformation rule (2.47) for $\hat{a}$, while using the two-dimensional version of the relation (2.42), we obtain

$$\hat{a}(z) = \sqrt{\frac{k}{2}}(r(0), t(0))M^{\mathrm{T}}(z)G\begin{pmatrix} \hat{x} \\ \hat{\vartheta} \end{pmatrix} \,, \tag{2.54}$$

where we used the identity (2.20) in the form $GM^{-1} = M^{\mathrm{T}}G$. The equivalence of (2.53) and (2.54) is in obvious accordance with the identity (2.50).

2.4.2 Astigmatic Gaussian modes

The formulation that we have given for the modes in one transverse dimension allows a direct generalization to two transverse dimensions. In that case we must have two lowering operators rather than one. Since these operators must return to their initial form after a full round trip, they must be determined by the eigenvectors of the round-trip ray matrix M_{rt}. In analogy to the expression (2.53), we introduce the two z dependent lowering operators

$$\hat{a}_i(z) = \sqrt{\frac{k}{2}}\mu_i^{\mathrm{T}} M^{\mathrm{T}}(z) G \begin{pmatrix} \hat{\rho} \\ \hat{\theta} \end{pmatrix} , \tag{2.55}$$

in terms of the two eigenvectors μ_i of M_{rt} with $i = 1, 2$. By the same argument as given for equation (2.54), these operators obey the transformation rule (2.48), and in the reference plane at $z = 0$ they are given by

$$\hat{a}_i(0) = \sqrt{\frac{k}{2}}\mu_i^{\mathrm{T}} G \begin{pmatrix} \hat{\rho} \\ \hat{\theta} \end{pmatrix} . \tag{2.56}$$

Over a full round trip, they transform as

$$\hat{a}_i(2L) = e^{i\chi_i}\hat{a}_i(0) , \tag{2.57}$$

in terms of the eigenvalues (2.24) corresponding to μ_i. By using the identities (2.25), one verifies that the ladder operators obey the commutation rules

$$[\hat{a}_i(z), \hat{a}_i^{\dagger}(z)] = 1 . \tag{2.58}$$

By using the identities $\mu_1^{\dagger} G \mu_2 = \mu_1^{\mathrm{T}} G \mu_2 = 0$, we find that other commutators vanish, so that $[\hat{a}_2, \hat{a}_1^{\dagger}] = [\hat{a}_2, \hat{a}_1] = 0$. For notational convenience we combine the two lowering operators into a vector of operators

$$\hat{A} = \begin{pmatrix} \hat{a}_1 \\ \hat{a}_2 \end{pmatrix} , \tag{2.59}$$

for all values of z. In analogy to equation (2.43), this can be written as

$$\hat{A} = \sqrt{\frac{k}{2}} \left(\mathsf{R}^{\mathrm{T}}\hat{\theta} - \mathsf{T}^{\mathrm{T}}\hat{\rho} \right) , \tag{2.60}$$

where now R and T are z dependent 2×2 matrices. Comparison with equation (2.55) shows that in the reference plane $z = 0$ the two matrices $\mathsf{R}^{\mathrm{T}}(0)$ and $\mathsf{T}^{\mathrm{T}}(0)$ can be combined into a single 2×4 matrix, where the two rows coincide with the transposed eigenvectors μ_i^{T}. This gives the formal identification

$$\begin{pmatrix} \mathsf{R}(0) \\ \mathsf{T}(0) \end{pmatrix} = (\mu_1 \; \mu_2) . \tag{2.61}$$

Equation (2.60) then shows that the z dependence of R and T can formally be expressed as

$$\begin{pmatrix} \mathsf{R}(z) \\ \mathsf{T}(z) \end{pmatrix} = M(z) \begin{pmatrix} \mathsf{R}(0) \\ \mathsf{T}(0) \end{pmatrix} , \tag{2.62}$$

where in the right-hand side a 4×4 matrix multiplies a 4×2 matrix, producing a 4×2 matrix. The behavior of M as a function of z is fully determined by the expressions (2.17) and (2.18) for free propagation and at passage of a lens. It follows that during free propagation, T is constant, while R obeys the differential equation $d\mathsf{R}/dz = \mathsf{T}$. At passage through a lens with focal matrix F, R does not change, whereas the change in T is given by

$$\mathsf{T}_{\text{out}} = \mathsf{T}_{\text{in}} - \mathsf{F}^{-1}\mathsf{R} . \tag{2.63}$$

The fundamental mode $|u_{00}(z)\rangle$ in the astigmatic cavity is defined by the requirement that it obeys the paraxial wave equation, and that it gives zero when acted on with the lowering operators $\hat{a}_i$. It is easy to check that these conditions are obeyed by the normalized mode function

$$u_{00}(\rho, z) = \sqrt{\frac{k}{\pi \det \mathsf{R}}} \exp\left(\frac{ik\rho^{\mathrm{T}}\mathsf{T}\mathsf{R}^{-1}\rho}{2}\right) \equiv \sqrt{\frac{k}{\pi \det \mathsf{R}}} \exp\left(-\frac{k\rho^{\mathrm{T}}\mathsf{S}\rho}{2}\right) \tag{2.64}$$

in terms of the z dependent matrices R and T. The matrix $\mathsf{S} = -i\mathsf{T}\mathsf{R}^{-1}$ is symmetric and its real part S_{r} is positive definite, as can be checked by using the properties of the eigenvectors μ_i derived in section 2.2. Because of the definitions of R and T in terms of the eigenvectors of the round-trip ray matrix M_{rt}, the fundamental mode returns to itself after a round trip, as expressed by

$$|u_{00}(2L)\rangle = e^{-i(\chi_1+\chi_2)/2}|u_{00}(0)\rangle . \tag{2.65}$$

Higher-order modes are defined by repeated application of the raising operators, which gives

$$|u_{nm}(z)\rangle = \frac{1}{\sqrt{n!m!}} \left(\hat{a}_1^\dagger(z)\right)^n \left(\hat{a}_2^\dagger(z)\right)^m |u_{00}(z)\rangle . \tag{2.66}$$

The set of modes functions $|u_{nm}(z)\rangle$ is complete and orthonormal in each transverse plane. Because of the round-trip properties (2.57) of the ladder operators, the modes transform over a round trip as

$$|u_{nm}(2L)\rangle = e^{-i(n+1/2)\chi_1 - i(m+1/2)\chi_2}|u_{nm}(0)\rangle . \tag{2.67}$$

The requirement that the electric field of a mode, which is proportional to $u_{nm}(\rho, z)\exp(ikz)$, picks up a phase that is a multiple of 2π, gives the resonance condition for the wave number

$$2kL - \left(n + \frac{1}{2}\right)\chi_1 - \left(m + \frac{1}{2}\right)\chi_2 = 2\pi q , \tag{2.68}$$

so that the frequency of the mode specified by the transverse mode numbers n and m, and the longitudinal mode number q is

$$\omega = \frac{c}{2L}\left\{2\pi q + \left(n + \frac{1}{2}\right)\chi_1 + \left(m + \frac{1}{2}\right)\chi_2\right\} . \tag{2.69}$$

Apparently, the general astigmatism does not show up in the frequency spectrum of the cavity. All that can be seen is the presence of two different round-trip Gouy phases. There are two different ways in which the corresponding frequency spectrum can be degenerate. For a cavity that has cylinder symmetry the two eigenvalue spectrum of the ray matrix is degenerate (i.e., $\chi_1 = \chi_2$) and its modes are frequency degenerate in the total mode number $n + m$. As a result any linear combination of modes with the same total mode number is a mode too. The second kind of degeneracy arises when one of the Gouy phases is a rational fraction of 2π. Then the combs of modes at different values of q overlap so that many different modes appear at the same frequency.

2.5 Physical properties of the cavity modes

2.5.1 Symmetry properties

So far we have described the modes as a periodic solution of the paraxial equation in the lens guide that is equivalent to the cavity. The electric and magnetic field in the cavity are obtained by refolding the periodic lens-guide fields (2.30) and (2.31). The fields in two successive intervals with length L in the lens guide then give the fields propagating back and forth inside the cavity. The electric field (2.30) in the lens guide then gives the expression for the field in the cavity

$$\mathbf{E}_{\text{cavity}}(\mathbf{r}, t) = \text{Re}\left\{E_0 \epsilon f(\rho, z) i e^{-i\omega t}\right\} \tag{2.70}$$

for $0 < z < L$, with

$$f(\rho, z) = \frac{1}{i}\left\{u(\rho, z)e^{ikz} - u(\rho, -z)e^{-ikz}\right\} . \tag{2.71}$$

The minus sign in (2.71) ensures that the mirror surfaces coincide with a nodal plane. This follows from the relation (2.63) between the input and the output of a lens. Applied to the lens at $z = 0$, this shows that in the lens guide the transverse profile $u(\rho, 0^{\pm})$ just left and right of lens 1 can be written as

$$u(\rho, 0^{\pm}) = u_1(\rho) \exp\left(\mp \frac{ik\rho^{\mathrm{T}} \mathsf{F}_1^{-1} \rho}{4}\right) , \tag{2.72}$$

where u_1 may be viewed as the transverse profile halfway lens 1. Substitution in equation (2.71) shows that the cavity field f near mirror 1 is given by $2u_1(\rho) \sin\left(kz - k\rho^{\mathrm{T}} \mathsf{F}_1^{-1} \rho/4\right)$. Since the value of k obeys the resonance condition (2.68), which makes $u(\rho, z) \exp(ikz)$ periodic, a similar argument holds for mirror 2. When $u_2(\rho)$ is defined as the periodic lens-guide field $u(\rho, z) \exp(ikz)$ at the plane halfway lens 2, the cavity field f near mirror 2 (where $z \approx L$) is $2u_2(\rho) \sin\left(k(z - L + k\rho^{\mathrm{T}} \mathsf{F}_2^{-1} \rho/4)\right)$.

The corresponding expression for the magnetic field in the cavity is

$$\mathbf{B}_{\text{cavity}}(\mathbf{r}, t) = \text{Re}\left\{E_0(\mathbf{e}_z \times \epsilon) b(\rho, z) e^{-i\omega t}\right\} , \tag{2.73}$$

with

$$b(\rho, z) = \frac{1}{c}\left\{u(\rho, z)e^{ikz} + u(\rho, -z)e^{-ikz}\right\} , \tag{2.74}$$

for $0 < z < L$. The expression (2.74) for the magnetic field has a plus sign, arising from the fact that the propagation direction $\mathbf{e}_z$ in (2.31) is replaced by $-\mathbf{e}_z$ for the field component propagating in the negative direction. Near mirror 1, the magnetic field function b is given by $2u_1(\rho)\cos\left(kz - k\rho^{\mathrm{T}}\mathsf{F}_1^{-1}\rho/4\right)/c$, while near mirror 2 we find $b(\rho, z) = 2u_2(\rho)\cos\left(k(z - L + k\rho^{\mathrm{T}}\mathsf{F}_2^{-1}\rho/4)\right)/c$.

The paraxial field in the cavity as described here arises from refolding a periodic field in the lens guide that propagates in the positive direction. We could just as well start from a lens guide field propagating in the negative z direction. Such a field is obtained by replacing $u(\rho, z)\exp(ikz)$ by its complex conjugate in equation (2.30). This leads to an alternative expression for the cavity field in the form (2.70) with f given by $[u^*(\rho, z)\exp(-ikz) - u^*(\rho, -z)\exp(ikz)]/i$. For a non-degenerate mode, this alternative expression for f must be proportional to the expression (2.71). This leads to the symmetry relation

$$u(\rho, -z) = u^*(\rho, z) , \tag{2.75}$$

apart from an overall phase factor. This shows that the mode functions $f(\rho, z)$ and $b(\rho, z)$ are real, so that they can be expressed as

$$f(\rho, z) = 2\,\mathrm{Im}\left\{u(\rho, z)e^{ikz}\right\} \qquad \text{and} \qquad b(\rho, z) = \frac{2}{c}\,\mathrm{Re}\left\{u(\rho, z)e^{ikz}\right\} . \tag{2.76}$$

From equations (2.70) and (2.73) we find that in a non-degenerate paraxial mode of a two-mirror cavity the electric and the magnetic field can be written as

$$\mathbf{E}_{\mathrm{cavity}}(\mathbf{r}, t) = -f(\rho, z)\mathrm{Im}\left\{E_0\epsilon e^{-i\omega t}\right\} \tag{2.77}$$

and

$$\mathbf{B}_{\mathrm{cavity}}(\mathbf{r}, t) = b(\rho, z)\mathrm{Re}\left\{E_0(\mathbf{e}_z \times \epsilon)e^{-i\omega t}\right\} , \tag{2.78}$$

which are products of a real function of position and a real function of time. Both fields take the form of a standing wave, with phase difference $\pi/2$. The curved transverse nodal planes of the electric field are determined by the requirement that $u(\rho, z)\exp(ikz)$ is real. These nodal planes coincide with the antinodal planes of the magnetic field.

2.5.2 Shape of the modes

It is interesting to notice that the real and the imaginary part of the complex propagating field in the lens guide correspond to the electric and magnetic field in the cavity, as given by the expression

$$u(\rho, z)e^{ikz} = cb(\rho, z) + if(\rho, z) . \tag{2.79}$$

This shows that the nodal planes of the electric or the magnetic field in the cavity are wavefronts of the traveling wave in the lens guide.

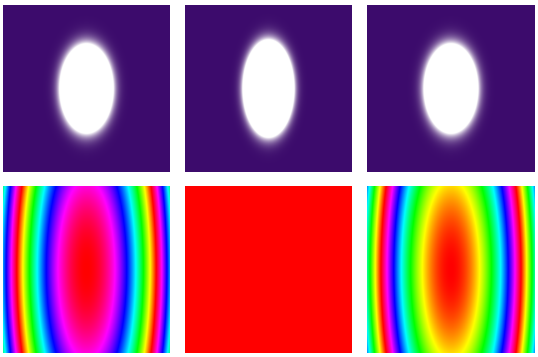

Figure 2.5: Intensity (top) and false-color phase (bottom) patterns of the fundamental mode of a lens guide with simple astigmatism. The corresponding cavity consists of two identical astigmatic mirrors with focal lengths $f_\xi = L$ and $f_\eta = 10L$, where L is the mirror separation. The ξ and η directions of the mirrors are aligned along the horizontal and vertical directions. From left to right the plots show the mode structure close to mirror 1, in the transverse plane in between the mirrors and close to mirror 2. The color code used to plot the phase patterns is periodic; from 0 to 2π the color changes in a continuous fashion from red via yellow, green, blue and purple back to red.

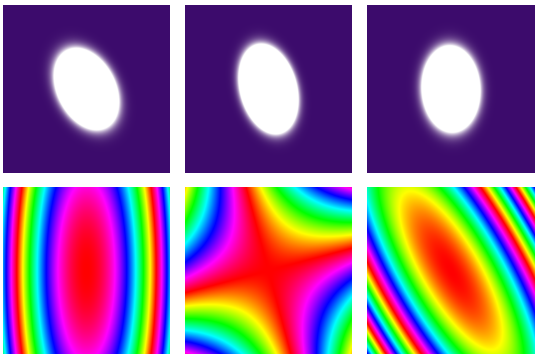

Figure 2.6: Intensity (top) and false-color phase (bottom) patterns of the fundamental mode of a lens guide with general astigmatism. The corresponding cavity consists of two identical astigmatic mirrors with focal lengths $f_\xi = L$ and $f_\eta = 10L$, where L is the mirror separation. Compared to the plots in figure 2.5, the right mirror is rotated over $\pi/6$ in the positive (counterclockwise) direction. From left to right the plots show the mode structure close to mirror 1, in the transverse plane in between the mirrors and close to mirror 2. The color code used to plot the phase patterns is periodic; from 0 to 2π the color changes in a continuous fashion from red via yellow, green, blue and purple back to red.

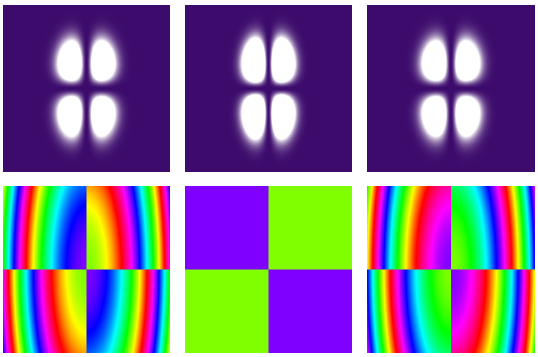

Figure 2.7: Intensity (top) and false-color phase (bottom) patterns of the (1, 1) mode of a lens guide with simple astigmatism. The corresponding cavity consists of two identical astigmatic mirrors with focal lengths $f_\xi = L$ and $f_\eta = 10L$, where L is the mirror separation. The ξ and η directions of the mirrors are aligned along the horizontal and vertical directions. From left to right the plots show the mode structure close to mirror 1, in the transverse plane in between the mirrors and close to mirror 2. The color code used to plot the phase patterns is periodic; from 0 to 2π the color changes in a continuous fashion from red via yellow, green, blue and purple back to red.

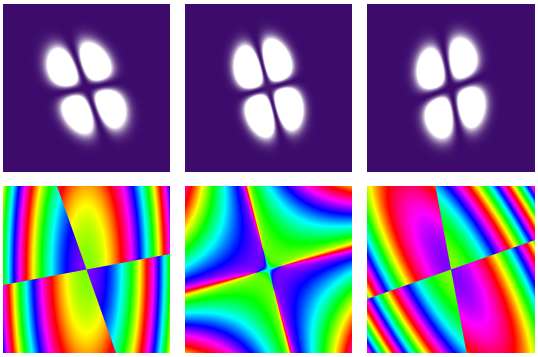

Figure 2.8: Intensity (top) and false-color phase (bottom) patterns of the (1, 1) mode of a lens guide with general astigmatism. The corresponding cavity consists of two identical astigmatic mirrors with focal lengths $f_\xi = L$ and $f_\eta = 10L$, where L is the mirror separation. Compared to the plots in figure 2.7, the right mirror is rotated over $\pi/6$ in the positive (counterclockwise) direction. From left to right the plots show the mode structure close to mirror 1, in the transverse plane in between the mirrors and close to mirror 2. The color code used to plot the phase patterns is periodic; from 0 to 2π the color changes in a continuous fashion from red via yellow, green, blue and purple back to red.

From the symmetry property (2.75) it follows that the periodic lens-guide field $u(\rho, z)\exp(ikz)$ is real in the transverse plane halfway each of the lenses. Since this conclusion holds for modes of all orders, also the ladder operators $\hat{a}_i$ can be chosen real in these two symmetry planes. As a result, the higher-order modes have the nature of astigmatic Hermite-Gaussian modes, with a pattern of two sets of parallel straight nodal lines. However, nodal lines in these two sets are not orthogonal in the case of a twisted cavity.

In the free space between the mirrors of a twisted cavity the modes attain a structure with vortices, arising from an elliptical rather than a linear nature of the distribution of transverse momentum. Only in the special case of simple astigmatism, the modes have a Hermite-Gaussian structure in all transverse planes, with rectangular patterns of nodal lines that are aligned to the axes of the two mirrors.

2.5.3 Orbital angular momentum

As a result of the twisted boundary conditions that are imposed by two astigmatic mirrors in non-parallel alignment, the cavity modes become twisted as well. Both the elliptical intensity distribution of the fundamental cavity mode as well as its elliptical or hyperbolic curves of constant phase change their orientation under propagation from one mirror to the other. This tumbling gives rise to orbital angular momentum in the cavity modes [17]. In the higher-order modes both the general astigmatism and the vortices, which appear in intermediate transverse planes, contribute to the orbital angular momentum [16].

The leading-order contribution to the orbital angular momentum per unit length in a monochromatic paraxial beam, as characterized by equations (2.30) and (2.31), is longitudinal. Its z component can be expressed as [43, 6]

$$\mathcal{L} = \frac{\epsilon_0|E_0|^2}{2i\omega}\int d_2\rho\; u^*(\rho,z,t)\left(x\frac{\partial}{\partial y} - y\frac{\partial}{\partial x}\right)u(\rho,z,t)\;. \tag{2.80}$$

In terms of the transverse position and momentum operators this can be rewritten as $N\hbar\langle u(z)|\hat{\rho}\times k\hat{\theta}|u(z)\rangle$, where $N = \epsilon_0|E_0|^2/(2\hbar\omega)$ is the number of photons per unit length and $\times$ denotes a cross product in the transverse plane. By the virtue of equation (2.60) and its hermitian conjugate, the canonical operators $\hat{\rho}$ and $\hat{\theta}$ can be expressed in terms of the ladder operators $\hat{A}$ and $\hat{A}^\dagger$. This leads to an expression for the orbital angular momentum in the (n,m) cavity mode in terms of the vectors $r_{1,2}(0)$ and $t_{1,2}(0)$. It can be cast in the following form

$$\begin{aligned}\mathcal{L}_{nm} = N\hbar\langle u_{nm}(z)|\hat{\rho}\times k\hat{\theta}|u_{nm}(z)\rangle = \\ N\hbar\left\{\left(n+\frac{1}{2}\right)\mathrm{Re}(r_1^*(0)\times t_1(0)) + \left(m+\frac{1}{2}\right)\mathrm{Re}(r_2^*(0)\times t_2(0))\right\}.\end{aligned} \tag{2.81}$$

This very natural expression of the orbital angular momentum clearly shows its origin in the geometry of the twisted cavity. In terms of the eigenvectors μ_1 and μ_2, it may be rewritten as

$$\mathcal{L}_{nm} = N\hbar\left\{\left(n+\frac{1}{2}\right)\frac{\mu_1^\dagger GJ\mu_1}{2} + \left(m+\frac{1}{2}\right)\frac{\mu_2^\dagger GJ\mu_2}{2}\right\}, \tag{2.82}$$

where

$$J = \begin{pmatrix} 0 & 1 & 0 & 0 \\ -1 & 0 & 0 & 0 \\ 0 & 0 & 0 & 1 \\ 0 & 0 & -1 & 0 \end{pmatrix} \tag{2.83}$$

is the generator of rotations of a ray (ρ, θ) in the transverse plane, i.e., $M_{\text{rot}}(\alpha) = e^{-\alpha J}$ is the ray matrix $\in Sp(4, \mathbb{R})$ that rotates both the transverse position and the propagation direction of a ray over an angle α. From the fact that the ray matrix for free propagation (2.17) commutes with J, it is clear that the orbital angular momentum in the cavity modes is conserved under free propagation from one mirror to the other. Since the lens-guide mode profiles close to the lenses are real apart from the curved wave fronts, which locally fit on the mirror surfaces, it follows that they are converted into their complex conjugates when passing a lens. As a result, the orbital angular momentum in the cavity mode changes sign when the beam passes a lens (mirror) so that there is no net orbital angular momentum in the cavity field as characterized by equations (2.70) and (2.73).

2.6 Examples

We illustrate the intensity and phase structure and the orbital angular momentum of twisted cavity modes by investigating a specific example. We consider a cavity that consists of two identical astigmatic mirrors with focal lengths $f_\xi = L$ and $f_\eta = 10L$, where L is the mirror separation. The cavity has simple astigmatism when the mirrors are in parallel (or anti-parallel) alignment whereas it has general astigmatism when they are non-aligned. It is geometrically stable for all (relative) orientations of the mirrors.

2.6.1 Mode structure

It is convenient to plot the intensity and phase patterns in the corresponding lens guide. In figures 2.5 and 2.6, we show the transverse intensity and phase patterns of the fundamental lens-guide mode both in the immediate neighborhood of the lenses (mirrors) and in the transverse plane between them. The plots in figure 2.5 correspond to the case in which the ξ and η directions of the mirrors are aligned along the horizontal and vertical directions. In this case, the cavity has transverse symmetry directions along the axes of the mirrors. The elliptical intensity patterns of the fundamental mode are aligned along these symmetry directions. Since the mirrors have different radii of curvature along their axes, the diffraction of the mode is (slightly) different for the two directions so that the ellipticity of the curves of constant intensity varies under propagation from one lens to the other. The phase patterns close to the mirrors confirm that the wave fronts of the lens-guide mode fit on the mirror surfaces. Since the cavity mirrors are identical, the lens guide has an additional inversion-symmetry plane in between the lenses (mirrors). As a result, this plane is the focal plane of the lens-guide modes

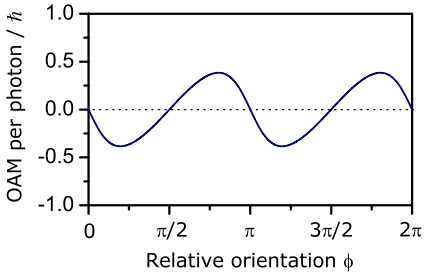

Figure 2.9: Orbital angular momentum in the $(1, 1)$ mode of a lens guide corresponding to a cavity with two identical astigmatic mirrors as a function of the relative orientation of the mirrors. The mirrors have focal lengths $f_\xi = L$ and $f_\eta = 10L$, where L is the mirror separation and $\phi = 0$ corresponds to the case in which the mirrors are aligned.

so that the wave fronts of the fundamental mode in the immediate neighborhood of this plane are flat.

The plots in figure 2.6 show the fundamental lens-guide mode in the case in which the right mirror is rotated over $\pi/6$ in the positive (counterclockwise) direction. This obviously introduces a twist in the mode. The wave fronts close to the lenses (mirrors) fit on the lenses (mirrors) while the orientation of the ellipses of constant intensity reflects their non-parallel alignment. As a result of the twist, the inversion symmetry in the transverse plane between the lenses is broken and the focal planes for the two transverse components do not coincide. In between the focal planes, the lines of constant phase are hyperbolas rather than ellipses.

As an example of a higher-order mode, we show the intensity and phase patterns of the $(1, 1)$ lens-guide mode. The plots in figure 2.7 show the intensity and phase patterns of the $(1, 1)$ mode in the case in which the mirrors are aligned. The mode is aligned along the mirror axes and, although propagation from one lens to the other does affect the scaling of the mode pattern along the symmetry axes, propagation does not affect its orientation. The mode takes the form of a Hermite-Gaussian in all transverse planes, which has two mutually perpendicular lines of zero intensity (line dislocations) in the transverse plane. Up to phase jumps of π, which are due to the dislocations, the phase structure in the immediate neighborhood of the lenses reflects the shape of the mirrors. The plots in figure 2.8 show how the phase and intensity patterns of the $(1, 1)$ mode change when the cavity is twisted. In this case, the intensity patterns close to the mirrors are not aligned along the mirror axes and the lines of zero intensity are no longer mutually perpendicular. The orientation of both the phase and the intensity patterns as well as the orientation of the line dislocations change upon propagation from one mirror to the other. Moreover, the mode is Hermite-Gaussian only in the immediate neighborhood of the lenses. In other transverse planes, it takes the form of a generalized Gaussian mode [44] and has elliptical vortices, rather than line dislocations, in the transverse plane. These are visible in the middle plots in figure 2.8.

2.6.2 Orbital angular momentum

The amount of orbital angular momentum in twisted cavity modes depends on the (relative) orientation of the mirrors. If the mirrors are in parallel or anti-parallel alignment, the cavity has simple astigmatism so that the orbital angular momentum vanishes. For intermediate orientations, the lens-guide modes do contain orbital angular momentum. A typical example of its dependence on the relative orientation of the mirrors is shown in figure 2.9. As was mentioned already, there is no net orbital angular momentum in the corresponding cavity field. The cavity mirrors invert the orbital angular momentum while reflecting the light, which implies that they experience a torque. This torque on mirror 2 amounts to $2c\mathcal{L}_{nm}$ while mirror 1 experiences the opposite torque. If the mirrors were allowed to rotate freely, the configurations with simple astigmatism (and therefore vanishing OAM) could either be stable or metastable. If $\mathcal{L}_{nm}$ goes through zero with a negative slope as a function of the orientation of mirror 2, the OAM of the modes gives rise to a torque that tends to restore the configuration. If $\mathcal{L}_{nm}$ goes through zero with a positive slope it is the other way around. The results shown in figure 2.9 indicate that the configuration that combines the largest and smallest radii of curvature is the stable one.

2.7 Discussion and conclusions

We have presented an algebraic method to obtain the complete and orthonormal set of paraxial modes of a geometrically stable two-mirror cavity with astigmatism. If the axes of the two mirrors are parallel, the modes take a factorized form and the problem of finding them is equivalent to the case of a single transverse dimension. In that case standard analytical techniques suffice to find expressions of the cavity modes. Finding expressions of the cavity modes is considerably more complex when the astigmatic mirror are non-parallel. In that case, the mode fields propagating between the mirrors display general astigmatism and no simple analytical approach is known to solve the problem of finding them.

An essential ingredient in our characterization of the cavity modes is the real 4×4 ray matrix M_{rt}, which is a purely geometric concept from ray optics and describes the transformation of a ray over one round trip through the cavity. We have argued that a cavity is geometrically stable only if the absolute values of all four eigenvalues of the round-trip ray matrix M_{rt} are equal to 1. Because of the special (group-theoretical) properties of the round-trip ray matrix, the requirement of geometric stability implies that both the eigenvectors and the corresponding eigenvalues form complex conjugate pairs. The arguments of the unitary eigenvalues play the role of round-trip Gouy phases χ_1 and χ_2 and determine the frequency spectrum according to equation (2.69). The spatial structure of the cavity modes is fully determined by the eigenvectors. They depend on the transverse reference plane that is taken as the start of a round trip. The eigenvalues are independent of the choice of the reference plane. As indicated in equation (2.61) and (2.62), the eigenvectors determine two 2×2 matrices $\mathsf{R}(z)$ and $\mathsf{T}(z)$, which vary along the optical axis of the lens guide that corresponds to the cav-

ity. The Gaussian fundamental mode depends on these two matrices according to equation (2.64). Higher order modes arise after repeated application of bosonic raising operators as in equation (2.66), where these operators are specified by equations (2.59) and (2.60). These algebraic expressions can be used directly to calculate the mode profiles.

The spatial structure and physical properties of twisted cavity modes are significantly different from those of non-twisted (separable) cavity modes. The intensity and phase patterns of twisted modes tumble under propagation from one mirror to the other. As a result, there is orbital angular momentum in these modes. Moreover, the higher-order modes contain optical vortices in the transverse planes between the mirrors.

Since the paraxial wave equation (2.32), which describes free propagation of a paraxial beam, is identical in form to the Schrödinger equation of a free particle in two dimensions, the methods and results of this chapter can be applied to study the time evolution of the quantum states of a particle in free space. In the Schrödinger equation, the longitudinal coordinate z is replaced by time, while the two transverse coordinates x and y are replaced by three spatial coordinates. In that case, the approach discussed in this chapter involves three pairs of bosonic ladder operators, which characterize a complete and orthonormal set of exact wave-packet solutions of the Schrödinger equation.

3

Twisted light between rotating mirrors

3.1 Introduction

The possibly very rich structure of optical cavity modes is fully determined by the boundary condition that the electric field must vanish on the mirror surfaces. This implies that the wave fronts (surfaces of equal phase) of a mode that propagates inside the cavity fit on the mirror surfaces. As a result, the mirror surfaces are nodal planes of the standing wave pattern that is formed inside the cavity. The common approach to finding the modes of a paraxial optical cavity is by considering a freely propagating Gaussian beam and requiring its wave fronts to fit on the mirror surfaces [12]. This is straightforward in the standard case of a cavity with two spherical mirrors. The resulting equation can be solved to obtain the beam parameters that characterize a complete and orthonormal set of Hermite-Gaussian modes. Geometric stability comes in as the necessary and sufficient condition for a cavity to have stationary modes and the round-trip Gouy phases determine the corresponding frequency spectrum. This approach allows for generalization to the case of astigmatic mirrors, which are curved differently in two mutually perpendicular transverse directions, provided that the mirror axes are parallel. The problem of finding the paraxial modes of a cavity with non-aligned astigmatic mirrors requires far more advanced analytical [38, 34] or, as discussed in the previous chapter, algebraic techniques.

In this chapter we consider an additional, and surprisingly different, source of complexity. We study the propagation and diffraction of light inside a two-mirror cavity that is rotating at a uniform velocity about its optical axis. It remains true that the electric field vanishes

on the mirror surfaces. Since cavity modes are usually defined as monochromatic solutions of the wave equation that obey the boundary conditions imposed by the mirrors, the mode concept requires special attention in this time-dependent case. As opposed to, for instance, vibration, uniform rotation is homogeneous in time, which means that all instants of time, and therefore all cavity round trips, are equivalent. In this special case, it is natural to require that modes adopt the time-dependence of the cavity so that they rotate along with the mirrors. We show that this property can be used as a defining property of rotating cavity modes. As an example, we consider the case of a rotating astigmatic two-mirror cavity. We generalize the geometric-algebraic method that we have developed in the previous chapter to derive explicit expressions of the rotating cavity modes and apply these to study some of their physical properties.

The material in this chapter is organized as follows. In the next section we discuss the perturbative approach to the paraxial approximation [45] and its generalization to the time-dependent case [46]. This helps us to ensure the consistency of our approach in that we retain all terms up to the same order of the expansion. In section 3.3 and section 3.4 we generalize the operator description of paraxial wave optics [42] to account for the time-dependence of a rotating cavity and show how modes can be defined in such a system. Explicit expressions of the rotating cavity modes are derived in section 3.5 and section 3.6, where we also discuss some of their physical properties. In section 3.7 we focus on the role of spatial symmetries in special limiting cases while section 3.8 is devoted to the orbital angular momentum in the rotating cavity modes. Explicit results for specific cases are briefly discussed in section 3.9.

3.2 Time-dependent paraxial propagation

The spatial structure of an optical beam is characterized by a vector field $\mathbf{u}(\mathbf{r}, t)$, which describes the spatial and temporal variations of the vector components of the field that are slow compared to those arising from the carrier wave. The profile $\mathbf{u}(\mathbf{r}, t)$ defines the electric field of the beam by

$$\mathbf{E}(\mathbf{r}, t) = \mathrm{Re}\left\{E_0 \mathbf{u}(\mathbf{r}, t)\, e^{ikz - i\omega t}\right\} , \tag{3.1}$$

where E_0 is an amplitude factor and $\omega = ck$ is the frequency of the carrier wave, with k the wave number and c the speed of light. In vacuum the electric field obeys the wave equation

$$\nabla^2 \mathbf{E} = \frac{1}{c^2} \frac{\partial^2 \mathbf{E}}{\partial t^2} , \tag{3.2}$$

with the additional requirement that it has a vanishing divergence

$$\nabla \cdot \mathbf{E} = 0 . \tag{3.3}$$

Essential for the paraxial approximation is that the beam has a small opening angle, which we indicate by the smallness parameter δ. Then the beam waist is of the order of the parameter γ, and the diffraction length (or Rayleigh range) is of the order of the parameter b, where

$$\frac{1}{k} = \delta\gamma = \delta^2 b . \tag{3.4}$$

So the diffraction length is much larger than the beam waist, which is much larger than the wavelength. The smallness of δ ensures that the variations of the profile $\mathbf{u}(\mathbf{r}, t)$ with the longitudinal coordinate z are slow compared to the variations with the transverse coordinates $\rho = (x, y)^{\mathrm{T}}$, which are, in turn, slow compared to the variations of the carrier wave $\exp(ikz)$ with z. By using δ as an expansion parameter, the time-independent paraxial wave equation (2.32) can be obtained directly from the wave equation (3.2) while resolving the apparent paradox that paraxial fields cannot have a completely vanishing divergence [45]. As we shall discuss in a moment, this approach allows for generalization to the time-dependent case [46].

Time dependent optical fields necessarily have spectral structure in addition to their spatial structure. The concept of a mode loses its meaning if the difference in diffraction of the frequency components becomes significant, i.e., if the diffraction due to the time dependence of the profile becomes important. Conversely, we shall show that the mode concept remains meaningful if the time scale for variation of the cavity boundaries is slower than the transit time through the focal range of the beam. This transit time is of the order of

$$a = \frac{b}{c} = \frac{1}{\omega\delta^2} \; . \tag{3.5}$$

In order to obtain the time-dependent paraxial wave equation, the profile $\mathbf{u}$ is expanded in powers of the opening angle δ

$$\mathbf{u}(\mathbf{r}, t) = \sum_{n=0}^{\infty} \delta^n \mathbf{u}^{(n)}(\mathbf{r}, t) \; . \tag{3.6}$$

Since we need to account for the (relative) order of the magnitudes of the derivatives of $\mathbf{u}$, it is convenient to introduce the scaled variables $\xi = x/\gamma$, $\eta = y/\gamma$, $\zeta = z/b$ and $\tau = t/a$. In these variables, the derivatives can be treated as being of the same order in δ. Substituting the expression (3.1) for the electric field in the wave equation (3.2) then gives

$$\left(\frac{\partial^2}{\partial\xi^2} + \frac{\partial^2}{\partial\eta^2} + 2i\frac{\partial}{\partial\zeta} + 2i\frac{\partial}{\partial\tau}\right)\mathbf{u}(\mathbf{r}, t) = \delta^2\left(\frac{\partial^2}{\partial\tau^2} - \frac{\partial^2}{\partial\zeta^2}\right)\mathbf{u}(\mathbf{r}, t) \; , \tag{3.7}$$

while the transversality condition (3.3) yields

$$\delta\left(\frac{\partial u_x}{\partial\xi} + \frac{\partial u_y}{\partial\eta}\right) = -\delta^2\frac{\partial u_z}{\partial\zeta} - iu_z \; . \tag{3.8}$$

It is natural to assume that to zeroth order the z component of $\mathbf{u}$ vanishes, and equation (3.8) shows that such a solution can be found. Then to zeroth order of the paraxial approximation the electric field lies in the transverse plane. In the special case of uniform polarization it can be written as

$$\mathbf{u}^{(0)}(\mathbf{r}, t) = \epsilon u(\mathbf{r}, t) \; , \tag{3.9}$$

where ϵ is a transverse polarization vector. The scalar profile $u(\mathbf{r}, t)$ obeys the time-dependent paraxial wave equation

$$\left(\frac{\partial^2}{\partial x^2} + \frac{\partial^2}{\partial y^2} + 2ik\frac{\partial}{\partial z} + \frac{2ik}{c}\frac{\partial}{\partial t}\right)u(\mathbf{r}, t) = 0 \; . \tag{3.10}$$

The expansion (3.6) then shows that all even orders of the transverse components are coupled by equation (3.7) while all odd orders can be assumed to vanish. Equation (3.8) connects odd orders of the z component to the even orders of the transverse components, which implies that all even orders (including the zeroth) of the longitudinal component vanish. The first-order contribution to the profile is longitudinal and by using equation (3.8) it can be expressed in the zeroth order term

$$\delta\mathbf{u}^{(1)}(\mathbf{r},t) = \frac{i}{k}\left(\epsilon_x\frac{\partial}{\partial x} + \epsilon_y\frac{\partial}{\partial y}\right)u(\mathbf{r},t)\mathbf{e}_z \,, \tag{3.11}$$

where $\mathbf{e}_z$ is the unit vector in the z direction.

Up to first order of the paraxial approximation, finding the modes of a cavity with rotating mirrors requires solving the time-dependent paraxial wave equation (3.10) with the boundary condition that the electric field (3.1) vanishes at the mirror surfaces at all times. The range of validity of this time-dependent wave equation provides a natural upper limit to the rotation frequency of the mirrors. In a typical experimental set-up the diffraction length of the modes of an optical cavity is of the order of magnitude of the mirror separation, so that the period of the rotation of the mirrors can be at most comparable to the cavity round-trip time. This yields an upper bound to the rotation frequency Ω

$$\Omega \lesssim \frac{c\pi}{L} \,, \tag{3.12}$$

where L is the mirror separation and c is the speed of light. The average lifetime of a photon inside the cavity, which we leave out of our consideration here, provides a natural lower bound to the rotation frequency of the mirrors.

3.3 Operator description of time-dependent paraxial wave optics

3.3.1 Operators and transformations

The standard time-independent paraxial wave equation follows if we omit the time derivative in equation (3.10). This has the same structure as the Schrödinger equation for a free particle in two dimensions, with k taking the place of $m/\hbar$ and the longitudinal coordinate z playing the role of time. This analogy can be exploited by adopting the Dirac notation of quantum mechanics to describe classical light beams [42]. This naturally leads to an operator description of paraxial wave optics. Here, we show that this description can be generalized to include the time dependence of the scalar beam profile $u(\rho,z,t)$, even though the time dependence of an optical beam does not have an analogue in quantum mechanics.

We associate to the beam profile $u(\rho,z,t)$ a vector $|u(z,t)\rangle$ in the Hilbert space of paraxial modes of the radiation field

$$u(\rho,z,t) = \langle\rho|u(z,t)\rangle \,, \tag{3.13}$$

where $|\rho\rangle$ is an eigenstate of the transverse position operator $\hat{\rho} = (\hat{x},\hat{y})^{\mathrm{T}}$. The corresponding momentum operator can be represented by $k\hat{\theta} = (k\hat{\vartheta}_x, k\hat{\vartheta}_y)^{\mathrm{T}} = -i(\partial/\partial x, \partial/\partial y)^{\mathrm{T}}$. The

transformations of paraxial propagation and lossless optical elements such as thin lenses can be expressed as unitary transformations in the transverse mode space. Expressing the time-dependent paraxial wave equation (3.10) in terms of the momentum operators gives

$$\left(\frac{\partial}{\partial z}+\frac{1}{c}\frac{\partial}{\partial t}\right)|u(z,t)\rangle=-\frac{ik}{2}\hat{\theta}^2|u(z,t)\rangle\,, \tag{3.14}$$

which is formally solved by

$$|u(z,t)\rangle=\exp\left(-\frac{ikz}{2}\hat{\theta}^2\right)|u(0,t-z/c)\rangle=\hat{U}_{\mathrm{f}}(z)|u(0,t-z/c)\rangle\,, \tag{3.15}$$

where $\hat{U}_{\mathrm{f}}(z)$ denotes the unitary operator that describes free propagation of a paraxial beam. This result shows that the time-dependent paraxial wave equation (3.10) describes paraxial beam propagation while incorporating retardation effects. A thin spherical lens imposes a Gaussian phase profile. Hence, the transformation caused by such a lens can be expressed as [27]

$$|u_{\mathrm{out}}\rangle=\exp\left(-\frac{ik\hat{\rho}^2}{2f}\right)|u_{\mathrm{in}}\rangle\,, \tag{3.16}$$

where f is the focal length of the lens. The generalization of this transformation to the case of a lens that has astigmatism is given by

$$|u_{\mathrm{out}}\rangle=\exp\left(-\frac{ik\hat{\rho}^{\mathrm{T}}\mathsf{F}^{-1}\hat{\rho}}{2}\right)|u_{\mathrm{in}}\rangle=\hat{U}_{\mathrm{l}}(\mathsf{F})|u_{\mathrm{in}}\rangle\,, \tag{3.17}$$

where F is a real and symmetric 2×2 matrix. The eigenvalues of F characterize the focal lengths of the lens while the, mutually orthogonal, real eigenvectors fix its orientation in the transverse plane.

3.3.2 Rotating lenses and frequency combs

The unitary operator that rotates a scalar function about the z axis can be expressed as

$$\hat{U}_{\mathrm{rot}}(\alpha)=\exp(-i\alpha\hat{L}_z)\,, \tag{3.18}$$

where α is the rotation angle and $\hat{L}_z=\hat{\rho}\times k\hat{\theta}=-i(x\partial/\partial y-y\partial/\partial x)=-i\partial/\partial\phi$ is the z component of the orbital angular momentum operator. The inverse of this rotation is a rotation in the opposite direction, so that $\hat{U}^{\dagger}_{\mathrm{rot}}(\alpha)=\hat{U}_{\mathrm{rot}}(-\alpha)$. The transformation of a rotated lens can be expressed as

$$\hat{U}_{\mathrm{rot}}(\alpha)U_{\mathrm{l}}(\mathsf{F})\hat{U}^{\dagger}_{\mathrm{rot}}(\alpha)\,. \tag{3.19}$$

This (anti-Heisenberg) transformation property makes sense if one realizes that rotating a lens is equivalent to rotating the profile in the opposite direction, applying the lens and rotating the profile backward. The beam transformation caused by an astigmatic lens (3.17) only involves

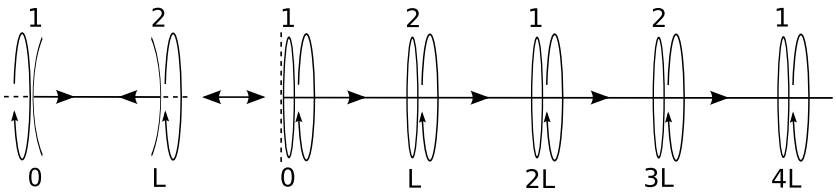

Figure 3.1: Unfolding a rotating optical cavity into an equivalent periodic lens guide. The mirrors are replaced by rotating lenses with the same focal lengths and the $z = 0$ reference plane is indicated by the dashed line.

the position operator $\hat{\rho} = (\hat{x}, \hat{y})^{\mathrm{T}}$. The anti-Heisenberg transformation of the position operator under a rotation about the z axis (3.18) can be expressed as

$$\hat{U}_{\mathrm{rot}}(\alpha)\hat{\rho}\hat{U}^{\dagger}_{\mathrm{rot}}(\alpha) = \begin{pmatrix} \cos\alpha & \sin\alpha \\ -\sin\alpha & \cos\alpha \end{pmatrix}\hat{\rho} = \mathsf{P}^{\mathrm{T}}(\alpha)\hat{\rho}\,, \tag{3.20}$$

with $\mathsf{P}(\alpha)$ a two-dimensional rotation matrix. By using this transformation property of the position operators, the transformation of a rotated lens (3.19) can be expressed as

$$\hat{U}_{\mathrm{l}}\Big(\mathsf{P}(\alpha)\mathsf{F}\mathsf{P}^{\mathrm{T}}(\alpha)\Big)\,. \tag{3.21}$$

For a lens rotating at angular velocity Ω, the rotation angle is $\alpha = \Omega t$, so that the time-dependent beam transformation caused by the rotating lens is given by $\hat{U}_{\mathrm{l}}(\mathsf{F}(t))$ where $\mathsf{F}(t) = \mathsf{P}(\Omega t)\mathsf{F}(0)\mathsf{P}^{\mathrm{T}}(\Omega t)$. Without loss of generality we can choose the real and symmetric matrix $\mathsf{F}(t)$ diagonal at $t = 0$

$$\mathsf{F}(0) = \begin{pmatrix} f_\xi & 0 \\ 0 & f_\eta \end{pmatrix}\,. \tag{3.22}$$

By using equations (3.19-3.22) and introducing cylindrical coordinates with $x = R\cos\phi$, $y = R\sin\phi$, the time-dependent transformation of a rotating lens can be expressed as

$$\hat{U}_{\mathrm{l}}(\mathsf{F}(t)) = \exp\Big[-\frac{ikR^2}{4}\left(f_\xi^{-1} + f_\eta^{-1}\right) - \frac{ikR^2}{4}\left(f_\xi^{-1} - f_\eta^{-1}\right)\cos\left(2\Omega t - 2\phi\right)\Big]\,. \tag{3.23}$$

Using the Jacobi-Anger expansion of a plane wave in cylindrical waves: $\exp(iz\cos\phi) = \sum_{l=-\infty}^{\infty} i^l J_l(z)\exp(il\phi)$, where J_l are Bessel functions of the first kind [47], this result can be rewritten as:

$$\begin{aligned}\hat{U}(\mathsf{F}(t)) = \exp\Big[-\frac{ikR^2}{4}\left(f_\xi^{-1} + f_\eta^{-1}\right)\Big]\times \\ \sum_l \left\{J_l\left(\frac{ikR^2}{4}\left(f_\xi^{-1} - f_\eta^{-1}\right)\right)\exp\Big[-2il\Big(\Omega t + \phi + \frac{\pi}{4}\Big)\Big]\right\}\,.\end{aligned} \tag{3.24}$$

It follows that a rotating lens introduces frequency side bands in a monochromatic optical field at frequencies $\omega \pm 2p\Omega$ with $p \in \mathbb{Z}$ [48].

3.4 Modes in a rotating cavity

3.4.1 Lens guide picture

In order to describe the evolution of a profile vector $|u(z,t)\rangle$ inside a rotating cavity it is convenient to unfold the cavity into an equivalent lens guide. As illustrated in figure 3.1, the mirrors are replaced by lenses with the same focal lengths. Rather than describing the bouncing back and forth inside the cavity we describe the propagation along the axis of the lens guide, with coordinate z. The dashed line on the left of the first lens in figure 3.1 indicates the transverse reference plane of the lens guide, which is positioned at $z = 0$. The profile in any transverse plane of the lens guide is connected to the profile in the input plane by a unitary transformation. Just as in equation (3.15), this time-dependent connection involves retardation, as described by

$$|u(z,t)\rangle = \hat{U}(z,t)|u(0,t-z/c)\rangle \; . \tag{3.25}$$

The unitary operator $\hat{U}(z,t)$ can be constructed by successive application of the transformations of the optical elements and free propagation that are in between the reference plane and the z plane in the correct order. We need only two different transformation operators for the lenses in the lens guide, which we denote for simplicity as $\hat{U}_1(t)$ and $\hat{U}_2(t)$. For the lens guide that corresponds to a cavity rotating at the uniform angular velocity Ω, these time-dependent operators are given by equation (3.19) with rotation angle $\alpha = \Omega t$, so that

$$\hat{U}_i(t) = \hat{U}_{\rm rot}(\Omega t)\hat{U}_1(\mathsf{F}_i(0))\hat{U}^\dagger_{\rm rot}(\Omega t) \; , \tag{3.26}$$

with $i = 1, 2$ labeling the two lens types. Since the orientations of the rotating lenses depend on time, retardation effects must be included. As an example we give the operator that connects the profile vectors in transverse planes that are separated by one period of the lens guide

$$\hat{U}(2L,t) = \hat{U}_{\rm f}(L)\hat{U}_2(t-L/c)\hat{U}_{\rm f}(L)\hat{U}_1(t-2L/c) \; . \tag{3.27}$$

Obviously, all lenses that correspond to the same mirror of the cavity have the same orientation at any instant of time. Nevertheless, as a result of the finiteness of the speed of light, the orientation of two lenses that correspond to the same mirror of the cavity is perceived differently by a light pulse that propagates through the lens guide.

3.4.2 Rotating modes

Cavity modes are resonant field distributions inside an optical cavity. In a stationary cavity, a field pattern is resonant only if it repeats itself after each round trip through the cavity. The natural generalization of this mode criterion to the rotating case is by requiring that the field pattern in the corresponding lens guide is the same in every period, at a single given instant of time. This implies that the mode vector $|u(0,t)\rangle$ in the reference plane for a given value of

t repeats itself after one period $2L$ up to a phase factor

$$|u(2L,t)\rangle = e^{-i\chi}|u(0,t)\rangle \ . \tag{3.28}$$

The phase χ generalizes the Gouy phase for the round trip in a stationary cavity. Since the lens guide is rotating at a uniform velocity Ω, this mode criterion (3.28) can be obeyed only if the mode pattern rotates along with the lenses, so that the time dependence of a mode vector must be determined by

$$|u(z,t)\rangle = \hat{U}_{\rm rot}(\Omega t)|v(z)\rangle \ . \tag{3.29}$$

The homogeneous time dependence of this profile (3.29) can be eliminated by introducing the z dependent profile

$$|v(z)\rangle = |u(z,0)\rangle \ , \tag{3.30}$$

which has the significance of the profile vector in the co-rotating frame. By combining the relation (3.29) with equations (3.25-3.27), we find that the propagation of a beam profile in this frame is governed by the general relation

$$|v(z)\rangle = \hat{U}(z,0)\hat{U}_{\rm rot}(-\Omega z/c)|v(0)\rangle \ , \tag{3.31}$$

so that the product $\hat{U}(z,0)\hat{U}_{\rm rot}(-\Omega z/c)$ can be viewed as the operator for free propagation in the co-rotating frame. In the special case of the propagation over one period of the lens guide, we find

$$|v(2L)\rangle = \hat{U}_{\rm rt}\hat{U}^{\dagger}_{\rm rot}(\Omega t)|u(0,t)\rangle = \hat{U}_{\rm rt}|v(0)\rangle \ , \tag{3.32}$$

where $\hat{U}_{\rm rt}$ is given by the expression

$$\hat{U}_{\rm rt} = \hat{U}_{\rm f}(L)\hat{U}_{\rm rot}(-\Omega L/c)\hat{U}_2(0)\hat{U}_{\rm f}(L)\hat{U}_{\rm rot}(-\Omega L/c)\hat{U}_1(0) \tag{3.33}$$

and has the significance of the transformation operator over a single period of the lens guide in the co-rotating frame. Notice that the operator for free evolution $\hat{U}_{\rm f}$ is denoted as a function of length while the lens operators $\hat{U}_i$ are denoted as a function of time and the rotation operator $\hat{U}_{\rm rot}$ is denoted as a function of angle.

Now the mode criterion (3.28) in the reference plane $z = 0$ in the rotating frame is obeyed by the eigenvectors of the round-trip operator $\hat{U}_{\rm rt}$. Once these mode vectors are determined, we can use the propagation equation (3.15) and the time dependence (3.29) to obtain the shape of the modes at other time instants, and at any position within a period of the lens guide. The eigenvalues, which are specified by the phase angles χ, determine the resonance frequencies of the modes. In the next section we shall indicate how the modes can be obtained explicitly from a ladder-operator method.

3.5 Ray matrices and ladder operators

3.5.1 Time-dependent ray matrices

The transverse spatial structure of paraxial modes in cavities with spherical mirrors is known to be similar to the spatial structure of the stationary states of a two-dimensional quantum

harmonic oscillator [12]. Complete sets of modes can be generated by using bosonic ladder operators [33]. In chapter 2, we have derived a ladder operator method to find explicit expressions of the paraxial modes of an optical cavity that has general astigmatism. These ladder operators are conveniently expressed in terms of the eigenvectors of the ray matrix for one period in the lens guide, or, equivalently, for one round trip in the cavity. Here we generalize this approach to account for the time dependence that arises from the rotation of the cavity. In this case, also the ray matrices depend on time.

In geometric paraxial optics, a light ray is specified by its position $\rho = (x, y)^{\mathrm{T}}$ and its propagation direction $\theta = \partial\rho/\partial z$ in the transverse plane z. They can conveniently be combined into a four-dimensional column vector

$$\mathscr{r}(z) = \begin{pmatrix} \rho(z) \\ \theta(z) \end{pmatrix} . \tag{3.34}$$

The linear transformation of a ray $\mathscr{r}$ through a paraxial astigmatic optical system can be described by a product of 4×4 ray matrices, which generalize the well-known $ABCD$ matrices to the case of two independent transverse dimensions [12]. Here, we shall construct the ray matrix $M(z)$ that describes the transformation of a ray through the lens guide from the reference plane at $z = 0$ to the transverse plane z. In wave optics, the position of a light beam is the expectation value of the operator $\hat{\rho}$, while its propagation direction is the expectation value of $\hat{\theta}$, which is the ratio of the transverse and the longitudinal momentum. This is confirmed by the fact that the Heisenberg evolution of the operator vector $\hat{\mathscr{r}} = (\hat{\rho}, \hat{\theta})^{\mathrm{T}}$ reproduces the ray matrix, as exemplified by the general identity

$$\hat{U}^{\dagger}(z) \begin{pmatrix} \hat{\rho} \\ \hat{\theta} \end{pmatrix} \hat{U}(z) = M(z) \begin{pmatrix} \hat{\rho} \\ \hat{\theta} \end{pmatrix} . \tag{3.35}$$

The propagation operator $\hat{U}$ acts on the operator nature of $\hat{\rho}$ and $\hat{\theta}$, while the matrix M acts on the four-dimensional ray vector. This relation may be viewed as the optical analogue of the Ehrenfest theorem in quantum mechanics [49]. Note that the commutation relations for the components of the position and propagation-direction operators take the form

$$[\hat{\rho}_x, \hat{\theta}_x] = [\hat{\rho}_y, \hat{\theta}_y] = i\lambda = i/k . \tag{3.36}$$

The ray matrix $M(z)$ for propagation from the plane $z = 0$ to the plane z of the lens guide can be constructed as the product of the ray matrices for the regions of free propagation and the lenses in between these planes in the right order. The ray matrix for free propagation is described by

$$\hat{U}_{\mathrm{f}}^{\dagger}(z) \begin{pmatrix} \hat{\rho} \\ \hat{\theta} \end{pmatrix} \hat{U}_{\mathrm{f}}(z) = \begin{pmatrix} 1 & z1 \\ 0 & 1 \end{pmatrix} \begin{pmatrix} \hat{\rho} \\ \hat{\theta} \end{pmatrix} = M_{\mathrm{f}}(z) \begin{pmatrix} \hat{\rho} \\ \hat{\theta} \end{pmatrix} , \tag{3.37}$$

where 1 and 0 are the 2×2 unit and zero matrices respectively. The transformation for a thin astigmatic lens can be expressed as

$$\hat{U}_{\mathrm{l}}^{\dagger}(\mathsf{F}) \begin{pmatrix} \hat{\rho} \\ \hat{\theta} \end{pmatrix} \hat{U}_{\mathrm{l}}(\mathsf{F}) = \begin{pmatrix} 1 & 0 \\ -\mathsf{F}^{-1} & 1 \end{pmatrix} \begin{pmatrix} \hat{\rho} \\ \hat{\theta} \end{pmatrix} = M_{\mathrm{l}}(\mathsf{F}) \begin{pmatrix} \hat{\rho} \\ \hat{\theta} \end{pmatrix} . \tag{3.38}$$

The ray matrix of a rotation about the z axis follows from the identity

$$\hat{U}^{\dagger}_{\mathrm{rot}}(\alpha)\begin{pmatrix}\hat{\rho}\\ \hat{\theta}\end{pmatrix}\hat{U}_{\mathrm{rot}}(\alpha)=\begin{pmatrix}\mathsf{P}(\alpha) & 0\\ 0 & \mathsf{P}(\alpha)\end{pmatrix}\begin{pmatrix}\hat{\rho}\\ \hat{\theta}\end{pmatrix}=M_{\mathrm{rot}}(\alpha)\begin{pmatrix}\hat{\rho}\\ \hat{\theta}\end{pmatrix}. \tag{3.39}$$

The identities (3.35) and (3.38) remain valid for rotating lenses, which makes both the operators $\hat{U}$ and the ray matrices M depend on time. The transformation of a time-dependent ray in the reference plane to another transverse plane z is given by

$$\text{ɾ}(z,t)=M(z,t)\,\text{ɾ}(0,t-z/c)) \tag{3.40}$$

in analogy to equation (3.25). A co-rotating incident ray in the reference plane must give a co-rotating ray everywhere in the lens guide, and the ray matrices in the rotating frame become independent of time. In complete analogy to equation (3.32), this implies that the transformation of a ray in the rotating frame over one period from the reference plane is given by the round-trip ray matrix

$$M_{\mathrm{rt}}=M_{\mathrm{f}}(L)M_{\mathrm{rot}}(-\Omega L/c)M_2(0)M_{\mathrm{f}}(L)M_{\mathrm{rot}}(-\Omega L/c)M_1(0)\,, \tag{3.41}$$

with $M_1(0)$ and $M_2(0)$ the ray matrices for the lenses 1 and 2 at time 0.

Any ray matrix that describes the transformation of a (sequence of) lossless optical elements obeys the following identity

$$M^{\mathrm{T}}GM=G\,,\qquad\text{where}\qquad G=\begin{pmatrix}0 & 1\\ -1 & 0\end{pmatrix}. \tag{3.42}$$

This property generalizes the requirement that the determinant of a ray matrix must be equal to 1 to optical systems that have two independent transverse dimensions. It is easy to show that the ray matrices that we have used obey this identity (3.42). The product of matrices that obey equation (3.42) obeys it as well and in mathematical terms the set of 4×4 matrices that obey this identity forms the real symplectic group $\mathrm{Sp}(4,\mathbb{R})$. Both the underlying algebra and the physics of such linear phase space transformations have been studied in detail, see, for instance, reference [39].

3.5.2 Ladder operators in reference plane

The similarity between Hermite-Gaussian modes of a cavity with spherical mirrors and harmonic-oscillator eigenstates can be traced back to the fact that in the paraxial limit the Heisenberg evolution (3.35) of the position and propagation-direction operators $\hat{\rho}$ and $\hat{\theta}$ is linear, so that ladder operators, which are linear in these operators, preserve their general shape under propagation and optical elements. In chapter 2 we have demonstrated that the ladder operators that generate the modes of a cavity with non-parallel astigmatic mirrors are determined by the eigenvectors of the round-trip ray matrix. In the rotating frame, the relation between the propagation operators and the ray matrix for a round trip is basically the same as for a

stationary one, and equations (3.33) and (3.41) are obviously analogous. This allows us to apply the same technique to obtain expressions for the modes of the rotating cavity. In order to define the ladder operators we shall need the eigenvectors and eigenvalues of the ray matrix equation (3.41). Stability of the rotating cavity requires that the eigenvalues are unitary, and since the matrix M_{rt} is real, this implies that its eigenvectors come in two pairs μ_1, μ_1^* and μ_2, μ_2^* that are each other's complex conjugate. The eigenvalue relations are written as

$$M_{\mathrm{rt}}\mu_1 = e^{i\chi_1}\mu_1 \quad \text{and} \quad M_{\mathrm{rt}}\mu_2 = e^{i\chi_2}\mu_2 \; . \tag{3.43}$$

From the general property (3.42) of ray matrices one directly obtains the generalized (symplectic) orthogonality properties

$$\mu_1^{\mathrm{T}} G \mu_2 = \mu_1^{\dagger} G \mu_2 = 0 \; , \tag{3.44}$$

while the eigenvectors can be normalized in order to obey the identities

$$\mu_1^{\dagger} G \mu_1 = \mu_2^{\dagger} G \mu_2 = 2i \; . \tag{3.45}$$

We shall now prove that the ladder operators that define the shape of the modes in the reference plane $z = 0$ at time 0 are easily expressed in terms of the eigenvectors μ_1 and μ_2 of the ray matrix M_{rt}. Following the approach discussed in the previous chapter, we introduce two lowering operators

$$\hat{a}_i = \sqrt{\frac{k}{2}} \mu_i G \begin{pmatrix} \hat{\rho} \\ \hat{\theta} \end{pmatrix} \; , \tag{3.46}$$

where $i = 1, 2$. From the generalized orthonormality properties (3.44) and (3.45) of the eigenvectors μ_i combined with the canonical commutation rules (3.36) it follows that the ladder operators obey the bosonic commutation rules

$$\left[\hat{a}_i, \hat{a}_j^{\dagger}\right] = \delta_{ij} \; . \tag{3.47}$$

Any set of ladder operators that obey these commutation relations defines a complete and orthonormal set of transverse modes according to

$$|v_{nm}\rangle = \frac{1}{\sqrt{n!m!}} \left(\hat{a}_1^{\dagger}\right)^n \left(\hat{a}_2^{\dagger}\right)^m |v_{00}\rangle \; . \tag{3.48}$$

Apart from an overall phase factor, the fundamental mode (or ground state in the terminology of quantum mechanics) $|v_{00}\rangle$ is determined by the requirement that $\hat{a}_1|v_{00}\rangle = \hat{a}_2|v_{00}\rangle = 0$. The bosonic ladder operators obviously determine a complete and orthogonal set of modes in the reference plane $z = 0$. A more explicit expression of the fundamental mode will be given below. In chapter 5 we shall derive analytical expressions of the higher-order modes.

3.5.3 Ladder operators in arbitrary transverse plane

The eigenvectors $\mu_i(0) = \mu_i$ refer to the transformation from the reference plane at $z = 0$ to the plane $z = 2L$, in the rotating frame. We also need the modes $|v_{mn}(z)\rangle$, and therefore the eigenvectors $\mu_i(z)$ in an arbitrary transverse plane z in the lens guide, in the rotating frame. The basic time-dependent transformation of a ray is given by equation (3.40), so that

$$\mu_i(z) = M(z,0)M_{\rm rot}(-\Omega z/c)\mu_i(0) \tag{3.49}$$

in analogy to equation (3.31) for the beam profile propagation in the rotating frame. In the special case of propagation over one period, we should take $z = 2L$. Then the ray transformation in (3.49) is $M_{\rm rt}$, which gives

$$\mu_i(2L) = e^{i\chi_i}\mu_i(0)\ . \tag{3.50}$$

For notational convenience we separate the four-dimensional eigenvectors in their two-dimensional subvectors as

$$\mu_i(z) = \begin{pmatrix} r_i(z) \\ t_i(z) \end{pmatrix}\ . \tag{3.51}$$

Then we compose two 2×2 matrices out of the column vectors $r_i(z)$ and $t_i(z)$, by the definition

$$\mathsf{R}(z) \equiv (r_1(z), r_2(z)) \qquad \text{and} \qquad \mathsf{T}(z) \equiv (t_1(z), t_2(z))\ . \tag{3.52}$$

The relations (3.44) and (3.45) can be summarized as

$$\mathsf{R}^{\rm T}\mathsf{T} - \mathsf{T}^{\rm T}\mathsf{R} = 0 \qquad \text{and} \qquad \mathsf{R}^{\dagger}\mathsf{T} - \mathsf{T}^{\dagger}\mathsf{R} = 2i\mathsf{1} \tag{3.53}$$

in all transverse planes z.

The dependence of the ladder operators on z in the rotating frame is determined by the requirement that when acting on a rotating solution of the time-dependent paraxial wave equation, they must produce another solution. In view of equation (3.31), this requirement takes the form

$$\hat{a}_i(z) = \hat{U}(z,0)U_{\rm rot}(-\Omega z/c)\hat{a}_i(0)U^{\dagger}_{\rm rot}(-\Omega z/c)\hat{U}^{\dagger}(z,0)\ . \tag{3.54}$$

In the right-hand sides of this equation the propagation operators $\hat{U}$ act on the operators $\hat{\rho}$ and $\hat{\theta}$. In accordance with the general Ehrenfest relation (3.35), and the relation (3.42), this gives rise to a product $GM^{-1} = M^{\rm T}G$ when we substitute the expression (3.46) for the lowering operator. This leads to the conclusion that the z dependent lowering operator obeys the relation

$$\hat{a}_i(z) = \sqrt{\frac{k}{2}}\mu_i(z)G\begin{pmatrix} \hat{\rho} \\ \hat{\theta} \end{pmatrix} = \sqrt{\frac{k}{2}}(r_i(z)\hat{\theta} - t_i(z)\hat{\rho}) \tag{3.55}$$

for all values of z.

3.6 Structure of the modes

3.6.1 Algebraic expressions of the modes

The fundamental mode $|v_{00}(z)\rangle$ in the rotating frame obeys the requirement that the lowering operators $\hat{a}_i(z)$ give zero when acting on it for all transverse planes z in the lens guide. An explicit analytical expression of the normalized mode function as it propagates through the lens guide can be found after a slight generalization of our results for a stationary cavity discussed in chapter 2. There we have shown that the fundamental mode can be expressed in terms of the z dependent eigenvectors, which give rise to the 2×2 matrices $\mathsf{R}(z)$ and $\mathsf{T}(z)$. For rotating cavities, the same result applies in the rotating frame, where the time dependence disappears. In the rotating frame, the beam profile of the fundamental mode is given by the general Gaussian expression

$$v_{00}(R,z) = \langle\rho|v_{00}(z)\rangle = \sqrt{\frac{k}{\pi \det \mathsf{R}(z)}}\exp\left(\frac{ik\rho^{\mathrm{T}}\mathsf{T}(z)\mathsf{R}^{-1}(z)\rho}{2}\right) . \tag{3.56}$$

From the properties (3.53) of the matrices R and T it follows that the matrix $\mathsf{S} = -i\mathsf{T}\mathsf{R}^{-1}$ is symmetric. In the intervals between the lenses, the corresponding time-dependent mode $|u_{00}(z,t)\rangle = \hat{U}_{\mathrm{rot}}(\Omega t)|v_{00}(z)\rangle$ obeys the time-dependent paraxial wave equation (3.10), and the input-output relation for $|u_{00}(z,t)\rangle$ across a lens of type 1 or 2 corresponds to the lens operator $\hat{U}_1(t)$ or $\hat{U}_2(t)$ as in equation (3.17).

The periodicity (3.50) of the eigenvectors μ_i ensures that the matrix $\mathsf{S}(z) = -i\mathsf{T}(z)\mathsf{R}^{-1}(z)$ is periodic with period $2L$. Moreover, the determinant of R picks up a phase factor after one period, according to the identity

$$\det \mathsf{R}(2L) = e^{i(\chi_1+\chi_2)}\det \mathsf{R}(0) . \tag{3.57}$$

As a result, the fundamental mode (3.56) picks up a phase factor $\exp(-i(\chi_1+\chi_2)/2)$ after a period of the lens guide, or over a cavity round trip.

The higher-order modes $|v_{nm}(z)\rangle$ in the rotating frame are obtained from the fundamental mode by using the z dependent version of (3.48)

$$|v_{nm}(z)\rangle = \frac{1}{\sqrt{n!m!}}\left(\hat{a}_1^\dagger(z)\right)^n\left(\hat{a}_2^\dagger(z)\right)^m|v_{00}(z)\rangle . \tag{3.58}$$

The periodicity (3.50) of the eigenvector is reflected in a similar periodicity of the lowering operator, in the form

$$\hat{a}_i(z+2L) = e^{i\chi_i}\hat{a}_i(z) , \tag{3.59}$$

which in turn will give rise to a periodicity of the modes in the rotating frame $|v_{nm}(z)\rangle$. From this equation we find that the raising operator gets an additional phase $\exp(-i\chi_i)$ after a round trip. The phase factor picked up by the mode $|v_{nm}\rangle$ (or by the time-dependent mode $|u_{nm}\rangle$) is therefore specified by the relation

$$|v_{nm}(2L)\rangle = e^{-i\chi_1(n+1/2)-i\chi_2(m+1/2)}|v_{nm}(0)\rangle . \tag{3.60}$$

The resonant wave numbers of the modes follow from the requirement that the complex electric field

$$\mathbf{E}_{nm}(\rho, z, t) = E_0 \epsilon u_{nm}(\rho, z, t)\, e^{ikz - i\omega t} \tag{3.61}$$

is periodic over a round trip. This implies that the wave number k of the transverse modes must obey the identity

$$2kL - \chi_1\left(n + \frac{1}{2}\right) - \chi_2\left(m + \frac{1}{2}\right) = 2\pi q \tag{3.62}$$

where $q \in \mathbb{Z}$ is the longitudinal mode index. Note that the round-trip Gouy phases χ_1 and χ_2, and thereby the resonant wavelengths are affected by the rotation. This is obvious since they arise from the eigenvalues of the round-trip ray matrix M_{rt}, which according to equation (3.41) contains the angular velocity Ω.

3.6.2 Spectral structure

Just as in equation (3.29), the time-dependent mode as viewed from the (non-rotating) laboratory frame follows from the mode $|v_{nm}(z)\rangle$ by a simple rotation, so that:

$$|u_{nm}(z, t)\rangle = \hat{U}_{\mathrm{rot}}(\Omega t)|v_{nm}(z)\rangle\ . \tag{3.63}$$

The mode function $u_{nm}(\rho, z, t) = \langle\rho|u_{nm}(z, t)\rangle$ is a co-rotating solution of the time-dependent paraxial wave equation (3.10). Since this mode function depends on time, the electric field (3.61) is no longer monochromatic. The spectral structure follows directly from the polar expansion

$$u_{nm}(\rho, z, t) = u_{nm}(R, \phi - \Omega t, z) = \sum_l g_{nml}(R, z) e^{il(\phi - \Omega t)}\ . \tag{3.64}$$

From this result it is clear that the rotation of a mode converts the l^{th} Fourier component along the azimuthal angle ϕ of the spatial distribution to a frequency component $\omega + l\Omega$. Since the fundamental Gaussian mode (3.56) is even under inversion in the transverse plane $\rho \to -\rho$, the expansion (3.64) for u_{00} contains only even values of l, so that the fundamental mode only contains side bands at frequencies $\omega + 2p\Omega$ with $p \in \mathbb{Z}$ and $\omega = ck$. The ladder operators $\hat{a}_i$ are obviously odd under this inversion, so that the modes $|u_{nm}\rangle$ with even values of $n+m$ only contain the even sidebands $\omega + 2p\Omega$, while the modes with odd values of $n + m$ only contain the odd sidebands $\omega + (2p + 1)\Omega$. The separation between neighboring sidebands is always equal to 2Ω, which reflects that the cavity returns to an equivalent orientation after a rotation over an angle of 180°.

3.6.3 The cavity field

We have unfolded a cavity with rotating mirrors into a lens guide with rotating lenses and described a method to obtain expressions of the transverse modes that are reproduced after

each period of the lens guide. In order to obtain an expression of the electric field inside the cavity, the lens-guide modes must be folded back into the cavity

$$\mathbf{E}_{\rm cav}(\mathbf{r},t) = \mathrm{Re}\Big\{ -i\epsilon E_0 \left[u(\rho,z,t)e^{ikz} - u(\rho,2L-z,t)e^{-ikz} \right] e^{-i\omega t} \Big\} \tag{3.65}$$

for $0 < z < L$. In the transverse planes near the two mirrors the two terms between the square brackets differ by phase factors $\exp(-ik\rho^{\rm T}\mathsf{F}_{1,2}^{-1}(t)\rho/2)$. For $z \simeq 0$ and $z \simeq L$ the electric field can be expressed as

$$\mathbf{E}_{\rm cav}(\mathbf{r},t) = 2\mathrm{Re}\left\{ \epsilon E_0 f_{1,2}(\rho,t) \sin\left(kz \mp \frac{k\rho^{\rm T}\mathsf{F}_{1,2}^{-1}\rho}{4} \right) e^{-i\omega t} \right\} , \tag{3.66}$$

where the $-$ and $+$ signs apply near mirror 1 and 2 respectively and $f_{1,2}(\rho,t)$ is the profile in the imaginary plane halfway the lenses in the lens guide picture. The sine term in equation (3.65) is the natural generalization of a standing wave to a field with transverse spatial structure. It shows that the electric field vanishes on the mirror surfaces even if the mode profiles halfway the mirrors $f_{1,2}(\rho,t)$ have phase structure so that the wave fronts of the field (3.65) do not fit on the mirror surfaces.

3.7 Spatial symmetries

As discussed in the previous chapter (section 2.5), the lens guide corresponding to a stationary two-mirror cavity has inversion symmetry in the imaginary planes halfway the lenses. Rotation breaks this symmetry and no spatial symmetries remain in the case of a rotating cavity with general astigmatism. This is different in the case of a rotating cavity with simple astigmatism. In this section, we give a more formal description of the inversion symmetry of a stationary cavity as well as of the spatial symmetries associated with simple astigmatism. We show that both survive in a modified fashion in the case of a rotating cavity with simple astigmatism.

3.7.1 Inversion symmetry of a stationary cavity

We consider inversion $z_{\rm s} + z \to z_{\rm s} - z$ of the lens guide with respect to a given transverse plane $z_{\rm s}$. As indicated in figure 3.2, the propagation direction of a ray $\theta = \partial\rho/\partial z$ picks up a minus sign under $z_{\rm s} + z \to z_{\rm s} - z$ so that the transformation of a ray $\mathscr{r}^{\rm T} = (\rho^{\rm T}, \theta^{\rm T})$ under this inversion is given by

$$\begin{pmatrix} \rho \\ \theta \end{pmatrix} \to N \begin{pmatrix} \rho \\ \theta \end{pmatrix} \qquad \text{with} \qquad N = \begin{pmatrix} 1 & 0 & 0 & 0 \\ 0 & 1 & 0 & 0 \\ 0 & 0 & -1 & 0 \\ 0 & 0 & 0 & -1 \end{pmatrix} \equiv \begin{pmatrix} 1 & 0 \\ 0 & -1 \end{pmatrix} . \tag{3.67}$$

As a result, the inverted transformation corresponding to a ray matrix M takes the following modified form

$$NM^{-1}N^{\rm T} = M . \tag{3.68}$$

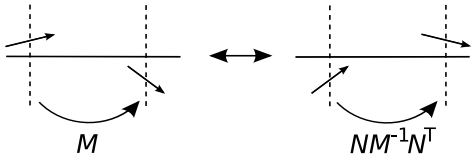

Figure 3.2: Inversion of an optical set-up. When both a ray trajectory and the elements of which the set-up consists are inverted with respect to some transverse plane z_s, the angles ϑ_x and ϑ_y, which specify the propagation direction of a ray, change sign. This is accounted for by the matrix N as defined in equation (3.67).

If the lens guide has inversion symmetry with respect to the plane $z = z_\mathrm{s}$, the ray matrix $M_\mathrm{rt}(z_\mathrm{s})$ that describes the transformation of a round trip starting from this plane must be equal to the corresponding inverted transformation, so that

$$NM_\mathrm{rt}^{-1}(z_\mathrm{s})N^\mathrm{T} = M_\mathrm{rt}(z_\mathrm{s}) \,. \tag{3.69}$$

In terms of the eigenvectors μ_i of the round-trip ray matrix $M_\mathrm{rt}(z_\mathrm{s})$, this symmetry property implies that

$$M_\mathrm{rt}(z_\mathrm{s})\mu_i(z_\mathrm{s}) = NM_\mathrm{rt}^{-1}(z_\mathrm{s})N^\mathrm{T}\mu_i(z_\mathrm{s}) = \lambda_i\mu_i(z_\mathrm{s}) \,, \tag{3.70}$$

where $\lambda_i = \exp(-i\chi_i)$ are the corresponding unitary eigenvalues. Using that $\mu_i^*(z_\mathrm{s})$ is an eigenvector of $M_\mathrm{rt}^{-1}(z_\mathrm{s})$ with eigenvalue λ_i, we find that inversion symmetry implies that

$$N\mu_i(z_\mathrm{s}) = \mu_i^*(z_\mathrm{s}) \,. \tag{3.71}$$

It follows that $r_i(z_\mathrm{s})$ and $\mathsf{R}(z_\mathrm{s})$ are real while $t_i(z_\mathrm{s})$ and $\mathsf{T}(z_\mathrm{s})$ are purely imaginary. As a result, both the fundamental mode (3.56) and the ladder operators (3.46) are real in the symmetry plane so that all modes are real in that plane.

Rotation obviously breaks the inversion symmetry in the transverse planes halfway the lenses and the round-trip ray matrix in the co-rotating frame (3.41) does not obey the identity (3.69). As a result the mode profiles halfway the lenses $f_{1,2}(\rho, t)$ are not real in general and contribute to the phase structure of the cavity field close to the mirrors (3.66).

3.7.2 Simple astigmatism

The lens guide corresponding to a stationary two-mirror cavity with simple astigmatism has symmetry directions parallel to the mirror axes in all transverse planes. These symmetry directions arise from the invariance of the cavity under reflections in the planes through the mirror axes and the cavity axis. In terms of the round-trip ray matrix $M(z)$, this symmetry

property can be expressed as

$$QM_{\mathrm{rt}}(z)Q^{\mathrm{T}} = M_{\mathrm{rt}}(z) \qquad \text{with} \qquad Q = \begin{pmatrix} 1 & 0 & 0 & 0 \\ 0 & -1 & 0 & 0 \\ 0 & 0 & 1 & 0 \\ 0 & 0 & 0 & -1 \end{pmatrix} \equiv \begin{pmatrix} \mathsf{Q} & 0 \\ 0 & \mathsf{Q} \end{pmatrix} . \tag{3.72}$$

The transformation Q describes a reflection in the xz plane. Similarly, $-Q$ describes a reflection in yz plane. In terms of the eigenvectors, this invariance (3.72) implies that $Q\mu_i(z) = \mu_i(z)$ so that $\mathsf{QR} = \mathsf{R}$ and $\mathsf{QT} = \mathsf{T}$. It follows that $u(\rho, z) = u(\mathsf{Q}\rho, z)$ so that the phase and intensity patterns of all the modes are aligned along the symmetry directions.

One may show easily that a stationary or rotating cavity with general astigmatism as well as a rotating cavity with simple astigmatism lacks the symmetry described by equation (3.72).

3.7.3 Rotating cavities with simple astigmatism

Rotation breaks both the inversion symmetry of a stationary cavity (3.69) and the spatial symmetries arising from simple astigmatism (3.72). As a result, no spatial symmetries remain in the case of a rotating cavity with general astigmatism. In the special case of a rotating cavity with simple astigmatism, however, one may prove explicitly that both symmetries survive when combined with inversion of the rotation direction $\Omega \to -\Omega$. These statements can be expressed as

$$QM_{\mathrm{rt}}(z;\Omega)Q^{\mathrm{T}} = M_{\mathrm{rt}}(z;-\Omega) , \tag{3.73}$$

and

$$NM_{\mathrm{rt}}^{-1}(z_{\mathrm{s}};\Omega)N^{\mathrm{T}} = M_{\mathrm{rt}}(z_{\mathrm{s}};-\Omega) , \tag{3.74}$$

where z_{s} is an inversion-symmetry plane and $M_{\mathrm{rt}}(z;-\Omega)$ is the ray matrix that describes the transformation of a round trip starting from a transverse plane z. The ray matrix $M_{\mathrm{rt}}(z;-\Omega)$ depends on the rotation frequency Ω according to equation (3.41). Combining equations (3.73) and (3.74) yields

$$QNM_{\mathrm{rt}}^{-1}(z;\Omega)(QN)^{\mathrm{T}} = M_{\mathrm{rt}}(z;\Omega) . \tag{3.75}$$

In terms of the eigenvectors $\mu_i(z;\Omega)$ this implies that

$$QN\mu_i(z;\Omega) = \mu_i^*(z;\Omega) , \tag{3.76}$$

from which we conclude that $\mathsf{QR}(z;\Omega) = \mathsf{R}^*(z;\Omega)$ and $\mathsf{QT}(z;\Omega) = -\mathsf{T}^*(z;\Omega)$ so that $v(\mathsf{Q}\rho, z) = v^*(\rho, z)$. As a result, the intensity patterns $|u(\rho, z, t)|^2$ of the modes of a rotating cavity with simple astigmatism are aligned along the mirror axes at all times, while the phase patterns are not.

3.8 Orbital angular momentum

In section 2.5.3, we have shown that the twisted boundary conditions that are imposed by a pair of non-parallel astigmatic mirrors induce orbital angular momentum in the modes of such a cavity. In the present case of a rotating cavity, we expect the twisted mode propagation in the rotating frame (3.31) combined with non-isotropic boundary conditions to give rise to orbital angular momentum as well. In this section we analyze the orbital angular momentum in rotating cavity modes. We discuss the contribution due to their phase structure and show that the physical rotation of the mode patterns contributes only in higher-order of δ. As a result this contribution is significant only in special cases where the orbital angular momentum due to the mode structure vanishes [19, 20].

The leading-order contribution to the orbital angular momentum per unit length in a monochromatic paraxial field is given by equation (2.80). The obvious extension of this result to the present case of polychromatic modes involves a summation over the frequency components $\omega + l\Omega$ with $l \in \mathbb{Z}$. Substitution of the spectral expansion (3.64) then gives the following expression for the orbital angular momentum in the rotating cavity modes (3.63)

$$\mathcal{L}_{nm} = \sum_{l=-\infty}^{\infty} \frac{\epsilon_0 |E_0|^2}{2(\omega + l\Omega)} \int_0^{2\pi} d\phi \int_0^{\infty} RdR\; l|g_{nml}(R,z)|^2 \,. \tag{3.77}$$

Using that the rotation frequency Ω is of the order of δ^2 smaller than the optical frequency ω, the leading-order contribution to the orbital angular momentum can be expressed as

$$\mathcal{L}^{(0)}_{nm} = \frac{\epsilon_0 |E_0|^2}{2\omega} \sum_{l=-\infty}^{\infty} \int_0^{2\pi} d\phi \int_0^{\infty} RdR\; l|g_{nml}(R,z)|^2 = N\hbar \langle v_{nm}(z)|\hat{\rho} \times k\hat{\theta}|v_{nm}(z)\rangle \,, \tag{3.78}$$

where the superscript (0) refers to the fact that this contribution is of order 0 in Ω/ω. This contribution obviously has the significance of the orbital angular momentum in the co-rotating frame and it is due to the spatial phase and intensity structure of the modes. Its dependence on the rotation frequency Ω can be traced back to fact that the round-trip ray matrix in the rotating frame (3.41) depends on Ω so that the same is true for the modes $|v_{nm}(z)\rangle$. In analogy with equation (2.81), this result (3.78) can be expressed in terms of the eigenvectors of the round-trip ray matrix (3.41)

$$\mathcal{L}^{(0)}_{nm} = N\hbar \left\{ \left(n + \frac{1}{2}\right) \mathrm{Re}\big(r_1^*(z) \times t_1(z)\big) + \left(m + \frac{1}{2}\right) \mathrm{Re}\big(r_2^*(z) \times t_2(z)\big) \right\} , \tag{3.79}$$

where $N = \epsilon_0 |E_0|^2/(2\hbar\omega)$ is the number of photons per unit length and $r_i(z)$ and $t_i(z)$ are related to the eigenvectors $\mu_i(z)$ of the round-trip ray matrix (3.41) by equations (3.51) and (3.49). Since free space is isotropic, $\mathcal{L}^{(0)}_{nm}$ is conserved under propagation from one mirror to the other. In the special case of a rotating cavity with simple astigmatism, the modified inversion symmetry (3.75) requires that the orbital angular momentum takes the same value $0 < z < L$ and $L < z < 2L$ so that the modes do not exert a torque on the mirrors. This

is not true if the cavity has general astigmatism. In that case both the astigmatism and the rotational deformation of the modes contribute to the orbital angular momentum, which takes different values in the two intervals of the lens guide. As a result, rotating modes with general astigmatism do exert a torque on the mirrors. However, also in the general-astigmatic case, there is net orbital angular momentum in the rotating cavity field. In this respect, rotating cavity modes with general astigmatism are different from their stationary counterparts.

The next-to-leading-order contribution to the orbital angular momentum is of the order of $\Omega/\omega \sim \delta^2$ smaller than the leading order term (3.78). It is non-negligible only in specific cases where the orbital angular momentum due to the spatial structure of the modes vanishes, for instance, for reasons of symmetry. It can be expressed as

$$\mathcal{L}^{(1)}_{nm} = -\frac{\epsilon_0 |E_0|^2 \Omega}{2\omega^2} \sum_{l=-\infty}^{\infty} \int_0^{2\pi} d\phi \int_0^{\infty} R dR \, l^2 |g_{nml}(R,z)|^2 \, . \tag{3.80}$$

This contribution is due to the fact that the mode patterns $u_{nm}(z,t)$ (3.64) in the laboratory frame rotate as a function of time. This general expression of the orbital angular momentum in a paraxial mode that does not possess orbital angular momentum in the co-rotating frame, is a slight generalization of the results in references [19] and [20]. A naive interpretation of the fact the rotational contribution to the orbital angular momentum is always negative would be that a light field has a negative moment of inertia. However, even in free space rotation has significant effects on the spatial and spectral structure of a light field so that it does not at all resemble a rigid body. As a result the concept of a moment of inertia is ill-defined in this wave-mechanical context [19, 20].

3.9 Examples

We illustrate some of the physical properties of rotating cavity modes by investigating two specific examples. We discuss the spatial structure of the intensity patterns of rotating cavity modes both in case of simple and in case of general astigmatism. The spectral structure of simple-astigmatic rotating cavity modes is discussed as well. Typical examples of the dependence of the orbital angular momentum on the rotation frequency are discussed in the next chapter, while the rotational deformation of the phase structure of optical cavity modes is discussed in detail in chapter 5.

3.9.1 Rotating simple astigmatism

The simplest realization of a uniformly rotating cavity consists of a stationary spherical and a rotating astigmatic (or cylindrical) mirror. In the absence of rotation the modes of such a cavity are astigmatic Hermite-Gaussian modes [12]. A cavity of this type has transverse symmetry directions parallel to the mirror axes along which the modes scale differently. Typical examples of the intensity patterns of astigmatic Hermite-Gaussian modes in the immediate neighborhood of the mirrors are shown in the upper windows in figure 3.3. Notice that the

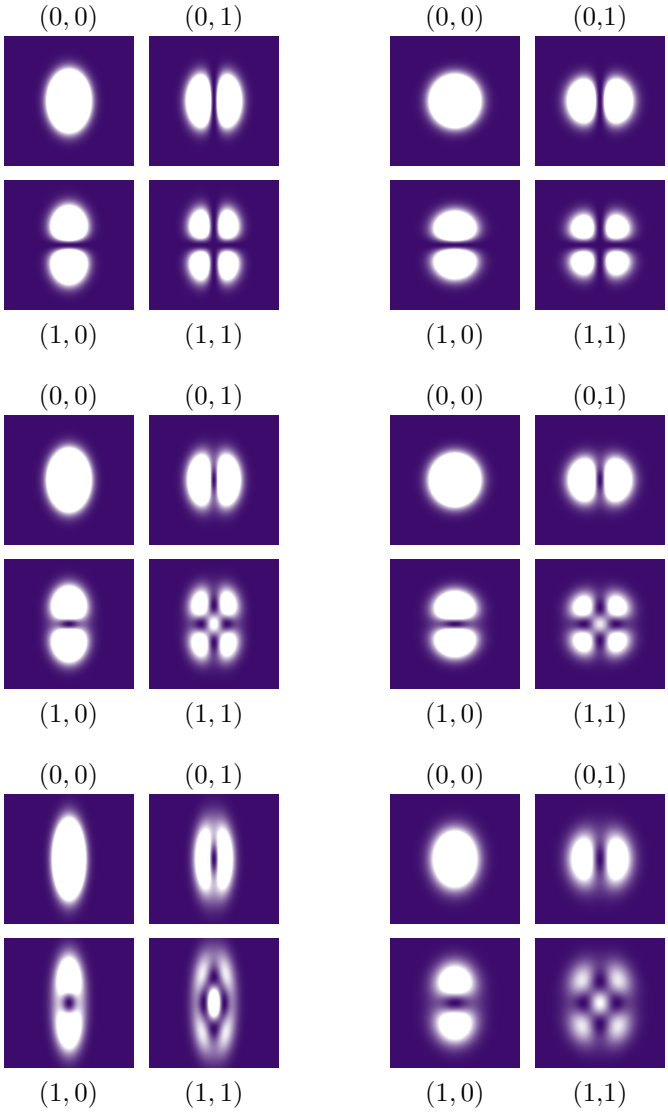

Figure 3.3: Intensity patterns of the $(0, 0)$, $(0, 1)$, $(1, 0)$ and $(1, 1)$ modes of the cavity between a stationary spherical and a rotating astigmatic mirror for different values of the rotation frequency Ω. The plots in the left column show the intensity patterns near the spherical mirror while the plots in right column show the intensity pattern near the astigmatic mirror. The radius of curvature of the spherical mirror is $4L$, where L is the mirror separation. The radius of curvature of the astigmatic mirror in the horizontal direction of the plot is equal to 2L while its radius of curvature in the vertical direction is 20L. From the top to the bottom the rotation frequency is increased from $\Omega = 0$ to $\Omega = c\pi/(30L)$ and $\Omega = c\pi/(6L)$.

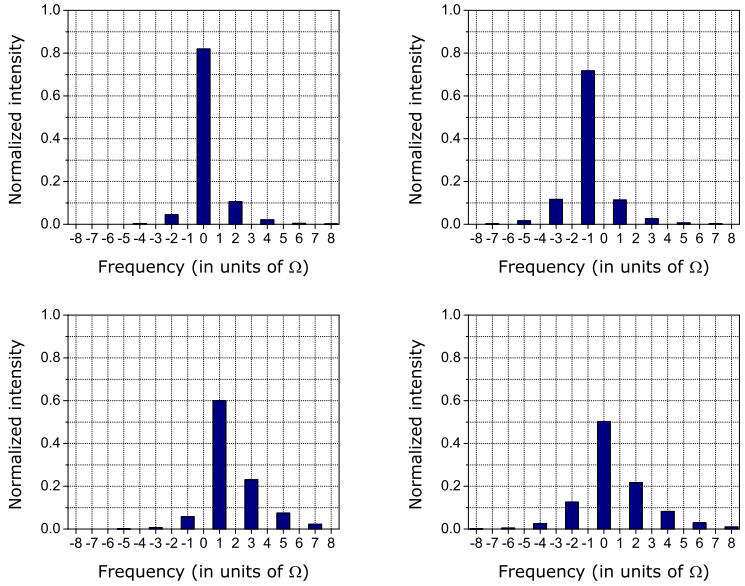

Figure 3.4: Spectral structure of the $(0,0)$, $(0,1)$, $(1,0)$ and $(1,1)$ modes of the cavity between a stationary spherical and rotating astigmatic mirror. The radius of curvature of the spherical mirror is equal to $4L$, where L is the mirror separation and the radii of curvature of the astigmatic mirror are equal to $2L$ and $20L$ respectively. The rotation frequency is equal to $\Omega = c\pi/(6L)$.

astigmatism of the intensity patterns is most pronounced on the spherical mirror. This is due to the fact that the astigmatism of a mirror is visible in the intensity pattern of the reflected beam only after free propagation over some distance.

If the astigmatic mirror is put into rotation the mode structure changes significantly. This is shown in the other two windows of figure 3.3. As a result of the rotation, the cavity is no longer invariant under reflection in the planes through the mirror axes and the cavity axis. In the special case of simple astigmatism, it is invariant under reflection in these planes combined with inversion of the rotation direction. As a result, the intensity patterns of the modes are still aligned along the mirror axes but the phase distributions are not. Rotation also breaks the inversion symmetry of the corresponding lens guide in the imaginary planes halfway the mirrors. As a result, the higher-order modes are no longer Hermite-Gaussian modes but generalized Gaussian modes with a nature in between Hermite- and Laguerre-Gaussian modes [44]. As a result, phase singularities (optical vortices) appear, which are best visible in the center of the $(0,1)$ and $(1,0)$ modes in figure 3.3.

The spectral structure of the rotating modes is illustrated in figure 3.4. These spectra show that the modes are confined spectrally and confirm that they only have odd or even

frequency components depending on the parity of the total mode number $n + m$. Due to the reflection symmetry in the planes through the mirror axes and the cavity axis, the orbital-angular-momentum spectrum of cavity modes with simple astigmatism is symmetric, i.e., $g_l(\rho) = g_{-l}(\rho)$ in the absence of rotation. Rotation breaks this symmetry, as is confirmed by the spectra in figure 3.4.

3.9.2 Rotating general astigmatism

The mode structure becomes significantly more complex if the cavity has general astigmatism, which is the case if it consists of two non-aligned astigmatic mirrors. Such a cavity does not have reflection symmetry planes through the optical axis. In the stationary case, the corresponding lens guide does have inversion symmetry in the imaginary plane halfway the lenses so that the higher-order modes close to the mirrors have the nature of astigmatic Hermite-Gaussian modes. Typical examples of the modes of a stationary astigmatic cavity with general astigmatism are shown in the upper window of figure 3.5.

At first sight one might guess that physical rotation of the mirrors effectively modifies their relative orientation so that it can help to reduce the effect of general astigmatism. This is not the case. The effect of rotation of the mirrors is essentially different from the effect of general astigmatism. This is illustrated in the lower window of figure 3.5. The rotation frequency is chosen such that the rotation angle after one round trip is equal but opposite to the angle between the orientations of the two mirrors. Putting the mirrors into physical rotation breaks the inversion symmetry so that the modes are no longer Hermite-Gaussian but generalized Gaussian modes that have general astigmatism. As a result, again, vortices appear.

3.10 Discussion and conclusion

In this chapter we have derived an algebraic method to obtain explicit expressions of the paraxial modes of an astigmatic optical cavity that is put into uniform rotation about its optical axis. Uniform rotation is homogeneous in time so that the explicit time-dependence of a rotating cavity can be eliminated by a transformation to the co-rotating frame. Its paraxial modes can then be obtained as solutions of the time-dependent paraxial wave equation (3.10) that are stationary in the rotating frame, i.e., rotate along with the mirrors in the laboratory frame. Up to first order of the paraxial approximation, the boundary condition that the electric field vanishes on the mirror surfaces is not affected by the transformation to the co-rotating frame. Mixing of the electric and magnetic fields is a second-order, relativistic, effect. The rotating cavity modes are thus obtained as stationary solutions in the co-rotating frame that vanish on the mirror surfaces. The regime of validity of the time-dependent paraxial wave equation provides a natural upper limit for the rotation frequency (3.12).

The method that we have used to derive expressions of the rotating cavity modes generalizes the ladder-operator method that we have introduced in the previous chapter to this

time-dependent case. It involves two pairs of bosonic ladder operators that generate a complete and orthogonal set of modes in the rotating frame (3.48). The transformation of the ladder operators from a reference plane in the co-rotating frame to an arbitrary transverse plane (3.54) can be expressed in terms of the 4×4 ray matrix that describes the linear transformation of a ray through the same system. As a result, the ladder operators that generate the cavity modes can be constructed from the eigenvectors of the ray matrix for a round trip in the co-rotating frame (3.41). Just as in the case of a cavity with stationary mirrors, geometric stability turns out to be the necessary and sufficient condition for the rotating cavity to have modes. The time-dependent expressions of the the modes $|u(z,t)\rangle$ in an external observer's frame can be obtained from the corresponding modes in the rotating frame $|v(z)\rangle$ by using equation (3.29).

In the rotating frame, the ray and wave dynamics is modified even though the ray matrices do not depend on time. In section 3.7, we have studied how rotation modifies the symmetry properties of a cavity and its modes while rotational effects on their orbital angular momentum were discussed in section 3.8. In section 3.9 we have shown how the mode structure is affected by rotation for different values of the rotation frequency and that the modes remain spectrally confined as well. In the last part of section 3.9 we have studied the interplay between general astigmatism and rotation. In both cases the cavity no longer has inversion symmetry so that the higher order modes are generalized Gaussian modes that have a nature in between Hermite-Gaussian and Laguerre-Gaussian modes with optical vortices.

The mode criterion that we have formulated in this chapter hinges upon the homogeneous time dependence of a rotating cavity and cannot be generalized to cavities with mirrors that rotate at different frequencies. In principle one can define the period of such a system by considering the number of round trips that is needed for both mirrors to return to positions that are equivalent to their initial positions. Once this period is determined, the method that we have developed here can be applied to find its modes, provided that the cavity is geometrically stable at all times. Preliminary numerical calculations, however, suggest that geometric stability is a heavy requirement in this, non-homogeneous, case.

The set-up that we have discussed in this chapter is hard to realize experimentally. In section 5.5 we shall discuss several possible routes towards experimental realization of a set-up that captures the essential optical properties a rotating astigmatic two-mirror cavity. Moreover, the methods that we have developed here provide a much more general framework to cope with propagation and retardation in optical set-ups that have elements with time-dependent settings. The only restriction is that the time-dependent paraxial approximation, which we have formulated in section 3.2, is justified.

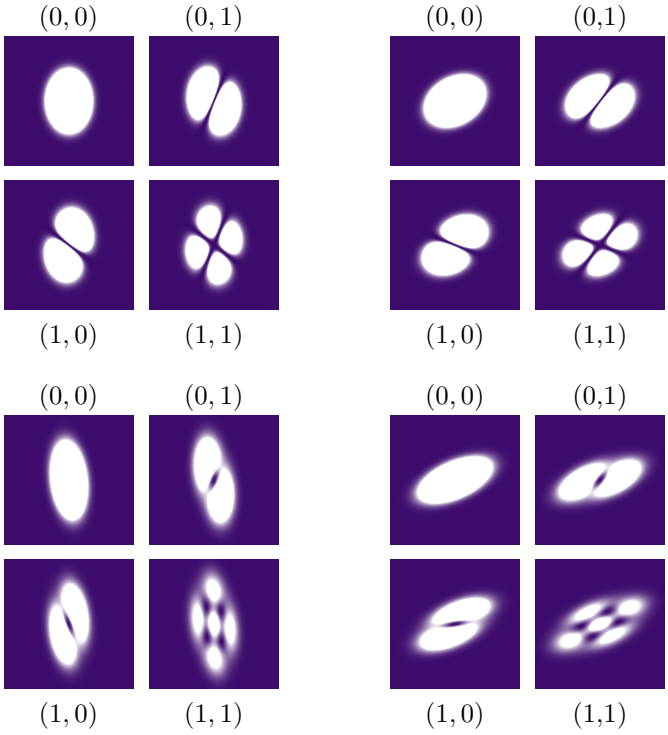

Figure 3.5: Modes of an optical cavity between two identical but non-aligned rotating astigmatic mirrors for different rotation frequencies. The mirrors have radii of curvature that are equal to $2L$ and $20L$. The axes of the right mirror coincide with the horizontal and vertical directions of the plots while the axes of the left mirror are rotated over an angle $-\pi/3$. From the top to the bottom the rotation frequency is increased from $\Omega = 0$ to $\Omega = c\pi/(6L)$. The latter frequency is chosen such that the angle over which the mirrors are rotated after each round trip is equal but opposite to the angle between the orientations of the two mirrors.

4

Rotational stabilization and destabilization of an optical cavity

4.1 Introduction

Stability is a very distinctive property of the dynamics of a physical system. Characteristic for unstable dynamics is that an arbitrary initial state evolves into a rapidly diverging state. Examples range from the simple case of a particle on the top of a hill to a wealth of instabilities that can be observed and characterized in fluids and plasmas. External motion has significant effects on the dynamics of physical systems and may modify its stability properties. This is exemplified by the Paul trap [50], or more generally by a time-orbiting potential trap [51], in which a particle is trapped in an oscillating potential from which it would escape in the stationary case. The Paul trap is a close analogue of the rotational stabilization of a particle in a saddle-point potential [52]. Another well-known example of rotational stabilization is the gyroscope. Similar behavior has also been observed in thermodynamically large systems such as granular matter [53] and fluids [54].

In recent years, optical cavities with moving elements have become topical. State-of-the-art experiments focus on opto-mechanical oscillators driven by radiation pressure [55, 56] and cavity-assisted trapping and cooling [57, 58, 59]. Possible applications range from weak-force detection [60] to fundamental research on quantum entanglement [61, 62] and decoherence [63, 64] on macroscopic scales. In addition to the longitudinal radiation pressure, electromagnetic fields can exert transverse forces due to their phase structure [65]. A specific

example is the transfer of optical orbital angular momentum [21], which can give rise to a torque along the propagation axis of the beam. Recently, it has been shown that this torque can in principle be sufficiently large to trap and cool the rotational degrees of freedom of a mirror in a cavity-assisted set-up [25]. In this chapter, we focus on the complementary question: How does rotation of a mirror affect the optical properties of a cavity and, in particular, its (in)stability? As such, the work presented here constitutes the first analysis of rotational effects on stability in optics.

We consider a cavity that consists of two mirrors facing each other. In the standard case both mirrors are spherical. Depending on their focusing properties, a ray that is coupled into such a cavity can either be captured, or escape after a finite (and typically small) number of round trips. In the latter case the cavity is geometrically unstable whereas it is stable in the former one. The stability criterion for this system can be expressed as [12]

$$0 < g_1 g_2 < 1 \,, \tag{4.1}$$

where $g_{1,2} = 1 - L/R_{1,2}$ with $R_{1,2} = 2f_{1,2}$ the radii of curvature of the two mirrors, $f_{1,2}$ the corresponding focal lengths and L the mirror separation. The optical properties of unstable cavities are fundamentally different from those of their stable counterparts [12]. Since a geometrically stable cavity has the ability to confine light, its modes are spatially confined and stationary. An unstable cavity, on the other hand, cannot confine light and is intrinsically lossy even if the mirrors are perfectly reflecting. As a result, the propagation of light inside an unstable cavity is dominated by diffraction at the sharp edges of the mirrors [66] and its "modes" are self-similar diverging patterns that have a fractal nature [67]. Instability is a necessary condition for an optical cavity to display chaotic behavior [68].

We consider rotations about the optical axis of a cavity and expect an effect only if at least one of the mirrors is astigmatic (or cylindrical), so that the cavity lacks axial symmetry. In general, both mirrors can be astigmatic with non-parallel axes but, for simplicity, we first focus on a cavity that consists of a cylindrical (c) and a spherical (s) mirror. The more general case of a cavity with two astigmatic mirrors is briefly discussed in section 4.4. In the simple case of a cavity with one spherical and one astigmatic mirror, the curvature of each mirror can be specified by a single g parameter so that the configuration space, spanned by g_s and g_c, is two-dimensional. In the absence of rotation the stability criterion in the plane through the optical axis in which the cylindrical mirror is curved is of the form of equation (4.1): $0 < g_\mathrm{s} g_\mathrm{c} < 1$. In the other perpendicular plane through the cavity axis, in which the cylindrical mirror is flat, the stability criterion reads: $0 < g_\mathrm{s} < 1$. As is indicated in the stability diagram in the upper left window in figure 4.1, stable (dark blue) areas appear where both criteria are met. The cavity is partially stable (light blue) in areas where only one of the two is fulfilled. When a cavity is partially stable, both a ray that is coupled into it and its modes are confined in one of the two transverse directions only. One may guess that rotation disturbs the confinement of the light by the mirrors so that all (partially) stable cavities will eventually lose stability if the rotation frequency is sufficiently increased. However, we will show that this is not the case and that rotation has surprisingly rich and distinct effects on the

stability of a two-mirror cavity.

4.2 Stability of a rotating cavity

In order to describe the diffraction of light inside a rotating cavity, we use the paraxial approximation [45] and its generalization to the time-dependent case [46]. We write the transverse electric field of a propagating mode as

$$\mathbf{E}(\mathbf{r},t) = \mathrm{Re}\left\{E_0 \epsilon u(\mathbf{r},t) e^{ikz-i\omega t}\right\} , \tag{4.2}$$

where E_0 is the amplitude of the field, ϵ is the polarization, k is the wave number and $\omega = ck$ is the optical frequency with c the speed of light. The large-scale spatial structure and slow temporal variations of the electric field are characterized by the complex scalar profile $u(\mathbf{r},t)$. In lowest order of the paraxial approximation and under the assumption that the time dependence of the profile is slow compared to the optical time scale, the electric field is purely transverse and the profile $u(\mathbf{r},t)$ obeys the time-dependent paraxial wave equation

$$\left(\nabla_\rho^2 + 2ik\frac{\partial}{\partial z} + \frac{2ik}{c}\frac{\partial}{\partial t}\right) u(\mathbf{r},t) = 0 , \tag{4.3}$$

with $\nabla_\rho^2 = \partial^2/\partial x^2 + \partial^2/\partial y^2$. If we omit the derivative with respect to time, this equation reduces to the standard paraxial wave equation, which describes the diffraction of a freely propagating stationary paraxial beam. The additional time derivative accounts for the time dependence of the profile and incorporates retardation between distant transverse planes.

The dynamics of light inside a cavity is governed by the boundary condition that the electric field vanish on the mirror surfaces. For a rotating cavity, this boundary condition is explicitly time dependent. This homogeneous time dependence vanishes in a co-rotating frame where it is sufficient to consider time-independent propagating modes $v(\mathbf{r})$. The transformation that connects $v(\mathbf{r})$ and $u(\mathbf{r},t)$ takes the form

$$u(\mathbf{r},t) = \hat{U}_{\mathrm{rot}}(\Omega t) v(\mathbf{r}) , \tag{4.4}$$

where Ω is the rotation frequency and $\hat{U}_{\mathrm{rot}}(\alpha) = \exp(-i\alpha\hat{L}_z)$ is the operator that rotates a scalar function over an angle α about the z axis with $\hat{L}_z = -i(x\partial/\partial y - y\partial/\partial x)$ the z component of the orbital angular momentum operator. Substitution of the rotating mode (4.4) in the time-dependent wave equation (4.3) gives

$$\left(\nabla_\rho^2 + 2ik\frac{\partial}{\partial z} + \frac{2\Omega k}{c}\hat{L}_z\right) v(\mathbf{r}) = 0 \tag{4.5}$$

for $v(\mathbf{r})$. The transformation to a rotating frame gives rise to a Coriolis term, in analogy with particle mechanics. Since ∇_ρ^2 and $\hat{L}_z$ commute, the formal solution of equation (4.5) can be expressed as

$$v(\rho,z) = \hat{U}_{\mathrm{f}}(z)\hat{U}_{\mathrm{rot}}\left(-\frac{\Omega z}{c}\right) v(\rho,0) \equiv \hat{U}(z) v(\rho,0) , \tag{4.6}$$

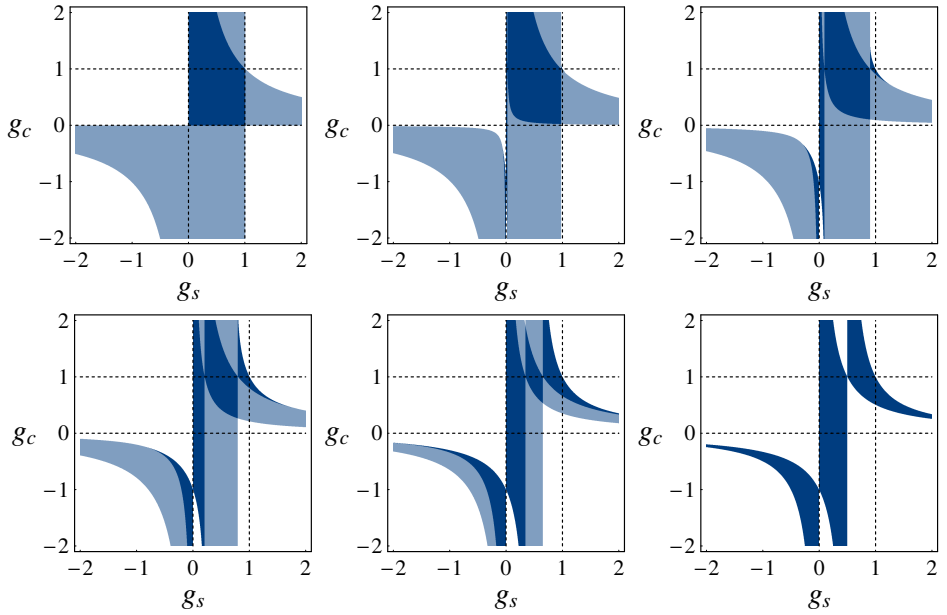

Figure 4.1: Stable (dark blue), partially stable (light blue) and unstable (white) areas of the configuration space (g_s, g_c) for a cavity that consists of a stationary spherical and a rotating cylindrical mirror, for different rotation frequencies. From left to right and from top to bottom the rotation frequency is increased in equal steps $\Omega_0/20$ from 0 to $\Omega_0/4$.

where $\rho = (x, y)^{\mathrm{T}}$ and $\hat{U}_{\mathrm{f}}(z) = \exp\left(\frac{iz}{2k}\nabla_\rho^2\right)$ is the unitary operator that describes free propagation of a paraxial beam in a stationary frame. The operator $\hat{U}(z)$ has the significance of the propagator in the rotating frame. The rotation operator arises from the Coriolis term in equation (4.5) and gives the propagating modes a twisted nature.

The transformation of paraxial modes under propagation and optical elements can be expressed in terms of a ray ($ABCD$) matrix [12, 32]. The standard 2×2 ray matrices that describe optical elements with axial symmetry can be found in any textbook on optics. The ray matrix of a composite system can be constructed by multiplying the ray matrices that describe the optical elements and the distances of free propagation between them, in the proper order. Generalization to astigmatic optical elements is straightforward and requires 4×4 ray matrices [12]. The ray matrix that describes propagation in a rotating frame is, analogous to equation (4.6), given by $M(z) = M_{\mathrm{f}}(z)M_{\mathrm{rot}}(-\Omega z/c)$, where $M_{\mathrm{f}}(z)$ is the 4×4 ray matrix that describes free propagation over a distance z and $M_{\mathrm{rot}}(\alpha)$ is the 4×4 ray matrix that rotates the position ρ and propagation direction θ of a ray $\mathscr{z}^{\mathrm{T}} = (\rho^{\mathrm{T}}, \theta^{\mathrm{T}})$ over an angle α about the z axis. Starting at the entrance plane of the spherical mirror, the time-independent ray matrix that describes a round trip through the rotating cavity in the co-rotating frame is

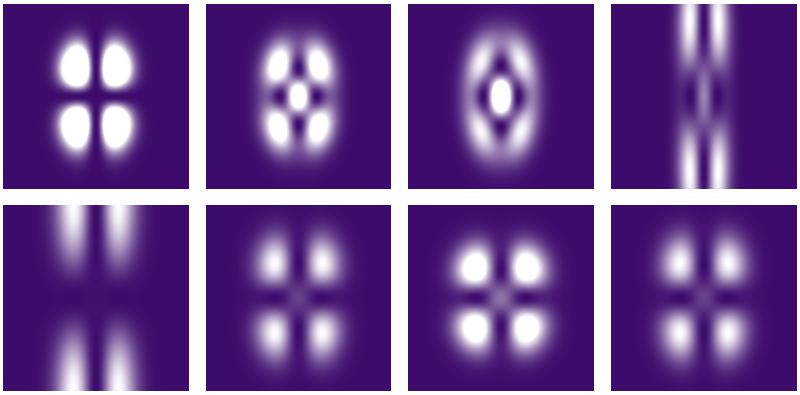

Figure 4.2: Transverse intensity patterns in the co-rotating frame of the $(1, 1)$ mode of cavity I (top), which is specified by $(g_s, g_c) = (\frac{3}{4}, \frac{1}{2})$ and destabilized by rotation, and cavity II (bottom), which is specified by $(g_s, g_c) = (-\frac{3}{4}, -\frac{1}{2})$ and stabilized by rotation, for increasing rotation frequencies. From left to right it increases from 0 to $0.166\Omega_0$ for cavity I and from $0.21\Omega_0$ to $\Omega_0/4$ for cavity II. The plots show the mode patterns close to the spherical mirror and the vertical direction corresponds to the direction in which the cylindrical mirror is flat.

then

$$M_{\mathrm{rt}} = M(L) \cdot M_{\mathrm{c}} \cdot M(L) \cdot M_{\mathrm{s}} \,, \tag{4.7}$$

where L is the mirror separation and M_{s} and M_{c} are the ray matrices for the spherical and the cylindrical mirror. They are fully determined by the radii of curvature and the orientation of the mirrors in the transverse plane. Explicit expressions of these ray matrices are given in sections 2.2 and 3.5.

Typically, the round-trip ray matrix (4.7) has four distinct time-independent eigenvectors μ_i with corresponding eigenvalues λ_i. In the rotating frame, any time-dependent incident ray $\mathscr{r}_0^{\mathrm{T}}(t) = \left(\rho^{\mathrm{T}}(t), \theta^{\mathrm{T}}(t)\right)$ can be expanded as $\mathscr{r}_0(t) = \sum_i a_i(t)\mu_i$. After n times bouncing back and forth between the mirrors, the ray evolves into $\mathscr{r}_n(t + 2nL/c) = \sum_i a_i(t)\lambda_i^n\mu_i$. The possibly complex eigenvalues have the significance of the magnification of the eigenvector after one round trip and it follows that a cavity is stable only if all four eigenvalues have absolute value 1. As shown in chapter 2, the eigenvalues of any physical ray matrix come in pairs λ and λ^{-1} so that possible deviations from $|\lambda| = 1$ appear in two of the four eigenvalues at the same time. If only two eigenvalues have absolute value 1, the cavity is partially stable. The eigenvalues of the round-trip ray matrix (4.7) do not depend on the frame of reference, and it follows that the same is true for the notion of stability.

A ray that is bounced back and forth inside the cavity hits a mirror at time intervals L/c. Since a rotation over π turns an astigmatic mirror to an equivalent orientation, it follows that the stability of a cavity is not affected by a change in the rotation frequency $\Omega \to \Omega + p\Omega_0$

with integer p and $\Omega_0 = c\pi/L$. In the present case, in which one of the mirrors is spherical, a ray hits the cylindrical mirror at time intervals $2L/c$ so that the eigenvalues λ_i are periodic with $\Omega_0/2$. Moreover, an astigmatic cavity is not gyrotropic so that the eigenvalues do not depend on the sign of Ω. It follows that it is sufficient to only consider rotation frequencies in the range $0 < \Omega < \Omega_0/4$.

By using the expression of the ray matrix in the co-rotating frame (4.7) and the stability criterion that its eigenvalues must have a unit length, we find the stable, partially stable and unstable sections in the configuration space $(g_\mathrm{s}, g_\mathrm{c})$ for different values of the rotation frequency. The results are shown in figure 4.1. These plots reveal that, already at relatively small rotation frequencies, quite drastic changes take place. For instance, near $(g_\mathrm{s}, g_\mathrm{c}) = (1, 0)$ stable configurations are destabilized to become (partially) unstable, while partially stable geometries near the negative g_c axis are stabilized by the rotation. An optical cavity can thus both lose and gain the ability to confine light due to the fact that it rotates. It is noteworthy that some configurations, for example those with small and positive g_s and g_c, are first partially destabilized by rotation, but retrieve stability if the rotation frequency is further increased. Another remarkable feature of the plots in figure 4.1 is the absence of partially stable areas in the lower right plot. As we will argue below, this is more generally true for the rotation frequency $\Omega_0/4$. In this specific case, the boundaries of stability are given by the hyperbolas $g_c = 1/(2g_s)$ and $g_c = 1/(2g_s - 1)$ and their asymptotes.

4.3 Signatures of stabilization and destabilization

As discussed in chapter 3, the structure of the modes of a rotating cavity is fully determined by the eigenvectors μ_i. The modes are defined as co-rotating solutions of the time-dependent paraxial wave equation (4.3) that vanish on the mirror surfaces. Geometric stability comes in as the necessary and sufficient requirement for them to exist. Here, we illustrate the effect of rotational (de)stabilization on the mode structure by considering two cases of a cavity with a spherical and a cylindrical mirror. Cavity I is specified by $(g_\mathrm{s}, g_\mathrm{c}) = (\frac{3}{4}, \frac{1}{2})$. It is stable in the absence of rotation and destabilized at a rotation frequency $\Omega = \Omega_0/6$. Cavity II is specified by the parameter values $(g_\mathrm{s}, g_\mathrm{c}) = (-\frac{3}{4}, -\frac{1}{2})$. It is partially stable in the absence of rotation and stabilized by rotation at $\Omega \simeq 0.2098\Omega_0$. The effect of rotation on the spatial structure of the modes of cavities I and II is shown in figure 4.2. The upper frames show the transverse spatial structure on the spherical mirror of the $(1, 1)$ mode of cavity I. From left to right the rotation frequency increases from 0 to $0.166\Omega_0$ in equal steps. In the absence of rotation (left frame) the mode is an astigmatic Hermite-Gaussian mode. Due to rotation, the mode is deformed to a generalized Gaussian mode with a nature in between Hermite-Gaussian and Laguerre-Gaussian modes [44]. As a result, phase singularities or so-called optical vortices [14], which are visible as points with zero intensity, appear. For rotation frequencies close to $\Omega_0/6$, the mode loses its confinement in the vertical direction. This reflects the fact that the cavity approaches a region of partial instability. The lower frames in figure 4.2 show the intensity pattern on the spherical mirror of the $(1, 1)$ mode of cavity II, which is stabilized

by rotation. From left to right the rotation frequency is increased from $0.21\Omega_0$ to $0.25\Omega_0$ in equal steps. As a result of the rotation we retrieve a mode that is confined in both directions and is similar to a Hermite-Gaussian mode. Deformation of the mode due to the rotation is more pronounced for even larger values of the rotation frequency.

Obviously, the horizontal and vertical directions in figure 4.2, which correspond to the curved and flat directions of the cylindrical mirror, are lines of symmetry. In the special case of a rotation frequency $\Omega_0/4$, the cylindrical mirror is rotated over $\pi/2$ after each round trip so that its orientation is periodic with two round-trip times as a period. This causes the diagonal lines between the horizontal and vertical directions to be lines of symmetry of the round-trip ray matrix (4.7) and the intensity patterns. This explains the apparent absence of astigmatism in the lower right plot of figure 4.2. This additional symmetry also causes the four eigenvalues λ_i to have the same absolute value, which explains the absence of partial stability in the lower right plot of figure 4.1.

Although the intensity patterns of the modes are aligned along the axes of the cylindrical mirror, their phase patterns are not. These attain a twist that is a signature of orbital angular momentum [21, 17], proportional to $\int d\rho v^*(\rho, z)\hat{L}_z v(\rho, z)$. The dependence of this orbital angular momentum in the $(1, 1)$ mode of cavity I on the rotation frequency is shown in figure 4.3 (left plot). The orbital angular momentum shows a divergence at $\Omega_0/6$, which arises from the induced instability of the cavity. The opposite happens for cavity II (right plot), which is stabilized by rotation. In this case the orbital angular momentum decreases with increasing rotation frequencies and eventually vanishes for $\Omega = \Omega_0/4$ due to the additional symmetry at this specific rotation frequency. The vanishing orbital angular momentum does not imply that there is no vorticity in the modes at this rotation frequency. The two contributions to the orbital angular momentum add up to zero for modes with two equal mode numbers.

4.4 Two astigmatic mirrors

Some features of the set-up that we have discussed so far are specific for the relatively simple geometry we have looked at. In particular, the plots in figure 4.1 show that no cavity with one spherical and one cylindrical mirror that is unstable in the absence of rotation can be (partially) stabilized by rotation. This is different in more general cases. As an example, we consider a cavity with two astigmatic mirrors. We take one of the radii of curvature of each of the mirrors fixed while we vary the others. In this case the corresponding parameter space, spanned by the g parameters corresponding to the varying radii of curvature, is again two-dimensional. The radii of curvature are chosen such that the g parameters are given by $(3/4, g_1)$ for mirror 1 and $(g_2, 3/4)$ for mirror 2. The alignment of the mirrors is such that the g_1 direction of mirror 1 is parallel to the $3/4$ direction of mirror 2 (and vice versa) so that the cavity has simple astigmatism. In the absence of rotation each of the symmetry planes through the mirror axes and the cavity axis can be considered as a cavity with two spherical mirrors. The corresponding stability criteria are given by $0 < 3g_1/4 < 1$ for one symmetry plane and $0 < 3g_2/4 < 1$ for the other. As is indicated in the upper left window in figure 4.4,

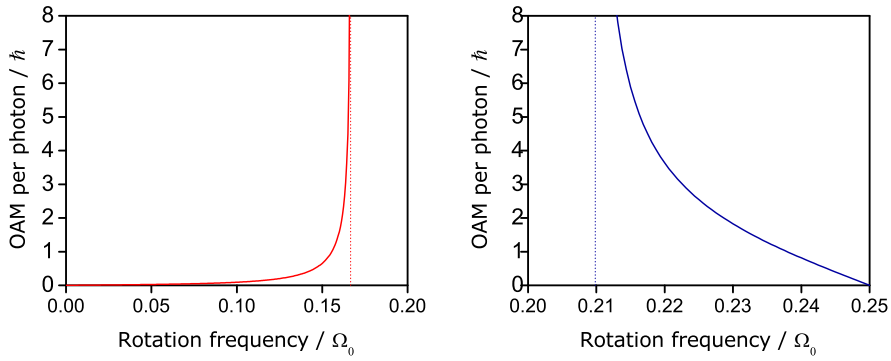

Figure 4.3: Dependence on the rotation frequency of the orbital angular momentum per photon in the $(1, 1)$ mode of cavity I (left), which is destabilized by rotation, and cavity II (right), which is stabilized by rotation.

these criteria are met in strips in the configuration space (g_1, g_2). A cavity with two astigmatic mirrors lacks the additional symmetry at $\Omega_0/4$ so that we need to consider rotation frequencies in the range $0 < \Omega < \Omega_0/2$. As the other windows in figure 4.4 reveal, again rotation has profound effects on the (in)stability of the cavity. One of the striking differences with the plots in figure 4.1 is that some unstable geometries, in particular close to $(g_1, g_2) = (1, 1)$ are fully stabilized by rotation at relatively small values of the rotation frequency. At the specific value of the rotation frequency $\Omega_0/2$, the mirrors are rotated over $\pi/2$ while the light propagates from one mirror to the other. From the stability point of view, this situation is equivalent to the case in which the mirrors are in the anti-parallel alignment and non-rotating. In that case, the stability criteria can be expressed as $0 < g_1 g_2 < 1$, which gives rise to hyperbolic boundaries of stability, and $0 < 9/16 < 1$, which is always fulfilled. As a result the cavity is partially stable in all cases and fully stable between the hyperbola $g_1 = 1/g_2$ and the $g_1 = 0$ and $g_2 = 0$ axes in the configuration space. This is confirmed by the stability diagram in the lower right window in figure 4.4. As a result of the fact that all geometries are (at least) partially stable at the rotation frequency $\Omega_0/2$, there is a strange discontinuity in the stability diagrams. Here, it occurs at $\Omega \simeq 0.27\Omega_0$. At this value of the rotation frequency many unstable geometries are suddenly partially stabilized while stable geometries are fully destabilized. Partially stable configurations are both stabilized to become stable and destabilized to become unstable. However, no configurations are stable through this sharp transition, which, physically speaking, corresponds to the boundary between "similar to anti-parallel alignment" and "similar to parallel alignment" of the mirrors.

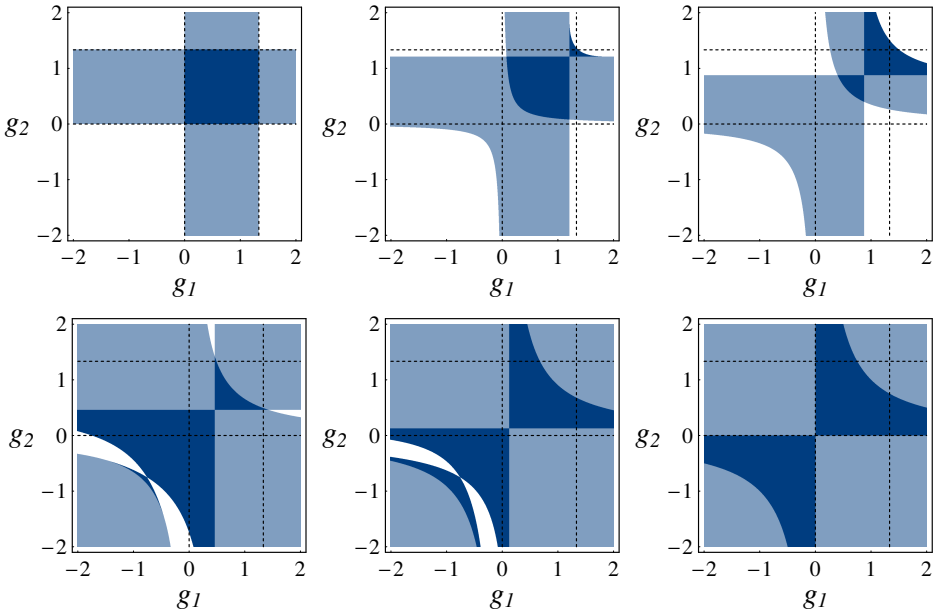

Figure 4.4: Stable (dark blue), partially stable (light blue) and unstable (white) areas of the configuration space (g_1, g_2) for a cavity that consists of two astigmatic mirrors, for different rotation frequencies. The g parameters corresponding to the radii of curvature of mirror 1 are given by $(3/4, g_1)$ while the g parameters for mirror 2 are given by $(g_2, 3/4)$. From left to right and from top to bottom the rotation frequency is increased in equal steps $\Omega_0/20$ from 0 to $\Omega_0/4$.

4.5 Conclusion

We have investigated rotationally induced transitions between the areas of stability and partial instability of an astigmatic two-mirror cavity. This is the first example of an optical system where stability can be induced or removed by rotation. Mechanical systems with dynamical stabilization are the Paul trap and the gyroscope. The most obvious signatures of rotational (de)stabilization are the modification of the mode confinement and the divergence of the orbital angular momentum, discussed in section 4.3 and respectively shown in figures 4.2 and 4.3. The spatial structure of the rotating cavity modes may be difficult to measure, but since their orbital angular momentum components appear at different frequencies due to the rotational Doppler shift [48, 69], it should be possible to resolve the divergence of the orbital angular momentum spectroscopically. The effects of transverse rotations on the optical properties of a cavity are significantly more complex than the resonance shifts that are associated with small longitudinal displacements of the mirrors. This may have important consequences in cavity-assisted opto-mechanical experiments in which the rotational degrees of freedom of

a mirror are addressed.

Although the set-up that we have studied here is rather specific, our method, which is exact in the paraxial limit, can be applied to more complex optical systems. Moreover, it should also be applicable to other, mathematically similar, wave-mechanical systems. Examples include the quantum-mechanical description of a particle in a rotating, partially stable potential and rotating acoustical cavities. In particular, the modification of the mode confinement and the rotationally induced angular momentum are expected to have analogues in such systems.

5

Rotationally induced vortices in optical cavity modes

5.1 Introduction

Rotation is a very natural source of vorticity: when a glass of water is stirred, a vortex appears at the center. Such a vortex is a singularity of the water current and it is of the same type as the vortex that appears above a sink. When a glass of water is put into uniform rotation, for instance by placing it on a turntable, the water current vanishes at the rotation axis but is not singular. It has been known for over half a century that this is different in case of a superfluid [70]. Due to the zero viscosity of, and the vortex quantization in, a superfluid, uniform rotations induce a regular pattern of equally charged vortices. Vortices appear only if the rotation frequency exceeds a certain critical value and their number increases if the rotation frequency is further increased. Eventually rotation may destabilize the superfluid. More recently, similar experiments have been performed with Bose-Einstein condensates of dilute gases both by optically stirring the condensate [71] and by trapping it in a rotating elliptical potential [72].

During the past decades, optical vortices and their propagation have attracted a significant amount of attention [73, 74, 75, 76, 77, 78]. An optical vortex is a singularity of the phase of an optical beam and is characterized by its position in the transverse plane, its topological charge and its morphology. The vortex charge is determined by the total phase change $2\pi q$ along a contour around the vortex center and must be integer for reasons of continuity. As

opposed to the vortices that appear in superfluids and Bose-Einstein condensates, optical vortices can be elliptical; their morphology is characterized by the partial derivatives of the beam profile close to the vortex center and can be represented by a point on a sphere [79]. The polar angle on the sphere determines the degree of ellipticity while the azimuthal angle fixes the orientation in the transverse plane. The interplay between astigmatism and the propagation of optical vortices may give rise to very rich behavior [80, 81, 82]. The dynamics of optical vortices in a laser cavity has also been studied [83].

In view of the recent interest in effects of rotating elements on optical beams [69] and the physical properties of rotating mode patterns [19, 20], the above-mentioned examples of rotationally induced vortices in material systems raise the question if and how rotation induces vorticity in light fields [84]. In this chapter we address this topic by studying the optical properties of a two-mirror cavity that is put into rotation about its optical axis. This set-up is schematically drawn in figure 5.1. We expect an effect of rotation only if the cavity lacks rotational symmetry. In analogy with the rotating elliptical potential in which Bose-Einstein condensates can be trapped, we break the rotational symmetry by taking at least one of the mirrors cylindrical or astigmatic. In the absence of rotation, such a cavity has astigmatic Hermite-Gaussian modes [12], which have lines of zero intensity (line dislocations) in the transverse plane. We show that rotation deforms the cavity modes into generalized Gaussian modes [44] and that the line dislocations are deformed into optical vortices (point singularities in the transverse plane). We study the properties of these rotationally induced optical vortices.

This chapter is organized as follows. In the next section we briefly review the propagation of optical fields through time-dependent systems, focus on the specific case of a rotating astigmatic cavity and summarize the ladder-operator method that we have introduced in chapter 3. In the third section, we characterize the degrees of freedom associated with the astigmatism and vorticity of the rotating cavity modes and apply the analogy with the quantum-mechanical harmonic oscillator to derive analytical expressions of the rotating cavity modes. These are used to discuss some general properties of the vortices that appear in these modes. In the fourth section we show and discuss some explicit results for a specific realization of a uniformly rotating two-mirror cavity.

5.2 Paraxial wave optics between rotating mirrors

5.2.1 Mode propagation in a rotating cavity

The mathematical description of the propagation of light through optical systems simplifies significantly if the paraxial approximation is applied. This approximation is almost always justified in experimental set-ups with optical beams. In the present case of a rotating cavity, we must account for effects that arise from the time dependence of the mirror settings. Assuming that the rotation frequency Ω is much smaller than the optical frequency ω, we use the generalization of the paraxial approximation to the time-dependent case [46]. In this approximation, the electric field is purely transverse. For a propagating mode it can be written

as

$$\mathbf{E}(\mathbf{r},t) = \mathrm{Re}\left\{E_0 \epsilon u(\mathbf{r},t) e^{ikz - i\omega t}\right\} , \tag{5.1}$$

where E_0 is the amplitude of the field, ϵ is the transverse polarization, k is the wave number and $\omega = ck$ is the optical frequency with c the speed of light. The complex scalar profile $u(\mathbf{r},t)$ characterizes the large-scale spatial structure and slow temporal variations of the field. It obeys the time-dependent paraxial wave equation

$$\left(\nabla_\rho^2 + 2ik\frac{\partial}{\partial z} + \frac{2ik}{c}\frac{\partial}{\partial t}\right) u(\rho,z,t) = 0 , \tag{5.2}$$

with $\rho = (x,y)^{\mathrm{T}}$ and $\nabla_\rho^2 = \partial^2/\partial x^2 + \partial^2/\partial y^2$ is the transverse Laplacian. If we omit the derivative with respect to time, this equation reduces to the standard paraxial wave equation, which has the same form as the Schrödinger equation for a free particle in two dimensions, z playing the role of time. It describes the diffraction of a freely propagating stationary paraxial beam. The time derivative in equation (5.2) accounts for the time dependence of the profile and incorporates retardation between distant transverse planes.

In addition to diffraction, the propagation of the light inside a cavity is governed by the boundary condition that the electric field must vanish on the mirror surfaces. In case of a rotating cavity this boundary condition is explicitly time dependent. A natural way to eliminate this time dependence is by transforming to a co-rotating frame, where it is sufficient to consider the behavior of time-independent propagating modes $v(\mathbf{r})$. The transformation that connects the profile in the rotating frame to the profile in the stationary frame can be expressed as

$$u(\rho,z,t) = \hat{U}_{\mathrm{rot}}(\Omega t) v(\rho,z) , \tag{5.3}$$

where Ω is the rotation frequency and $\hat{U}_{\mathrm{rot}}(\alpha) = \exp(-i\alpha\hat{L}_z)$ is the operator that rotates a scalar function over an angle α about the z axis with $\hat{L}_z = -i(x\partial/\partial y - y\partial/\partial x)$ the z component of the orbital angular momentum operator. Substitution of the rotating mode (5.3) in the time-dependent paraxial wave equation (5.2) yields the wave equation for $v(\rho,z)$

$$\left(\nabla_\rho^2 + 2ik\frac{\partial}{\partial z} + \frac{2\Omega k}{c}\hat{L}_z\right) v(\rho,z) = 0 . \tag{5.4}$$

In the rotating frame, the retardation term is replaced by a Coriolis term, which is familiar from particle mechanics. Since ∇_ρ and $\hat{L}_z$ commute, the formal solution of the paraxial wave equation in the rotating frame (5.4) can be expressed as

$$v(\rho,z) = \hat{U}_{\mathrm{f}}(z)\hat{U}_{\mathrm{rot}}\left(-\frac{\Omega z}{c}\right) v(\rho,0) \equiv \hat{U}(z) v(\rho,0) , \tag{5.5}$$

where $\hat{U}_{\mathrm{f}}(z) = \exp\left(\frac{iz}{2k}\nabla_\rho^2\right)$ is the propagator corresponding to the time-independent paraxial wave equation and describes free propagation of a paraxial beam in a stationary frame. The operator $\hat{U}(z)$ has the significance of the propagator in the rotating frame. The rotation operator arises from the Coriolis term in equation (5.4) and gives the propagating modes a twisted nature.

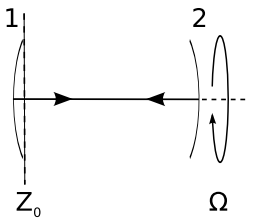

Figure 5.1: Schematic plot of the set-up that we study in this chapter: an astigmatic two-mirror cavity that is put into rotation about its optical axis. The rotation frequency is denoted Ω and z_0 indicates the transverse reference plane.

5.2.2 The modes of a rotating cavity

In a stationary cavity, modes are usually defined as stationary solutions of the time-dependent paraxial wave equation (5.2) that vanish on the mirror surfaces [12]. The transverse profiles of these modes are reproduced after each round trip up to a Gouy phase factor $\exp(-i\chi)$, which determines the resonant wave numbers. From equation (5.1) it follows that the electric field picks up a phase $2kL - \chi$, where L is the mirror separation, after each round trip so that the resonance condition reads $2kL - \chi = 2\pi q$ with $q \in \mathbb{Z}$. The necessary and sufficient condition for a stationary cavity to have long-lived modes is that it is geometrically stable, i.e., that the round-trip Gouy phases χ are real so that the magnification $|\exp(-i\chi)|$ is equal to 1.

Since a rotating cavity is time-dependent, we cannot expect time-independent modes in this case. A natural and continuous generalization of the mode criterion to the rotating case is to require that the modes adopt the time-dependence of the cavity, i.e., that they rotate along with the mirrors. These modes are time-independent in the co-rotating frame so that they obey equation (5.4) and vanish on the mirror surfaces. As discussed in the previous chapter, the interplay between rotation and stability gives rise to surprisingly rich behavior, but geometrically stable rotating two-mirror cavities exist. In chapter 3, we have derived an analytical-algebraic method to find explicit expressions of their modes. The method involves two pairs of bosonic ladder operators in the spirit of the quantum-mechanical harmonic oscillator that generate a complete and orthogonal set of cavity modes. In a given transverse reference plane, which we take close to the first mirror and denote by $z = z_0$ as is indicated in figure 5.1 the profiles of the cavity modes can be expressed as

$$v_{nm}(\rho, z_0) = \frac{1}{\sqrt{n!m!}} \left(\hat{a}_1^\dagger(z_0)\right)^n \left(\hat{a}_2^\dagger(z_0)\right)^m v_{00}(\rho, z_0) \,, \tag{5.6}$$

where $\hat{a}_1^\dagger(z_0)$ and $\hat{a}_2^\dagger(z_0)$ are the two raising operators in the reference plane. The fundamental mode $v_{00}(z_0)$ is fixed up to a phase factor by the requirement that acting on it with the corresponding lowering operators must give zero, i.e., $\hat{a}_1(z_0)v_{00}(z_0) = \hat{a}_2(z_0)v_{00}(z_0) = 0$. The ladder operators are linear combinations of the position operators $\hat{\rho} = (x, y)$ and the conjugate

momentum operators $k\hat{\theta} = -i\nabla_\rho$ with k the wave number of the mode. The expectation values $\langle v|\hat{\rho}|v\rangle$ and $\langle v|\hat{\theta}|v\rangle$ have the significance of the average transverse position and the average propagation direction of the beam. The position and propagation direction operators obey canonical commutation relations $[\hat{\rho}_i, k\hat{\theta}_j] = i\delta_{ij}$, where the indices i and j run over x and y and with δ_{ij} the Kronecker delta function. In the reference plane z_0 the lowering operators can be expressed as

$$\hat{a}_i(z_0) = \sqrt{\frac{k}{2}}\left(r_i^{\mathrm{T}}(z_0)\hat{\theta} - t_i^{\mathrm{T}}(z_0)\hat{\rho}\right) , \tag{5.7}$$

where the index i runs over 1 and 2. The complex vectors $t_i(z_0)$ and $r_i(z_0)$ have two components and are chosen such that $\mu_i^{\mathrm{T}} = (r_i^{\mathrm{T}}, t_i^{\mathrm{T}})$ is an eigenvector of the round-trip ray matrix in the co-rotating frame. In the present case of an astigmatic optical cavity, this is a real 4×4 matrix, which can be expressed as

$$M_{\mathrm{rt}} = M_1 \cdot M(L) \cdot M_2 \cdot M(L) , \tag{5.8}$$

where $M(z) = M_{\mathrm{f}}(z) \cdot M_{\mathrm{rot}}(-\Omega z/c)$ is the ray matrix that corresponds to $\hat{U}(z)$ and describes free propagation in the co-rotating frame, $M_{\mathrm{f}}(z)$ is the ray matrix that describes propagation in a stationary frame and $M_{\mathrm{rot}}(\alpha)$ is the ray matrix that describes a rotation over an angle α in the transverse plane. The ray matrices $M_{1,2}$ describe the mirrors 1 and 2 respectively and are fully determined by their radii of curvature and orientation in the transverse plane. These ray matrices are the generalizations to the astigmatic case of the standard 2×2 ray matrices, which can be found in any textbook on optics. Explicit expressions of the 4×4 ray matrices are given in section 3.5.

As opposed to the unitary propagator $\hat{U}(z)$ and the rotation operator $\hat{U}_{\mathrm{rot}}(\alpha)$, which act in the Hilbert space of transverse modes, ray matrices describe real linear transformations in the transverse phase space (ρ, θ). Formally speaking, this phase space is a symplectic manifold and the real and linear transformations that preserve its mathematical structure form the real symplectic group $Sp(\mathbb{R}, 4)$. Symplectic groups and various physically relevant aspects of symplectic geometry have been studied in detail, see, for instance, reference [39]. The ladder operators act in the mode space, but since they are constructed from the ray vectors $\mu_i^{\mathrm{T}} = (r_i^{\mathrm{T}}, t_i^{\mathrm{T}})$ and transform accordingly, the algebraic properties of the round-trip ray matrix (5.8) are essential for the ladder operator approach to be applicable. From these properties, it follows that its eigenvalues are either real or pairwise complex conjugate phase factors. The rotating cavity is geometrically stable only in the latter case. In this case, the corresponding pairwise complex conjugate eigenvectors $\mu_{1,2}^{\mathrm{T}} = (r_i^{\mathrm{T}}, t_i^{\mathrm{T}})$ and $\mu_i^{\dagger} = (r_i^{\dagger}, t_i^{\dagger})$ can be chosen such that

$$r_i^{\mathrm{T}}(z_0)t_j(z_0) - t_i^{\mathrm{T}}(z_0)r_j(z_0) = 0 , \tag{5.9}$$

and

$$r_i^{\dagger}(z_0)t_j(z_0) - t_i^{\dagger}(z_0)r_j(z_0) = 2i\delta_{ij} , \tag{5.10}$$

where the indices i and j take the values 1 and 2. The complex conjugate eigenvectors $\mu_{1,2}^{\dagger}$ generate the raising operators $\hat{a}_{1,2}^{\dagger}$ according to equation (5.7) and the special properties of the

eigenvectors (5.9) and 5.10) guarantee that the ladder operators obey bosonic commutation relations

$$[a_i(z_0), a_j(z_0)] = 0 \qquad \text{and} \qquad [\hat{a}_i(z_0), \hat{a}_j^\dagger(z_0)] = \delta_{ij} \,, \tag{5.11}$$

where the indices i and j run over 1 and 2, so that the modes (5.6) form a complete and orthonormal set in the transverse reference plane.

The four eigenvalues of the round-trip ray matrix (5.8) can be written as $\exp(i\chi_{1,2})$ and $\exp(-i\chi_{1,2})$, where $\chi_{1,2}$ are the round-trip Gouy phases that are picked up by the lowering operators. They determine the resonant wave numbers for the (n, m) cavity mode according to

$$2kL - \chi_1\left(n + \frac{1}{2}\right) - \chi_2\left(m + \frac{1}{2}\right) = 2\pi q \,, \tag{5.12}$$

where $q \in \mathbb{Z}$ is the longitudinal mode index.

The ladder operators that generate the rotating cavity modes in an arbitrary transverse plane inside the cavity can be constructed according to equation (5.7) and its hermitian conjugate by using that the z dependent eigenvectors $\mu_i^{\mathrm{T}}(z) = (r_i^{\mathrm{T}}(z), t_i^{\mathrm{T}}(z))$ are given by

$$\begin{pmatrix} r_i(z) \\ t_i(z) \end{pmatrix} = M(z - z_0) \begin{pmatrix} r_i(z_0) \\ t_i(z_0) \end{pmatrix} . \tag{5.13}$$

The properties given by equations (5.9) and (5.10) are preserved under this transformation so that the ladder operators obey the bosonic commutation relations (5.11) in all transverse planes.

So far, we have considered only the mode that propagates from left to right (from mirror 1 to mirror 2 in figure 5.1). By using the ray matrix that describes one of the mirrors (say mirror 2), one can construct the ladder operators that generate the modes that propagate in the opposite direction

$$\begin{pmatrix} r_i^{\leftarrow}(z) \\ t_i^{\leftarrow}(z) \end{pmatrix} = M(z_0 + L - z) \cdot M_2 \cdot M(z_0 + L - z) \begin{pmatrix} r_i^{\rightarrow}(z) \\ t_i^{\rightarrow}(z) \end{pmatrix} . \tag{5.14}$$

The actual field inside the cavity is a linear combination of the left and right propagating modes and can be expressed as

$$\mathbf{E}_{nm}(\mathrm{r}, t) = \mathrm{Re}\Big\{ -iE_0\epsilon(v_{nm}^{\rightarrow}(\rho, z)e^{ikz - i\omega t} - v_{nm}^{\leftarrow}(\rho, z)e^{-ikz - i\omega t})\Big\} \,, \tag{5.15}$$

where the minus sign accounts for the fact that a mode changes sign when it is reflected by a mirror. In the rest of this chapter, we focus on the mode profile $v_{nm}(\rho, z)$ rather than on the actual cavity field (5.15), since this is the profile that would be measured in any realistic experiment. The expressions of the modes that we have given in this section hold in the co-rotating frame, the corresponding expressions of the rotating mode patterns $u_{nm}(\rho, z, t)$ in the stationary frame can be obtained by applying equation (5.3).

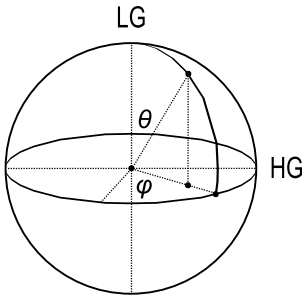

Figure 5.2: The Hermite-Laguerre sphere, which describes the degrees of freedom associated with the nature of higher-order paraxial optical modes. Each point $(\varphi_{\mathrm{HL}}, \vartheta_{\mathrm{HL}})$ corresponds to a complete and orthonormal set of modes; the poles $(\vartheta_{\mathrm{HL}} = 0, \pi)$ correspond to Laguerre-Gaussian modes while points on the equator $(\vartheta_{\mathrm{HL}} = \pi/2)$ correspond to Hermite-Gaussian modes. Intermediate values of the polar angle ϑ_{HL} give rise to generalized Gaussian modes. The azimuthal angle φ_{HL} determines the orientation of the higher-order mode patterns in the transverse plane.

5.3 Ladder operators and vortices

5.3.1 Analytical expressions of the modes

In order to derive more explicit expressions of the rotating cavity modes (5.6), we combine the vectors $r_{1,2}$ and $t_{1,2}$ in two matrices, which are defined as

$$\mathsf{R}(z) = (r_1(z), r_2(z)) \qquad \text{and} \qquad \mathsf{T}(z) = (t_1(z), t_2(z)) \,, \tag{5.16}$$

The special properties (5.9) and (5.10) can then be summarized as

$$\mathsf{R}^{\mathrm{T}}\mathsf{T} - \mathsf{T}^{\mathrm{T}}\mathsf{R} = 0 \quad \text{and} \quad \mathsf{R}^{\dagger}\mathsf{T} - \mathsf{T}^{\dagger}\mathsf{R} = 2i\mathsf{1} \,. \tag{5.17}$$

As was mentioned already, the fundamental mode $v_{00}(\rho, z)$ is fixed by the requirement that acting on it with both lowering operators must give 0. The two first order differential equations that are thus obtained have the solution

$$v_{00}(\rho, z) = \sqrt{\frac{k}{\pi \det \mathsf{R}(z)}} \exp\left(-\frac{k\rho^{\mathrm{T}}\mathsf{S}(z)\rho}{2}\right) \,, \tag{5.18}$$

where $\mathsf{S} = -i\mathsf{T}\mathsf{R}^{-1}$ is a 2×2 matrix. It makes sense to decompose S into its real and imaginary parts $\mathsf{S} = \mathsf{S}_{\mathrm{r}} + i\mathsf{S}_{\mathrm{i}}$. The matrices S_{r} and S_{i}, respectively, characterize the astigmatism of the Gaussian intensity and phase patterns. From the properties of R and T (5.17) it can be shown easily that S is symmetric and that its real part S_{r} is positive definite so that the mode profile is square-integrable. The profile in equation (5.18) has been normalized properly. In order to

characterize the other degrees of freedom, it is convenient to rewrite the z dependent lowering operators (5.7) as

$$\begin{pmatrix} \hat{a}_1(z) \\ \hat{a}_2(z) \end{pmatrix} = \sqrt{\frac{k}{2}} \left(\mathsf{R}^{\mathrm{T}}(z)\hat{\theta} - \mathsf{T}^{\mathrm{T}}(z)\hat{\rho} \right) = \sqrt{\frac{k}{2}} \mathsf{R}^{\mathrm{T}}(z) \left(\hat{\theta} - i\mathsf{S}(z)\hat{\rho} \right) . \tag{5.19}$$

By using equation (5.17) we find that $\mathsf{R}\mathsf{R}^{\dagger} = \mathsf{S}_{\mathrm{r}}^{-1}$ so that $\mathsf{R}^{\mathrm{T}}(z)$ can be written as $\sigma(z)\mathsf{S}(z)_{\mathrm{r}}^{-1/2}$, where σ is a unitary 2×2 matrix. Notice that S_{r} is real, symmetric and positive definite so that $\mathsf{S}_{\mathrm{r}}^{-1/2}$ is well defined. By making use of the operator identity $e^{A}Be^{-A} = B + [A, B] + \frac{1}{2!}[[A, [A, B]] + ...$ and the canonical commutation relations $[\hat{\rho}, k\hat{\theta}] = i\delta_{ij}$ we find that

$$\mathsf{S}_{\mathrm{i}}\hat{\rho} + \hat{\theta} = e^{-ik\rho\mathsf{S}_{\mathrm{i}}\rho/2}\hat{\theta}e^{ik\rho\mathsf{S}_{\mathrm{i}}\rho/2} \tag{5.20}$$

so that the z dependent lowering operators can be expressed as

$$\begin{pmatrix} \hat{a}_1 \\ \hat{a}_2 \end{pmatrix} = -i\sqrt{\frac{k}{2}}\sigma e^{-ik\rho\mathsf{S}_{\mathrm{i}}\rho/2} \left(\mathsf{S}_{\mathrm{r}}^{1/2}\hat{\rho} + i\mathsf{S}_{\mathrm{r}}^{-1/2}\hat{\theta} \right) e^{ik\rho\mathsf{S}_{\mathrm{i}}\rho/2} . \tag{5.21}$$

By introducing real scaled coordinates $\rho' = \sqrt{k}\mathsf{S}_{\mathrm{r}}^{1/2}\rho$ that account for the astigmatism of the intensity pattern, the product of $\sqrt{k/2}$ and the linear combination of $\hat{\rho}$ and $\hat{\theta}$ between the brackets takes the form of the lowering operators of a dimensionless quantum-mechanical harmonic oscillator in two dimensions. From right to left, both the z dependent lowering operators (5.21) and the corresponding raising operators $\hat{a}_{1,2}^{\dagger}$ first remove the curved wave front, then modify the mode pattern and eventually restore the wave front again. The unitary matrix σ describes the additional degrees of freedom, which characterize the nature and orientation of the higher-order modes. Overall phase factors in the rows of σ do not affect the mode structure in a given transverse plane z and without loss of generality we can fix its determinant such that $\sigma \in SU(2)$. Since σ is unitary, its rows are not independent and we can write

$$\sigma = \begin{pmatrix} \sigma_x & \sigma_y \\ -\sigma_y^* & \sigma_x^* \end{pmatrix} , \tag{5.22}$$

with $|\sigma_x|^2 + |\sigma_y|^2$. In complete analogy with the Poincaré sphere for polarization vectors (or the Bloch sphere for spin-1/2 states) the degrees of freedom associated with the complex vector (σ_x, σ_y) can be mapped onto the so-called Hermite-Laguerre sphere [17]. As is indicated in figure 5.2, every point on the sphere corresponds to two pairs of bosonic ladder operators that generate a complete set of higher-order modes. In this respect, it is different from the Poincaré and Bloch spheres, on which every point corresponds to a single state. The poles on the Hermite-Laguerre sphere correspond with $(\sigma_x, \sigma_y) = (1, \pm i)/\sqrt{2}$ and yield ladder operators that generate Laguerre-Gaussian modes. Points on the equator correspond to $(\sigma_x, \sigma_y) = (\cos\varphi_{\mathrm{HL}}, \sin\varphi_{\mathrm{HL}})$ and give rise to Hermite-Gaussian modes. Intermediate values of the polar angle $0 < \vartheta_{\mathrm{HL}} < \pi/2$ correspond to generalized Gaussian modes [44]. The azimuthal angle φ_{HL} fixes the orientation of the higher-order mode patterns in the transverse

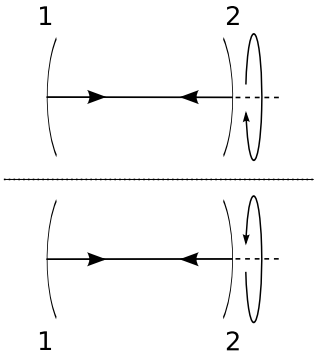

Figure 5.3: A stationary cavity with simple astigmatism is equivalent to its mirror image (the dashed line indicates the mirror plane). Since the rotation direction changes sign under this reflection, rotation breaks this symmetry.

plane. The rows of σ (5.22) correspond to antipodal points on the sphere so that it is, strictly speaking, sufficient to consider one of the hemispheres only. In general, the separation of the degrees of freedom in terms of the symmetric matrix S, which characterizes the astigmatism, and the unitary matrix σ, which determines the nature of the higher order modes, is local in the sense that it only holds in a single transverse plane z. The evolution of σ under propagation and optical elements depends on the astigmatism and vice versa.

Using the defining identity of the Hermite polynomials $H_n(x)\exp(-x^2/2) = (x - \frac{\partial}{\partial x})^n \exp(-x^2/2)$ and the binomial expansion $(a+b)^n = \sum_{p=0}^{n} \binom{n}{p} a^p b^{n-p}$ for $[a,b] = 0$ the normalized higher order modes can be expressed as

$$v_{nm}(\rho', z) = \left(\frac{k(\det \mathsf{S}_\mathrm{r})^{1/2}}{\pi}\right)^{1/2} \exp\left(-\frac{\rho'(1 + i\mathsf{S}_\mathrm{r}^{-1/2}\mathsf{S}_\mathrm{i}\mathsf{S}_\mathrm{r}^{-1/2})\rho'}{2}\right) \times$$
$$\sum_{p=0}^{n}\sum_{q=0}^{m} \binom{n}{p}\binom{m}{q} (i)^{n+m} (\sigma^*_{x'})^p \left(\sigma_{y'}\right)^q \left(\sigma^*_{y'}\right)^{n-p} (\sigma_{x'})^{m-q} \times H_{k+l}(x') H_{n+m-k-l}(y') \,, \quad (5.23)$$

where $\rho' = (x', y')^\mathrm{T}$ are the scaled coordinates that account for the astigmatism of the intensity patterns. The above expression holds in the co-rotating frame. The corresponding expression for the rotating modes $u_{nm}(\rho', z, t)$ in the stationary frame, can be obtained by applying equation (5.3).

5.3.2 Vortices in higher order modes

As discussed in section 3.7, a stationary two-mirror cavity has inversion symmetry in the imaginary transverse planes halfway the lenses of the corresponding lens guide. In case of a cavity with simple astigmatism, the symmetry property (3.72) is equivalent to the statement

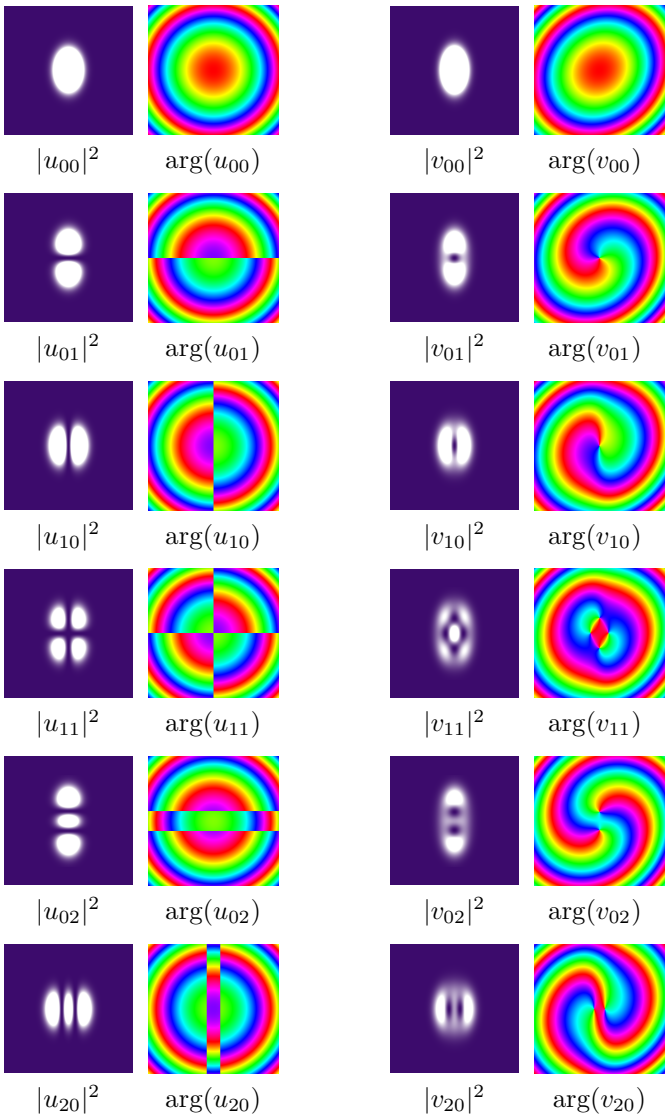

Figure 5.4: Intensity and false-color phase patterns of the first few modes of an optical cavity consisting of a spherical and a stationary (left) and rotating (right) cylindrical mirror. The radius of curvature of the spherical mirror is equal to $4L$, with L the mirror separation. The radius of curvature of the cylindrical mirror is equal to $2L$. The plots show the mode patterns in the co-rotating frame close to the spherical mirror. The cylindrical mirror is flat in the vertical direction. In the right plots, the rotation frequency is equal to $\Omega_0/10$ with $\Omega_0 = c\pi/L$. The color code used to plot the phase patterns is periodic; from 0 to 2π the color changes in a continuous fashion from red via yellow, green, blue and purple back to red.

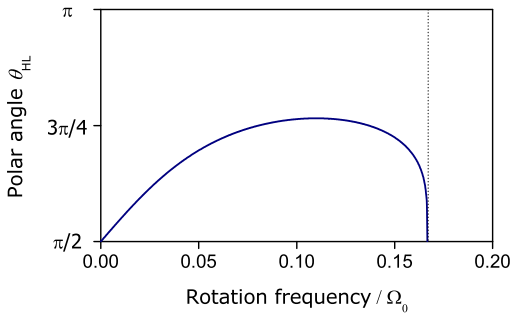

Figure 5.5: Dependence on the rotation frequency Ω of the polar angle ϑ_{HL} on the Hermite-Laguerre sphere for a cavity consisting of a spherical and a rotating cylindrical mirror. The characterization of the modes in terms of $(\varphi_{\mathrm{HL}}, \vartheta_{\mathrm{HL}})$ is local and the plot specifies the nature of the higher-order modes in the transverse plane close to the spherical mirror.

that a stationary cavity must have the same modes as its mirror image, as illustrated in figure 5.3, where the mirror plane is parallel to one of the planes through the mirror axes and the cavity axis. This symmetry implies that the cavity modes are real apart from the overall curved wave fronts. This symmetry property holds for modes of all order so that the higher order modes are Hermite-Gaussian. Hermite-Gaussian modes do have line dislocations (lines across which the phase jumps by π) in the transverse plane, but do not have vortices. As discussed in section 3.7, the inversion symmetry in case of a stationary cavity with general astigmatism is more subtle. In that case, the cavity modes are real only in the immediate neighborhood of the mirrors.

Rotation obviously breaks the inversion symmetry of a stationary cavity. As a result, the modes of a rotating cavity have additional phase structure. The fundamental mode attains a twist; although the electric field vanishes on the mirror surfaces, its wave fronts do not fit their local curvature. From equation (5.18), it is clear that no vortices can appear in the fundamental mode. Vortices appear as zeros of the polynomial part of the profile of the higher order modes (5.23). Due to the rotation of the cavity, the line dislocations in the higher-order Hermite-Gaussian modes are deformed into elliptical vortices.

From the fact that σ (5.22) is a unitary matrix, it follows that the two raising operators $\hat{a}^\dagger_{1,2}$ generate vortices with opposite charge. As a result, the vortices that appear at the center of the v_{01} and v_{10} modes have equal but opposite topological charges ± 1. Since both vortices are spherical (canonical) in the scaled coordinates, their morphologies are determined only by the astigmatism of the intensity pattern. In general, the raising operators split, displace and introduce vortices in the cavity modes so that the vortex pattern in the higher-order modes (5.23) can be very complicated. More explicit expressions have been given only in limiting cases [80, 81].

The fundamental mode contains only even powers of the position coordinates $\rho = (x, y)^{\mathrm{T}}$

and is even under inversion in the transverse plane: $\rho \to -\rho$. The ladder operators are linear in the position and propagation-direction operators and are obviously odd under this inversion. It follows that the rotating cavity modes (5.23) are even or odd, depending on the parity of the total mode number $n + m$. Odd modes have a vortex at the center of the mode patterns, whereas even modes, in general, do not.

5.4 Examples

In this section we illustrate the rotational effects on the structure of two-mirror cavity modes by further investigating a specific example. We focus on a cavity consisting of a stationary spherical and a rotating cylindrical mirror, which is the simplest realization of a uniformly rotating two-mirror cavity. The radius of curvature of the spherical mirror is taken as $4L$, with L the mirror separation while the radius of curvature of the cylindrical mirror is chosen as $2L$. This cavity is geometrically stable for rotation frequencies up to $\Omega_0/6$, where $\Omega_0 = c\pi/L$ with c the speed of light, is the frequency corresponding to the cavity round-trip time.

In the absence of rotation, the modes $u_{nm}(\rho, z)$ of the cavity are defined as the stationary solutions of the time-dependent paraxial wave equation (5.2) that vanish on both mirror surfaces. The transverse intensity and phase patterns close to the spherical mirror of the zeroth, first and second order modes of the cavity are plotted in the left column of figure 5.4. Although the astigmatism is different in other transverse planes (in particular close to the cylindrical mirror), the modes are Hermite-Gaussian everywhere. Their phase structure clearly reflects the fact that the wave fronts fit the curvature of the (spherical) mirror. The phase structure of the higher-order modes reveals phase jumps of π (sign changes), which appear along horizontal and vertical lines in the transverse plane and arise from the Hermite-polynomials in equation (5.23). Although these line dislocations are not visible in the intensity patterns, they are physical and can be observed interferometrically.

If the cylindrical mirror is put into rotation, the mode structure changes significantly. The modes of a rotating cavity are defined as co-rotating solutions of equation (5.2), or equivalently solutions of equation (5.4), that vanish on the mirror surfaces. In the co-rotating frame, propagating modes attain a twist due to retardation, which is accounted for by the Coriolis term in equation (5.4). The effect of rotation on the intensity and phase patterns of the zeroth, first and second order cavity modes is illustrated in the right column of figure 5.4, for which the rotation frequency is equal to $\Omega_0/10$. The mode patterns are clearly affected by rotation. The intensity patterns become more similar to Laguerre-Gaussian modes and have obviously the structure of generalized Gaussian modes. Although the electric field vanishes on the mirror surface, the wave fronts no longer fit its curvature. This is most apparent in case of the fundamental mode $v_{00}(\rho, z)$, where the curves of constant phase close to the spherical mirror have become elliptical. The non-parallel orientation of the elliptical intensity and phase patterns of the fundamental mode $v_{00}(\rho, z)$ reflects its twisted nature. The higher-order modes also attain a twist. Moreover, vortices appear in their phase patterns. The results confirm that the vortices in the $v_{01}(\rho, z)$ and $v_{10}(\rho, z)$ have opposite charges and that only modes with odd

$n + m$ have a vortex at the center. In the modes with equal mode numbers n and m, vortices appear in pairs of equal but opposite charge so that the total vortex charge is equal to zero. As a result, the curves of constant phase that enclose all vortices are closed.

Due to a combined symmetry that survives rotation, the intensity patterns of the rotating modes are aligned along the axes of the cylindrical mirror while the phase patterns are not. As a result the azimuthal angle on the Hermite-Laguerre sphere φ_{HL}, which specifies the orientation of the higher-order mode patterns, does not depend on the rotation frequency. This is not true for the polar angle ϑ_{HL}, which specifies whether the modes are Hermite-Gaussian, Laguerre-Gaussian or generalized Gaussian modes and is a measure of the vorticity in their phase structure. Its dependence on the rotation frequency Ω is shown in figure 5.5. In general, the characterization of the cavity modes in terms of a point on the Hermite-Laguerre sphere is local and the plot in figure 5.5 characterizes the higher-order cavity modes close the the spherical mirror. It confirms that, due to the fact that rotation breaks the inversion symmetry of a stationary cavity, the cavity modes are continuously deformed from Hermite-Gaussian modes in the stationary case into generalized Gaussian modes in the rotating case. For not too large values of the rotation frequency, the rotationally induced vorticity is proportional to the rotation frequency. For larger values something surprising happens: at some point, the vorticity starts to decrease with increasing rotation frequencies and eventually the modes become Hermite-Gaussian again. This is due to the fact that this cavity is destabilized by rotation at a rotation frequency $\Omega_0/6$. At this point, the modes lose their confinement in one of the transverse directions (in this case in the vertical direction, i.e., the direction in which the cylindrical mirror is flat) so that the elliptical vortices are stretched to become line dislocations again. Although the vorticity in the modes disappears if this transition is approached, the orbital angular momentum diverges due to the diverging astigmatism. As we have shown in chapter 4, rotation may also stabilize a cavity that is unstable in the absence of rotation. In such cases we expect the opposite behavior. Due to the rotation of the cavity, we retrieve Hermite-Gaussian modes at the point where the cavity is stabilized, while mode deformation and induced vorticity appear for even larger values of the rotation frequency.

5.5 Some remarks on experimental issues

In chapters 3, 4 and 5, we have discussed various optical and opto-dynamical properties of astigmatic optical cavities with rotating mirrors. The essential feature that distinguishes those from their stationary counterparts is the retardation L/c of a light pulse after propagation from one mirror to the other. In the co-rotating frame, this gives rise to a twist $\Omega L/c$, which significantly modifies the mode structure and the focusing properties of the cavity. Since the speed of light is very large, experimental observation of the effects that we have studied requires very large values of the rotation frequency Ω. In this section we discuss some possibilities and limitations of several routes towards realization of an experimental set-up that captures the essential features of the one that we have studied in this thesis.

Under typical experimental conditions, the distance between the mirrors of a paraxial

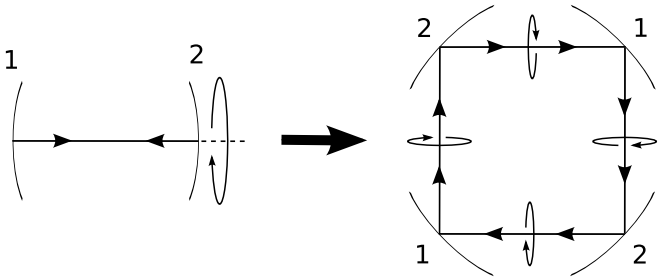

Figure 5.6: A rotating two-mirror cavity can be unfolded into a stationary four-mirror ring cavity that captures the essential optical properties of the rotating cavity. The image rotators between the mirror rotate the mode profile over an angle $\Omega L/c$ in order to account for the twist of the modes under propagation in the rotating frame.

optical cavity ranges from a few centimeters to several meters. In this case, the rotation frequency Ω_0, which corresponds to the cavity round-trip time is of the order of 10^8 hertz so that observation of the effects that we have discussed here, requires mechanical rotation frequencies of 1 to 10 megahertz. Mechanical vibration frequencies close to this range have been achieved with a piezoelectric actuator [85]. Developing a similar device to simulate rotations at megahertz frequencies is challenging but seems, at least in principle, not impossible.

Lower values of the rotation frequency require larger values of the mirror separation. Currently, high-finesse optical cavities as large as 2 to 4 kilometers are being operated in attempts to optically detect gravitational waves [86]. In such a set-up rotation frequencies of a few kilohertz would suffice. However, the mirrors that are used in these set-ups are large and, therefore, heavy so that achieving mechanical rotation at kilohertz frequencies without too much distortion is anything but straightforward. Moreover, fabrication of an astigmatic mirror of this size is not at all trivial.

Another, perhaps more realistic, dynamical approach could be to apply a rotating astigmatic mode pattern, which can be constructed from its stationary Doppler-shifted frequency components [48], to optically induce a rotating refractive-index pattern in a material with a Kerr nonlinearity. Such a pattern could be used in transmission to realize a two-mirror cavity with a rotating lens. The optical properties of such a cavity could be observed at another wavelength. The rotation frequency that can be achieved in this set-up is eventually limited by the dynamical response of the Kerr medium.

In addition to the dynamical realizations, one could try to mimic the twisted mode propagation in the rotating frame by using image rotators. Since it is essential that back and forth propagating modes attain a twist in the same direction, a two-mirror cavity with an image rotator between the mirrors does not do the job. Instead, one should use a ring resonator with four, pairwise identical, mirrors in which the light passes an image rotator after each mirror, as indicated in figure 5.6. Although the settings of the optical elements in this set-up

are time-independent, it does capture the essential optical properties of a rotating two-mirror cavity. A difficulty with this set-up is that the clockwise and counterclockwise propagating modes are frequency degenerate. In a passive set-up one of the two modes can be selected by injecting light in one direction only. In an active realization, this degeneracy could be lifted by applying the polarization degree of freedom.

5.6 Conclusion and outlook

In this chapter, we have applied the ladder-operator that we introduced in chapter 3 to study the vortices that appear in the modes of an astigmatic two-mirror cavity when it is put into rotation about the optical axis. The modes of a rotating cavity are defined as solutions of the time-dependent paraxial wave equation (5.2) that rotate along with the cavity and vanish on the mirror surfaces. This mode criterion is a continuous generalization of the requirement that the modes of a stationary cavity are stationary solutions of equation (5.2) that vanish on the mirror surfaces. The rotating cavity modes are stationary solutions in a co-rotating frame where mode propagation is twisted due to the finite speed of light. As a result, rotation deforms the astigmatic Hermite-Gaussian modes of a stationary cavity into generalized Gaussian modes. The line dislocations in the Hermite-Gaussian modes are deformed into elliptical vortices. In chapter 4, we have shown that rotation can destabilize a two-mirror cavity that is stable in the absence of rotation. When such a transition is approached, the cavity modes lose their confinement in one transverse direction so that the elliptical vortices are stretched to become line dislocations again. This is illustrated in figure 5.5.

An interesting but open question is how rotation would affect the optical properties of a geometrically unstable cavity, especially when close to the rotationally induced transition from an unstable to a stable geometry. A geometrically unstable cavity is intrinsically lossy [12] and the propagation of light inside an unstable cavity is dominated by diffraction at the sharp edges of the mirrors [66]. Both mathematically and physically this system is fundamentally different from the stable cavities that we have studied here and it is not possible to apply or generalize our method to such a system.

As opposed to a normal fluid, a spatially confined optical cavity mode attains vorticity when it is put into uniform rotation. In this respect, it has some similarity with superfluids and Bose-Einstein condensates. Compared to those systems, however, optical beams have many more degrees of freedom to cope with rotation. A Bose-Einstein condensate arises as the collective ground state of an ensemble of interacting bosons (usually atoms) in thermal equilibrium. It is a gauge-symmetry-broken state that is characterized by its uniform phase. The only way in which such a system can attain orbital angular momentum, is by locally creating cylindrically symmetric vortices while keeping its phase fixed elsewhere. As a result, vortices appear only when the rotation frequency exceeds a certain threshold and the number of vortices increases when the rotation frequency is further increased. For optical cavity modes, on the other hand, both the astigmatism of the phase and intensity patterns and the properties of the optical vortices are affected by rotation. Both contribute to the or-

bital angular momentum [17], which typically increases with increasing values of the rotation frequency even though the number of vortices does, in general, not increase.

6

Geometric phases for astigmatic optical modes of arbitrary order

6.1 Introduction

In the twenty-five years that have passed since Berry published his landmark paper [87], the geometric phase has turned out to be a very unifying concept in physics. Various phase shifts and rotation angles both in classical and quantum physics have been proven to originate from the geometry of the underlying parameter space. One of the first examples was given by Pancharatnam [88] who discovered that the phase shift due to a cyclic transformation of the polarization of an optical field is equal to half the enclosed area on the Poincaré sphere for polarization states. Other optical examples of geometric phases are the phase shift that arises from the variation of the direction of the wave vector of an optical field through a fiber [89] and the phase that is associated with the cyclic manipulation of a squeezed state of light [90]. The Gouy phase shift, which is due to the variation of the beam parameters (the beam width and the radius of curvature of the wave front) of a Gaussian optical beam, can also be interpreted geometrically [91].

In analogy with the geometric phase for polarization (or spin) states of light, van Enk has proposed a geometric phase that arises from cyclic mode transformations of paraxial optical beams carrying orbital angular momentum [92]. The special case of isotropic first-order modes is equivalent to the polarization case [93] and, as was experimentally demonstrated by Galvez et. al., the geometric phase shift acquired by a first-order mode that is transformed along a closed trajectory on the corresponding Poincaré sphere also equals half the enclosed surface on this sphere [94]. Similar experiments have been performed with second-order modes [95], in particular to show that exchange of orbital angular momentum is necessary for a non-trivial geometric phase to occur [96]. However, in the general case of isotropic modes of order N, the connection with the geometry of the $N + 1$-dimensional mode space is not at all obvious.

In this chapter, we present a complete and general analysis of the phase shift of transverse optical modes of arbitrary order when propagating through a paraxial optical set-up, thereby resolving this issue. Paraxial optical modes with different transverse mode indices (n, m) are connected by bosonic ladder operators in the spirit of the algebraic description of the quantum-mechanical harmonic oscillator and complete sets of transverse modes $|u_{nm}\rangle$ can thus be obtained from two pairs of ladder operators [17]. We show that the geometries of the subspaces of modes with fixed transverse mode numbers n and m, which are closed under mode transformations, are all carbon copies of the geometry underlying the ladder operators. We fully characterize this geometry including both the generalized beam parameters, which characterize the astigmatism and orientation of the intensity and phase patterns of a Gaussian fundamental mode, and the degrees of freedom associated with the nature and orientation of the higher-order modes. We find a dynamical and a geometric contribution to the phase shift of a mode under propagation through an optical set-up, which both have a clear significance in terms of this parameter space.

The material in this chapter is organized as follows. In the next section we briefly summarize the operator description of paraxial wave optics. We discuss its group-theoretical structure, which is essential for our ladder-operator approach, and show how paraxial ray optics emerges from it. In section 6.3 we discuss how complete basis sets of transverse modes can be obtained from two pairs of bosonic ladder operators. We discuss the transformation properties of the ladder operators, and, thereby, of the modes and characterize the ten degrees of freedom that are associated with the choice of a basis of transverse modes. Two of those degrees of freedom relate to overall phase factors of the ladder operators and, therefore, of the modes. In section 6.4, we show that the variation of these phases under propagation through a set-up originates from the variation of the other parameters. We discuss an analogy with the Aharonov-Bohm effect in quantum mechanics and show that both contributions to the phase shift are geometric in that they are fully determined by the trajectory through the parameter space. However, only the geometric contribution relates to the geometry of this space. Section 6.5 is devoted to the specific, but experimentally relevant, case of mode transformations of non-astigmatic modes. In the final section, we summarize our results and draw our conclusions.

6.2 Canonical description of paraxial optics

6.2.1 Position and propagation direction as conjugate variables

A monochromatic paraxial beam of light that propagates along the z direction is conveniently described by the complex scalar profile $u(\rho, z)$, which characterizes the spatial structure of the field beyond the structure of the carrier wave $\exp(ikz - i\omega t)$. The two-dimensional vector $\rho = (x, y)^{\mathrm{T}}$ denotes the transverse coordinates. The electric and magnetic fields of the beam can be expressed as

$$\mathbf{E}(\rho, z, t) = \mathrm{Re}\left\{E_0 \epsilon u(\rho, z) e^{ikz - i\omega t}\right\} \tag{6.1}$$

and

$$\mathbf{B}(\rho, z, t) = \mathrm{Re}\left\{\frac{E_0}{c}(\mathbf{e}_z \times \epsilon) u(\rho, z) e^{ikz - i\omega t}\right\} , \tag{6.2}$$

where E_0 is the amplitude of the field, ϵ is the transverse polarization, $\mathbf{e}_z$ is the unit vector along the propagation direction and $\omega = ck$ is the optical frequency with c the speed of light. The slowly varying amplitude $u(\rho, z)$ obeys the paraxial wave equation

$$\left(\nabla_\rho^2 + 2ik\frac{\partial}{\partial z}\right) u(\rho, z) = 0 , \tag{6.3}$$

where $\nabla_\rho^2 = \partial^2/\partial x^2 + \partial^2/\partial y^2$ is the transverse Laplacian. Under the assumption that the transverse variation of the field appears on a much larger length scale than the wavelength, this description of paraxial wave optics is consistent with Maxwell's equations in free space [45].

The paraxial wave equation (6.3) has the form the Schrödinger equation for a free particle in two dimensions. The longitudinal coordinate z plays the role of time while the transverse coordinates $\rho = (x, y)^{\mathrm{T}}$ constitute the two-dimensional space. This analogy allows us to adopt the Dirac notation of quantum mechanics to describe the evolution of a classical wave field [42]. In the Schrödinger picture, we introduce state vectors $|u(z)\rangle$ in the Hilbert space L^2 of square-integrable transverse states of the wave field, where the z coordinate parameterizes the trajectory along which the field propagates. The states are properly normalized $\langle u(z)|u(z)\rangle = 1$ for all z and the field profile in real space can be expressed as $u(\rho, z) = \langle \rho|u(z)\rangle$. Just as in quantum mechanics, the transverse coordinates may be viewed as a hermitian vector operator $\hat{\rho} = (\hat{x}, \hat{y})^{\mathrm{T}}$ acting on the Hilbert space. The derivatives with respect to these coordinates constitute canonically conjugate operators. Rather than the conjugate transverse momentum operator $-i\partial/\partial\rho$, which has the significance of the normalized transverse momentum of the field, it is convenient to construct the propagation-direction operator by dividing the transverse momentum operator by the normalized longitudinal momentum k. Thus, we obtain the hermitian vector operator $\hat{\theta} = (\hat{\vartheta}_x, \hat{\vartheta}_y)^{\mathrm{T}} = -(i/k)(\partial/\partial x, \partial/\partial y)^{\mathrm{T}}$. The transverse position and propagation-direction operators obey the canonical commutation rules

$$[\hat{\rho}_a, k\hat{\theta}_b] = i\delta_{ab} , \tag{6.4}$$

where the indices a and b run over the x and y components. In analogy with quantum mechanics, we introduce the transverse field profile in propagation-direction representation

$$\tilde{u}(\theta, z) = \langle \theta | u(z) \rangle = \frac{k}{2\pi} \int d_2\rho \; u(\rho, z) e^{-ik\theta^{\mathrm{T}}\rho} \; , \tag{6.5}$$

which is the two-dimensional Fourier transform of $u(\rho, z)$ and characterizes the transverse propagation-direction distribution of the field.

In geometric optics, a ray of light is fully characterized in a transverse plane z by its transverse position ρ and propagation direction θ, which are usually combined in the four-dimensional ray vector $\mathscr{z}^{\mathrm{T}} = (\rho^{\mathrm{T}}, \theta^{\mathrm{T}})$. The operator description of paraxial wave optics may be viewed as a formally quantized (wavized) description of light rays, where ρ and θ have been replaced by hermitian operators $\hat{\rho}$ and $\hat{\theta}$ that obey canonical commutation rules (6.4) and $1/k = \lambda\!\!\!^{-}$ plays the role of $\hbar$ [31]. These operators are conveniently combined in the ray operator $\hat{\mathscr{z}}^{\mathrm{T}} = (\hat{\rho}^{\mathrm{T}}, \hat{\theta}^{\mathrm{T}})$. In analogy with quantum mechanics, where the expectation values of the position and momentum operators have a clear classical significance in the limit $\hbar \to 0$, a paraxial wave field reduces to a ray in the limit of geometric optics $\lambda\!\!\!^{-} \to 0$. Its transverse position and propagation direction in the transverse plane z are characterized by the expectation values $\langle u(z)|\hat{\rho}|u(z)\rangle$ and $\langle u(z)|\hat{\theta}|u(z)\rangle$.

6.2.2 Group-theoretical structure of paraxial wave and ray optics

Both the diffraction of a paraxial beam under free propagation, as described by the paraxial wave equation (6.3), and the transformations due to lossless optical elements can be expressed as unitary transformations $|u_{\mathrm{out}}\rangle = \hat{U}|u_{\mathrm{in}}\rangle$ on the transverse state of the field. In general, a unitary operator can be expressed as

$$\hat{U}(\{a_j\}) = e^{-i\sum_j a_j \hat{T}_j} \; , \tag{6.6}$$

where $\{a_j\}$ is a set of real parameters and $\{\hat{T}_j\}$ a set of hermitian generators, i.e., $\hat{T}_j^{\dagger} = T_j$. In the present case of paraxial propagation and paraxial (first-order) optical elements, the generators are quadratic forms in the transverse position and propagation-direction operators. This is exemplified by the paraxial wave equation (6.3), which in operator notation takes the following form

$$\frac{\partial}{\partial z}|u(z)\rangle = -\frac{ik}{2}\hat{\theta}^2|u(z)\rangle \tag{6.7}$$

and is formally solved by

$$|u(z)\rangle = \exp\left(-\frac{ikz\hat{\theta}^2}{2}\right)|u(0)\rangle \; . \tag{6.8}$$

This shows that that free propagation of a paraxial field is generated by $k\hat{\theta}^2/2$, which is obviously quadratic in the canonical operators. Since the ray operator $\hat{\mathscr{z}}$ has four components, the number of squares of the operators is four while the number of mixed products is $\binom{4}{2} = 6$,

which gives a total of ten quadratic forms. They are hermitian and can be chosen as

$$T_1 = \hat{x}^2\,, \quad T_2 = \hat{y}^2\,, \quad T_3 = \hat{x}\hat{y}\,, \quad T_4 = \tfrac{k}{2}\left(\hat{x}\hat{\vartheta}_x + \hat{\vartheta}_x\hat{x}\right)\,, \quad T_5 = \tfrac{k}{2}\left(\hat{y}\hat{\vartheta}_y + \hat{\vartheta}_y\hat{y}\right)\,,$$
$$T_6 = k\hat{x}\hat{\vartheta}_y\,, \quad T_7 = k\hat{y}\hat{\vartheta}_x\,, \quad T_8 = k^2\hat{\vartheta}_x\hat{\vartheta}_y\,, \quad T_9 = k^2\hat{\vartheta}_x^2 \quad \text{and} \quad T_{10} = k^2\hat{\vartheta}_y^2\,. \tag{6.9}$$

In terms of these generators, free propagation of a paraxial beam (6.8) is described by

$$|u(z)\rangle = \exp\left(-\frac{i\left(\hat{T}_9 + \hat{T}_{10}\right)z}{2k}\right)|u(0)\rangle\,. \tag{6.10}$$

The mixed product $\hat{T}_8$ appears in the generator of free propagation through an anisotropic medium, i.e., a medium in which the refractive index depends on the propagation direction θ. In that case the propagator can be expressed as $\exp(-ik\hat{\theta}^{\mathrm{T}}\mathsf{N}^{-1}\hat{\theta}z/2)$, where N is a real and symmetric matrix that characterizes the (quadratic) variation of the refractive index with the propagation direction. If the anisotropy of the refractive index is not aligned along the ϑ_x and ϑ_y directions, this transformation involves $\hat{T}_8$. A thin astigmatic lens imposes a Gaussian phase profile. The unitary transformation that describes it can be expressed as

$$|u_{\mathrm{out}}\rangle = \exp\left(-\frac{ik\rho^{\mathrm{T}}\mathsf{F}^{-1}\rho}{2}\right)|u_{\mathrm{in}}\rangle\,, \tag{6.11}$$

where F is a real and symmetric 2×2 matrix whose eigenvalues correspond to the focal lengths of the lens while the corresponding, mutually perpendicular, eigenvectors fix its orientation in the transverse plane. In the general case of an astigmatic lens that is not aligned along the x and y directions, this transformation involves the generators $\hat{T}_1$, $\hat{T}_2$ and $\hat{T}_3$. A rotation of the beam profile in the transverse plane can be represented by

$$|u_{\mathrm{rot}}\rangle = e^{-i(\hat{T}_6 - \hat{T}_7)\phi}|u\rangle\,, \tag{6.12}$$

where $\hat{T}_6 - \hat{T}_7 = -i(x\partial/\partial y - y\partial/\partial x)$ is the orbital angular momentum operator and ϕ is the rotation angle. The operators $\hat{T}_4$ and $\hat{T}_5$ generate transformations that rescale a field profile along the x and y directions respectively, i.e.,

$$u_{\mathrm{out}}(x,y,z) = \langle\rho|u_{\mathrm{out}}(z)\rangle = \langle\rho|e^{i\log(c_x)\hat{T}_4 + i\log(c_y)\hat{T}_5}|u_{\mathrm{in}}(z)\rangle = \sqrt{c_x c_y}\; u_{\mathrm{in}}(c_x x, c_y y, z)\,. \tag{6.13}$$

Physically speaking, such transformations correspond to the deformation of a field profile due to refraction at the interface between two dielectrics with different refractive indices.

From the canonical commutation relations (6.4), it follows that the commutator of any two generators (6.9) is a linear combination of the generators. In mathematical terms, the algebra of the generators is closed, which means that $[\hat{T}_k, \hat{T}_l] = i\sum_m g_{klm}\hat{T}_m$ with real structure constants g_{klm}. We shall prove that the unitary transformations (6.6) with the generators (6.9) form a ten-parameter Lie group. For reasons that will become clear this group is called the metaplectic group $Mp(4)$.

Since the states $|u(z)\rangle$ are normalized, the expectation values $\langle u(z)|\hat{\rho}|u(z)\rangle$ and $\langle u(z)|\hat{\theta}|u(z)\rangle$ have the significance of the average transverse position and the average propagation direction of the field. A special property of the unitary transformations in equation (6.6) with the quadratic generators given by (6.9), is that the Heisenberg transformation $\hat{U}^\dagger\,\hat{\mathscr{z}}\,\hat{U}$ of the vector operator $\hat{\mathscr{z}}^{\mathrm{T}} = (\hat{\rho}^{\mathrm{T}}, \hat{\theta}^{\mathrm{T}})$ is linear, so that it can be expressed as

$$\hat{U}^\dagger(\{a_j\})\,\hat{\mathscr{z}}\,\hat{U}(\{a_j\}) = M(\{a_j\})\,\hat{\mathscr{z}}\ , \tag{6.14}$$

where $M(\{a_j\})$ is the 4×4 ray matrix that describes the transformation of a ray $\mathscr{z}^{\mathrm{T}} = (\rho^{\mathrm{T}}, \theta^{\mathrm{T}})$ under the optical element that is described by the state-space operator $\hat{U}(\{a_j\})$. The defining properties of the position and momentum operators, i.e., that they are hermitian and obey canonical commutation rules (6.4), are preserved under this unitary Heisenberg transformation. It follows that $M(\{\alpha_j\})$ is real and obeys the identity

$$M^{\mathrm{T}}(\{a_j\})GM(\{a_j\}) = G \qquad \text{with} \qquad G = \begin{pmatrix} 0 & 1 \\ -1 & 0 \end{pmatrix}, \tag{6.15}$$

where 0 and 1 denote the 2×2 zero and unit matrices respectively, so that G is a 4×4 matrix. This identity (6.14) ensures that the operator expectation values $\langle u(z)|\,\hat{\mathscr{z}}\,|u(z)\rangle$ of the transverse position and propagation direction transform as a ray, i.e., trace out the path of a ray when the field propagates through an optical set-up. This shows how paraxial ray optics emerges from paraxial wave optics and, as such, the identity (6.14) may be viewed as an optical analogue of the Ehrenfest theorem in quantum mechanics [49]. The manifold of rays $\mathscr{z}$ constitutes a phase space in the mathematical sense. The real and linear transformations on this manifold that obey the relation (6.15), or, equivalently, preserve the canonical commutation rules (6.4), are ray matrices. The product of two ray matrices is again a ray matrix so that ray matrices form a group. The group of real 4×4 ray matrices, which preserve the bilinear form $\mathscr{z}^{\mathrm{T}}G\mathscr{z}$, where $\mathscr{z}$ and $\mathscr{z}$ are ray vectors, is called the symplectic group $Sp(4,\mathbb{R})$. The term symplectic, which is a syllable-by-syllable translation of the Latin "complex" to Ancient Greek and literally means "braided together", refers to the fact that a phase space is a joint space of position and propagation direction (momentum). The 4×4 ray matrices in $Sp(4,\mathbb{R})$ emerge from a set of unitary state-space transformations, which, as one may prove from equation (6.14), constitute a group under operator multiplication. As was mentioned already, this group is called the metaplectic group $Mp(4)$. For real rays $\mathscr{z}\,,\mathscr{z}\ \in\mathbb{R}^4$, the products $\mathscr{z}^{\mathrm{T}}G\mathscr{z}$ and $\mathscr{z}^{\mathrm{T}}G\mathscr{z}$ vanish. The product $\mathscr{z}^{\mathrm{T}}G\mathscr{z}$ does not vanish and is obviously conserved under paraxial propagation and optical elements. It is called the Lagrange invariant [29, 97] and has the significance of the phase-space extent of a pair of rays $\mathscr{z}$ and $\mathscr{z}$. Conservation of this quantity is an optical analogue of Liouville theorem in statistical mechanics.

The commutators of the quadratic generators $\hat{T}_j$ and the position and propagation-direction operators are linear in these operators, so that we can write

$$-i[\hat{T}_j,\,\hat{\mathscr{z}}] = J_j\,\hat{\mathscr{z}}\ , \tag{6.16}$$

where the 4×4 matrices J_j are real. Explicit expressions of these matrices are given in appendix 6.A. Applying equation (6.14) to infinitesimal transformations immediately shows that the ray matrix corresponding to the unitary state-space operator in equation (6.6) is given by

$$M(\{\alpha_j\}) = e^{-\sum_j \alpha_j J_j} \ . \tag{6.17}$$

Equation (6.16) provides a general relationship between the generators $\{\hat{T}_j\}$ of the unitary state-space transformations (6.6) and the generators $\{J_j\}$ of the corresponding ray matrices (6.17). By applying equation (6.15) to infinitesimal transformations, one finds that the generators obey $J_j^{\mathrm{T}} G + G J_j = 0$. Moreover, from equation (6.16) one may prove that

$$[[\hat{T}_i, \hat{T}_j], \hat{z}\,] = [J_i, J_j]\,\hat{z} \ . \tag{6.18}$$

Using the Lie algebra $[\hat{T}_k, \hat{T}_l] = i \sum_m g_{klm} \hat{T}_m$ we find that $[J_k, J_l] = -\sum_m g_{klm} J_m$. This proves that the metaplectic and symplectic groups are homomorphic, i.e., for every $\hat{U} \in Mp(4)$ there is a corresponding $M \in Sp(4, \mathbb{R})$. The reverse of this statement is not true; a ray matrix M fixes a corresponding transformation $\hat{U}$ up to an overall phase. The homomorphism is an isomorphism up to this phase.

By using equation (6.15) and the expressions of the unitary transformations (6.10), (6.11), (6.12) and (6.13) or, equivalently, the relation between (6.16) the sets of generators $\{\hat{T}_j\}$ and $\{J_j\}$ and the definition (6.17) of the ray matrices, one finds the 4×4 ray matrices that describe propagation, a thin lens, a rotation in the transverse plane and the rescaling of a beam profile due to refraction at the interface between two dielectrics. These ray matrices, some of which have been given explicitly in sections 2.2 and 3.5, generalize the well-known ABCD matrices to the case of two independent transverse degrees of freedom [12].

The group-theoretical structure that we have discussed in this section can easily be generalized to the case of D spatial dimensions. In that case there are $2D$ canonical operators. These give rise to $2D + \binom{2D}{2} = 2D^2 + D$ linearly independent quadratic forms, which generate state-space transformations that constitute the metaplectic group $Mp(2D)$. The corresponding ray matrices obey the $2D-$dimensional generalization of equation (6.15) and form the corresponding symplectic group $Sp(2D, \mathbb{R})$. In case of a single transverse dimension, the three hermitian quadratic forms can be chosen as x^2, $k(\hat{x}\hat{\vartheta}_x + \hat{\vartheta}_x \hat{x})/2$ and $k^2 \hat{\vartheta}_x^2$. In the analogous case of the quantum-mechanical description of a particle in three dimensions, the number of quadratic forms is twenty-one.

6.3 Basis sets of paraxial modes

6.3.1 Ladder operators

As a result of the quadratic nature of the generators (6.9), a, possibly astigmatic, Gaussian beam profile at the $z = 0$ input plane of a paraxial optical set-up will retain its Gaussian shape in all other transverse planes z. This is the general structure of a transverse fundamental

mode. Complete sets of higher-order transverse modes that preserve their general shape under paraxial propagation and paraxial optical elements can be obtained by repeated application of bosonic raising operators $\hat{a}_p^\dagger(0)$ in the $z = 0$ plane [33]. In the present case of two transverse dimensions, we need two independent raising operators so that $p = 1, 2$. Both the raising operators and the corresponding lowering operators $\hat{a}_p(0)$ are linear in the transverse position and propagation-direction operators $\hat{\rho}$ and $\hat{\theta}$. Their transformation property under unitary transformations $\in Mp(4)$ follows from the requirement that acting with a transformed ladder operator on a transformed state must be equivalent to transforming the raised or lowered state, i.e.,

$$\hat{a}_{\text{out}}^{(\dagger)}|u_{\text{out}}\rangle = \hat{a}_{\text{out}}^{(\dagger)}\hat{U}|u_{\text{in}}\rangle = \hat{U}\hat{a}_{\text{in}}^{(\dagger)}|u_{\text{in}}\rangle \, . \tag{6.19}$$

In view of the unitarity of $\hat{U}$, this requires that

$$\hat{a}_{\text{out}}^{(\dagger)} = \hat{U}\hat{a}_{\text{in}}^{(\dagger)}\hat{U}^\dagger \, . \tag{6.20}$$

Since the generators (6.9) are quadratic in the position and propagation-direction operators, the ladder operators preserve their general structure and remain linear in these operators under this transformation (6.20). Moreover, their bosonic nature is preserved so that they obey the commutation rules

$$[\hat{a}_p(z), \hat{a}_q^\dagger(z)] = \delta_{pq} \tag{6.21}$$

in all transverse planes z of the optical set-up if (and only if) they obey bosonic commutation rules in the $z = 0$ plane. When the fundamental Gaussian mode $|u_{00}(z)\rangle$ is chosen such that the lowering operators give zero when acting upon it, i.e., $\hat{a}_1(z)|u_{00}(z)\rangle = \hat{a}_2(z)|u_{00}(z)\rangle = 0$, the commutation rules (6.21) guarantee that the modes

$$|u_{nm}(z)\rangle = \frac{1}{\sqrt{n!m!}} \left(\hat{a}_1^\dagger(z)\right)^n \left(\hat{a}_2^\dagger(z)\right)^m |u_{00}(z)\rangle \, , \tag{6.22}$$

form a complete set in all transverse planes z. For a given optical system, the complete set of modes is thus fully characterized by the choice of the two bosonic ladder operators $\hat{a}_p(0)$ in the reference plane $z = 0$.

In chapter 2, we have shown that, in the special case of an astigmatic two mirror-cavity, the ladder operators, and thereby the cavity modes, can be directly obtained as the eigenvectors of the ray matrix for one round trip inside the cavity. In the present case of an open system, we are free to choose the parameters that specify the ladder operators in the $z = 0$ input plane. A convenient way to do this is to choose an arbitrary ray matrix $M_0 \in Sp(4, \mathbb{R})$. This ray matrix can be chosen independent of the properties of the optical system, and of the ray matrices that describe the transformations of its elements. However, as we shall see, a necessary and sufficient restriction is that M_0 has four eigenvectors μ for which the matrix element $\mu^\dagger G \mu$ does not vanish. It is obvious that this matrix element is purely imaginary so that the eigenvectors must be complex. Since M_0 is real, this implies that for each eigenvector μ_p also μ_p^* is one of the eigenvectors so that the eigenvectors come in two complex conjugate

pairs, obeying the eigenvalue relations $M_0\mu_p = \lambda_p\mu_p$ and $M_0\mu_p^* = \lambda_p^*\mu_p^*$, with $p = 1, 2$. Without loss of generality we can assume that the matrix elements $\mu_p^\dagger G\mu_p$ are positive imaginary. Then we can write

$$\mu_p^\dagger G\mu_p = 2i \qquad \text{and} \qquad \mu_p^{\mathrm{T}} G\mu_p = 0\,, \tag{6.23}$$

where $p = 1, 2$. The first relation can be assured by proper normalization of the eigenvectors, whereas the second follows from the antisymmetry of G. By taking matrix elements of the symplectic identity $M_0^{\mathrm{T}} G M_0 = G$, we find the relations

$$\lambda_p^*\lambda_q\mu_p^\dagger G\mu_q = \mu_p^\dagger G\mu_q \qquad \text{and} \qquad \lambda_p\lambda_q\mu_p^{\mathrm{T}} G\mu_q = \mu_p^{\mathrm{T}} G\mu_q\,. \tag{6.24}$$

Assuming that the two eigenvalues λ_1 and λ_2 are different, we conclude that

$$\mu_1^\dagger G\mu_2 = 0 \qquad \text{and} \qquad \mu_1^{\mathrm{T}} G\mu_2 = 0\,. \tag{6.25}$$

When the eigenvalues are degenerate, i.e., $\lambda_1 = \lambda_2$, one can find infinitely many pairs of linearly independent vectors μ_1 and μ_2 that obey these symplectic orthonormality properties. Following the approach discussed in chapter 2, we now specify the ladder operators in the $z = 0$ input plane by the expressions

$$\hat{a}_p(0) = \sqrt{\frac{k}{2}}\mu_p^{\mathrm{T}} G\,\hat{\boldsymbol{\varepsilon}} \qquad \text{and} \qquad \hat{a}_p^\dagger(0) = \sqrt{\frac{k}{2}}\mu_p^\dagger G\,\hat{\boldsymbol{\varepsilon}}\,. \tag{6.26}$$

The symplectic orthonormality properties (6.23) and (6.25) of the eigenvectors μ_p and μ_p^* ensure that the ladder operators in the input plane obey bosonic commutation relations (6.21). From the general transformation property of the ladder operators (6.20), combined with the Ehrenfest relation (6.14) between $\hat{U}$ and M, one may show that the ladder operators in other transverse planes z are given by the same expressions (6.26) when μ_p is replaced by $\mu_p(z) = M(z)\mu_p$. Here, $M(z)$ is the ray matrix that describes the transformation of ray from the $z = 0$ input plane to the transverse plane z. It can be constructed by multiplying the ray matrices that describe the optical elements of which the set-up consists and free propagation between them in proper order. The fact that the properties (6.23) and (6.25) are conserved under symplectic transformations $\in Sp(4, \mathbb{R})$ confirms that the ladder operators remain bosonic in all transverse planes of the set-up.

Since the modes are fully characterized by the choice of two complex vectors μ_p, we expect that the expectation values of physically relevant operators can be expressed in terms of these vectors. The average transverse position and momentum of the beam trace out the path of a ray. This implies that the expectation values $\langle u_{nm}|\hat{\rho}|u_{nm}\rangle$ and $\langle u_{nm}|\hat{\theta}|u_{nm}\rangle$ vanish. In appendix 6.B we prove, however, that the expectation values of the generators $\hat{T}_j$ are, in general, different from zero and can be expressed as

$$\langle u_{nm}|\hat{T}_j|u_{nm}\rangle = \frac{1}{2}\left\{\left(n + \frac{1}{2}\right)\mu_1^\dagger G J_j \mu_1 + \left(m + \frac{1}{2}\right)\mu_2^\dagger G J_j \mu_2\right\}\,. \tag{6.27}$$

This result generalizes the expression (2.82) of the orbital angular momentum in twisted cavity modes that we derived in chapter 2. It is noteworthy that these properties of the modes

are fully characterized by the generators J_j and the complex ray vectors μ_p, which both have a clear geometric-optical significance.

Finally, it is worthwhile to notice that the results of this section remain valid when the number of (transverse) dimensions is different. In particular, the same method gives explicit expressions for complete orthogonal sets of time-dependent wave functions that solve the Schrödinger equation of a free particle in three-dimensional space.

6.3.2 Degrees of freedom in fixing a set of modes

We have shown that there is a one-to-one correspondence between the defining properties of a ray matrix, i.e., that it is real and obeys the identity (6.15), and the properties (6.23) and (6.25) of the complex eigenvectors μ_p that ensure that the ladder operators (6.26) are bosonic. This implies that all different basis sets of complex vectors μ_p that obey these identities must be related by symplectic transformations, i.e., each of these sets can be written as $\{M\mu_p\} \cup \{M\mu_p^*\}$, with $M \in Sp(4,\mathbb{R})$ and $\{\mu_p\} \cup \{\mu_p^*\}$ the set of complex eigenvectors of a specific ray matrix $M_0 \in Sp(4,\mathbb{R})$. Since $\{M\mu_p\} \cup \{M\mu_p^*\}$ constitutes the set of eigenvectors of MM_0M^{-1}, it follows that the freedom in choosing a set of complex vectors that generate two pairs of bosonic ladder operators (6.26) is equivalent to the freedom of choosing a ray matrix $M \in Sp(4,\mathbb{R})$. As a result, the number of independent parameters associated with this choice is equal to the number of generators of $Sp(4,\mathbb{R})$, which is ten. In order to give a physical interpretation of these degrees of freedom, we follow the characterization discussed in chapter 5 and decompose the complex ray vectors into two-dimensional subvectors so that $\mu_p^{\mathrm{T}}(z) = (r_p^{\mathrm{T}}(z), t_p^{\mathrm{T}}(z))$. In terms of these subvectors, the ladder operators take the following form

$$\hat{a}_p(z) = \sqrt{\frac{k}{2}}(r_p^{\mathrm{T}}(z)\hat{\theta} - t_p^{\mathrm{T}}(z)\hat{\rho}) \qquad \text{and} \qquad \hat{a}_p^{\dagger}(z) = \sqrt{\frac{k}{2}}(r_p^{\dagger}(z)\hat{\theta} - t_p^{\dagger}(z)\hat{\rho}) \,, \tag{6.28}$$

where $p = 1, 2$. An explicit expression of the Gaussian fundamental mode can be given if we combine the two-dimensional column vectors r_p and t_p into

$$\mathsf{R}(z) = (r_1(z), r_2(z)) \qquad \text{and} \qquad \mathsf{T}(z) = (t_1(z), t_2(z)) \,. \tag{6.29}$$

The objects R and T take the form of 2×2 matrices, but since r_p and t_p are transverse vectors, R and T do not transform as such under ray-space transformations $\in Sp(4,\mathbb{R})$ nor under transformations on the transverse plane. The symplectic orthonormality properties (6.23) and (6.25) of the vectors μ_p can be expressed as

$$\mathsf{R}^{\dagger}(z)\mathsf{T}(z) - \mathsf{T}^{\dagger}(z)\mathsf{R}(z) = 2i\mathsf{1} \qquad \text{and} \qquad \mathsf{R}^{\mathrm{T}}(z)\mathsf{T}(z) - \mathsf{T}^{\mathrm{T}}(z)\mathsf{R}(z) = \mathsf{0} \,, \tag{6.30}$$

and hold for all values of z. Now, the fundamental transverse mode in plane z can be written as

$$u_{00}(\rho, z) = \sqrt{\frac{k}{\pi \det \mathsf{R}(z)}} \exp\left(-\frac{k\rho^{\mathrm{T}}\mathsf{S}(z)\rho}{2}\right) \,, \tag{6.31}$$

where $\mathsf{S} = -i\mathsf{T}\mathsf{R}^{-1}$. As opposed to R and T, S is a 2×2 matrix in the transverse plane and transforms accordingly. It can be checked directly that acting upon $|u_{00}(z)\rangle$ with the lowering operators $\hat{a}_1(z)$ and $\hat{a}_2(z)$ gives zero. The fundamental mode (6.31) is properly normalized and has been constructed such that it solves the paraxial wave equation (6.3) under free propagation. Moreover, one may check that it transforms properly under the transformations of optical elements. The second relation in equation (6.30) guarantees that S is symmetric. This is obvious when we multiply the relation from the left with $(\mathsf{R}^{\mathrm{T}})^{-1}$, and from the right with R^{-1}. The real and imaginary parts S_{r} and S_{i} of S respectively characterize the astigmatism of the intensity and phase patterns. The real part can be written as $\mathsf{S}_{\mathrm{r}} = (-i\mathsf{T}\mathsf{R}^{-1} + i(\mathsf{R}^{\dagger})^{-1}\mathsf{T}^{\dagger})/2$. With the first relation in equation (6.30) this shows that $\mathsf{R}\mathsf{S}_{\mathrm{r}}\mathsf{R}^{\dagger} = \mathsf{1}$. This leads to the identity

$$\mathsf{R}\mathsf{R}^{\dagger} = \mathsf{S}_{\mathrm{r}}^{-1} \,, \tag{6.32}$$

which shows that S_{r} is positive definite. As a result, the curves of constant intensity in the transverse plane are ellipses. Moreover, the fundamental mode is square-integrable. Depending on the sign of $\det \mathsf{S}_{\mathrm{i}}(z)$ the curves of constant phase in the transverse plane are ellipses, hyperbolas or parallel straight lines. Under free propagation, S is a slowly varying smooth function of z. Optical elements, on the other hand, may instantaneously modify the astigmatism. The astigmatism of both the intensity and the phase patterns is characterized by two widths in mutually perpendicular directions and one angle that specifies the orientation of the curves of constant intensity or phase. The total number of degrees of freedom that specify the astigmatism, and, thereby, the matrix symmetric S, is thus equal to six.

Two of the remaining four degrees of freedom are related to the nature and orientation of the higher-order mode patterns. From equation (6.32), we find that R can be expressed as $\mathsf{S}_{\mathrm{r}}^{-1/2}\sigma^{\mathrm{T}}$, where σ is a unitary 2×2 matrix. Notice that S_{r} is real and positive so that $\mathsf{S}_{\mathrm{r}}^{-1/2}$ is well-defined. It is illuminating to rewrite the complex ray vectors μ_1 and μ_2 as

$$\begin{pmatrix} \mu_1 & \mu_2 \end{pmatrix} = \begin{pmatrix} \mathsf{R} \\ \mathsf{T} \end{pmatrix} = \begin{pmatrix} 1 & 0 \\ -\mathsf{S}_{\mathrm{i}} & 1 \end{pmatrix} \begin{pmatrix} \mathsf{S}_{\mathrm{r}}^{-1/2} & 0 \\ 0 & \mathsf{S}_{\mathrm{r}}^{1/2} \end{pmatrix} \begin{pmatrix} \sigma^{\mathrm{T}} & 0 \\ 0 & \sigma^{\mathrm{T}} \end{pmatrix} \begin{pmatrix} \tilde{\mu}_x & \tilde{\mu}_y \end{pmatrix} , \tag{6.33}$$

where $\tilde{\mu}_x = (1, 0, i, 0)^{\mathrm{T}}$ and $\tilde{\mu}_y = (0, 1, 0, i)^{\mathrm{T}}$ are the complex ray vectors that correspond to the ladder operators that generate the stationary states of an isotropic harmonic oscillator in two dimensions. The first matrix in the second right-hand-side of this expression (6.33) is the ray matrix that describes the transformation of a thin astigmatic lens. It imposes the elliptical or hyperbolic wave front of the optical modes on the harmonic oscillator functions. The second matrix has the form of the ray matrix that describes the deformation of a mode due to refraction. It rescales the modes along two mutually perpendicular transverse directions and accounts for the astigmatism of the intensity patterns. The third matrix involves the complex matrix σ and obeys the generalization of equation (6.15) to complex matrices. Since it is complex, however, it is not a ray matrix $\in Sp(4, \mathbb{R})$. In order to clarify its significance, we rewrite equation (6.33) in terms of the ladder operators, which are conveniently combined in the vector operator $(\hat{a}_1, \hat{a}_2)^{\mathrm{T}}$. By using the definition if the ladder operators (6.26) and the

Ehrenfest relation (6.14), the transformation in equation (6.33) can be expressed as

$$\begin{pmatrix} \hat{a}_1 \\ \hat{a}_2 \end{pmatrix} = \sqrt{\frac{k}{2}}(\mathsf{R}^{\mathrm{T}}\hat{\theta} - \mathsf{T}^{\mathrm{T}}\hat{\rho}) = \\ -i\sqrt{\frac{k}{2}}\sigma \exp\left(-\frac{ik\rho^{\mathrm{T}}\mathsf{S}_i\rho}{2}\right)\left(\mathsf{S}_r^{1/2}\hat{\rho} + i\mathsf{S}_r^{-1/2}\hat{\theta}\right)\exp\left(\frac{ik\rho^{\mathrm{T}}\mathsf{S}_i\rho}{2}\right). \quad (6.34)$$

The linear combination of the position and momentum operators between the brackets takes the form of the lowering-operator vector for an isotropic harmonic oscillator in two dimensions. Again, the 2×2 matrix S_r accounts for the astigmatism of the intensity patterns by rescaling the ladder operators and, therefore, the modes they generate. The exponential terms take the form of the mode-space transformation for a thin astigmatic lens and impose the curved wave fronts. From right to left, the lowering operators (6.34) as well as the corresponding raising operators, first remove the curved wave front, then modify the mode patterns and eventually restore the wave front again. The 2×2 matrix σ is a unitary transformation in the space of the lowering operators $\hat{a}_1$ and $\hat{a}_2$ and transforms accordingly. It arises from the $U(2)$ symmetry of the isotropic harmonic oscillator in two dimensions and accounts for the fact that any, properly normalized, linear combination of bosonic lowering operators yields another bosonic lowering operator. Up to overall phases, to which we come in a moment, this transformation can be parameterized as $\hat{a}_1 \to \eta_1\hat{a}_1 + \eta_2\hat{a}_2$ and $\hat{a}_2 \to -\eta_1^*\hat{a}_1 + \eta_2^*\hat{a}_2$ with $|\eta_1|^2 + |\eta_2|^2 = 1$. The two obvious degrees of freedom that are associated with the spinor $\eta = (\eta_1, \eta_2)^{\mathrm{T}}$ are the relative amplitude and the relative phase of its components. Analogous to the Poincaré sphere for polarization states (or the Bloch sphere for spin-1/2 states), they can be mapped onto a sphere. For reasons that will become clear, this sphere is called the Hermite-Laguerre sphere [17]. Since η_1 and η_2 are spinor components in a linear rather than a circular basis, this mapping takes the following form

$$\eta = \begin{pmatrix} \eta_1 \\ \eta_2 \end{pmatrix} = \frac{1}{\sqrt{2}}\begin{pmatrix} e^{\frac{i\varphi}{2}}\cos\frac{\vartheta}{2} + e^{-i\frac{\varphi}{2}}\sin\frac{\vartheta}{2} \\ -ie^{\frac{i\varphi}{2}}\cos\frac{\vartheta}{2} + ie^{-i\frac{\varphi}{2}}\sin\frac{\vartheta}{2} \end{pmatrix}, \quad (6.35)$$

where ϑ and φ are the polar and azimuthal angles on the sphere. The mapping is such that the north pole ($\vartheta = 0$) corresponds to ladder operators that generate astigmatic Laguerre-Gaussian modes with positive helicity. The south pole ($\vartheta = \pi$) corresponds to Laguerre-Gaussian modes with the opposite helicity while the equator ($\vartheta = \pi/2$) corresponds to Hermite-Gaussian modes. Other values of the polar angle ϑ correspond to generalized Gaussian modes [44]. The azimuth angle φ determines the transverse orientation of the higher-order mode patterns. Since paraxial optical modes are invariant under rotations over π in the transverse plane, the mapping in equation (6.35) is such that a rotation over φ on the sphere corresponds to a rotation of the mode pattern over $\phi = \varphi/2$.

The unitary matrix that describes the ladder operator transformation corresponding to the spinor η is constructed as

$$\sigma_0(\eta) = \begin{pmatrix} \eta_1 & \eta_2 \\ -\eta_2^* & \eta_1^* \end{pmatrix}, \quad (6.36)$$

where the second row is fixed up to a phase factor by the requirement that σ_0 must be unitary. With this convention, the two rows of sigma correspond to antipodal points on the Hermite-Laguerre sphere. Completely fixing the matrix $\sigma \in U(2)$, however, requires four independent degrees of freedom. The remaining two, which are not incorporated in η, are phase factors. Any matrix $\sigma \in U(2)$ can be written as

$$\sigma = \begin{pmatrix} e^{i\chi_1} & 0 \\ 0 & e^{i\chi_2} \end{pmatrix} \sigma_0(\eta) \; . \tag{6.37}$$

The phase factors $\exp(i\chi_p)$ correspond to overall phases of the vectors μ_p and, therefore, of the ladder operators (6.26). The vectors μ_p can be written as

$$\mu_p = e^{i\chi_p} \nu_p(\mathsf{S}, \eta) \; , \tag{6.38}$$

where $p = 1, 2$ and $\nu_p(\mathsf{S}, \eta)$ is completely determined by S and η according equation (6.33), σ being replaced by $\sigma_0(\eta)$. Although the vectors ν_1 and ν_2 obey symplectic orthonormality conditions (6.23) and are, therefore, not independent, the phases χ_1 and χ_2 are independent. From equation (6.37) and the fact that $\mathsf{R} = \mathsf{S}_\mathrm{r}^{-1/2} \sigma^\mathrm{T}$ it is clear that the argument of $\det \mathsf{R}$ is equal to $\chi_1 + \chi_2$ so that the overall phase of the fundamental mode (6.31) is given by $-(\chi_1 + \chi_2)/2$. The overall phases of the two raising operators are respectively $-\chi_1$ and $-\chi_2$, so that the phase factors in the higher order modes $|u_{nm}(z)\rangle$ are given by $\exp(-i\chi_{nm})$ with

$$\chi_{nm} = \left(n + \frac{1}{2}\right)\chi_1 + \left(m + \frac{1}{2}\right)\chi_2 \; . \tag{6.39}$$

In a single transverse plane, such overall phase factors do not modify the physical properties of the mode pattern. The evolution of these phase under propagation and optical elements, however, can be measured interferometrically.

The astigmatism of the modes, as characterized by the 2×2 matrix S, can be modified in any desired way by appropriate combinations of the optical elements that we have discussed in section 6.2. As will be discussed in section 6.5, the degrees of freedom associated with the spinor η can be manipulated by mode convertors and image rotators. Although we shall see that variation of the phase factors $\exp(i\chi_p)$ is, in general, unavoidable when the other parameters are modified, we show here that it is possible to construct a ray matrix $\in Sp(4, \mathbb{R})$ that solely changes these phase factors. Such a ray matrix is defined by the requirement that

$$M_\chi(\{\chi_p\}) \begin{pmatrix} \mu_1 & \mu_2 & \mu_1^* & \mu_2^* \end{pmatrix} = \begin{pmatrix} e^{i\chi_1}\mu_1 & e^{i\chi_2}\mu_2 & e^{-i\chi_1}\mu_1^* & e^{-i\chi_2}\mu_2^* \end{pmatrix} \; , \tag{6.40}$$

so that the vectors μ_p and μ_p^* are eigenvectors of M_χ. The corresponding eigenvalues are unitary. In terms of R and T this relation can be expressed as

$$M_\chi(\{\chi_p\}) \begin{pmatrix} \mathsf{R} & \mathsf{R}^* \\ \mathsf{T} & \mathsf{T}^* \end{pmatrix} = \begin{pmatrix} \mathsf{R} & \mathsf{R}^* \\ \mathsf{T} & \mathsf{T}^* \end{pmatrix} \begin{pmatrix} \mathsf{C} & 0 \\ 0 & \mathsf{C}^* \end{pmatrix} \; , \tag{6.41}$$

where

$$\mathsf{C} = \begin{pmatrix} e^{i\chi_1} & 0 \\ 0 & e^{i\chi_2} \end{pmatrix} \; . \tag{6.42}$$

By using that

$$\begin{pmatrix} \mathsf{R} & \mathsf{R}^* \\ \mathsf{T} & \mathsf{T}^* \end{pmatrix}^{-1} = \frac{1}{2i}\begin{pmatrix} -\mathsf{T}^\dagger & \mathsf{R}^\dagger \\ \mathsf{T}^{\mathrm{T}} & -\mathsf{R}^{\mathrm{T}} \end{pmatrix}, \tag{6.43}$$

which follows directly from the identities in equation (6.30), we find that M_χ can be expressed as

$$M_\chi(\{\chi_p\}) = \frac{1}{2i}\begin{pmatrix} \mathsf{R} & \mathsf{R}^* \\ \mathsf{T} & \mathsf{T}^* \end{pmatrix}\begin{pmatrix} \mathsf{C} & 0 \\ 0 & \mathsf{C}^* \end{pmatrix}\begin{pmatrix} -\mathsf{T}^\dagger & \mathsf{R}^\dagger \\ \mathsf{T}^{\mathrm{T}} & -\mathsf{R}^{\mathrm{T}} \end{pmatrix} = \frac{1}{2i}\begin{pmatrix} -\mathsf{RCT}^\dagger + \mathsf{R}^*\mathsf{C}^*\mathsf{T}^{\mathrm{T}} & \mathsf{RCR}^\dagger - \mathsf{R}^*\mathsf{C}^*\mathsf{R}^{\mathrm{T}} \\ -\mathsf{TCT}^\dagger + \mathsf{T}^*\mathsf{C}^*\mathsf{T}^{\mathrm{T}} & \mathsf{TCR}^\dagger - \mathsf{T}^*\mathsf{C}^*\mathsf{R}^{\mathrm{T}} \end{pmatrix} \tag{6.44}$$

This ray matrix adds overall phases $\exp(\pm i\chi_p)$ to the eigenvectors μ_p and μ_p^*. It is real and one may check that it obeys the identity (6.15) so that it is a physical ray matrix $\in Sp(4,\mathbb{R})$.

In this section, we have argued that the number of degrees of freedom associated with the choice of two pairs of ladder operators that generate a basis set of modes in a transverse plane z is equal to number of generators of $Sp(4,\mathbb{R})$, which is ten. We have shown that six of those are related to the astigmatism of the modes as characterized by a the complex and symmetric 2×2 matrix S. Two of the other four are angles on the Hermite-Laguerre sphere that characterize a spinor η, which determines the nature and orientation of the higher-order modes. The remaining two are overall phases of the ladder operators. All these degrees of freedom can be manipulated in any desired way by choosing a suitable ray matrix $\in Sp(4,\mathbb{R})$.

6.3.3 Gouy phase

In the limiting case of non-astigmatic modes that propagate through an isotropic optical system the 2×2 matrix S is a symmetric matrix with degenerate eigenvalues so that it can be considered a scalar $s = s_\mathrm{r} + is_\mathrm{i}$. If we choose $\sigma_0 = 1$, the higher-order modes are Hermite-Gaussian. In that case, the complex ray vectors are given by $\mu_1 = (r,0,t,0)^{\mathrm{T}}$ and $\mu_2 = (0,r,0,t)^{\mathrm{T}}$, with $r,t\in\mathbb{C}$. The symplectic normalization condition (6.23) implies that $r^*t - t^*r = 2i$. The real part s_r of $s = -it/r$ determines the beam width $w = \sqrt{2/(ks_r)}$ of the fundamental mode while the imaginary part s_i fixes the radius of curvature of its wave fronts according to $R = 1/s_\mathrm{i}$. Under free propagation over a distance z, the vectors μ_1 and μ_2 transform according to

$$\mu_1(z) = \begin{pmatrix} r+zt \\ 0 \\ t \\ 0 \end{pmatrix} \quad\text{and}\quad \mu_2(z) = \begin{pmatrix} 0 \\ r+zt \\ 0 \\ t \end{pmatrix}. \tag{6.45}$$

The parameters r, t and s remain scalar and free propagation does not introduce an overall phase difference between μ_1 and μ_2 so that η, or, equivalently σ_0, is independent of z. Without loss of generality we can choose $z = 0$ to coincide with the focal plane of the mode, which

implies that $s \in \mathbb{R}$ so that $r^*t = -t^*r = i$. Since s_r, and, therefore, $\mathsf{R} = \sigma_0 s_r$ cannot pick up a phase, we find that

$$\chi(z) - \chi(0) = \arg\left(\frac{r + zt}{r}\right) = \arctan\left(\frac{tz}{r}\right) = \arctan\left(\frac{z}{z_R}\right) , \tag{6.46}$$

where $z_R = ir/t$ is the Rayleigh range. This is the well-known Gouy phase for a Gaussian mode [12]. Since the vectors μ_1 and μ_2 pick up an overall phase $\chi(z)$, the raising operators pick up a phase $-\chi(z)$. The phase shift of the higher-order modes (6.22) is then given by $\exp(-i(n + m + 1)\chi)$ and depends on the total mode number $N = n + m$ only. As a result of this degeneracy, the same expression holds in the non-astigmatic case with $\sigma_0 \neq 1$. In that case, it is still true that the components of η are independent of z.

Generalization to astigmatic modes is straightforward only if the modes have simple astigmatism and if the orientation of the higher-order mode patterns is aligned along the astigmatism of the fundamental mode. In that case, the vectors μ_p pick up different Gouy phases and the components of η are independent of z. As will be discussed in section 6.5, this is not true in the case of non-astigmatic modes that propagate through an optical set-up with simple astigmatism. In the more general case of modes with general astigmatism that propagate through an arbitrary set-up of paraxial optical elements, the z dependence of S depends on η and vice versa [17]. In this case no simple expressions of the Gouy phases can be derived. The phase in equation (6.39) may be viewed as the ultimate generalization of the Gouy phase within paraxial wave optics.

6.4 The geometric interpretation of the variation of the phases χ_{nm}

6.4.1 Evolution of the phases χ_{nm}

In this section we show that variation of the phase differences χ_p between μ_p and ν_p (6.38) is, in general, unavoidable under (a sequence of) mode transformations that modify the degrees of freedom associated with S and η. From the discussion in the previous section it is clear that the generalized Gouy phases were defined such that they vary only under transformations that involve free propagation. However, for later purposes, it is convenient to formulate the description of mode transformations that give rise to phase shifts in a slightly more general way.

Suppose that the unitary state-space transformation that describes (a part of) a trajectory through the parameter space is given by $\hat{U}(\zeta) = \exp(-i\hat{T}\zeta)$, where $\hat{T}$ is a (linear combination of the) generator(s) defined in equation (6.9) and ζ is a real parameter that parameterizes the trajectory. In this case, the ζ dependent ladder operators (6.20) obey the anti-Heisenberg equation of motion

$$\left[\hat{a}^{(\dagger)}(\zeta), \hat{T}\right] = -i\frac{\partial \hat{a}^{(\dagger)}}{\partial \zeta} . \tag{6.47}$$

In terms of the complex ray vectors $\mu_p(\zeta)$ and the ray matrix $M(\zeta) = \exp(-J\zeta)$ that corresponds to $\hat{U}(\zeta)$ according to relation (6.14), this equation of motion takes the form of a

symplectic Schrödinger equation and can be expressed as

$$\frac{\partial \mu_p}{\partial \zeta} = -J\mu_p(\zeta) \, . \tag{6.48}$$

Substitution of $\mu_p(\zeta) = \exp(i\chi_p)\nu_p(\zeta)$ yields after dividing by $\exp(i\chi_p)$

$$i\frac{\partial \chi_p}{\partial \zeta}\nu_p(\zeta) + \frac{\partial \nu_p}{\partial \zeta} = -J\nu_p(\zeta) \, . \tag{6.49}$$

By multiplying from the left with $\nu_p^\dagger G$, using the normalization condition $\nu_p^\dagger G \nu_p = 2i$ and rearranging the terms we find that

$$\frac{\partial \chi_p}{\partial \zeta} = \frac{1}{2}\left\{ \nu_p^\dagger G J \nu_p + \nu_p^\dagger G \frac{\partial \nu_p}{\partial \zeta} \right\} \, . \tag{6.50}$$

The generator J represents a conserved quantity. Hence, the first term between the curly brackets does not depend on the parameter ζ and the above equation (6.50) can be integrated to obtain

$$\chi_p(\zeta) = \frac{1}{2}\left\{ \left(\nu_p^\dagger G J \nu_p\right)\zeta + \int_0^\zeta d\zeta' \nu_p^\dagger G \frac{\partial \nu_p}{\partial \zeta'} \right\} \, . \tag{6.51}$$

The first term between the curly brackets constitutes a dynamical contribution to the phase shift and arises from the fact that J corresponds to a constant of motion. The second term, on the other hand, relates to the geometry of the complex ray space and is the natural generalization of Berry's geometric phase to this case. In the next section, we derive an equivalent expression from which the geometric significance of the phase shifts (6.51) is more obvious.

6.4.2 Analogy with the Aharonov-Bohm effect

In quantum mechanics, it is well-known that the coupling of a particle with charge q to the magnetic vector potential $\mathbf{A}(\mathbf{r})$ gives rise to a measurable phase shift $(q/\hbar)\int_C \mathbf{A}\cdot d\mathbf{r}$ of the wave function when the particle moves along a trajectory $C = \mathbf{r}(t)$. This effect occurs even when the magnetic field $\mathbf{B} = \nabla \times \mathbf{A}$ vanishes everywhere along the trajectory and is known as the Aharonov-Bohm effect [98].

The physical properties that are associated with the wave function that describes a particle in quantum mechanics are not affected by the transformation $\psi(\mathbf{r}, t) \rightarrow \exp(i\phi(\mathbf{r}))\psi(\mathbf{r}, t)$. The Schrödinger equation is obviously not invariant under this local $U(1)$ gauge transformation. When gauge invariance of the Schrödinger equation is imposed, the vector potential $\mathbf{A}(\mathbf{r})$ arises as the corresponding gauge field. In this picture, the Aharonov-Bohm phase is due to the coupling to a gauge field, the conserved charge q being the coupling constant. As such it is a direct consequence of the $U(1)$ gauge invariance of quantum electrodynamics.

In this section, we point out an analogy between the generalized Gouy phase and the Aharonov-Bohm effect. This gives some new insights in the nature and origin of this geometric phase and allows us to derive an expression of the phase (6.51) from which its

origin in the geometry of the underlying parameter space is obvious. It is convenient to combine the parameters that characterize the eight degrees of freedom that are associated with the matrix S and the spinor η into a vector $\vec{\mathcal{R}} = (\mathcal{R}_1, \mathcal{R}_2, ...)^{\mathrm{T}}$. The corresponding differential operator, which is a vector in the eight-dimensional parameter space, is defined as $\vec{\nabla}_{\vec{\mathcal{R}}} = (\partial/\partial\mathcal{R}_1, \partial/\partial\mathcal{R}_2, ...)^{\mathrm{T}}$.

The physical properties, for example those in equation (6.27), of the transverse mode fields (6.22), which are generated by the ladder operators constructed from the vectors μ_p, are not affected by transformations of the type

$$\mu_p \to e^{i\psi_p(\vec{\mathcal{R}})}\mu_p \ , \tag{6.52}$$

where $p = 1, 2$. This symmetry property can be thought of as local $U(1) \otimes U(1)$ gauge invariance. The ray matrix $\in Sp(4, \mathbb{R})$ that describes such gauge transformations (6.52) figures in equation (6.44). As shown in appendix 6.C, the two corresponding real generators J_{χ_p} can be constructed from the eigenvectors μ_p. The vector μ_1 is an eigenvector of J_{χ_1} with eigenvalue $-i$. Since J_{χ_1} is real, the complex conjugate vector μ_1^* is an eigenvector of J_{χ_p} with eigenvalue i. Moreover, $J_{\chi_1}\mu_2 = J_{\chi_1}\mu_2^* = 0$. Similarly, μ_2 and μ_2^* are eigenvectors of J_{χ_2} with eigenvalues $-i$ and i and $J_{\chi_2}\mu_1 = J_{\chi_2}\mu_1^* = 0$. Since invariance under the gauge transformation (6.52) is a local and continuous symmetry, it gives rise to conserved Noether charges. The gauge transformations are generated by two different generators, hence there are two Noether charges, which can be expressed as $v_p^\dagger G J_{\chi_p} v_p/2 = 1$, where the factor $1/2$ arises from the fact that a symplectic vector space is a joint space of position and momentum and where we have used that $J_{\chi_p} v_p = -i$ and $v_p^\dagger G v_p = 2i$. In appendix 6.C, we prove that the corresponding state-space generators $\hat{T}_{\chi_p}$ can be expressed as $\left(\hat{a}_p^\dagger \hat{a}_p + \hat{a}_p \hat{a}_p^\dagger\right)/2$ so that the charges of a mode (6.22) are given by $\langle u_{nm}|\hat{T}_{\chi_1}|u_{nm}\rangle = (n + 1/2)$ and $\langle u_{nm}|\hat{T}_{\chi_2}|u_{nm}\rangle = (m + 1/2)$. Since the gauge transformation in equation (6.44) is constructed from the eigenvectors μ_p, it varies throughout the parameters space. As a result, the generators $\hat{T}_{\chi_p}$ can be constructed only locally and vary through the parameter space according to the ladder-operator transformation in equation (6.20). However, since the modes also vary, it follows that Noether charges $(n + 1/2)$ and $(m + 1/2)$ of the modes $|u_{nm}\rangle$ are globally conserved.

In terms of $\vec{\mathcal{R}}$ and $\vec{\nabla}_{\vec{\mathcal{R}}}$, the equations of motion of the vectors μ_p (6.48) can be rewritten as

$$\left(\vec{\nabla}_{\vec{\mathcal{R}}}\mu_p\right) \cdot \frac{\partial\vec{\mathcal{R}}}{\partial\zeta} = -J\mu_p \ . \tag{6.53}$$

These equations are obviously not invariant under the gauge transformations (6.52). Imposing gauge invariance yields the modified equations of motion

$$\left(\left(\vec{\nabla}_{\vec{\mathcal{R}}} + i\vec{A}_p\right)v_p\right) \cdot \frac{\partial\vec{\mathcal{R}}}{\partial\zeta} = -Jv_p \ , \tag{6.54}$$

where the gauge fields $\vec{A}_p$ are vector fields in the parameter space of $\vec{\mathcal{R}}$ that are defined by their transformation property under the gauge transformations (6.52)

$$\vec{A}_p \to \vec{A}_p - \vec{\nabla}_{\vec{\mathcal{R}}}\psi_p \ . \tag{6.55}$$

With these transformation properties, the equation of motion (6.54) is manifestly invariant under the gauge transformations (6.52). The general solution of this equation (6.54) can be expressed as

$$\nu_p = \mu_p e^{-i\int_C \vec{A}_p \cdot d\vec{\mathcal{R}}} , \tag{6.56}$$

where C is a trajectory $\vec{\mathcal{R}}(\zeta)$ and μ_p solves the equation of motion without the gauge field (6.53). In full analogy with the Aharonov-Bohm effect, this shows that the phase difference between μ_p and ν_p is due to the fact that the latter is coupled to the gauge field $\vec{A}_p$. Since we have defined the vectors μ_p so as to include the appropriate geometric-phase factor while they are not coupled to the gauge fields, the coupling of ν_p to the gauge fields removes the geometric phase rather than introducing it. The geometric origin of the phases is evident in that they are determined only by the trajectory C and do not depend on the velocity $\partial\vec{\mathcal{R}}/\partial\zeta$. By using equation (6.54) they can be expressed as

$$\chi_p = \int_C \vec{A}_p \cdot d\vec{\mathcal{R}} = \frac{1}{2}\int_0^{\zeta} d\zeta' \left\{ \nu_p G J \nu_p + \left(\nu_p^\dagger G \vec{\nabla}_{\mathcal{R}} \nu_p\right) \cdot \frac{\partial \vec{\mathcal{R}}}{\partial \zeta} \right\} , \tag{6.57}$$

which is in obvious agreement with equation (6.51).

In analogy with the Aharonov-Bohm effect, the Noether charges $\nu_p^\dagger G J_{\chi_p} \nu_p/2 = 1$ determine the strength of the coupling of the vectors μ_p to the gauge fields $\vec{A}_p$. This is consistent with the fact that the vectors ν_p pick up phases χ_p. The Noether charges of the modes (6.22), however, are equal to $n + 1/2$ and $m + 1/2$ and depend on the mode numbers n and m. As a result, the modes $|u_{nm}\rangle$ couple differently to the (corresponding state-space) gauge fields and, therefore, experience different phase shifts. This is in obvious agreement with equation (6.39).

The Noether currents $(\nu_p^\dagger G J_{\chi_p} \nu_p/2)\partial\vec{\mathcal{R}}/\partial\zeta = \partial\vec{\mathcal{R}}/\partial\zeta$ are uniform throughout the parameters space of $\vec{\mathcal{R}}$. It follows that the "physical" fields or Berry curvatures $F_{\alpha\beta} = \partial_\alpha (A_p)_\beta - \partial_\beta (A_p)_\alpha$, where the indices α and β run over the parameter-space vector components, are constant so that the gauge fields $\vec{A}_p(\vec{\mathcal{R}})$ cannot possess any non-trivial dynamics. Attributing the generalized Gouy phases χ_p to coupling to gauge fields $\vec{A}_p$, which do not have any dynamical properties in their own rights, may seem a bit tautological. On the other hand, the analysis discussed here shows that the structure that underlies the generalized Gouy phase shifts (6.39) is that of a gauge theory. In this picture, the appearance of phase shifts under propagation through an optical set-up is the unavoidable consequence of the $U(1)\times U(1)$ gauge invariance of the dynamics of paraxial optical modes, or, equivalently, of the fact that the mode charges $n + 1/2$ and $m + 1/2$ are conserved under state-space transformations $\in Mp(4, \mathbb{R})$.

The connection between the gauge invariance as discussed here does not depend on the specific structure of the symplectic vector space. Our results as well as the Aharonov-Bohm effect indicate that there is a more general connection between local gauge invariance and the appearance of geometric phases, see, for instance, reference [99].

6.5 Geometric phases for non-astigmatic modes

6.5.1 Ray matrices on the Hermite-Laguerre sphere

A particulary interesting limiting case of the geometric phases that we discuss in this chapter, are the phase shifts due to mode conversions on the Hermite-Laguerre sphere, each point on which characterizes a basis set of higher-order modes. We focus on non-astigmatic modes in their focal planes so that S can be considered a real scalar $s \in \mathbb{R}$. We shall construct ray matrices and corresponding state-space operators that solely modify the degrees of freedom associated with the Hermite-laguerre sphere and study the geometric phases arising from such transformations.

The azimuth angle φ on the Hermite-Laguerre sphere specifies the orientation in the transverse plane of the set of higher-order modes. It can be modified by the rotation operator $\exp(-i\varphi\hat{s}_3)$, where $\hat{s}_3 = k(\hat{x}\hat{\vartheta}_y - \hat{y}\hat{\vartheta}_x)/2 = (\hat{T}_6 - \hat{T}_7)/2$ is the corresponding generator. The factor $1/2$ accounts for the fact that a rotation angle φ on the Hermite-Laguerre sphere corresponds to a $\phi = \varphi/2$ in the transverse plane. For reasons that will become clear, the ray matrix that describes a rotation in a plane parallel to an equatorial plane on the Hermite-Laguerre sphere is denoted M_3. It takes the following form

$$M_3(\varphi) = e^{-\varphi\Sigma_3} = \begin{pmatrix} \mathsf{P}\left(\frac{\varphi}{2}\right) & 0 \\ 0 & \mathsf{P}\left(\frac{\varphi}{2}\right) \end{pmatrix} = \begin{pmatrix} \cos\left(\frac{\varphi}{2}\right) & -\sin\left(\frac{\varphi}{2}\right) & 0 & 0 \\ \sin\left(\frac{\varphi}{2}\right) & \cos\left(\frac{\varphi}{2}\right) & 0 & 0 \\ 0 & 0 & \cos\left(\frac{\varphi}{2}\right) & -\sin\left(\frac{\varphi}{2}\right) \\ 0 & 0 & \cos\left(\frac{\varphi}{2}\right) & \sin\left(\frac{\varphi}{2}\right) \end{pmatrix}, \quad (6.58)$$

where $\Sigma_3 = (J_6 - J_7)/2$ is the corresponding ray-space generator and $\mathsf{P} \in SO(2)$ is a 2×2 rotation matrix. When this ray matrix acts on an arbitrary pair of complex ray vectors μ_p that obey the identities (6.23) and (6.25), the matrix S transforms according to $\mathsf{S} \to \mathsf{PSP}^{\mathrm{T}}$. In the present case of scalar S, this transformation only modifies the orientation of the mode patterns and does not affect S.

Another class of transformations that solely act upon the Hermite-Laguerre sphere are those that describe mode converters. Mode converters consists of a pair of astigmatic or cylindrical lenses [100]. The distance between the lenses and their radii of curvature are chosen such that the Gouy phase shift introduces a phase difference ϑ between the eigenvectors μ_1 and μ_2 of the transformation of the mode converter. If the input and output plane of the mode converter are chosen such that they respectively coincide with focal planes of the incident and outgoing modes and if the modes are matched to the mirrors so that S is scalar and equal to 1 in appropriate units determined by the mirrors, the eigenvectors of the mode converter are given by $\tilde{\mu}_1 = (1, 0, i, 0)^{\mathrm{T}}$ and $\tilde{\mu_2} = (0, 1, 0, i)^{\mathrm{T}}$ and their complex conjugates. The ray matrix that describes the transformation that introduces a phase difference ϑ between

$\tilde{\mu}_1$ and $\tilde{\mu}_2$ can then be constructed as

$$M_1(\vartheta) = e^{-\vartheta\Sigma_1} = \begin{pmatrix} \cos\left(\frac{\vartheta}{2}\right) & 0 & \sin\left(\frac{\vartheta}{2}\right) & 0 \\ 0 & \cos\left(\frac{\vartheta}{2}\right) & 0 & -\sin\left(\frac{\vartheta}{2}\right) \\ -\sin\left(\frac{\vartheta}{2}\right) & 0 & \cos\left(\frac{\vartheta}{2}\right) & 0 \\ 0 & \sin\left(\frac{\vartheta}{2}\right) & 0 & \cos\left(\frac{\vartheta}{2}\right) \end{pmatrix}, \tag{6.59}$$

where $\Sigma_1 = k(J_1 - J_2)/4 + (J_9 - J_{10})/(4k)$ is the corresponding generator. Again, one may prove easily that this transformation does not affect the astigmatic degrees of freedom if S is scalar and equal to 1. The corresponding state-space generator is given by $\hat{s}_1 = k(\hat{T}_1 - \hat{T}_2)/4 + (\hat{T}_9 - \hat{T}_{10})/(4k) = k(\hat{x}^2 - \hat{y}^2 + \hat{\vartheta}_x^2 - \hat{\vartheta}_y^2)/4$.

So far, we have constructed two of the three ray matrices that only modify the nature and orientation of the higher-order modes. The third corresponds to a mode converter in a basis that is rotated over $\pi/4$ in the transverse plane, or, equivalently over $\pi/2$ in the equatorial plane of the Hermite-Laguerre sphere. The ray matrix that describes such a transformation can be obtained as

$$M_2(\vartheta) = M_3(\pi/4)M_1(\vartheta)M_3^{-1}(\pi/4) = e^{-\vartheta\Sigma_2} = \begin{pmatrix} \cos\left(\frac{\vartheta}{2}\right) & 0 & 0 & \sin\left(\frac{\vartheta}{2}\right) \\ 0 & \cos\left(\frac{\vartheta}{2}\right) & \sin\left(\frac{\vartheta}{2}\right) & 0 \\ 0 & -\sin\left(\frac{\vartheta}{2}\right) & \cos\left(\frac{\vartheta}{2}\right) & 0 \\ -\sin\left(\frac{\vartheta}{2}\right) & 0 & 0 & \cos\left(\frac{\vartheta}{2}\right) \end{pmatrix}, \tag{6.60}$$

where $\Sigma_2 = kJ_3/2 + J_8/(2k)$ is the corresponding generator. The corresponding state-space generator is given by $\hat{s}_2 = k\hat{T}_3/2 + \hat{T}_8/(2k) = k(xy + \hat{\vartheta}_x\hat{\vartheta}_y)/2$. Since M_3 and M_1 do not affect the astigmatic degrees of freedom if S is scalar and equal to 1, it follows that the same is true for M_3.

By using the canonical commutation relations (6.4) and the definitions of the generators $\hat{s}_1$, $\hat{s}_2$ and $\hat{s}_3$ in terms of the canonical operators, one may easily show that the generators obey an $SU(2)$ algebra

$$[\hat{s}_1, \hat{s}_2] = i\hat{s}_3 \tag{6.61}$$

and cyclic permutations. The ray-space generators obey

$$[\Sigma_1, \Sigma_2] = \Sigma_3 \tag{6.62}$$

so that the matrices $i\Sigma_1$, $i\Sigma_2$ and $i\Sigma_3$ also constitute an $SU(2)$ algebra. Thus we have obtained both a metaplectic and a symplectic realization of an $SU(2)$ algebra. This proves the well-known fact that $SU(2)$ is a subgroup of $Mp(4)$ and, therefore, of $Sp(4, \mathbb{R})$.

6.5.2 Spinor transformations

Since the generators Σ_1, Σ_2 and Σ_3 constitute an $SU(2)$ algebra, an arbitrary pair of ray vectors μ_p on the Hermite-Laguerre sphere can be expressed as a linear combination of the

eigenvectors of one of these generators. In analogy with section 6.3, where we introduced the components of η as the coefficients of the expansion of an arbitrary bosonic lowering operator in terms of the two lowering operators for a harmonic oscillator in two dimensions, we can write an arbitrary pair of complex ray vectors on the Hermite-Laguerre sphere as

$$\mu_1 = \eta_1\tilde{\mu}_1 + \eta_2\tilde{\mu}_2 \qquad \text{and} \qquad \mu_2 = -\eta_2^*\tilde{\mu}_1 + \eta_1^*\tilde{\mu}_2 \,, \tag{6.63}$$

where $\tilde{\mu}_1 = (1,0,i,0)^{\mathrm{T}}$ and $\tilde{\mu}_2 = (1,0,i,0)^{\mathrm{T}}$ are eigenvectors of Σ_1 with eigenvalues $-i$ and i respectively, (they are also eigenvectors of $J_{\mathrm{HO}} = k(J_1+J_2)/4+(J_9+J_{10})/(4k)$ with degenerate eigenvalues i). Notice that, analogous to the construction in section 6.3 and the mapping in equation (6.35), the components of η are spinor components in a linear rather than in a circular basis. The symplectic orthogonality properties (6.23) and (6.25) require that the expansions in equation (6.63) do not involve the complex conjugate vectors μ_p^*. Moreover, they ensure normalization of η such that $|\eta_1|^2 + |\eta_2|^2 = 1$.

Since the ray matrices M_1, M_2 and M_3, as defined in equations (6.59), (6.60) and (6.58), only modify the degrees of freedom associated with η, these transformations can be expressed in the two-dimensional spinor space. In particular, the transformation described by M_3 (6.58) can be expressed as

$$\begin{pmatrix} \eta_1 \\ \eta_2 \end{pmatrix} \to \begin{pmatrix} \cos\left(\frac{\varphi}{2}\right) & -\sin\left(\frac{\varphi}{2}\right) \\ \sin\left(\frac{\varphi}{2}\right) & \cos\left(\frac{\varphi}{2}\right) \end{pmatrix} \begin{pmatrix} \eta_1 \\ \eta_2 \end{pmatrix} = e^{-i\varphi\tau_3/2} \begin{pmatrix} \eta_1 \\ \eta_2 \end{pmatrix} , \tag{6.64}$$

where

$$\tau_3 = \begin{pmatrix} 0 & -i \\ i & 0 \end{pmatrix} \tag{6.65}$$

is the corresponding generator. Similarly, the transformations (6.59) and (6.60) of mode converters can be rewritten in terms of the spinor components as

$$\begin{pmatrix} \eta_1 \\ \eta_2 \end{pmatrix} \to \begin{pmatrix} e^{\frac{i\vartheta}{2}} & 0 \\ 0 & e^{\frac{-i\vartheta}{2}} \end{pmatrix} \begin{pmatrix} \eta_1 \\ \eta_2 \end{pmatrix} = e^{-i\vartheta\tau_1/2} \begin{pmatrix} \eta_1 \\ \eta_2 \end{pmatrix} \tag{6.66}$$

and

$$\begin{pmatrix} \eta_1 \\ \eta_2 \end{pmatrix} \to \begin{pmatrix} \cos\left(\frac{\vartheta}{2}\right) & i\sin\left(\frac{\vartheta}{2}\right) \\ i\sin\left(\frac{\vartheta}{2}\right) & \cos\left(\frac{\vartheta}{2}\right) \end{pmatrix} \begin{pmatrix} \eta_1 \\ \eta_2 \end{pmatrix} = e^{-i\varphi\tau_2/2} \begin{pmatrix} \eta_1 \\ \eta_2 \end{pmatrix} , \tag{6.67}$$

where the corresponding spinor generators are given by

$$\tau_1 = \begin{pmatrix} -1 & 0 \\ 0 & 1 \end{pmatrix} \qquad \text{and} \qquad \tau_2 = \begin{pmatrix} 0 & -1 \\ -1 & 0 \end{pmatrix} . \tag{6.68}$$

As a result of the fact that we have the defined the spinor components with respect to the eigenvectors of Σ_1 rather than of Σ_3, the spinor generators τ_1, τ_2 and τ_3 take the form of Pauli matrices in a rotated basis. They also form an $SU(2)$ algebra, i.e., $[\tau_1, \tau_2] = i\tau_3$ and cyclic

permutations. This algebra is closed and the matrix transformations of η on the Hermite-Laguerre sphere that are generated by τ_1, τ_2 and τ_3 are analogues of Jones matrices in polarization optics.

Since the complex vectors $\tilde{\mu}_1$ and $\tilde{\mu}_2$ are eigenvectors of Σ_1 with eigenvalues $-i$ and i respectively, the spinor corresponding to a point (ϕ, θ) on the Hermite-Laguerre sphere can be expressed as

$$\eta(\phi,\theta) = (-i)^{1/2} e^{-i(\phi+\pi/2)\tau_3} e^{-i\theta\tau_1} e^{i\pi\tau_2/2} \begin{pmatrix} 1 \\ 0 \end{pmatrix}, \tag{6.69}$$

where the factor $(-i)^{1/2} = \exp(-i\pi/4)$ is introduced to make this identity consistent with equation (6.35).

6.5.3 Mode-space transformations

In dimensionless notation, the lowering operators corresponding to the complex ray vectors $\tilde{\mu}_p$ can be expressed as

$$\hat{b}_x = \sqrt{\frac{k}{2}}(\hat{x} + i\hat{\vartheta}_x) \qquad \text{and} \qquad \hat{b}_y = \sqrt{\frac{k}{2}}(\hat{y} + i\hat{\vartheta}_y)\,. \tag{6.70}$$

The corresponding raising operators $\hat{b}_x^\dagger$ and $\hat{b}_y^\dagger$ generate the set of harmonic-oscillator states in two dimensions $|v_{nm}\rangle$ according to equation (6.22), the raising operators being replaced by the harmonic-oscillator raising operators. This set corresponds to $\eta = (1,0)^{\mathrm{T}}$, which is on the equator of the Hermite-Laguerre sphere. The antipodal point $\eta = (0,1)^{\mathrm{T}}$ gives rise to the same set of modes $|v_{mn}\rangle$, the mode indices being interchanged. The modes corresponding to an arbitrary point on the Hermite-Laguerre sphere can be expanded as

$$|u_{nm}(\eta)\rangle = \frac{1}{\sqrt{n!m!}} \left(\eta_1^* \hat{b}_x^\dagger + \eta_2^* \hat{b}_y^\dagger\right)^n \left(-\eta_2 \hat{b}_x^\dagger + \eta_1 \hat{b}_y^\dagger\right)^m |v_{00}\rangle\,. \tag{6.71}$$

By using that $[\hat{b}_x^\dagger, \hat{b}_y^\dagger] = 0$, this can be rewritten as

$$|u_{nm}(\eta)\rangle = \sum_{p=0}^{n}\sum_{q=0}^{m} \sqrt{\frac{(n+m-p-q)!(p+q)!}{n!m!}} \binom{n}{p}\binom{m}{q} \times (\eta_1^*)^{n-p}(\eta_2^*)^p(-\eta_2)^{m-q}(\eta_1)^q |v_{(n+m-p-q)(p+q)}\rangle\,, \tag{6.72}$$

which expresses the transformed state $|u_{nm}(\eta)\rangle$ as an expansion in two-dimensional harmonic-oscillator states of the same order $N = n+m$. Conversely, this result shows that the subspaces of modes of fixed order $N = n + m$ are closed under transformations (mode conversions) on the Hermite-Laguerre sphere.

In general, the subspace of modes of fixed order N is an $N + 1$-dimensional subspace of the Hilbert space of transverse states of the field. The unitary transformations on this subspace form the group $SU(N + 1)$. Only in the special case of first order modes, the most general unitary transformation is equivalent to the $SU(2)$ transformation that figures

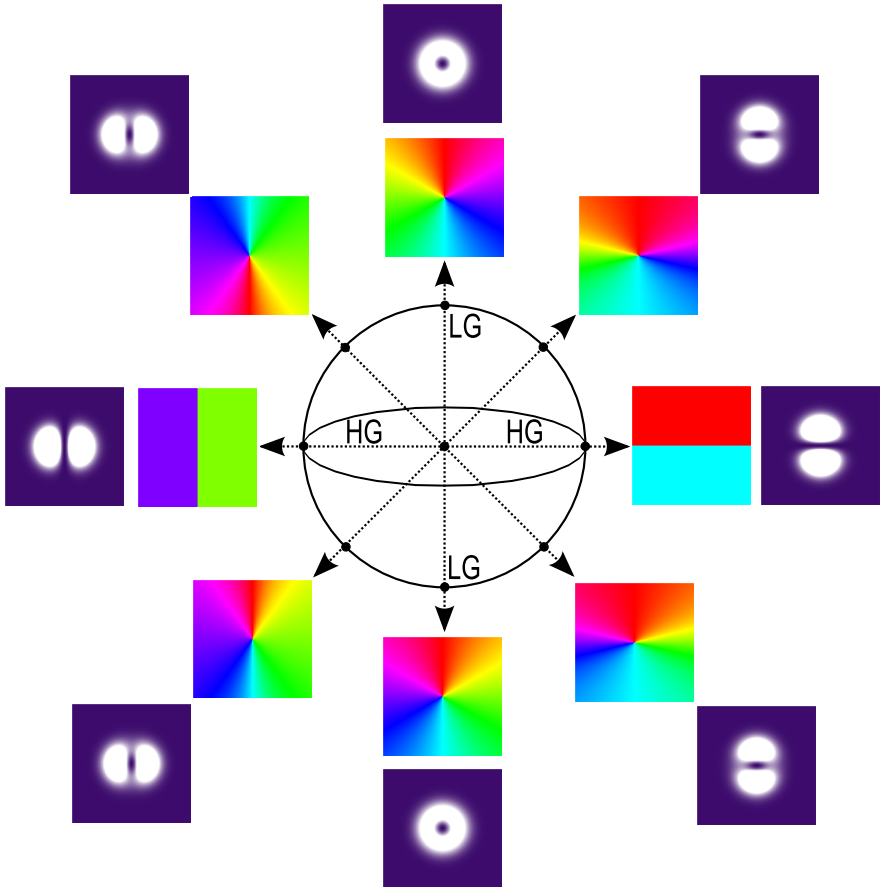

Figure 6.1: Intensity and false-color phase patterns of the modes that lie in the $\varphi = 0$ plane of the Hermite-Laguerre, or, equivalently, Poincaré sphere for the non-astigmatic first-order modes $|u_{01}\rangle$. The north and a south poles ($\vartheta = 0, \pi$) respectively correspond to Laguerre-Gaussian modes with $l = n - m = -1$ and $l = m - n = 1$. On both poles $p = \min(n, m) = 0$. The modes on the equator ($\vartheta = \pi/2$) are Hermite-Gaussian while modes for intermediate values of ϑ are generalized Gaussian modes. The color coding in the phase patterns is such that the color changes in a continuous fashion from red via yellow, green, blue and purple back to red when the phase changes from 0 to 2π.

in equation (6.72). It follows that the subspace of first-order modes is isomorphic to the Hermite-Laguerre sphere for the ladder operators. This sphere, which is an analogue of the Poincaré sphere for polarization states [93], as well as the intensity and phase structure of some of the modes that lie on it, is plotted in figure 6.1. In the general case of $N > 1$, $SU(2)$ is a subgroup of the group $SU(N+1)$ of unitary transformations on the subspace of modes of fixed order N. This accounts for the fact that only specific transformations on the Hilbert space of transverse states of the field can be achieved by mode converters and image rotators. In case of $N > 1$, the transformation in equation (6.72) gives rise to a sphere for each combination (n, m) of the transverse mode numbers. Since $|u_{nm}(\eta)\rangle$ and $|u_{mn}(\eta)\rangle$ correspond to antipodal points on the same sphere, it follows that, depending on the parity of N, only $(N+2)/2$ (for even N) or $(N+1)/2$ (for odd N) of these spheres are independent, i.e., not related by rotations over π. All of these spheres are isomorphic to the Hermite-Laguerre sphere for the ladder operators. Since, in general, the modes on a given sphere cannot be expressed as a linear combination of the modes on the poles, it follows that, for $N > 1$, these spheres are not Poincaré spheres in the strict sense. The two spheres for second-order modes, as well as the intensity and phase patterns of some of the modes that lie on them, are plotted in figure 6.2.

The mode-transformation in equation (6.72), together with the matrix representation of the spinor transformation that we have discussed above, provides a matrix description of beam transformations of non-astigmatic optical modes of arbitrary order. It generalizes the description discussed in references [101, 102], which applies to first order modes.

By inverting the relations in equation (6.70) and their hermitian conjugates, the position and propagation-direction operators can be expressed in terms of the ladder operators. Using this result, the state-space generators can be written as $\hat{s}_1 = (\hat{b}_x^\dagger \hat{b}_x - \hat{b}_y^\dagger \hat{b}_y)/2$, $\hat{s}_2 = (\hat{b}_x^\dagger \hat{b}_y + \hat{b}_x \hat{b}_y^\dagger)/2$ and $\hat{s}_3 = (\hat{b}_x^\dagger \hat{b}_y - \hat{b}_x \hat{b}_y^\dagger)/(2i)$, which is a Schwinger representation of the $SU(2)$ algebra. Here, the $SU(2)$ algebra (6.61) is ensured by the boson commutation relations (6.21). This representation provides a complete and closed description of the modes and transformations on the Hermite-Laguerre sphere in terms of the ladder operators.

6.5.4 Geometric phases and the Aharonov-Bohm analogy

The spinor η, as defined by equation (6.35), is completely determined by the azimuthal and polar angles on the Hermite-Laguerre sphere. The reverse of this statement is not true; choosing a point on the Hermite-Laguerre sphere fixes a properly normalized spinor $\xi^\dagger \xi = 1$ up to an overall phase factor so that $\xi = \exp(i\chi)\eta(\phi, \xi)$ with $\chi \in \mathbb{R}$. In the limiting case of transformations on the Hermite-Laguerre sphere, it follows from equation (6.63), or from the equivalent expansion in terms of the lowering operators in equation (6.70), that the two raising operators $a_1^\dagger$ and $\hat{a}_2^\dagger$ pick up equal but opposite phases $-\chi$ and χ respectively. The modes $|u_{nm}(\eta)\rangle$ (6.71) pick up a phases $\exp(-i\chi_{nm})$ with

$$\chi_{nm} = (n - m)\chi \, . \tag{6.73}$$

Such phases do not modify the physical properties of the modes but their variation under (a sequence of) transformations on the Hermite-Laguerre sphere can be measured interferometrically. Analogous to the discussion in section 6.4, we shall show that the variation χ has a geometric interpretation in terms of the Hermite-Laguerre sphere. We consider (a sequence of) state-space transformations that only modify the degrees of freedom associated with the nature and orientation of the higher-order modes. The evolution of the ladder operators under such transformations is described by the anti-Heisenberg equation of motion (6.47) when $\hat{T}$ is replaced by a generator $\hat{s}/2$, which is a linear combination of $\hat{s}_1$, $\hat{s}_2$ and $\hat{s}_3$, and ζ parameterizes a trajectory on the Hermite-Laguerre sphere. The factor $1/2$ in the generator is introduced for notational convenience. In terms of a spinor ξ, the equation of motion (6.48) takes the following form

$$\frac{\partial \xi}{\partial \zeta} = -\frac{i\tau\xi(\zeta)}{2} \,, \tag{6.74}$$

where τ is the spinor generator that corresponds to $\hat{s}$. It is a linear combination of τ_1, τ_2 and τ_3. The spinor ξ picks up the appropriate phase factor. Substitution of $\xi = \exp(i\chi)\eta$ gives

$$i\eta\frac{\partial \chi}{\partial \zeta} + \frac{\partial \eta}{\partial \zeta} = -\frac{i\tau\eta}{2} \,. \tag{6.75}$$

Using that $\eta^\dagger\eta = 1$, this result can be rewritten as

$$\frac{\partial \chi}{\partial \zeta} = i\eta^\dagger\frac{\partial \eta}{\partial \zeta} - \frac{\eta^\dagger\tau\eta}{2} \,. \tag{6.76}$$

The generator τ represents a constant of motion so that this result can be integrated to yield

$$\chi(\zeta) = -\frac{(\eta^\dagger\tau\eta)\zeta}{2} + i\int_0^\zeta d\zeta' \eta^\dagger\frac{\partial \eta}{\partial \zeta'} \,. \tag{6.77}$$

This result can also be obtained directly from substitution of the complex ray vectors μ_p, as defined by equation (6.63), in the general expression of the geometric phase shift (6.51). The first term in equation (6.51) arises from the fact that $\tau/2$ represents a conserved quantity. The second term constitutes the well-known geometric phase shift that is experienced by a spinor when it is transported along a trajectory on the Hermite-Laguerre sphere. Analogous to the discussion in section 6.4, both contributions are geometric in that they are fully determined by the trajectory on the Hermite-Laguerre sphere but only the second relates to the geometry of the Hermite-Laguerre sphere. It is natural to use spherical coordinates $\vec{\mathcal{R}} = (r\sin(\vartheta)\cos(\varphi), r\sin(\vartheta)\sin(\varphi), r\cos(\vartheta))^{\mathrm{T}}$ to parameterize points on the Hermite-Laguerre sphere. For a closed trajectory that consists of geodesics, the first contribution in equation (6.77) vanishes [103]. Then, the phase shift (6.77) can be rewritten as

$$\chi = i\int_0^z dz' \eta^\dagger\frac{\partial \eta}{\partial z'} = i\int_0^z dz' \eta^\dagger\left(\vec{\nabla}_{\vec{\mathcal{R}}}\eta\right)\cdot\frac{\partial \vec{\mathcal{R}}}{\partial z'} = i\oint_C \eta^\dagger\left(\vec{\nabla}_{\vec{\mathcal{R}}}\eta\right)\cdot d\vec{\mathcal{R}} \,, \tag{6.78}$$

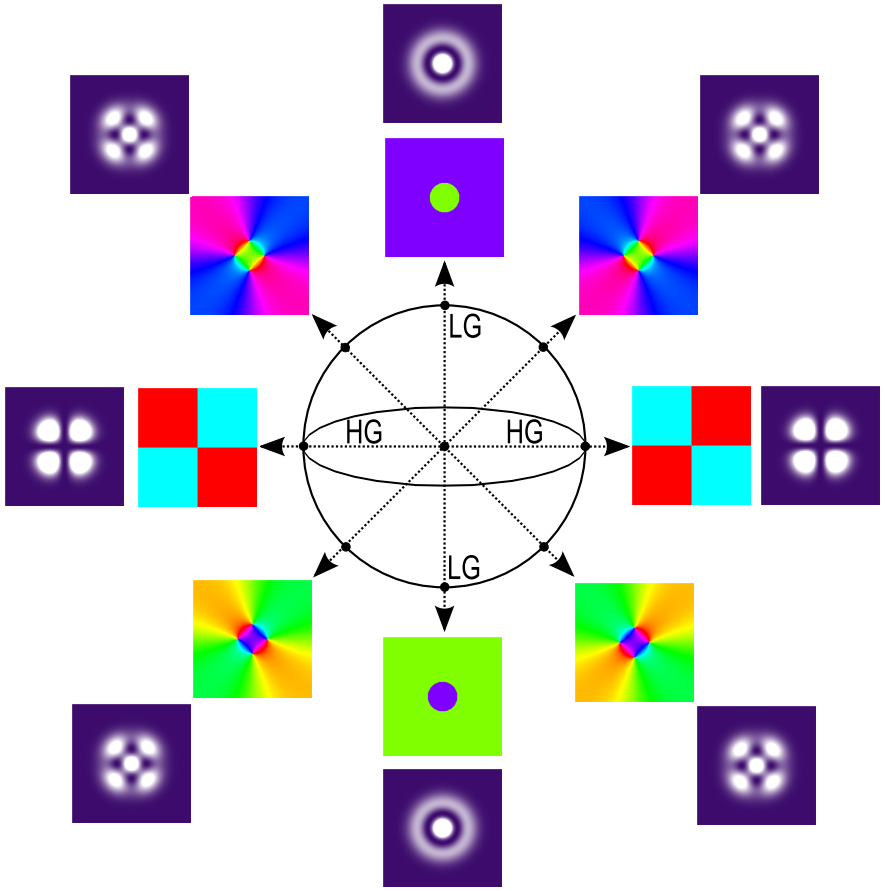

Figure 6.2: Intensity and false-color phase patterns of the modes that lie in the $\varphi = 0$ plane of two the Hermite-Laguerre spheres for non-astigmatic second-order modes $|u_{11}\rangle$ (this page) and $|u_{02}\rangle$ (next page). In the figure on this page, the north and south poles ($\vartheta = 0, \pi$) respectively correspond to Laguerre-Gaussian modes with $l = n - m = m - n = 0$ and $p = \min(n, m) = 0$ while the modes on the equator ($\vartheta = \pi/2$) are Hermite-Gaussian. The intermediate modes are generalized Gaussian modes. In the figure on the next page the north and south poles ($\vartheta = 0, \pi$) respectively correspond to a Laguerre-Gaussian mode

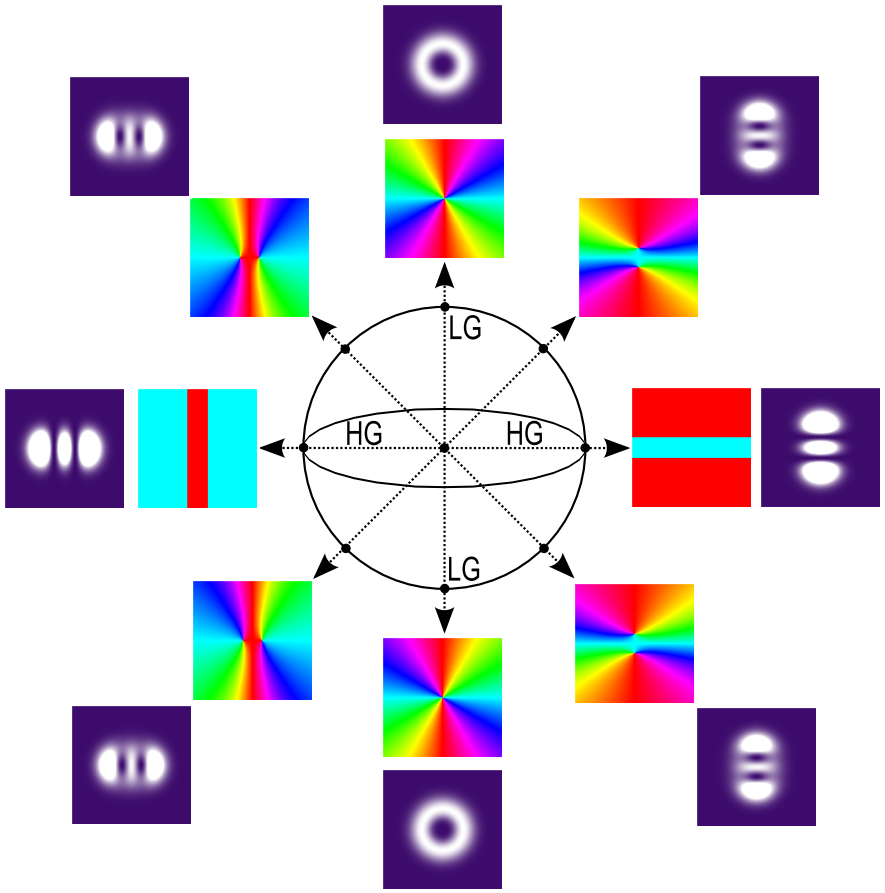

(continued) with $l = n - m = -2$ and $l = m - n = 2$. In both cases $p = \min(n, m) = 1$. Again, the modes on the equator ($\vartheta = \pi/2$) are Hermite-Gaussian while generalized Gaussian modes appear for intermediate values of ϑ. The color coding in the phase patterns is such that the color changes in a continuous fashion from red via yellow, green, blue and purple back to red when the phase changes from 0 to 2π. Both spheres are carbon-copies of the Hermite-Laguerre sphere on which every point characterizes two pairs of bosonic ladder operators.

where $\vec{\nabla}_{\vec{\mathcal{R}}}$ is the gradient in spherical coordinates and $C = \vec{\mathcal{R}}(z)$ is a closed trajectory on the Hermite-Laguerre sphere. In the Aharonov-Bohm picture, this phase shift is due to the coupling of η to a gauge field that arises from the $U(1)$ gauge invariance of the spinor dynamics. Comparison with equation (6.56) shows that this gauge field is given by

$$\vec{A} = \eta^{\dagger}\left(\vec{\nabla}_{\vec{\mathcal{R}}}\eta\right) . \tag{6.79}$$

By using the gradient in spherical coordinates and equation (6.35) $\vec{A}$ can be written as

$$\vec{A} = \frac{i\cot\vartheta}{2r} . \tag{6.80}$$

The corresponding "magnetic" field or Berry curvature is given by

$$\vec{B} = \vec{\nabla}_{\vec{\mathcal{R}}} \times \vec{A} = -\frac{i}{2r^2} \tag{6.81}$$

and is homogeneous on the Hermite-Laguerre sphere. It may be viewed as the field of a monopole located at the center of the Hermite-Laguerre sphere. By the virtue of Stokes' theorem, the geometric phase can be expressed as

$$\chi = i\oint_C \eta^{\dagger}\left(\vec{\nabla}_{\vec{\mathcal{R}}}\eta\right)\cdot d\vec{\mathcal{R}} = i\oint_C \vec{A}\cdot d\vec{\mathcal{R}} = i\oint_{\mathcal{S}} \vec{B}\cdot d\vec{\mathcal{S}} = \frac{1}{2}\oint_{\mathcal{S}} d\Omega = \frac{1}{2}\Omega , \tag{6.82}$$

where $\mathcal{S}$ is the enclosed surface on the Hermite-Laguerre sphere and Ω is the solid angle. This result establishes the well-known connection between the geometric phase acquired by a spinor that is transported along a closed trajectory on the Hermite-Laguerre sphere and the enclosed solid angle Ω on the sphere. Since we have defined the phase picked up by the higher-order modes as $\exp(-i\chi_{nm})$ with $\chi_{nm} = (n-m)\chi$, the result in equation (6.82) has the opposite sign of the analogous result for the standard case in which a spinor with positive helicity picks up a phase shift $\exp(i\chi)$.

The phase shift the modes $|v_{nm}\rangle$, as given by equation (6.73), depends only on the difference between the mode numbers n and m. In the Aharonov-Bohm picture, $n-m$ has the significance of the topological charge of a non-astigmatic mode $|v_{nm}\rangle$ and determines the strength of the coupling to the (corresponding state-space) gauge field. For modes with equal mode numbers $n = m$, the topological charge vanishes so that they do not couple to the gauge field and, therefore, do not experience a phase shift. The orbital angular momentum in non-astigmatic modes $|v_{nm}\rangle$ can be expressed as $(n-m)\cos\vartheta$ [17] and is proportional to their topological charge. It follows that in the case of a non-astigmatic mode, the exchange of orbital angular momentum between the mode and the set-up through which it propagates is necessary for a non-trivial geometric phase to occur [96, 95].

In this section, we have studied the geometric phase that arises from (cyclic) transformations on the Hermite-Laguerre sphere for higher-order modes. We have constructed ray matrices that solely modify the nature and orientation of the higher-order modes and derived the corresponding spinor and mode-space transformations. In terms of the spinor η the phase

shift due to a (cyclic) transformation takes the familiar form of the geometric phase for a spinor. In experimental realizations, mode converters consist of pairs of astigmatic lenses in which the degrees of freedom associated with S are employed to achieve mode conversion [100]. As a result, there will be an additional contribution to the phase shift of the modes. This can be compensated for by measuring the interference between fields that have passed the same sequence of mode converters and image rotators but with different relative orientations [94].

6.6 Concluding remarks

We have explored the parameter space that is associated with the choice of a complete and orthonormal set of paraxial optical modes in the transverse plane. Modes are defined as solutions of the paraxial wave equation (6.3) that are fully characterized by a set of mode parameters whose variation through a paraxial optical set-up is described by the 4×4 ray matrix $M(z)$, which describes the transformation of a ray $r = (\rho, \theta)^{\mathrm{T}}$ from the $z = 0$ input plane of the set-up to the transverse plane z. Complete sets of transverse modes can be obtained from two pairs of bosonic ladder operators. The ladder operators are fully specified by two complex ray vectors μ_p with $p = 1, 2$, which characterize the mode parameters. Their variation through an optical set-up, and, thereby, the variation of the ladder operators, can conveniently be expressed in terms of $M(z)$. We have argued that there is a one-to-one correspondence between the algebraic properties of the ladder operators and the defining properties of a physical ray matrix $\in Sp(4, \mathbb{R})$, i.e., that it is real and obeys the identity (6.15). It follows that all sets of modes can be expressed in terms of two pairs of ladder operators and, moreover, that the freedom in choosing a set of modes is equivalent to the choice of an arbitrary ray matrix $M_0 \in Sp(4, \mathbb{R})$. Since $Sp(4, \mathbb{R})$ is a ten-parameter Lie group, the number of free parameters associated with this choice is equal to ten. A possible physical characterization of these degrees of freedom involves a symmetric 2×2 matrix S, which characterizes the astigmatism of the phase and intensity patterns of the fundamental mode, and a spinor η, which specifies the nature and orientation of the higher-order modes. The matrix S is fully specified by six parameters while characterization of η requires two independent parameters, which can be mapped on a Poincaré sphere. The remaining two degrees of freedom are overall phases of the ladder operators. They do not modify the physical properties of the modes in a given transverse plane z. Their variation through an optical set-up, however, gives rise to a generalized Gouy phase shift of the modes, which can be measured interferometrically. We have shown that both contributions to the variation of the overall phases through an optical set-up, as described by equation (6.51), are geometric in that they are fully determined by the trajectory $\vec{\mathcal{R}}(z)$ and do not depend on the velocity $\partial\vec{\mathcal{R}}/\partial z$. However, only the second contribution in equation (6.51) relates to the geometry of the parameter space. In the specific case of a closed trajectory on the Hermite-Laguerre sphere for non-astigmatic optical modes, the phase shifts of the two raising operators are equal but opposite. In full analogy with the Pancharatnam phase for polarization states, they are equal to half the enclosed surface on the sphere.

It is noteworthy that the overall phases χ_p of the vectors μ_p are in general only unambiguously defined in case of a closed trajectory. In particular, in the propagation-direction representation, the astigmatism of the fundamental mode $\tilde{u}_{00}(\theta, z)$ is fully specified by the symmetric matrix $\mathsf{V} = \mathsf{S}^{-1}$. Analogous to the discussion in section 6.3, the remaining degrees of freedom can be characterized by a unitary 2×2 matrix υ, which is defined such that $\mathsf{T} = \mathsf{V}_\mathrm{r}^{-1/2}\upsilon^\mathrm{T}$. It follows that υ and σ are related by $\sigma = -i\upsilon\mathsf{V}_\mathrm{r}^{-1/2}\mathsf{V}\mathsf{S}_\mathrm{r}^{1/2}$. In general $\det\left(\mathsf{V}_\mathrm{r}^{-1/2}\mathsf{V}\mathsf{S}_\mathrm{r}^{1/2}\right) \neq 1$ so that defining $\sigma = \mathsf{C}\sigma_0$ and $\upsilon = \mathsf{C}'\upsilon_0$ such that σ_0 and υ_0 have unit determinants, requires different phase matrices $\mathsf{C} \neq \mathsf{C}'$. The phase shift along a closed trajectory, however, does not depend on the phase convention used. In the limiting case of transformations of non-astigmatic modes in their focal planes, i.e., when S and V can be considered real scalars, the phases are also unambiguously defined along an open trajectory. All results presented in this chapter are, of course, independent of the phase convention that is chosen.

We have shown that the symplectic group of ladder-operator transformations $Sp(4, \mathbb{R})$ corresponds to the metaplectic group $Mp(4)$ of unitary transformations on the Hilbert space of state vectors $|u\rangle$. The metaplectic group constitutes a subgroup of the set of all possible unitary transformations. This accounts for the fact that only specific linear combinations of paraxial optical modes are modes as well, i.e., are fully characterized by a set of parameters whose variation through a paraxial optical set-up is fully described by the ray matrix $M(z)$. Each combination (n, m) of the transverse mode indices gives rise to a subspace of the Hilbert space of transverse states of the field, which is closed under metaplectic transformations. The geometries of these subspaces are all carbon copies of the geometry of the symplectic manifold underlying the ladder operators. In the limiting case of mode conversions of non-astigmatic modes, the metaplectic group reduces to $SU(2)$ and all those subspaces become spheres, which are all carbon copies of the Hermite-Laguerre sphere for the ladder operators.

We have pointed out an analogy between the Aharonov-Bohm effect in quantum electrodynamics and the generalized Gouy effect in classical wave mechanics. This reveals deep insights in the geometric origin of the latter. The physical properties of the modes (6.22) that are generated by two pairs of ladder operators are not affected by the $U(1)\otimes U(1)$ gauge transformation described by equation (6.52), or, equivalently (6.44). Imposing gauge invariance of the equations of motion (6.47) or (6.48), gives rise to two gauge fields $\vec{A}_p$ in the parameter space. Analogous to the Aharonov-Bohm effect, the geometric phase shift of the ladder operators through an optical set-up is due to the coupling these gauge fields. The raising and corresponding lowering operators have pairwise equal but opposite topological charges and experience opposite phase shifts. The topological charges of the modes $|u_{nn}\rangle$, i.e., the Noether charges that arise from the gauge invariance of the description of their propagation through an optical set-up, are given by $n + 1/2$ and $m + 1/2$ and depend on the mode numbers. As a result, the modes $|u_{nm}\rangle$ couple differently to the gauge fields and experience different phase shifts given by equation (6.39). Notice that the above-mentioned subspaces of modes with transverse mode indices n and m are all uniquely characterized by their coupling to the two (state-space) gauge fields. In the specific case of transformations on the Hermite-Laguerre

sphere for higher-order modes, the phase shifts of the two lowering operators are equal but opposite. In that case, the phase shift of the modes is given by equation (6.73). In the Aharonov-Bohm picture, the variation of this phase is due to the coupling of the spinor η to a single gauge field $\vec{A}$ that arises from the $U(1)$ gauge invariance of the spinor dynamics. The topological charge of the modes $|v_{nm}\rangle$ on the Hermite-Laguerre sphere is equal $n - m$ and the "magnetic" field (Berry curvature) due to the gauge field is uniform on the Hermite-Laguerre sphere. It may be viewed as the field of a monopole located at the center of the sphere.

Although we have focused on the optical case, the mathematical structure that underlies the ladder-operator method and the phase shifts that arise from the geometry underlying the ladder operators are more general. The ray space (ρ, θ) is a phase space in the mathematical sense and the operator description of paraxial wave optics that we have discussed in section 6.2 may be viewed as a formally quantized (wavized) description of rays. Although the interpretation is different, all this is in full analogy with the quantization of classical mechanics to obtain quantum mechanics. As a result, the methods and results of this chapter can be applied to the quantum-mechanical description of wave packets. The only restriction for the ladder-operator approach to apply is that the state-space generators (or Hamiltonian in the quantum language) are quadratic in the canonical operators. The methods and results in this chapter have been formulated such that it is evident how they can be generalized to account for more independent spatial dimensions. In the general case of D dimensions, the number of generators of $Mp(2D)$ and $Sp(2D, \mathbb{R})$ is equal to $2D^2 + D$, $D^2 + D$ of which are associated with a $D \times D$ symmetric matrix that generalizes S. The remaining D^2 parameters specify a unitary matrix $\in U(D)$, which generalizes σ, and corresponds to the choice of D orthonormal $D-$component spinors and D overall phase factors. The variation of the phases under propagation (evolution) have a geometric interpretation in terms of the other degrees of freedom.

Appendices

6.A The ray-space generators J_j

In this appendix we give explicit expressions of the ray-space generators J_j. They are defined by equation (6.16) and correspond to the state-space generators $\hat{T}_j$ as defined in equation (6.9). They are given by

$$J_1 = \frac{2}{k}\begin{pmatrix} 0 & 0 & 0 & 0 \\ 0 & 0 & 0 & 0 \\ 1 & 0 & 0 & 0 \\ 0 & 0 & 0 & 0 \end{pmatrix} \quad J_2 = \frac{2}{k}\begin{pmatrix} 0 & 0 & 0 & 0 \\ 0 & 0 & 0 & 0 \\ 0 & 0 & 0 & 0 \\ 0 & 1 & 0 & 0 \end{pmatrix} \quad J_3 = \frac{1}{k}\begin{pmatrix} 0 & 0 & 0 & 0 \\ 0 & 0 & 0 & 0 \\ 0 & 1 & 0 & 0 \\ 1 & 0 & 0 & 0 \end{pmatrix}$$

$$J_4 = \begin{pmatrix} -1 & 0 & 0 & 0 \\ 0 & 0 & 0 & 0 \\ 0 & 0 & 1 & 0 \\ 0 & 0 & 0 & 0 \end{pmatrix} \quad J_5 = \begin{pmatrix} 0 & 0 & 0 & 0 \\ 0 & -1 & 0 & 0 \\ 0 & 0 & 0 & 0 \\ 0 & 0 & 0 & 1 \end{pmatrix}$$

$$J_6 = \begin{pmatrix} 0 & 0 & 0 & 0 \\ -1 & 0 & 0 & 0 \\ 0 & 0 & 0 & 1 \\ 0 & 0 & 0 & 0 \end{pmatrix} \quad J_7 = \begin{pmatrix} 0 & -1 & 0 & 0 \\ 0 & 0 & 0 & 0 \\ 0 & 0 & 0 & 0 \\ 0 & 0 & 1 & 0 \end{pmatrix}$$

$$J_8 = k\begin{pmatrix} 0 & 0 & 0 & -1 \\ 0 & 0 & -1 & 0 \\ 0 & 0 & 0 & 0 \\ 0 & 0 & 0 & 0 \end{pmatrix} \quad J_9 = 2k\begin{pmatrix} 0 & 0 & -1 & 0 \\ 0 & 0 & 0 & 0 \\ 0 & 0 & 0 & 0 \\ 0 & 0 & 0 & 0 \end{pmatrix} \quad J_{10} = 2k\begin{pmatrix} 0 & 0 & 0 & 0 \\ 0 & 0 & 0 & -1 \\ 0 & 0 & 0 & 0 \\ 0 & 0 & 0 & 0 \end{pmatrix} \tag{6.83}$$

6.B Expectation values of the generators $\hat{T}_j$

This appendix is devoted to a proof of equation (6.27), which expresses the expectation values $\langle u_{nm}|\hat{T}_j|u_{nm}\rangle$ of the generators $\hat{T}_j$ in equation (6.9) in terms of the corresponding ray-space generators $\hat{J}_j$ as defined by equation (6.16). We prove this by mathematical induction. The special cases $\langle u_{00}|\hat{T}_j|u_{00}\rangle$ involve Gaussian standard integrals and can be proven explicitly. A formal proof by mathematical induction thus requires showing that the identity (6.27) holds for modes $|u_{n+1m}\rangle$ and $|u_{nm+1}\rangle$ if it holds for $|u_{nm}\rangle$. In order to prove this, we notice that

$$\langle u_{n+1m}|\hat{T}_j|u_{n+1m}\rangle = \frac{1}{n+1}\langle u_{nm}|\hat{a}_1\hat{T}_j\hat{a}_1^\dagger|u_{nm}\rangle \,. \tag{6.84}$$

Using that

$$\left[\hat{T}_j, \hat{a}_p\right] = \sqrt{\frac{k}{2}}\left(\mu_p^{\mathrm{T}} G\hat{T}_j\,\hat{\boldsymbol{z}} - \mu_p^{\mathrm{T}} G\,\hat{\boldsymbol{z}}\,\hat{T}_j\right) = \sqrt{\frac{k}{2}}\mu_p^{\mathrm{T}} G\left[\hat{T}_j, \hat{\boldsymbol{z}}\right] = i\sqrt{\frac{k}{2}}\mu_p^{\mathrm{T}} G J_j\,\hat{\boldsymbol{z}} \,, \tag{6.85}$$

this can be rewritten as

$$\left(\frac{1}{n+1}\right)\langle u_{nm}|\left(\hat{T}_j\hat{a}_1 - i\sqrt{\frac{k}{2}}\mu_1^{\mathrm{T}}GJ_j\,\hat{\varepsilon}\right)\hat{a}_1^\dagger|u_{nm}\rangle =$$

$$\langle u_{nm}|\hat{T}_j|u_{nm}\rangle - \left(\frac{i}{n+1}\right)\sqrt{\frac{k}{2}}\mu_1^{\mathrm{T}}GJ_j\langle u_{nm}|\,\hat{\varepsilon}\,\hat{a}_1^\dagger|u_{nm}\rangle\,. \tag{6.86}$$

The analogous result may be derived for $|u_{nm+1}\rangle$ and proving equation (6.27) thus boils down to proving that

$$-\left(\frac{i}{n+1}\right)\sqrt{\frac{k}{2}}\mu_p^{\mathrm{T}}GJ_j\langle u_{nm}|\,\hat{\varepsilon}\,\hat{a}_p^\dagger|u_{nm}\rangle = \frac{1}{2}\mu_p^\dagger GJ_j\mu_p = \frac{1}{2}\left(\mu_p^\dagger GJ_j\mu_p\right)^{\mathrm{T}} = \frac{1}{2}\mu_p^T GJ_j\mu_p^*\,, \tag{6.87}$$

where we used that $G^{\mathrm{T}} = -G$ and that $J^{\mathrm{T}}G = -GJ$. This expression can be rewritten as

$$\langle u_{nm}|\,\hat{\varepsilon}\,\hat{a}_p^\dagger|u_{nm}\rangle = i(n+1)\sqrt{\frac{1}{2k}}\mu_p^*\,, \tag{6.88}$$

which we also prove by mathematical induction. Again, the special case of $|u_{00}\rangle$ can be checked explicitly. In order to prove that it is true for $|u_{n+1m}\rangle$ and $|u_{nm+1}\rangle$, we use that

$$\left[\,\hat{\varepsilon}\,,\hat{a}_p^\dagger\right] = \hat{\varepsilon}\left(\sqrt{\frac{k}{2}}\mu_p^\dagger G\,\hat{\varepsilon}\right) - \left(\sqrt{\frac{k}{2}}\mu_p^\dagger G\,\hat{\varepsilon}\right)\hat{\varepsilon} = \sqrt{\frac{k}{2}}\left[\,\hat{\varepsilon}\,,r_p^*\hat{\theta} - t_p^*\hat{\rho}\right] = i\sqrt{\frac{1}{2k}}\mu_p^* \tag{6.89}$$

and find

$$\langle u_{n+1m}|\,\hat{\varepsilon}\,\hat{a}_1^\dagger|u_{n+1m}\rangle = \left(\frac{1}{n+1}\right)\langle u_{nm}|\hat{a}_1\,\hat{\varepsilon}\,\hat{a}_1^\dagger\hat{a}_1^\dagger|u_{nm}\rangle =$$

$$\left(\frac{1}{n+1}\right)\langle u_{nm}|\hat{a}_1\left(\hat{a}_1^\dagger\,\hat{\varepsilon}\, + i\sqrt{\frac{1}{2k}}\mu_1^*\right)\hat{a}_1^\dagger|u_{nm}\rangle = \langle u_{nm}|\,\hat{\varepsilon}\,\hat{a}_1^\dagger|u_{nm}\rangle + i\sqrt{\frac{1}{2k}}\mu_1^*\,. \tag{6.90}$$

The analogous result may be derived for $|u_{nm+1}\rangle$. This completes the proof of equation (6.88) and, thereby, of equation (6.27).

6.C Mode-space operators corresponding to the Noether charges

In this appendix we construct both the ray-space and the corresponding state-space generators of the $U(1)\otimes U(1)$ gauge transformations. The ray matrix that describes such transformations is given by equation (6.44). To first order in the phases χ_1 and χ_2 the matrix C (6.42) is given by

$$\mathsf{C} = \begin{pmatrix} 1+i\chi_1 & 0 \\ 0 & 1+i\chi_2 \end{pmatrix} = \begin{pmatrix} 1 & 0 \\ 0 & 1 \end{pmatrix} + \chi_1\begin{pmatrix} i & 0 \\ 0 & 0 \end{pmatrix} + \chi_2\begin{pmatrix} 0 & 0 \\ 0 & i \end{pmatrix}. \tag{6.91}$$

Substitution in equation (6.44) then gives

$$M_\chi(\{\chi_p\}) = 1 + \frac{\chi_1}{2}\begin{pmatrix} -r_1t_1^\dagger - r_1^*t_1^{\mathrm{T}} & r_1r_1^\dagger + r_1^*r_1^{\mathrm{T}} \\ -t_1t_1^\dagger - t_1^*t_1^{\mathrm{T}} & t_1r_1^\dagger + t_1^*r_1^{\mathrm{T}} \end{pmatrix} +$$

$$\frac{\chi_2}{2}\begin{pmatrix} -r_2t_2^\dagger - r_2^*t_2^{\mathrm{T}} & r_2r_2^\dagger + r_2^*r_2^{\mathrm{T}} \\ -t_2t_2^\dagger - t_2^*t_2^{\mathrm{T}} & t_2r_2^\dagger + t_2^*r_2^{\mathrm{T}} \end{pmatrix}, \tag{6.92}$$

where $r_1 t_1^\dagger = r_1 \otimes t_1^\dagger$ etcetera are direct vector products. From $M_\chi(\{\chi_p\}) = \exp\left(-\chi_p J_{\chi_p}\right) \simeq 1 - \chi_p J_{\chi_p}$, we find that

$$J_{\chi_p} = \frac{1}{2}\begin{pmatrix} r_p t_p^\dagger + r_p^* t_p^{\mathrm{T}} & -r_p r_p^\dagger - r_p^* r_p^{\mathrm{T}} \\ t_p t_p^\dagger + t_p^* t_p^{\mathrm{T}} & -t_p r_p^\dagger - t_p^* r_p^{\mathrm{T}} \end{pmatrix} \tag{6.93}$$

where $p = 1, 2$. These generators are 4×4 matrices in the ray space. By carefully inspecting the form of the direct products and the structure of the generators J_j as given in appendix 6.A we find that

$$\begin{aligned} \hat{T}_{\chi_p} = -\frac{k}{4}\Big\{ & r_p^{\mathrm{T}}\hat{\theta}\hat{\rho}^{\mathrm{T}} t_p^* + r_p^\dagger \hat{\theta}\hat{\rho}^{\mathrm{T}} t_p^{\mathrm{T}} - r_p^{\mathrm{T}}\hat{\theta}\hat{\theta}^{\mathrm{T}} r_p^* - r_p^\dagger \hat{\theta}\hat{\theta}^{\mathrm{T}} r_p^{\mathrm{T}} + \\ & t_p^{\mathrm{T}}\hat{\rho}\hat{\theta}^{\mathrm{T}} r_p^* + t_p^\dagger \hat{\rho}\hat{\theta}^{\mathrm{T}} r_p^{\mathrm{T}} - t_p^{\mathrm{T}}\hat{\rho}\hat{\rho}^{\mathrm{T}} t_p^* - t_p^\dagger \hat{\rho}\hat{\rho}^{\mathrm{T}} t_p^{\mathrm{T}} \Big\} . \end{aligned} \tag{6.94}$$

This can be rewritten as

$$\hat{T}_{\chi_p} = -\frac{k}{4}\left\{ \begin{pmatrix} -t_p^\dagger & r_p^\dagger \end{pmatrix} \begin{pmatrix} \hat{\rho}\hat{\rho}^{\mathrm{T}} & \hat{\rho}\hat{\theta}^{\mathrm{T}} \\ \hat{\theta}\hat{\rho}^{\mathrm{T}} & \hat{\theta}\hat{\theta}^{\mathrm{T}} \end{pmatrix} \begin{pmatrix} t_p \\ -r_p \end{pmatrix} + \begin{pmatrix} -t_p^{\mathrm{T}} & r_p^{\mathrm{T}} \end{pmatrix} \begin{pmatrix} \hat{\rho}\hat{\rho}^{\mathrm{T}} & \hat{\rho}\hat{\theta}^{\mathrm{T}} \\ \hat{\theta}\hat{\rho}^{\mathrm{T}} & \hat{\theta}\hat{\theta}^{\mathrm{T}} \end{pmatrix} \begin{pmatrix} t_p^* \\ -r_p^* \end{pmatrix} \right\} , \tag{6.95}$$

which equals

$$\begin{aligned} \hat{T}_{\chi_p} = \frac{k}{4}\left\{ \mu_p^\dagger G\hat{z}\ \ \hat{z}^{\mathrm{T}} G\mu_p + \mu_p^{\mathrm{T}} G\hat{z}\ \ \hat{z}^{\mathrm{T}} G\mu_p^* \right\} = \\ \frac{k}{2}\left\{ \mu_p^\dagger G\hat{z}\ \ \mu_p^{\mathrm{T}} G\hat{z} + \mu_p^{\mathrm{T}} G\hat{z}\ \ \mu_p^\dagger G\hat{z} \right\} = \frac{1}{2}\left(\hat{a}_p^\dagger \hat{a}_p + \hat{a}_p \hat{a}_p^\dagger \right) , \end{aligned} \tag{6.96}$$

where, we used that $\hat{z}^{\mathrm{T}} G\mu_p$ is scalar so that $\hat{z}^{\mathrm{T}} G\mu_p = (\hat{z}^{\mathrm{T}} G\mu_p)^{\mathrm{T}} = -\mu_p^{\mathrm{T}} G\hat{z}$.

7

An exact quantum theory of rotating light

7.1 Introduction

During the past decades, both the propagation and the diffraction of light through optical set-ups with rotating optical elements [104, 105, 48, 69], as well as the physical properties of rotating beams of light [19, 106, 20] have attracted a steady amount of attention. So far, both theoretical and experimental work has focused mainly on classical aspects of rotating light. Only recently, van Enk and Nienhuis have proposed a first quantum theory of rotating photons [107]. They construct rotating field operators as coherent superpositions of the field operators corresponding to the rotational Doppler-shifted [48] angular-momentum components of the field. In leading order of the paraxial approximation, the spin and orbital degrees of freedom of the radiation field decouple [45] and fields with a rotating polarization and a stationary spatial pattern can be constructed as superpositions of rotational Doppler-shifted circular-polarization states. Similarly, fields with a rotating mode pattern and a stationary polarization can be built up from the rotational Doppler-shifted angular-momentum components of the spatial field distribution. It is, of course, also possible to construct fields with both a rotating polarization and a rotating spatial pattern. Since, in the paraxial approximation, the polarization and spatial degrees of freedom are decoupled, the rotation frequencies may even have different values. The rotation of the polarization and spatial patterns of the fields that are thus constructed are uniform only in the paraxial limit. Moreover, the approach requires that the differences in diffraction of the Doppler-shifted angular-momentum components of the field are negligible, i.e that the the rotation frequency is small compared to the optical

frequency.

In this chapter, we introduce the first exact quantum theory of rotating light. We show that Maxwell's equations in free space have complete sets of solutions that rotate uniformly as a function of time, i.e., that are monochromatic in a rotating frame. Our approach does not necessarily involve paraxial approximations and both the spatial structure and the polarization of the rotating modes of free space rotate at a uniform velocity about the rotation axis. Once such rotating solutions have been obtained, quantization is relatively straightforward. We follow the standard procedure of canonical quantization and show that quantization in the co-rotating frame is consistent with quantization in the stationary frame. We show how this approach can be applied to obtain a quantum-mechanical description of the dynamics of the set of modes that obey rotating boundary conditions. We derive the paraxial counterpart of the exact theory and discuss quantization of the rotating cavity modes that we have studied in chapters 3 and 5 as an example.

The material in this chapter is organized as follows. In the next section, we summarize the equations of motion of the radiation field, show how they may be derived from the standard Lagrangian for the free electromagnetic field and discuss canonical quantization in the Coulomb gauge [5]. In section 7.3 we study the dynamics of light in a rotating frame and derive complete sets of monochromatic solutions of the wave equation in such a frame. The corresponding field operators in a stationary frame are introduced and discussed in section 7.4, where we also discuss quantization in the rotating frame. In the final section we summarize our results and draw our conclusions.

7.2 Preliminaries

7.2.1 Equations of motion of the free radiation field

It is well-known from textbook electrodynamics that the electric and magnetic fields are fully characterized by a scalar potential $\Phi(\mathbf{r},t)$ and a vector potential $\mathbf{A}(\mathbf{r},t)$. In terms of these potentials the fields are given by [4]:

$$\mathbf{B}(\mathbf{r},t) = \nabla \times \mathbf{A}(\mathbf{r},t) \qquad \text{and} \qquad \mathbf{E}(\mathbf{r},t) = -\nabla\Phi(\mathbf{r},t) - \frac{\partial \mathbf{A}}{\partial t}\,, \tag{7.1}$$

where c is the speed light. These definitions ensure that the homogeneous Maxwell equations are obeyed [4]. Although the fields are fully specified by the potentials $\Phi(\mathbf{r},t)$ and $\mathbf{A}(\mathbf{r},t)$, the reverse is not true; there is some arbitrariness (gauge freedom) in the choice of the potentials. The dynamics of the free radiation field is most conveniently described in the Coulomb gauge, which is defined by the requirement that [4]

$$\nabla \cdot \mathbf{A}(\mathbf{r},t) = 0\,. \tag{7.2}$$

In the absence of electric charges and currents, it follows from the inhomogeneous Maxwell equations that the scalar potential Φ vanishes while the vector potential obeys the wave equa-

tion

$$\left(\nabla^2 - \frac{1}{c^2}\frac{\partial^2}{\partial t^2}\right)\mathbf{A}(\mathbf{r},t) = 0\ , \tag{7.3}$$

which, together with the requirement that the field is divergence free (7.2), fully describes the dynamics of the free radiation field in the Coulomb gauge.

In general, the dynamics of the free electromagnetic field may be described by the Lagrangian [5]

$$L = \int d_3\mathbf{r}\ \mathcal{L}(\mathbf{A},\dot{\mathbf{A}}) = \frac{\epsilon_0}{2}\int d_3\mathbf{r}\left\{|\dot{\mathbf{A}}|^2 - c^2|(\nabla\times\mathbf{A})|^2\right\} = \frac{\epsilon_0}{2}\left\{\langle\dot{\mathbf{A}}|\dot{\mathbf{A}}\rangle - c^2\langle\nabla\times\mathbf{A}|\nabla\times\mathbf{A}\rangle\right\}\ , \tag{7.4}$$

where $\mathcal{L}$ is the Lagrangian density in real space and we have adopted the Dirac notation of quantum mechanics to denote the state of the classical radiation field. In case of the free radiation field it is natural to assume that the field $\mathbf{A}$ and its derivatives vanish at infinity while, for the radiation field enclosed by an ideal cavity with a perfectly conducting boundary, the Maxwell boundary conditions [4] require that $\mathbf{A}$ at the boundary is locally normal to it. In both cases, and under the assumption that the field is locally transverse so that it obeys equation (7.2), partial integration of the second term in equation (7.4) yields $\int d_3\mathbf{r}\ |\nabla\times\mathbf{A}|^2 = -\int d_3\mathbf{r}\ \mathbf{A}\cdot\left(\nabla^2\mathbf{A}\right)$. Using this, one may show that the Euler-Lagrange equation that derives from the Lagrangian (7.4) reproduces the wave equation (7.3). The canonical momentum density corresponding to the field $\mathbf{A}$ is given by

$$\mathbf{\Pi}_\mathbf{A} = \frac{\partial\mathcal{L}}{\partial\dot{\mathbf{A}}} = \epsilon_0\dot{\mathbf{A}}\ . \tag{7.5}$$

The Hamiltonian may be obtained as

$$H = \int d_3\mathbf{r}\left\{\mathbf{\Pi}_\mathbf{A}\cdot\dot{\mathbf{A}} - \mathcal{L}\right\} = \frac{1}{2\epsilon_0}\left\{\langle\mathbf{\Pi}_\mathbf{A}|\mathbf{\Pi}_\mathbf{A}\rangle + \epsilon_0^2c^2\langle\nabla\times\mathbf{A}|\nabla\times\mathbf{A}\rangle\right\} = \frac{1}{2\epsilon_0}\left\{\langle\mathbf{\Pi}_\mathbf{A}|\mathbf{\Pi}_\mathbf{A}\rangle - \epsilon_0^2c^2\langle\mathbf{A}|\nabla^2\mathbf{A}\rangle\right\}\ . \tag{7.6}$$

The second equality only holds in the Coulomb gauge as defined by equation (7.2). In this gauge, the corresponding Hamilton equations reproduce the wave equation (7.3).

7.2.2 Modes and quantization

Optical modes are usually defined as monochromatic solutions of the wave equation (7.3). Although the vector potential is real, it is convenient to allow for complex mode functions $\mathbf{F}_\lambda(\mathbf{r})$ so that the vector potential corresponding to a mode $\mathbf{F}_\lambda$ is given by $\mathbf{A}(\mathbf{r},t) = \mathrm{Re}\{\mathbf{F}_\lambda(\mathbf{r})\exp(-i\omega_\lambda t)\}$. The subscript λ denotes a set of mode indices, which characterizes the spatial and polarization structure of the mode function $\mathbf{F}_\lambda$. For a given set of modes, the amplitudes $\langle\mathbf{F}_\lambda|\mathbf{A}\rangle$ and their derivatives $\langle\mathbf{F}_\lambda|\dot{\mathbf{A}}\rangle$ obey harmonic equations of motion and it follows

that the radiation field can be quantized as a set of harmonic oscillators. In case of the free field it is customary to quantize the field in a basis of plane waves. It is well-known, however, that quantization can be performed in a manifestly basis-independent manner, which also applies to the case of a set of cavity modes with finite spatial extent [108]. For later reference, we briefly summarize the quantization of the radiation field in an orthonormal but otherwise arbitrary set of modes $\{\mathbf{F}_\lambda\}$. Since the complex vector potential corresponding to a mode $\mathbf{F}_\lambda$ is given by $\mathbf{F}_\lambda(\mathbf{r})\exp(-i\omega_\lambda t)$, it follows from the wave equation (7.3) that the mode functions obey the Helmholtz equation

$$\left(\nabla^2 + k_\lambda^2\right)\mathbf{F}_\lambda(\mathbf{r}) = 0\,, \tag{7.7}$$

where $k_\lambda^2 = \omega_\lambda^2/c^2$ so that also $\mathbf{F}_\lambda(\mathbf{r})\exp(i\omega_\lambda t)$ is a solution of the wave equation (7.3). However, since also $\mathbf{F}_\lambda^*(\mathbf{r})$ obeys the Helmholtz equation (7.7), and since $\mathrm{Re}\{\mathbf{F}_\lambda(\mathbf{r})e^{i\omega_\lambda t}\} = \mathrm{Re}\{\mathbf{F}_\lambda^*(\mathbf{r})e^{-i\omega_\lambda t}\}$, it follows that without loss of generality we can assume that $\omega_\lambda > 0$. It is convenient to define λ^* such that $\mathbf{F}_\lambda^*(\mathbf{r}) = \mathbf{F}_{\lambda^*}(\mathbf{r})$. Notice that this convention implies that, in general, λ^* is not the complex conjugate of λ. In the specific case of real mode functions $\mathbf{F}_\lambda = \mathbf{F}_\lambda^*$ it implies that $\lambda^* = \lambda$. The mode functions $\{\mathbf{F}_\lambda\}$ are eigenfunctions of the Hermitian operator ∇^2 and form, therefore, a complete basis in real space. This implies that any solution of the wave equation (7.3) can be expanded as

$$\mathbf{A}(\mathbf{r},t) = \sum_\lambda \langle\mathbf{F}_\lambda|\mathbf{A}(t)\rangle\mathbf{F}_\lambda(\mathbf{r})\,. \tag{7.8}$$

In order to quantize the field, we introduce the normal variables, which are defined as

$$a_\lambda(t) = \left(\frac{\epsilon_0}{2\hbar\omega_\lambda}\right)^{1/2}\left(i\langle\mathbf{F}_\lambda|\dot{\mathbf{A}}(t)\rangle + \omega_\lambda\langle\mathbf{F}_\lambda|\mathbf{A}(t)\rangle\right) \tag{7.9}$$

and

$$(a_{\lambda^*})^*(t) = \left(\frac{\epsilon_0}{2\hbar\omega_\lambda}\right)^{1/2}\left(-i\langle\mathbf{F}_\lambda|\dot{\mathbf{A}}(t)\rangle + \omega_\lambda\langle\mathbf{F}_\lambda|\mathbf{A}(t)\rangle\right)\,, \tag{7.10}$$

where we used that the physical field $\mathbf{A}$ and its time derivative $\dot{\mathbf{A}}$ are real. Notice that in case of real mode functions $\mathbf{F}_\lambda = \mathbf{F}_{\lambda^*}$ it follows that $a_\lambda = a_{\lambda^*}$. Inverting the definitions (7.9) and (7.10) yields

$$\mathbf{A}(\mathbf{r},t) = \sum_\lambda\left(\frac{\hbar}{2\epsilon_0\omega_\lambda}\right)^{1/2}\left(a_\lambda(t)\mathbf{F}_\lambda(\mathbf{r}) + a_\lambda^*(t)\mathbf{F}_\lambda^*(\mathbf{r})\right) \tag{7.11}$$

and

$$\dot{\mathbf{A}}(\mathbf{r},t) = -i\sum_\lambda\left(\frac{\hbar\omega_\lambda}{2\epsilon_0}\right)^{1/2}\left(a_\lambda(t)\mathbf{F}_\lambda(\mathbf{r}) - a_\lambda^*(t)\mathbf{F}_\lambda^*(\mathbf{r})\right)\,. \tag{7.12}$$

The corresponding expressions for the electric and magnetic fields can be obtained by applying equation (7.1). From equation (7.5), it follows that the canonical momentum density can be expressed as

$$\mathbf{\Pi}(\mathbf{r},t) = -i\sum_\lambda\left(\frac{\hbar\omega_\lambda\epsilon_0}{2}\right)^{1/2}\left(a_\lambda(t)\mathbf{F}_\lambda(\mathbf{r}) - a_\lambda^*(t)\mathbf{F}_\lambda^*(\mathbf{r})\right)\,. \tag{7.13}$$

Since the mode functions $\mathbf{F}_\lambda$ do not depend on time, equations (7.11) and (7.12) imply that

$$\dot{a}_\lambda(t) = -i\omega_\lambda a_\lambda(t) \ , \tag{7.14}$$

which also follows from the fact that the field (7.12) obeys the wave equation (7.3). Substitution in the Hamiltonian (7.6) gives

$$H = \sum_\lambda \frac{\hbar\omega_\lambda}{2} \left(a_\lambda^* a_\lambda + a_\lambda a_\lambda^*\right) \ , \tag{7.15}$$

which, in view of equation (7.14), does not depend on time and takes the form of the Hamiltonian of a harmonic oscillator for each mode $\mathbf{F}_\lambda$.

Canonical quantization of the field involves replacing the field and the canonical momentum density by hermitian vector operators $\hat{\mathbf{A}}$ and $\hat{\mathbf{\Pi}}$ whose components obey canonical commutation relations. In the Coulomb gauge these take the following form [5]

$$\left[\hat{A}_i(\mathbf{r}, t), \hat{\Pi}_j(\mathbf{r}', t)\right] = i\hbar\delta_\perp(\mathbf{r} - \mathbf{r}')\delta_{ij} \ , \tag{7.16}$$

where the indices i and j run over the vector components, $\delta_\perp(\mathbf{r} - \mathbf{r}')$ denotes the transverse delta function [5] and δ_{ij} denotes the Kronecker delta. As opposed to, for instance, ∇^2, which acts as an operator in the Hilbert space of physical states of the classical radiation field $\mathbf{A}(\mathbf{r}, t)$, the field and momentum operators $\hat{\mathbf{A}}(\mathbf{r}, t)$ and $\hat{\mathbf{\Pi}}(\mathbf{r}, t)$ are operators in the Hilbert space of quantum states of the radiation field. By replacing the classical field and momentum in the definitions of the normal variables (7.9) and (7.10) by the corresponding operators, one finds the operators $\hat{a}_\lambda$ and $\hat{a}_\lambda^\dagger$ that correspond to these variables. They obey boson commutation rules

$$\left[\hat{a}_\lambda, \hat{a}_{\lambda'}^\dagger\right] = \delta_{\lambda\lambda'} \ . \tag{7.17}$$

The operators $\hat{a}_\lambda^\dagger$ and $\hat{a}_\lambda$ respectively create and annihilate a photon in the mode $\mathbf{F}_\lambda$. The vacuum state, which is the quantum state of the field in which none of the modes $\mathbf{F}_\lambda$ contains photons, is defined by

$$\hat{a}_\lambda|\text{vac}) = 0 \qquad \forall\lambda \ , \tag{7.18}$$

where a bra vector $|...)$ with a round bracket denotes a vector in the Hilbert space of quantum states of the radiation field. Other states can be generated by acting with (functions of) the creation operators $\hat{a}_\lambda^\dagger$ on the vacuum. The quantum dynamics of the radiation field is governed by the Heisenberg equation of motion for the field operators, or, equivalently, the Schrödinger equation for the quantum states. The Hamilton operator takes the form of equation (7.15), the normal variables being replaced by the creation and annihilation operators. Similarly, the field and momentum operators take the form of equation (7.12) and (7.13), the creation and annihilation operators replacing the normal variables. The canonical commutation relations (7.16) are ensured by the boson commutation rules (7.17). The definition of the vacuum state (7.18), the field and momentum operators (7.16) and the Hamiltonian (7.15) provide a complete description of the quantum dynamics of the radiation field.

So far, we have assumed that $\{\mathbf{F}_\lambda\}$ constitutes a discrete set of modes. In case of a continuous set, the mode functions are normalized to δ functions and the summations over λ are replaced by integrals over the continuous variables that characterize the modes. In the particular case of normalized plane waves $\exp(i\mathbf{k}\cdot\mathbf{r})/(2\pi)^{3/2}$ the summations are replaced by $\sum_\lambda \to (2\pi)^{-3/2}\int d_3\mathbf{k}$.

7.3 Wave optics in a rotating frame

7.3.1 Equations of motion

In chapter 3, we have shown that the modes of an optical cavity that is put into uniform rotation about its optical axis can be defined as solutions of the time-dependent wave equation that rotate along with the mirrors. These solutions are monochromatic in the co-rotating frame. The corresponding complex fields, whose real parts correspond to the physical fields, are separable in space and time and, therefore, stationary in the co-rotating frame. We shall generalize the rotating-mode concept to the case of a freely propagating non-paraxial field and obtain complete sets of rotating modes of the free radiation field as monochromatic solutions in a rotating frame. First, we derive the equations of motion for light in a rotating frame.

Analogous to the discussion in chapter 5, we express the time-dependent vector potential in the stationary frame in terms of the vector potential in a rotating frame. The latter is denoted $\mathbf{C}(\mathbf{r},t)$. Since rotation of both the vector components and their spatial structure of a vector field in $\mathbb{R}^3$ is a real transformation of the field, it follows that $\mathbf{C}(\mathbf{r},t)$ can be defined real. It is related to the vector potential in the stationary frame by the identity

$$\mathbf{A}(\mathbf{r},t) = \langle\mathbf{r}|e^{-i\Omega t\hat{J}_z}|\mathbf{C}\rangle\ , \tag{7.19}$$

where $|\mathbf{r}\rangle$ is an eigenket of the position operator so that $\mathbf{C}(\mathbf{r},t) = \langle\mathbf{r}|\mathbf{C}\rangle$ is the real-space representation of the vector potential in the rotating frame. The operator $\exp(-i\hat{J}_z\Omega t)$ describes a time-dependent rotation of both the spatial structure and the polarization of a vector field, where Ω is the rotation frequency and $\hat{J}_z$ is the corresponding generator. By considering infinitesimal rotations $\exp(-i\alpha\hat{J}_z)\mathbf{A} = \mathbf{A} - i\alpha\hat{J}_z\mathbf{A} + O(\alpha^2)$ of both the vector components of a field $\mathbf{A}$ and their spatial structure, we find that $\hat{J}_z$ may be expressed as

$$\langle\mathbf{r}|\hat{J}_z|\mathbf{A}\rangle = \langle\mathbf{r}|\hat{L}_z + \hat{S}_z|\mathbf{A}\rangle \doteq -i\frac{\partial}{\partial\phi}\mathbf{A}(\mathbf{r},t) + i\begin{pmatrix}0&-1&0\\1&0&0\\0&0&0\end{pmatrix}\mathbf{A}(\mathbf{r},t)\ . \tag{7.20}$$

The spin part $\hat{S}_z$ acts upon the vector nature of the field and generates rotations of the vector components. The orbital part, on the other hand, solely acts upon the spatial structure of each of the vector components and generates rotations of their spatial patterns. Notice that the form of the real-space representation of $\hat{J}_z$, which figures in the second right-hand side in equation (7.20), confirms that the rotation of a vector field in $\mathbb{R}^3$ is a real transformation so that the vector potential can be assumed real in both frames.

Substitution of the rotating field $|\mathbf{A}\rangle = e^{-i\Omega t\hat{J}_z}|\mathbf{C}\rangle$ and its time derivative $|\dot{\mathbf{A}}\rangle = e^{-i\Omega t\hat{J}_z}\left(|\dot{\mathbf{C}}\rangle - i\Omega\hat{J}_z|\mathbf{C}\rangle\right)$ in the Lagrangian (7.4) yields the Lagrangian in the rotating frame

$$L_{\rm rot} = \frac{\epsilon_0}{2}\left\{\langle\dot{\mathbf{C}}|\dot{\mathbf{C}}\rangle + i\Omega\langle\mathbf{C}|\hat{J}_z|\dot{\mathbf{C}}\rangle - i\Omega\langle\dot{\mathbf{C}}|\hat{J}_z|\mathbf{C}\rangle + \Omega^2\langle\mathbf{C}|\hat{J}_z^2|\mathbf{C}\rangle - c^2\langle\nabla\times\mathbf{C}|\nabla\times\mathbf{C}\rangle\right\}\ , \quad (7.21)$$

where we have used that $\nabla\times(\hat{J}_z\mathbf{C}) = \hat{J}_z(\nabla\times\mathbf{C})$ so that $\langle\nabla\times\mathbf{A}|\nabla\times\mathbf{A}\rangle = \langle\nabla\times\mathbf{C}|\nabla\times\mathbf{C}\rangle$. Using the real-space representation of $\hat{J}_z$, which figures in equation (7.20), one may show that $\nabla\cdot(\hat{J}_z\mathbf{C}) = \hat{L}_z(\nabla\cdot\mathbf{C})$. It follows that the transversality condition (7.2) is not affected by a transformation to a rotating frame so that

$$\nabla\cdot\mathbf{C}(\mathbf{r},t) = 0\ . \quad (7.22)$$

By using that, for a transverse field, $\langle\nabla\times\mathbf{C}|\nabla\times\mathbf{C}\rangle = -\langle\mathbf{C}|\nabla^2\mathbf{C}\rangle$, the Euler-Lagrange equation for $\mathbf{C}(\mathbf{r},t)$ yields the wave equation in the rotating frame

$$\left(\nabla^2 + \frac{\Omega^2\hat{J}_z^2}{c^2} + \frac{2i\Omega\hat{J}_z}{c^2}\frac{\partial}{\partial t} - \frac{1}{c^2}\frac{\partial^2}{\partial t^2}\right)\mathbf{C}(\mathbf{r},t) = 0\ . \quad (7.23)$$

This equation can also be obtained directly from substitution of the rotating field (7.19) in the wave equation in the stationary frame (7.3). Notice that, $i\hat{J}_z$ is real so that the wave equation (7.23) in the rotating frame is real.

The canonical-momentum density in the rotating frame is given by

$$\mathbf{\Pi}_{\mathbf{C}}(\mathbf{r},t) = \frac{\partial\mathcal{L}}{\partial\dot{\mathbf{C}}} = \epsilon_0\left(\dot{\mathbf{C}}(\mathbf{r},t) - i\Omega\langle\mathbf{r}|\hat{J}_z|\mathbf{C}\rangle\right) = \epsilon_0\left(\dot{\mathbf{C}}(\mathbf{r},t) + i\Omega\langle\mathbf{C}|\hat{J}_z|\mathbf{r}\rangle\right)\ , \quad (7.24)$$

which is also real. By using the expression (7.5) of the momentum in a stationary frame and $|\dot{\mathbf{A}}\rangle = e^{-i\Omega t\hat{J}_z}\left(|\dot{\mathbf{C}}\rangle - i\Omega\hat{J}_z|\mathbf{C}\rangle\right)$, we find that

$$\mathbf{\Pi}_{\mathbf{A}}(\mathbf{r},t) = \langle\mathbf{r}|e^{-i\Omega t\hat{J}_z}|\mathbf{\Pi}_{\mathbf{C}}\rangle\ . \quad (7.25)$$

The Hamiltonian in the rotating frame can be expressed as

$$H_{\rm rot} = \mathbf{\Pi}_{\mathbf{C}}\cdot\dot{\mathbf{C}} - L = \frac{1}{2\epsilon_0}\langle\mathbf{\Pi}_{\mathbf{C}}|\mathbf{\Pi}_{\mathbf{C}}\rangle + i\Omega\langle\mathbf{\Pi}_{\mathbf{C}}|\hat{J}_z|\mathbf{C}\rangle - i\Omega\langle\mathbf{C}|\hat{J}_z|\mathbf{\Pi}_{\mathbf{C}}\rangle + \frac{\epsilon_0 c^2}{2}\langle\nabla\times\mathbf{C}|\nabla\times\mathbf{C}\rangle\ . \quad (7.26)$$

By using that the field is transverse (7.22), one may show that the Hamilton equations that derive from this Hamiltonian are equivalent to the wave equation in the rotating frame (7.23).

7.3.2 Rotating modes in free space

Analogous to the discussion in chapter 3, rotating modes of the free radiation field are defined as solutions of the wave equation (7.3) that are monochromatic in a rotating frame. In complex notation, such solutions can be expressed $\mathbf{C}(\mathbf{r},t) = \mathrm{Re}\{\mathbf{C}(\mathbf{r})\exp(-i\omega t)\}$, where $\mathbf{C}(\mathbf{r})$ is

the complex spatial vector potential in the rotating frame. Substitution in the wave equation in the rotating frame (7.23) gives

$$\left(\nabla^2 + \frac{\Omega^2 \hat{J}_z^2}{c^2} + \frac{2\omega\Omega \hat{J}_z}{c^2} + \frac{\omega^2}{c^2}\right)\mathbf{C}(\mathbf{r}) = 0 \,. \tag{7.27}$$

This equation plays the role analogous to that of the Helmholtz equation (7.7) in the rotating frame. Notice that due to the presence of $\hat{J}_z$, which is a purely imaginary operator, equation (7.27) is not real so that $\mathbf{C}(\mathbf{r})$ is, in general, a complex vector field.

Since $[\nabla^2, \hat{J}_z] = 0$, it follows that ∇^2 and $\hat{J}_z$ must have simultaneous eigenfunctions for which the wave equation (7.23) reduces to an algebraic equation, which can be solved to obtain a dispersion relation. We shall derive the simultaneous eigenfunctions of ∇^2 and $\hat{J}_z$, which allow us to obtain exact expressions of rotating modes in free space. For reasons of convenience, we first discuss the analogous case of a rotating scalar field $A(\mathbf{r}, t)$. Later on, we shall construct rotating complex vector fields $\mathbf{A}(\mathbf{r}, t)$ from these scalar ones. Analogous to equation (7.19), the negative frequency part of a rotating scalar field is defined as

$$A(\mathbf{r}, t) = e^{-i\hat{L}_z\Omega t} C(\mathbf{r}) e^{-i\omega t} \,, \tag{7.28}$$

where $C(\mathbf{r})$ is spatial field in the rotating frame. In case of a scalar field, equation (7.27) reduces to

$$\left(\nabla^2 + \frac{\Omega^2 \hat{L}_z^2}{c^2} + \frac{2\omega\Omega \hat{L}_z}{c^2} + \frac{\omega^2}{c^2}\right) C(\mathbf{r}) = 0 \,. \tag{7.29}$$

Since also $[\nabla^2, \hat{L}_z] = 0$ and since $\hat{L}_z$ and ∇^2 are both hermitian, $\hat{L}_z$ and ∇^2 must have an orthonormal set of simultaneous eigenfunctions for which the wave equation (7.29) becomes an algebraic equation. Since $[\hat{L}_z, -i\partial/\partial z] = 0$ and since the eigenfunctions of $\hat{L}_z$ are proportional to $\exp(il\phi)$ while the eigenfunctions of $-i\partial/\partial z$ are proportional to $\exp(iqz)$, it is natural to introduce cylindrical coordinates (R, ϕ, z) and look for solutions of the following type

$$C(R, \phi, z) = G(R) e^{il\phi} e^{iqz} \,, \tag{7.30}$$

with $l \in \mathbb{Z}$ and $q \in \mathbb{R}$. Substitution in the scalar wave equation (7.29) yields after rearranging the terms

$$\left(R^2 \frac{\partial^2}{\partial R^2} + R\frac{\partial}{\partial R} + (\kappa R)^2 - l^2\right) G(R) = 0 \,, \tag{7.31}$$

where $\kappa \in \mathbb{R}^+$ is defined by the dispersion relation

$$(\omega + l\Omega)^2 = c^2(\kappa^2 + q^2) \,. \tag{7.32}$$

The solutions of equation (7.31) are Bessel functions of the first kind $G_{\kappa l}(R) = J_l(\kappa R)$ so that a set of scalar Bessel mode functions can be introduced as

$$G_\lambda(\mathbf{r}) = \left(\frac{1}{2\pi}\right) J_l(\kappa R) e^{il\phi} e^{iqz} \,, \tag{7.33}$$

where $\lambda = (\kappa, l, q)$ denotes the set of spatial mode indices and the factor $1/(2\pi)$ is introduced for reasons of normalization. The corresponding frequencies can be obtained from (7.32)

$$\omega_{\lambda\pm} = \pm c\sqrt{\kappa^2 + q^2} - l\Omega \,. \tag{7.34}$$

For every solution G_λ with $\omega_{\lambda\pm}$, the mode function $G^*_\lambda = G_{\lambda^*}$ with $\lambda^* = (\kappa, -l, -q)$ obeys the scalar wave equation (7.29) with the frequencies $\omega_{\lambda^*\pm} = \pm c\sqrt{\kappa^2 + q^2} + l\Omega$. Since the mode functions are in general complex, the real scalar field in the rotating frame corresponding to the mode G_λ with $\omega_{\lambda+}$ is given by

$$C(\mathbf{r}, t) = \frac{e^{i\Omega t\hat{J}_z}\left(G_\lambda e^{-ic\sqrt{\kappa^2+q^2}t} + G_{\lambda^*}e^{ic\sqrt{\kappa^2+q^2}t}\right)}{2} \,, \tag{7.35}$$

where we have used that $\exp(-i\Omega t\hat{J}_z)$ is real. Since $\mathrm{Re}\left(G_\lambda e^{-ic\sqrt{\kappa^2+q^2}t}\right) = \mathrm{Re}\left(G_{\lambda^*}e^{ic\sqrt{\kappa^2+q^2}t}\right)$, it follows that without loss of generality we can choose

$$\omega_\lambda = c\sqrt{\kappa^2 + q^2} - l\Omega \qquad \text{so that} \qquad \omega_{\lambda^*} = c\sqrt{\kappa^2 + q^2} + l\Omega \,. \tag{7.36}$$

By using the orthonormality property of Bessel functions of the first kind [47], one may show that the mode functions $\{G_\lambda\}$ are normalized to δ functions

$$\langle G_\lambda | G_{\lambda'}\rangle = \int_0^\infty RdR \int_0^{2\pi} d\phi \int_{-\infty}^\infty dz\, G^*_\lambda(R, \phi, z) G_{\lambda'}(R, \phi, z) = \frac{1}{\kappa}\delta(\kappa - \kappa')\delta(q - q')\delta_{ll'} \,, \tag{7.37}$$

where $\delta(\kappa - \kappa')$ and $\delta(q - q')$ denote Dirac delta functions while $\delta_{ll'}$ denotes the Kronecker delta. By the Fourier-Bessel theorem and the Fourier theorem [47], the set of mode functions $\{G_\lambda\}$ constitutes a complete basis in real space.

It is clear that the vector field $(\mathbf{e}_z \times \nabla)A$ is locally transverse so that it obeys the transversality condition (7.2). It is easy to show that this is an exact solution of the wave equation (7.3) if (and only if) $A(\mathbf{r}, t)$ obeys the scalar equivalent of the wave equation. Since the corresponding electric field has a vanishing z component, it is customary to call this a transverse electric (TE) mode [4, 6]. The transversality condition (7.2) allows for two linearly independent polarization states. The other, for which the magnetic field is transverse (TM), can be constructed as $-(ic/\omega)\nabla \times (\mathbf{e}_z \times \nabla)A$, where ω is the frequency in a stationary frame. In general, the TE and TM mode functions corresponding to a set of scalar modes A are globally orthonormal. The vectorial mode functions corresponding the TE and TM Bessel modes can be expressed as

$$\mathbf{G}^{\mathrm{TE}}_\lambda(\mathbf{r}) = (\mathbf{e}_z \times \nabla)G_\lambda(\mathbf{r}) \tag{7.38}$$

and

$$\mathbf{G}^{\mathrm{TM}}_\lambda(\mathbf{r}) = \frac{-i}{\sqrt{\kappa^2 + q^2}}\nabla \times (\mathbf{e}_z \times \nabla)G_\lambda(\mathbf{r}) \,, \tag{7.39}$$

where $\sqrt{\kappa^2 + q^2}$ arises as the length of the wave vector of the Bessel modes in a stationary frame. The frequencies in the rotating frame depend on Ω and are given by (7.36). It is

convenient to define the subscript mode index of the vector fields such that it characterizes both the spatial and the polarization degrees of freedom associated with the modes. In order to do so, we introduce vectorial mode functions $\mathbf{G}_\mu$ with $\mu = (\lambda, \sigma)$, where σ runs over the TE and TM polarizations. One may prove that both the TE and TM mode are exact eigenstates of $\hat{J}_z$ with eigenvalues l, but not of $\hat{L}_z$ and $\hat{S}_z$ separately. Moreover, both are eigenfunctions of ∇^2 with eigenvalues $-(\kappa^2 + q^2)$, of $-i\partial/\partial z$ with eigenvalues q and of the transverse laplacian $\nabla_\rho^2 = \nabla^2 - \partial^2/\partial z^2$ with eigenvalues $-\kappa^2$. Analogous to equation (7.37), the vectorial mode functions $\mathbf{G}_\mu$ obey the closure relation

$$\langle \mathbf{G}_\mu | \mathbf{G}_{\mu'} \rangle = \int_0^\infty RdR \int_0^{2\pi} d\phi \int_{-\infty}^{\infty} dz\, \mathbf{G}_\mu^*(R, \phi, z) \cdot \mathbf{G}_{\mu'}(R, \phi, z) = \frac{1}{\kappa}\delta(\kappa - \kappa')\delta(q - q')\delta_{ll'}\delta_{\sigma\sigma'} \,, \tag{7.40}$$

where $\mu = (\kappa, l, q, \sigma)$. It follows that the set $\{\mathbf{G}_\mu\}$ of vectorial Bessel mode functions constitutes a complete basis of transverse vector fields in $\mathbb{C}^3$ so that the general solution of the wave equation in the rotating frame (7.23) can be expanded as

$$\mathbf{C}(\mathbf{r}, t) = \sum_\sigma \int_0^\infty \kappa d\kappa \int_{-\infty}^{\infty} dq \sum_l \langle \mathbf{G}_\mu | \mathbf{C}(t) \rangle \mathbf{G}_\mu(\mathbf{r}) \,. \tag{7.41}$$

Since the vectorial Bessel modes are eigenfunctions of $\hat{J}_z$ and, therefore, of the rotation operator $\exp(-i\alpha\hat{J}_z)$, it follows that the corresponding fields are monochromatic both in the rotating and in the stationary frame. As such, the Bessel modes $\{\mathbf{G}_\mu\}$ accommodate the transformations from a stationary to a rotating frame and vice versa.

7.3.3 Basis transformations

In this section we discuss how an arbitrary set of rotating modes, in particular the set of mode functions that obey rotating boundary conditions, can be expanded in the vectorial Bessel modes. We consider an orthonormal set of mode functions $\{\mathbf{V}_\nu\}$ that correspond to transverse and monochromatic fields in the rotating frame, i.e., vector fields in $\mathbb{C}^3$ that obey equations (7.22) and (7.23). Again, the subscript mode index ν characterizes both the spatial and polarization degrees of freedom. The frequency of the mode $\mathbf{V}_\nu$ is denoted ω_ν. Analogous to equation (7.41), the modes can be expanded as

$$\mathbf{V}_\nu(\mathbf{r}) = \sum_\sigma \int_0^\infty \kappa d\kappa \sum_l \int_{-\infty}^{\infty} dq\, \langle \mathbf{G}_\mu | \mathbf{V}_\nu \rangle \mathbf{G}_\mu(\mathbf{r}) \,, \tag{7.42}$$

where $\mu = (\kappa, l, q, \sigma)$ and the coefficients of the expansion are given by

$$\langle \mathbf{G}_\mu | \mathbf{V}_\nu \rangle = \int_0^\infty RdR \int_0^{2\pi} d\phi \int_0^\infty dq\, \mathbf{G}_\mu^*(R, \phi, z) \cdot \mathbf{V}_\nu(R, \phi, z) \,. \tag{7.43}$$

By using that both $\mathbf{V}_\mu$ and $\mathbf{G}_\nu$ correspond to monochromatic solutions of the wave equation in the rotating frame (7.23), one may show by partial integration that the matrix elements (7.43)

differ from 0 only if $\omega_\mu^2 = \omega_\nu^2$. This can be exploited by eliminating one of the spatial mode indices, for instance, $|q|$, in favor of the frequency $\omega = \omega_\nu$. For a fixed value of ω, the scalar mode functions (7.33) can be expressed as

$$H_\lambda(\mathbf{r};\omega) = \left(\frac{1}{2\pi}\right) J_l(\kappa R) e^{il\phi} e^{\pm \frac{iz}{c}\sqrt{\omega^2+2l\omega\Omega+l^2\Omega^2-c^2\kappa^2}} \ , \tag{7.44}$$

where $\lambda = (\kappa, l, \pm, \omega)$ and the + and − signs correspond to fields that propagate in the positive and negative z directions respectively. The corresponding vectorial modes $\mathbf{H}_\mu$ can be obtained by applying equations (7.38) and (7.39). In terms of these mode functions, the expansion (7.42) reduces to

$$\mathbf{V}_\nu(\rho, z) = \sum_\sigma \int_0^\infty \kappa d\kappa \sum_l \sum_\pm \langle \mathbf{H}_\mu | \mathbf{V}_\nu \rangle \mathbf{H}_\mu(\mathbf{r}) \ , \tag{7.45}$$

where the summation over ± denotes a summation over the two propagation directions along the z axis. If we limit the discussion to fields for which the expansion (7.44) only involves components with a fixed sign of q, the coefficients of the expansion (7.45) can be obtained from integration in the transverse plane

$$\langle \mathbf{H}_\nu | \mathbf{V}_\mu \rangle = \int_0^\infty R dR \int_0^{2\pi} d\phi \left(\mathbf{H}_\nu(R, \phi, z)\right)^* \cdot \mathbf{V}_\mu(R, \phi, z) \ . \tag{7.46}$$

This result shows that, for a given value of the frequency in the rotating frame ω and a given propagation direction along the z axis, the spatial dependence of a transverse vectorial mode is fully determined by the field pattern in a single transverse plane. In the more general case of monochromatic fields that contain components that propagate in both directions along the z axis, the field can be separated in two parts that propagate in opposite directions along the z axis. In that case, the analogous expressions can be derived for each of these two parts.

7.3.4 Rotating modes in the paraxial approximation

The expansion (7.45) of a set of monochromatic vectorial modes $\mathbf{V}_\mu$ in the basis of TE and TM modes corresponding to monochromatic scalar Bessel modes $H_\lambda(\mathbf{r})$ establishes the connection with the paraxial description discussed in chapter 3 in a very natural way. Essential to the paraxial approximation is the assumption that the field propagates mainly along a well-defined direction, so that the wave-vector components transverse to the dominant propagation direction are small compared to the length of the wave vector. In the case of the scalar monochromatic Bessel modes (7.44), this implies that $c^2\kappa^2 << \omega^2$. In the terminology of section 3.2, the ratio $c\kappa/\omega$ can be used as a smallness parameter δ. Analogous to the discussion in chapter 3, we also assume that $\Omega \sim \delta^2\omega$, which is a slowly-varying envelope approximation. Then, by expanding the square root in the argument of the exponent in equation (7.44) up to first order in powers of δ, the monochromatic scalar Bessel modes (7.44) reduce to

$$H_\lambda(\rho, z; \omega) \simeq \exp\left(\pm \frac{i\omega z}{c}\left(1 + \frac{l\Omega}{\omega} - \frac{c^2\kappa^2}{2\omega^2}\right)\right) H_\lambda(\rho, 0; \omega) \ , \tag{7.47}$$

where the + and − signs again correspond to fields that propagate in the positive and negative z directions. Since $\nabla_\rho^2 H_\lambda = -\kappa^2 H_\lambda$ and $\hat{L}_z H_\lambda = l H_\lambda$, the exponential term in equation (7.47) takes the form of the paraxial propagator in the rotating frame (3.31), acting on the transverse Bessel mode function $H_\lambda(\rho, 0)$, z being replaced by $-z$ for modes propagating in the negative z direction. This shows that the paraxial Bessel modes (7.47) are exact solutions of the paraxial wave equation in a rotating frame (5.4). The longitudinal components of the TM modes are of the order of δ smaller than the transverse components and, in leading order of the paraxial approximation, both the TE and the TM modes corresponding to the scalar mode functions (7.47) are polarized in the transverse plane. Moreover, the transverse variation of the polarization is slow compared to that of the transverse beam profile as characterized by $H_\lambda(\rho, z)$ so that, up to first order in δ, the transverse polarization of the Bessel modes can be chosen independent of the spatial mode indices. In the paraxial approximation, a vectorial Bessel mode $\mathbf{G}_\mu$ thus reduces to $\epsilon_\sigma H_\lambda$, where σ labels two linearly independent transverse polarization states and λ is a set of spatial mode indices. Analogous to the discussion above, the paraxial Bessel modes $\epsilon_\sigma H_\lambda$ constitute a complete basis set of paraxial modes. An arbitrary (set of) paraxial modes $\epsilon_\tau V_\lambda$, where τ labels the polarization states, can be expanded in this basis. In the case of the rotating cavity modes that we have described in chapters 3 and 5, the paraxial mode functions are given by $V_\lambda = v_{nm} \exp(ikz)$ with $\lambda = (n, m, k)$ the mode profiles in the rotating frame v_{nm} given by equation (3.58). The uniform polarization ϵ can be chosen independently of the spatial indices λ.

Notice that, analogous to the description in section 3.2, this approach is perturbative in that it allows for obtaining higher-order corrections by taking higher-order powers of δ into account. However, the spatial and polarization degrees of freedom are decoupled only in lowest non-vanishing order of the paraxial approximation.

7.4 Quantization

7.4.1 Normal variables for a rotating field

As discussed in the previous section, the vectorial Bessel mode functions accommodate the transformation from the rotating to the stationary frame and vice versa. In order to derive expressions of the normal variables associated with the Bessel-mode components of the field in a rotating frame, we substitute the expansion (7.41) in the expression (7.19) of the rotating field in the stationary frame and obtain

$$\mathbf{A}(\mathbf{r}, t) = \sum_\sigma \int_0^\infty \kappa d\kappa \sum_l \int_{-\infty}^\infty dq \, \langle \mathbf{G}_\mu | \mathbf{C} \rangle e^{-il\Omega t} \mathbf{G}_\mu(\mathbf{r}) \tag{7.48}$$

for the real vector potential in the stationary frame. Its time derivative can be expressed as

$$\dot{\mathbf{A}}(\mathbf{r}, t) = \sum_\sigma \int_0^\infty \kappa d\kappa \sum_l \int_{-\infty}^\infty dq \left(\langle \mathbf{G}_\mu | \dot{\mathbf{C}}(t) \rangle - il\Omega \langle \mathbf{G}_\mu | \mathbf{C}(t) \rangle \right) e^{-il\Omega t} \mathbf{G}_\mu(\mathbf{r}) \, . \tag{7.49}$$

From the definitions (7.9) and (7.10), we find that the normal variables corresponding to the Bessel-mode components of the rotating field are given by

$$a_\mu(t) = \left(\frac{\epsilon_0}{2\hbar c\sqrt{\kappa^2+q^2}}\right)^{1/2} e^{-il\Omega t}\Big(i\langle \mathbf{G}_\mu|\dot{\mathbf{C}}(t)\rangle + \omega_{\mu^*}\langle \mathbf{G}_\mu|\mathbf{C}(t)\rangle\Big) \tag{7.50}$$

and

$$a_{\mu^*}(t) = \left(\frac{\epsilon_0}{2\hbar c\sqrt{\kappa^2+q^2}}\right)^{1/2} e^{il\Omega t}\Big(i\langle \mathbf{G}_{\mu^*}|\dot{\mathbf{C}}(t)\rangle + \omega_{\mu}\langle \mathbf{G}_{\mu^*}|\mathbf{C}(t)\rangle\Big) \tag{7.51}$$

where $c\sqrt{\kappa^2+q^2}$ arises as the frequency of the Bessel modes in the stationary frame and ω_{μ^*} and ω_μ are given by equation (7.36). With the normal variables in equations (7.50) and (7.51), the field in the stationary frame and the corresponding momentum take the form of equations (7.12) and (7.13), the mode functions $\mathbf{F}_\lambda$ being replaced by the vectorial Bessel modes $\mathbf{G}_\mu$.

7.4.2 Normal variables in the rotating frame

In case of a complete set of rotating modes $\{\mathbf{V}_\mu\}$, it is more natural to describe the dynamics of the radiation field in terms of a set of normal variables that characterize the amplitudes and corresponding momenta in these rotating modes. In this section, we show that it is possible to introduce such variables and derive the corresponding Hamiltonian. The expressions in equations (7.50) and (7.51) suggest to introduce normal variables for the Bessel-mode components in the rotating frame as

$$c_\mu(t) = \left(\frac{\epsilon_0}{2\hbar c\sqrt{\kappa^2+q^2}}\right)^{1/2} \Big(i\langle \mathbf{G}_\mu|\dot{\mathbf{C}}(t)\rangle + \omega_{\nu^*}\langle \mathbf{G}_\mu|\mathbf{C}(t)\rangle\Big) \tag{7.52}$$

and

$$c_{\mu^*}(t) = \left(\frac{\epsilon_0}{2\hbar c\sqrt{\kappa^2+q^2}}\right)^{1/2} \Big(i\langle \mathbf{G}_{\mu^*}|\dot{\mathbf{C}}(t)\rangle + \omega_{\mu}\langle \mathbf{G}_{\nu^*}|\mathbf{C}(t)\rangle\Big)\,. \tag{7.53}$$

Notice that, although their shape is very similar to that of normal variables in a stationary frame, both the anti-symmetric way in which the frequencies ω_ν and ω_{ν^*} appear and the square-root factor, which involves the frequency of the Bessel mode in a stationary frame, are signatures of the fact that these are normal variables in a non-inertial frame. They are related to the normal variables (7.50) and (7.51) in the stationary frame by the unitary transformations

$$a_\mu(t) = e^{-il\Omega t}c_\mu(t) \qquad \text{and} \qquad a_{\mu^*}(t) = e^{il\Omega t}c_{\mu^*}(t)\,. \tag{7.54}$$

The field in the rotating frame and its derivative can be expressed as

$$\mathbf{C}(\mathbf{r},t) = \sum_\sigma \int_0^\infty \kappa d\kappa \sum_l \int_{-\infty}^\infty dq \left(\frac{\hbar}{2\epsilon_0 c\sqrt{\kappa^2+q^2}}\right)^{1/2} \Big(c_\mu(t)\mathbf{G}_\mu(\mathbf{r}) + c^*_\mu(t)\mathbf{G}_{\mu^*}(\mathbf{r})\Big) \tag{7.55}$$

and

$$\dot{\mathbf{C}}(\mathbf{r},t) = -i\sum_{\sigma}\int_0^\infty \kappa d\kappa \sum_l \int_{-\infty}^{\infty} dq \left(\frac{\hbar}{2\epsilon_0 c\sqrt{\kappa^2+q^2}}\right)^{1/2} \times \omega_\mu\Big(c_\mu(t)\mathbf{G}_\mu(\mathbf{r}) - c^*_\mu(t)\mathbf{G}_{\mu^*}(\mathbf{r})\Big)\,, \tag{7.56}$$

where we have used that $\omega_{\mu^*}+\omega_\mu = 2c\sqrt{\kappa^2+q^2}$ and $\omega_{\mu^*}-\omega_\mu = 2l\Omega$. Since the $\mathbf{G}_\mu$ and $\mathbf{G}_{\mu^*}$ obey the wave equation in the rotating frame at the frequencies ω_μ and $-\omega_\mu$, this result is consistent with the fact that $\mathbf{C}(\mathbf{r},t)$ obeys equation (7.23). By using equation (7.24), we find that

$$\mathbf{\Pi}_{\mathbf{C}}(\mathbf{r},t) = -i\sum_{\sigma}\int_0^\infty \kappa d\kappa \sum_l \int_{-\infty}^{\infty} dq \left(\frac{\hbar\epsilon_0 c\sqrt{\kappa^2+q^2}}{2}\right)^{1/2} \Big(c_\mu(t)\mathbf{G}_\mu(\mathbf{r}) - c^*_\mu(t)\mathbf{G}_{\mu^*}(\mathbf{r})\Big)\,. \tag{7.57}$$

The hamiltonian in the rotating frame (7.26) can be expressed as

$$H_{\rm rot} = \frac{1}{2}\sum_{\sigma}\int_0^\infty \kappa d\kappa \sum_l \int_{-\infty}^{\infty} dq\, \hbar\omega_\mu\Big(c^*_\mu c_\mu + c_\mu c^*_\mu\Big)\,. \tag{7.58}$$

The form of this Hamiltonian confirms that the harmonic structure of the dynamics of the modes survives in the rotating frame. The classical dynamics of the Bessel modes in the rotating frame is described the Hamilton equations with the Hamiltonian (7.58) and with the field and corresponding momentum as specified by equations (7.56) and (7.57).

From the expansion in equation (7.41), it follows that the normal variables that characterize the amplitude and momentum in a complete and orthonormal set of rotating modes $\{\mathbf{V}_\nu\}$ may be defined as properly normalized linear combinations of the normal variables for the Bessel modes, i.e.,

$$v_\nu(t) = \sum_{\sigma}\int_0^\infty \kappa d\kappa \sum_l \int_{-\infty}^{\infty} dq\, \langle \mathbf{V}_\nu|\mathbf{G}_\mu\rangle c_\mu(t) \tag{7.59}$$

and

$$v_{\nu^*}(t) = \sum_{\sigma}\int_0^\infty \kappa d\kappa \sum_l \int_{-\infty}^{\infty} dq\, \langle \mathbf{V}_{\nu^*}|\mathbf{G}_{\mu^*}\rangle c_{\mu^*}(t)\,, \tag{7.60}$$

where $\mu = (\kappa, l, q, \sigma)$. By using the definitions (7.52) and (7.53) of c_μ and c_{μ^*} and the fact that the matrix element $\langle \mathbf{V}_\nu|\mathbf{G}_\mu\rangle$ differs from zero only when $\omega^2_\nu = \omega^2_\mu$ while the matrix element $\langle \mathbf{V}_{\nu^*}|\mathbf{G}_{\mu^*}\rangle$ differs from zero only when $\omega^2_{\nu^*} = \omega^2_{\mu^*}$, we find that

$$v_\nu(t) = \sum_{\sigma}\int_0^\infty \kappa d\kappa \sum_l \int_{-\infty}^{\infty} dq \left(\frac{\epsilon_0}{2\hbar(\omega_\nu + l\Omega)}\right)^{1/2} \times \langle \mathbf{V}_\nu|\mathbf{G}_\mu\rangle\Big(i\langle \mathbf{G}_\nu|\dot{\mathbf{C}}(t)\rangle + (\omega_\nu + 2l\Omega)\langle \mathbf{G}_\mu|\mathbf{C}(t)\rangle\Big) \tag{7.61}$$

and

$$v_{\nu^*}(t) = \sum_\sigma \int_0^\infty \kappa d\kappa \sum_l \int_{-\infty}^\infty dq \left(\frac{\epsilon_0}{2\hbar(\omega_\nu - l\Omega)}\right)^{1/2} \times \langle \mathbf{V}_{\nu^*}|\mathbf{G}_{\mu^*}\rangle\Big(i\langle \mathbf{G}_{\nu^*}|\dot{\mathbf{C}}(t)\rangle + (\omega_\nu - 2l\Omega)\langle \mathbf{G}_{\mu^*}|\mathbf{C}(t)\rangle\Big) . \quad (7.62)$$

Notice that the normal variables (7.61) and (7.62) reduce to the ordinary normal variables in the stationary frame in the absence of rotation, i.e., for $\Omega = 0$. Using the completeness of the vectorial Bessel modes (7.40), the definitions in equations (7.59) and (7.60) can be inverted to obtain

$$c_\mu(t) = \sum_\nu \langle \mathbf{G}_\mu|\mathbf{V}_\nu\rangle v_\nu(t) \qquad \text{and} \qquad c_{\mu^*}(t) = \sum_\nu \langle \mathbf{G}_{\mu^*}|\mathbf{V}_{\nu^*}\rangle v_{\nu^*}(t) , \quad (7.63)$$

where we have assumed that $\{\mathbf{V}_\nu\}$ is a discrete set of modes. Again using that the matrix elements $\langle \mathbf{G}_\mu|\mathbf{V}_\nu\rangle$ differ from 0 only when $\omega_\mu^2 = \omega_\nu^2$, the Hamiltonian (7.58) can be expressed as

$$H_{\rm rot} = \frac{1}{2}\sum_\nu \hbar\omega_\nu\Big(v_\nu^* v_\nu + v_\nu v_\nu^*\Big) . \quad (7.64)$$

Thus, we have obtained a complete description of the classical dynamics of the radiation field in terms of normal variables for an orthonormal but otherwise arbitrary set of rotating modes $\{\mathbf{V}_\nu\}$.

7.4.3 Canonical quantization

In the stationary frame, quantization is performed by replacing the real field $\mathbf{A}$ and canonical momentum $\mathbf{\Pi}_\mathbf{A}$ by hermitian operators that obey canonical commutation rules (7.16). The normal variables a_μ, as specified by equation (7.50), and their complex conjugates a_μ^* become bosonic annihilation and creation operators. The field operator in the stationary frame takes the form of equation (7.12) when the modes $\mathbf{F}_\lambda$ are replaced by the Bessel modes $\mathbf{G}_\nu$ and the normal variables are replaced by the creation and annihilation operators. The quantum evolution of the rotating field operators is governed by the Heisenberg equation of motion. The Hamiltonian takes the form of equation (7.15) when the normal variables are replaced by the creation and annihilation operators that correspond to the normal variables defined in equation (7.50) and (7.51).

Quantization in the rotating frame involves replacing the field in the rotating frame $\mathbf{C}(\mathbf{r}, t)$ and the corresponding momentum $\mathbf{\Pi}_\mathrm{C}(\mathbf{r}, t)$ (7.24) by vector operators $\hat{\mathbf{C}}(\mathbf{r}, t)$ and $\hat{\mathbf{\Pi}}_\mathrm{C}(\mathbf{r}, t)$ whose components obey canonical commutation rules

$$\Big[\hat{C}_i(\mathbf{r}), \hat{\Pi}_{\mathbf{C}j}(\mathbf{r}')\Big] = i\hbar\delta_\perp(\mathbf{r} - \mathbf{r}')\delta_{ij} , \quad (7.65)$$

where the indices i and j run over the vector components. The other, independent, commutators of the components of $\hat{\mathbf{C}}$ and $\hat{\mathbf{\Pi}}_\mathrm{C}$ vanish. From the definition (7.19) of the complex field in the rotating frame and the expression (7.25) of the corresponding momentum, it is evident

that quantization in the rotating frame is consistent with quantization in the stationary frame. Substitution of the expansions (7.55) and (7.57) in the canonical commutation rules in the rotating frame (7.65) shows that also the normal variables in the rotating frame become bosonic creation and annihilation operators. This is in obvious agreement with the transformations in equation (7.54). Since the transformation described by the equations (7.59) and (7.60) is a properly normalized unitary transformation in the space of the normal variables, it follows that the same is true for the normal variables that describe the dynamics of the field in terms of the amplitudes and momenta of the rotating modes $\mathbf{V}_\mu$. The quantum dynamics in the rotating frame is described by the Heisenberg equation of motion with the Hamiltonian in equation (7.58) or, equivalently, (7.64) when the normal variables are replaced by creation and annihilation operators.

Notice, that since the transformation in equation (7.54), and also the transformations in equations (7.59) and (7.60), are properly normalized unitary transformations, the vacuum as perceived from the rotating frame is the same as that perceived from the stationary frame (7.18).

7.5 Summary, conclusion and outlook

In this chapter we have presented the first exact quantum-optical description of rotating light, or, equivalently, quantized the radiation field in an orthonormal but otherwise arbitrary basis of rotating modes $\{\mathbf{V}_\mu\}$. Rotating modes are defined as divergence free (7.22) monochromatic solutions of the wave equation in a rotating frame (7.23). In complex notation, these fields are separable in space and time so that the corresponding physical fields are stationary in the rotating frame. As a result, they rotate uniformly in a stationary frame. We have shown that the set of vectorial Bessel modes both with transverse electric (TE) and transverse magnetic (TM) polarization are exact eigenstates of $\hat{J}_z$ and, therefore, of the rotation operator $\exp(-i\Omega t\hat{J}_z)$. It follows that the fields corresponding to these modes only pick up a frequency shift under the transformation from a stationary to a rotating frame. As a result, the Bessel-mode fields are monochromatic in both frames. As the Bessel modes are monochromatic in the stationary frame, the free radiation field can be quantized in this basis in the usual way. Since they are also monochromatic in the rotating frame, an arbitrary rotating mode $\mathbf{V}_\mu$, which is monochromatic in the rotating frame, can be expanded in the subset of Bessel modes that have the same frequency in the rotating frame. The simple transformation property of Bessel modes to the stationary frame naturally leads to an expression of the field operator corresponding to the rotating mode as a linear combination of the field operators for the Bessel modes in the stationary frame. Alternatively, the field can be quantized directly in the rotating frame. We have shown that this is equivalent to quantization in the stationary frame.

The approach discussed in this chapter is particulary suited to describe the quantum dynamics of a set of modes that solve rotating boundary conditions, such as the rotating cavity modes discussed in chapters 3 and 5. In that respect it is complementary to the approach discussed in reference [107], where approximate rotating solutions in free space are constructed

from stationary ones. As opposed to reference [107], the theory presented here is exact and does not require paraxial and/or slowly-varying-envelope approximations. On the other hand, the approach in reference [107] is more flexible in that it allows for a quantum description of fields with a rotating polarization and/or a rotating mode pattern whereas the work discussed here only concerns uniformly rotating fields.

The method discussed in this chapter concerns quantization of the free radiation field in the Coulomb gauge. As a result, its validity is restricted to energy scales where vacuum fluctuations in full quantum electrodynamics (e.g. electron-positron pair creation) are negligible. A special property of the transformation to a rotating frame that we have applied in this chapter is that it does not affect the vacuum state of the radiation field. From a relativistic point-of-view, other definitions of the transformation to a rotating frame may be more natural [109, 110]. These lead to a different definition of the vacuum in the rotating frame [111]. The transformation to a rotating frame that we have used here is fundamentally different from the transformation to the co-moving frame of an orbiting observer. Also in that case the vacuum is perceived differently, which may be understood as an example of the Unruh effect [112].

The scalar Bessel beams G_λ that we have studied in section 7.3, were first proposed some twenty years ago [113, 114] and have been investigated in detail both theoretically and experimentally, see, for instance, reference [115] for a recent review. The vectorial Bessel beams $\mathbf{G}_\mu$ are less well-known but have also been studied before [6, 116]. Since the production of Bessel beams in experiments is well-established, it should be possible to construct the rotating fields that we have discussed in this chapter as a superposition of their rotational-Doppler shifted components. Production of quantum coherent superpositions of such modes is probably far more involved.

An interesting application of the theory discussed in this chapter would be to study the quantum interference of two single-photon fields that have the same spectral and spatial structure in a given transverse plane of their own co-rotating frames but rotate at different frequencies and, possibly, in opposite directions. From the results of section 7.3, it is clear that rotation has strong and distinct effects on the spectral and spatial structure of the modes. As a result, the probability of photon bunching in a quantum-interferometric set-up, which is essentially determined by the spatial and spectral overlap of the two modes, depends strongly on the two rotation frequencies.

Bibliography

[1] J. Kepler, *De cometis libelli tres* (AugustæVindelicorum, 1619).

[2] E. Hecht, *Optics*, Fourth edition (Addison Wesley, San Francisco, CA, 2001).

[3] J. C. Maxwell, *A dynamical theory of the electromagnetic field*, Phil. Trans. R. Soc. Lond. **155**, 459 (1865).

[4] J. D. Jackson, *Classical electrodynamics*, Third edition (John Wiley & Sons, Hoboken, NJ, 1999).

[5] C. Cohen-Tannoudji, J. Dupont-Roc, and G. Grynberg, *Photons and atoms: Introduction to quantum electrodynamics* (Wiley-VCH, Berlin, 1997).

[6] G. Nienhuis, *Angular momentum and vortices in optics* in *Structured light and its applications* (D. L. Andrews (Ed.), Elsevier, Amsterdam, 2008).

[7] E. Wigner, *On unitary representations of the inhomogeneous Lorentz group*, Ann. Math. **40**, 149 (1939).

[8] S. J. Van Enk and G. Nienhuis, *Commutation rules and eigenvalues of spin and orbital angular momentum of radiation fields*, J. Mod. Opt. **41**, 963 (1994).

[9] R. A. Beth, *Mechanical detection and measurement of the angular momentum of light*, Phys. Rev. **50**, 115 (1936).

[10] A. Ashkin, J. M. Dziedzic, J. E. Bjorkholm, and S. Chu, *Observation of a single-beam gradient force optical trap for dielectric particles*, Opt. Lett. **11**, 288 (1986).

[11] L. Allen, M. W. Beijersbergen, R. J. C. Spreeuw, and J. P. Woerdman, *Orbital angular momentum of light and the transformation of Laguerre-Gaussian laser modes*, Phys. Rev. A **45**, 8185 (1992).

[12] A. E. Siegman, *Lasers* (University Science Books, Sausalito, CA, 1986).

[13] P. Dirac, *Quantised singularities in the electromagnetic field*, Proc. Roy. Soc. A **133**, 60 (1931).

[14] M. R. Dennis, K. O'Holleran, and M. J. Padgett, *Singular optics: Optical vortices and polarization singularities*, Progr. Opt. **53**, 293 (2009).

[15] M. R. Dennis, Y. S. Kivshar, M. S. Soskin, and G. A. Swartzlander Jr., *Singular optics: More ado about nothing*, J. Opt. A: Pure Appl. Opt. **11**, 090201 (2009).

[16] A. Ya. Bekshaev, M. S. Soskin, and M. V. Vasnetsov, *Optical vortex symmetry breakdown and decomposition of the orbital angular momentum of light beams*, J. Opt. Soc. Am. A **20**, 1635 (2003).

[17] J. Visser and G. Nienhuis, *Orbital angular momentum of general astigmatic modes*, Phys. Rev. A **70**, 013809 (2004).

[18] J. A. Arnaud and H. Kogelnik, *Gaussian light beams with general astigmatism*, Appl. Opt **8**, 1687 (1969).

[19] A. Ya. Bekshaev, M. S. Soskin, and M. V. Vasnetsov, *Angular momentum of a rotating light beam*, Opt. Commun. **249**, 367 (2005).

[20] G. Nienhuis, *Polychromatic and rotating beams of light*, J. Phys. B: At. Mol. Opt. Phys. **39**, 529 (2006).

[21] G. Molina-Terriza, J. P. Torres, and L. Torner, *Twisted photons*, Nature Physics **3**, 305 (2007).

[22] A. Mair, A. Vaziri, G. Weihs, and A. Zeilinger, *Entanglement of the orbital angular momentum states of photons*, Nature **412**, 313 (2001).

[23] J. B. Pors, S. S. R. Oemrawsingh, A. Aiello, M. P. van Exter, E. R. Eliel, G. W. 't Hooft, and J. P. Woerdman, *Shannon dimensionality of quantum channels and its application to photon entanglement*, Phys. Rev. Lett. **101**, 120502 (2008).

[24] D. G. Grier, *A revolution in optical manipulation*, Nature **424**, 21 (2006).

[25] M. Bhattacharya and P. Meystre, *Using a Laguerre-Gaussian beam to trap and cool the rotational motion of a mirror*, Phys. Rev. Lett. **99**, 153603 (2007).

[26] C. Huygens, *Traité de la lumière* (Pierre vander Aa, Marchand Libraire, Leide, 1690).

[27] J. W. Goodman, *Introduction To Fourier Optics*, Second edition (McGraw-Hill Book Company, New York, NY, 1996).

[28] R. S. Longhurst, *Geometrical and physical optics*, Second edition (John Wiley & Sons, Hoboken, NJ, 1967).

[29] R. K. Luneburg, *Mathematical theory of optics* (University of California Press, Berkeley, CA, 1964).

[30] R. P. Feynman and A. R. Hibbs, *Quantum mechanics and path Integrals* (McGraw-Hill Book Company, New York, NY, 1965).

[31] D. Gloge and D. Marcuse, *Formal quantum theory of light rays*, J. Opt. Soc. Am. **59**, 1629 (1969).

[32] H. Kogelnik, *Imaging of optical modes - resonators with internal lenses*, Bell. Syst. Tech. J. **44**, 455 (1965).

[33] G. Nienhuis and L. Allen, *Paraxial wave optics and harmonic oscillators*, Phys. Rev. A **48**, 656 (1993).

[34] L. A. Belousova, *Theory of nonorthogonal resonators*, J. Appl. Spec. **30**, 172 (1979).

[35] J. L. Blows and G. W. Forbes, *Mode characteristics of twisted resonators composed of two cylindrical mirrors*, Opt. Express **2**, 184 (1998).

[36] D. Janner, G. D. Valle, G. Galzerano, and S. Longhi, *Stability of astigmatic and twisted optical lensguides*, Opt. Quant. Electron. **36**, 1061 (2004).

[37] V. L. Kasyutich, *Laser beam patterns of an optical cavity formed by two twisted cylindrical mirrors*, Appl. Phys. B **96**, 141 (2009).

[38] J. A. Arnaud, *Nonorthogonal optical waveguides and resonators*, Bell. Syst. Tech. J. **49**, 2311 (1970).

[39] V. Guilleman and S. Sternberg, *Symplectic techniques in physics* (Cambridge University Press, Cambridge, 1984).

[40] D. R. Herriott and H. J. Schulte, *Folded optical delay lines*, Appl. Opt. **4**, 883 (1965).

[41] Y. F. Chen, Y. P. Lan, and K. F. Huang, *Observation of quantum-classical correspondance from high-order transverse patterns*, Phys. Rev. A **68**, 043803 (2003).

[42] D. Stoler, *Operator methods in physical optics*, J. Opt. Soc. Am. **71**, 334 (1981).

[43] S. J. van Enk and G. Nienhuis, *Eigenfunction description of laser beams and orbital angular momentum of light*, Opt. Commun. **94**, 147 (1992).

[44] E. G. Abramochkin and V. G. Volostnikov, *Generalized Gaussian beams*, J. Opt. A: Pure Appl. Opt. **6**, S157 (2004).

[45] M. Lax, W. H. Louisell, and W. B. McKnight, *From Maxwell to paraxial wave optics*, Phys. Rev. A **11**, 1365 (1975).

[46] I. H. Deutsch and J. C. Garrison, *Paraxial quantum propagation*, Phys. Rev. A **43**, 2498 (1991).

[47] G. B. Arfken and H. J. Weber, *Mathematical methods for physicists*, Fifth edition (Academic Press, San Diego, CA, 2001).

[48] G. Nienhuis, *Doppler effect induced by rotating lenses*, Opt. Commun. **132**, 8 (1996).

[49] J. J. Sakurai, *Modern quantum mechanics*, Revised edition (Addison Wesley, San Francisco, CA, 1994).

[50] W. Paul and H. Steinwedel, *Ein neues Massenspektrometer ohne Magnetfeld*, Z. Naturforsch. A **8**, 448 (1953).

[51] W. Petrich, M. H. Anderson, J. R. Ensher, and E. A. Cornell, *Stable, tightly confining magnetic trap for evaporative cooling of neutral atoms*, Phys. Rev. Lett. **74**, 3352 (1995).

[52] R. Thompson, T. Harmon, and M. Ball, *The rotating-saddle trap: a mechanical analogy to RF-electric-quadrupole ion trapping?*, Can. J. Phys. **80**, 1433 (2002).

[53] O. Zik, D. Levine, S. G. Lipson, S. Shtrikman, and J. Stavans, *Rotationally induced segregation of granular materials*, Phys. Rev. Lett. **73**, 644 (1994).

[54] A. Salhi and C. Cambon, *Time-dependent rotating stratified shear flow: Exact solution and stability analysis*, Phys. Rev. E **75**, 016312 (2007).

[55] T. J. Kippenberg, H. Rokhsari, T. Carmon, A. Scherer, and K. J. Vahala, *Analysis of radiation-pressure induced mechanical oscillation of an optical microcavity*, Phys. Rev. Lett. **95**, 033901 (2005).

[56] T. Corbitt, D. Ottaway, E. Innerhofer, J. Pelc, and N. Mavalvala, *Measurement of radiation-pressure-induced optomechanical dynamics in a suspended Fabry-Perot cavity*, Phys. Rev. A **74**, 021802(R) (2006).

[57] P. F. Cohadon, A. Heidmann, and M. Pinard, *Cooling of a mirror by radiation pressure*, Phys. Rev. Lett. **83**, 3174 (1999).

[58] D. Kleckner and D. Bouwmeester, *Sub-Kelvin cooling of a micromechanical resonator*, Nature **444**, 75 (2006).

[59] S. Gröblacher, S. Gigan, H. R. Böhm, A. Zeilinger, and M. Aspelmeyer, *Radiation-pressure self-cooling of a micromirror in a cryogenic environment*, Europhys. Lett. **81**, 54003 (2008).

[60] M. Lucamarini, D. Vitali, and P. Tombesi, *Scheme for a quantum-limited force measurement with an optomechanical device*, Phys. Rev. A **74**, 063816 (2006).

[61] D. Vitali, S. Gigan, A. Ferreira, H. R. Böhm, P. Tombesi, A. Guerreiro, V. Vedral, A. Zeilinger, and M. Aspelmeyer, *Optomechanical entanglement between a movable mirror and a cavity field*, Phys. Rev. Lett. **98**, 030405 (2007).

[62] M. Bhattacharya, P.-L. Giscard, and P. Meystre, *Entangling the rovibrational modes of a macroscopic mirror using radiation pressure*, Phys. Rev. A **77**, 030303(R) (2008).

[63] J. Z. Bernad, L. Diosi, and T. Geszti, *Quest for quantum superpositions of a mirror: High and moderately low temperatures*, Phys. Rev. Lett. **97**, 250404 (2006).

[64] D. Kleckner, I. Pikovski, E. Jeffrey, L. Ament, E. Eliel, J. van den Brink, and D. Bouwmeester, *Creating and verifying a quantum superposition in a micro-optomechanical system*, New J. Phys. **10**, 095020 (2008).

[65] Y. Roichman, B. Sun, Y. Roichman, J. Amato-Grill, and D. G. Grier, *Optical forces arising from phase gradients*, Phys. Rev. Lett. **100**, 013602 (2008).

[66] W. H. Southwell, *Unstable-resonator-mode derivation using virtual-source theory*, J. Opt. Soc. Am. A **3**, 1885 (1986).

[67] G. P. Karman, G. S. McDonald, G. H. C. New, and J. P. Woerdman, *Fractal modes in unstable resonators*, Nature **402**, 138 (1999).

[68] G. Puentes, A. Aiello, and J. P. Woerdman, *Chaotic ray dynamics in an optical cavity with a beam splitter*, Opt. Lett. **29**, 929 (2004).

[69] J. Courtial, K. Dholakia, D. A. Robertson, L. Allen, and M. J. Padgett, *Measurement of the rotational frequency shift imparted to a rotating light beam possessing orbital angular momentum*, Phys. Rev. Lett. **80**, 3217 (1998).

[70] D. V. Osborne, *The rotation of liquid Helium II*, Proc. Phys. Soc. A **63**, 909 (1950).

[71] K. W. Madison, F. Chevy, W. Wohlleben, and J. Dalibard, *Vortex formation in a stirred Bose-Einstein condensate*, Phys. Rev. Lett. **84**, 806 (2000).

[72] E. Hodby, G. Hechenblaikner, S. A. Hopkins, O. M. Maragò, and C. J. Foot, *Vortex nucleation in Bose-Einstein condensates in an oblate, purely magnetic potential*, Phys. Rev. Lett. **88**, 010405 (2001).

[73] J. F. Nye and M. V. Berry, *Dislocations in wave trains*, Proc. R. Soc. Lond. A **336**, 165 (1974).

[74] G. Indebetouw, *Optical vortices and their propagation*, J. Mod. Opt. **40**, 73 (1993).

[75] D. Rozas, C. T. Law, and G. A. Swartzlander Jr., *Propagation dynamics of optical vortices*, J. Opt. Soc. Am. B **14**, 3054 (1997).

[76] I. Freund, *Optical vortex trajectories*, Opt. Commun. **181**, 19 (2000).

[77] K. O'Holleran, M. R. Dennis, F. Flossmann, and M. J. Padgett, *Fractality of light's darkness*, Phys. Rev. Lett. **100**, 053902 (2008).

[78] K. O'Holleran, M. R. Dennis, and M. J. Padgett, *Topology of Light's Darkness*, Phys. Rev. Lett. **102**, 143902 (2009).

[79] F. Roux, *Coupling of noncanonical optical vortices*, J. Opt. Soc. Am. B **21**, 664 (2003).

[80] A. Ya. Bekshaev, M. S. Soskin, and M. V. Vasnetsov, *Transformation of higher-order optical vortices upon focusing by an astigmatic lens*, Opt. Commun. **241**, 237 (2004).

[81] J. Visser, *Operator description of the dynamics of optical modes* (PhD thesis, Leiden University, 2005).

[82] R. K. Singh, P. Senthilkumaran, and K. Singh, *The effect of astigmatism on the diffraction of a vortex carrying beam with a Gaussian background*, J. Opt. A: Pure Appl. Opt. **9**, 543 (2007).

[83] K. Staliunas, *Dynamics of optical vortices in a laser beam*, Opt. Commun. **90**, 123 (1992).

[84] V. A. Pas'ko, M. V. Vasnetsov, and M. S. Soskin, *Generation of optical vortices by the periodic motion of a monochromatic source and its radiation spectrum*, J. Opt. A: Pure Appl. Opt. **11**, 094007 (2009).

[85] D. C. Roberts, H. Li, J. L. Steyn, K. T. Turner, R. Mlcak, L. Saggere, S. M. Spearing, M. A. Schmidt, and N. W. Hagood, *A high-frequency, high-stiffness piezoelectric actuator for microhydraulic applications*, Sensor. Actuat. A: Phys. **97-98**, 620 (2002).

[86] The LIGO scientific collaboration and the VIRGO collaboration, *An upper limit on the stochastic gravitational-wave background of cosmological origin*, Nature **460**, 990 (2009).

[87] M. V. Berry, *Quantal phase factors accompanying adiabatic changes*, Proc. R. Soc. Lond. A **392**, 45 (1984).

[88] S. Pancharatnam, *Generalized theory of interference, and its applications*, Proc. Ind. Acad. Sci. A **44**, 247 (1956).

[89] A. Tomita and R. Y. Chiao, *Observation of Berry's topological phase by use of an optical fiber*, Phys. Rev. Lett. **57**, 937 (1986).

[90] R. Y. Chiao and T. F. Jordan, *Lorentz-group Berry phases in squeezed light*, Phys. Lett. A **132**, 77 (1988).

[91] R. Simon and N. Mukunda, *Bargmann invariant and the geometry of the Güoy Effect*, Phys. Rev. Lett. **70**, 880 (1993).

[92] S. J. van Enk, *Geometric phase, transformations of gaussian beams and angular momentum transfer*, Opt. Commun. **102**, 59 (1993).

[93] M. Padgett and J. Courtial, *Poincaré-sphere equivalent for light beams containing orbital angular momentum*, Opt. Lett. **24**, 430 (1999).

[94] E. J. Galvez, P. R. Crawford, H. I. Sztul, M. J. Pysher, P. J. Haglin, and R. E. Williams, *Geometric phase associated with mode transformations of optical beams bearing orbital angular momentum*, Phys. Rev. Lett. **90**, 203901 (2003).

[95] E. J. Galvez and M. A. O'Connell, *Existence and absence of geometric phases due to mode transformations of high-order modes*, Proc. SPIE **5736**, 166 (2005).

[96] S. Tiwari, *Geometric phase in optics - quantal or classical*, J. Mod. Opt. **39**, 1097 (1992).

[97] M. Born and E. Wolf, *Principles of optics*, Sixth edition (Cambridge University Press, Cambridge, 1986).

[98] Y. Aharonov and D. Bohm, *Significance of electromagnetic potentials in the quantum theory*, Phys. Rev. **115**, 485 (1959).

[99] J. C. Garrison and R. Y. Chiao, *Geometrical phases from global gauge invariance of nonlinear classical field theories*, Phys. Rev. Lett. **60**, 165 (1988).

[100] M. W. Beijersbergen, L. Allen, H. E. L. O. van der Veen and J. P. Woerdman, *Astigmatic laser mode converters and transfer of orbital angular momentum*, Opt. Comm. **96**, 123 (1993).

[101] L. Allen, J. Courtial, and M. J. Padgett, *Matrix formulation for the propagation of light beams with orbital and spin angular momenta*, Phys. Rev. E **60**, 7497 (1999).

[102] L. Allen and M. J. Padgett, *Equivalent geometric transformations for spin and orbital angular momentum of light*, J. Mod. Opt. **54**, 487 (2007).

[103] R. Aleksiejunas and V. Ivaska, *Geometric phases for scalar wave superpositions*, Phys. Lett. A **235**, 1 (1997).

[104] B. A. Garetz and S. Arnold, *Variable frequency shifting of circularly polarized laser radiation via a rotating half-wave retardation plate*, Opt. Commun. **31**, 1 (1979).

[105] R. Simon, H. J. Kimble, and E. C. G. Sudarshan, *Evolving geometric phase and its dynamical manifestation as a frequency shift: An optical experiment*, Phys. Rev. Lett. **61**, 19 (1988).

[106] C. N. Alexeyev and M. A. Yavorsky, *Angular momentum of rotating paraxial light beams*, J. Opt. A: Pure Appl. Opt. **7**, 416 (2005).

[107] S. J. van Enk and G. Nienhuis, *Photons in polychromatic rotating modes*, Phys. Rev. A **76** (2007).

[108] I. H. Deutsch, *A basis-independent approach to quantum optics*, Am. J. Phys. **59**, 834 (1991).

[109] G. Trocheris, *Electrodynamics in a rotating frame of reference*, Philos. Mag. **40**, 1143 (1949).

[110] H. Takeno, *On relativistic theory of rotating disk*, Prog. Theor. Phys. **7**, 367 (1952).

[111] V. A. D. Lorenci and N. F. Svaiter, *A rotating quantum vacuum*, Found. Phys. **29**, 1233 (1999).

[112] W. G. Unruh, *Notes on black-hole evaporation*, Phys. Rev. D **14**, 870 (1976).

[113] J. Durnin, *Exact solutions for nondiffracting beams. I. The scalar theory*, J. Opt. Soc. Am. A **4**, 651 (1987).

[114] J. Durnin, J. J. Miceli, and J. H. Eberly, *Diffraction-free beams*, Phys. Rev. Lett. **58**, 1499 (1987).

[115] D. McGloin and K. Dholakia, *Bessel beams: diffraction in a new light*, Contemp. Phys. **46**, 15 (2005).

[116] A. V. Novitsky and D. V. Novitsky, *Negative propagation of vector Bessel beams*, J. Opt. Soc. Am. A **24**, 2844 (2007).

Samenvatting

In deze samenvatting bespreek ik de essentiële concepten en onderzoeksresultaten uit dit proefschrift op een manier waarop ze toegankelijk zijn voor wie niet zo goed ingevoerd is in de moderne natuur- en wiskunde dan wel niet zo vertrouwd is met de Engelstalige terminologie die gebruikt wordt. Zoals Einstein in een ander verband ooit opmerkte is het in de natuurkunde van belang de zaken zo eenvoudig voor te stellen als mogelijk, maar niet eenvoudiger. Om die reden probeer ik in deze samenvatting de essentie van dit proefschrift te vatten, maar vermijd ik oversimplificatie. De titel van dit boek laat zich het beste vertalen als 'Licht met een draai - straalaspecten in singuliere golf- en quantumoptica'. Na het lezen van deze samenvatting zou de betekenis van ieder van deze woorden en hun verband met het werk in dit proefschrift duidelijk moeten zijn.

Hoofdstuk 1: Verdraaid licht

Dit proefschrift gaat over licht. Fysisch gesproken is licht een electromagnetisch golfverschijnsel. Anders dan een golf die zich voortplant door een gitaarsnaar en waarin de uitwijking van de snaar ten opzichte van de evenwichtspositie trilt (oscilleert), bestaat licht uit twee oscillerende componenten. Zowel het electrische als het magnetische veld in een lichtbundel oscilleren in alle vlakken die loodrecht staan op de richting waarin de golf zich voortplant. Zulke vlakken worden transversale vlakken genoemd. Bovendien oscilleren de electrische en magnetische velden in onderling loodrechte richtingen. De richting waarin het electrische veld oscilleert, bepaalt de polarisatie van het licht. In een circulair gepolariseerde lichtbundel draait de polarisatie als functie van de tijd. In het eenvoudigste geval is de richting waarin het licht zich voortplant en de polarisatie overal hetzelfde. De locale voortplantingsrichting en polarisatie van het licht kunnen echter ook variëren als functie van de positie in de ruimte en als functie van de tijd. In dat geval heeft het licht ruimtelijke structuur. Dit proefschrift gaat over zulke structuren van licht. Voordat ik de andere hoofdstukken van dit proefschrift bespreek, zal ik kort aangeven waarom structuren van licht de interesse van natuurkundigen hebben. Deze interesse is tenminste drieledig.

Ten eerste kan de structuur van een lichtbundel en de interactie tussen het licht een deeltje aanleiding geven tot krachten en krachtmomenten op deeltjes. Hoewel zulke krachten onder realistische omstandigheden klein zijn (typisch enkele piconewtons), wordt dit principe onder meer gebruikt in het zogeheten optische pincet (optical tweezers) waarmee deeltjes vast-

gepakt en verplaatst kunnen worden. Daarnaast zijn optische krachten en krachtmomenten van belang in het vakgebied optomechanica waarin de gekoppelde (quantum)mechanica van het stralingsveld en een mechanische oscillator wordt gemanipuleerd en bestudeerd.

Daarnaast kan een lichtbundel interessante fysische eigenschappen hebben die samenhangen met zijn ruimtelijke structuur. Het belangrijkste voorbeeld hiervan is het baanimpulsmoment. Het impulsmoment is een grootheid die de hoeveelheid draaiing van een fysisch object karakteriseert (zoals de gewone lineaire impuls een maat is voor de hoeveelheid lineaire beweging van een object). Voor deeltjes zijn er twee verschillende bijdragen aan het totale impulsmoment die grofweg corresponderen met het draaien om de eigen as (tollen of spinnen) en het draaien om een andere as (meestal om een ander object). Een soortgelijke tweedeling bestaat ook voor het impulsmoment in licht dat één welbepaalde kleur heeft (monochromatisch licht). Enerzijds kan licht een spinimpuls moment hebben dat samenhangt met draaiing van zijn polarisatie. Anderzijds is er het baanimpulsmoment dat het gevolg is van specifieke structuren in de voortplantingsrichting van het licht in de bundel. In het laatste geval is het de energiestroom die draait om de as waarlangs de bundel zich voortplant. De meest voor de hand liggende bijdrage aan het impulsmoment in niet-monochromatische lichtbundels is wellicht het baanimpulsmoment als gevolg van fysieke draaiing van het bundelpatroon. Onder realistische omstandigheden is deze bijdrage echter veel kleiner dan de andere twee. In een baanbrekend experiment dat werd uitgevoerd in 2001 werd aangetoond dat lichtdeeltjes (fotonen) verstrengeld kunnen zijn in hun baanimpulsmoment. Verstrengeling is een merkwaardig quantummechanisch verschijnsel waarbij de individuele toestanden van twee deeltjes op verschillende plaatsen (bijvoorbeeld hun baanimpulsmomenten) volledig onbepaald zijn, terwijl hun gezamenlijke toestand (het totale baanimpulsmoment) goed gedefinieerd is. Wanneer de toestand van een van de deeltjes gemeten wordt, ligt de toestand van het andere deeltje instantaan vast. Quantumverstrengeling ligt aan de basis van onderzoek naar quantumcomputers en quantuminformatica. Aangezien het baanimpulsmoment samenhangt met de structuur van licht, is de structuur van licht een mogelijke kandidaat voor het coderen, manipuleren en transporteren van een pakketje quantuminformatie.

Afgezien van mogelijke toepassingen van optische krachten en quantumverstrengeling is er tenslotte ook interesse in de meer theoretische en mathematische aspecten van structuren van licht. Baanimpulsmoment in lichtbundels hangt vaak (maar, anders dan soms gedacht wordt, niet altijd) samen met de aanwezigheid van optische vortices. Dat zijn draaikolken in een lichtbundel. In het centrum van de vortex is het donker (zoals het in het oog van een orkaan niet stormt) en de variatie van de voortplantingsrichting van het licht rondom de vortex is zodanig dat het licht om het vortexcentrum heen draait. Het vortexpatroon in een lichtbundel kan zeer complex zijn en aanleiding geven tot topologisch interessante structuren als knopen en lussen. Het vakgebied dat zich bezighoudt met vortices en vortexpatronen in lichtbundels wordt singuliere optica genoemd.

Hoewel het foton inmiddels even ter sprake is geweest, hebben we het vooral gehad over licht als golfverschijnsel. Nadat in de negentiende eeuw het golfkarakter van licht zowel theoretisch als experimenteel uitgebreid bestudeerd was en goed begrepen werd, bleek in de eerste

helft van de twintigste eeuw dat licht ook een deeltjeskarakter heeft. Dat wordt beschreven door de quantummechanica of, meer specifiek, de quantumelectrodynamica (QED). In quantummechanische zin is licht niet óf een deeltje óf een golf, maar vertoont het eigenschappen van beide. Hoewel dit op het eerste gezicht tegenstrijdig lijkt, beschrijft de quantumelectrodynamica nauwkeurig hoe deze ogenschijnlijk verschillende gedaanten met elkaar samenhangen. Veel van de eerder genoemde eigenschappen vloeien voort uit het golfkarakter van licht en zijn dus uitstekend te beschrijven en te bestuderen door gebruikmaking van een klassieke (dat wil zeggen niet-quantummechanische) theorie. Bovendien is het formuleren van een quantummechanische beschrijving van licht in het algemeen relatief eenvoudig wanneer het klassieke golfgedrag goed begrepen wordt. Het grootste deel van dit proefschrift gaat dan ook over licht als klassiek golfverschijnsel. Alleen in hoofdstuk 7 bestuderen we quantumtoestanden van licht.

Hoofdstuk 2: Verdraaide resonatormodes

In het tweede hoofdstuk bestuderen we de ruimtelijke structuur van resonatormodes. Een resonator (ook wel trilholte) is een opstelling van twee, meestal gekromde, spiegels waartussen het licht heen en weer stuitert. Zo'n geometrie vormt het optische hart van iedere laser. Analoog aan een gitaarsnaar, waarin staande-golfpatronen ontstaan door het heen en weer bewegen van lopende golven, passen alleen specifieke patronen van licht precies tussen de twee spiegels. Zulke patronen worden modi (enkelvoud modus) of, in het Engels, modes (enkelvoud mode) van de resonator genoemd. Anders dan in een gitaarsnaar, waarvan de vaste uiteinden punten zijn, zijn de spiegels waaruit de resonator bestaat gekromd in het vlak loodrecht op de richting waarlangs het licht heen en weer stuitert. De modes moeten dus niet alleen tussen maar ook op de spiegeloppervlakken passen. Als gevolg hiervan hebben resonatormodes ook structuur in de vlakken loodrecht op de richting waarlangs het licht heen en weer stuitert (de transversale vlakken in de resonator). In het gebruikelijke geval zijn beide spiegels sferisch, dat wil zeggen dat ze de vorm hebben van een deel van een boloppervlak. In dit hoofdstuk zijn we echter geïnteresseerd in resonatormodes die verdraaid zijn. Daarmee bedoelen we dat ze vervormd zijn als een doek die uitgewrongen wordt. Om dat te bereiken moeten beide spiegels asferisch zijn. De eenvoudigste manier om een asferische spiegel te maken is door het spiegeloppervlak elliptisch te krommen. Daarmee wordt bedoeld dat het zo gekromd is dat de hoogtelijnen op het oppervlak ellipsen in plaats van cirkels zijn. Het oppervlak is dan verschillend gekromd in verschillende richtingen en we spreken wel van een astigmatische spiegel. Een resonator met twee astigmatische spiegels die een verschillende oriëntatie in het transversale vlak hebben, noemen we verdraaid. Omdat de modes van een resonator op beide spiegeloppervlakken passen, zijn de modes van een verdraaide resonator ook verdraaid. De structuur van de modes is zodanig dat hun oriëntatie in het transversale vlak verdraait terwijl het licht zich van de ene naar de andere spiegel voortplant. Het effect van het verdraaien van een resonator op de structuur van zijn modes is te zien in de figuren 2.5 en 2.6 op pagina 32. In figuur 2.5 tonen we de structuur van een mode van een resonator

waarvan beide spiegels astigmatisch zijn, maar dezelfde oriëntatie hebben. In dat geval is de resonator niet verdraaid. De paarswitte plaatjes tonen het intensiteitspatroon. Dat is wat men zou zien wanneer men een foto van het licht zou maken. De kleurenplaatjes tonen de vorm van het golffront van het licht. Een golffront is een denkbeeldig oppervlak dat elkaar aanrakende golftoppen (of dalen) met elkaar verbindt. Denk bijvoorbeeld aan de cirkels die zichtbaar zijn rondom de plaats waar een steen in het water gegooid is. De linker en rechter figuren tonen de transversale modestructuur vlakbij de spiegels. De golffronten hebben de elliptische vorm van de spiegels aangenomen. Ook de intensiteitpatronen zijn elliptisch. Omdat de spiegels identiek zijn, is het golffront in het vlak tussen de spiegels vlak. De plaatjes in figuur 2.6 tonen hoe de structuur van deze mode verandert wanneer een van de spiegels (in dit geval de rechter) verdraaid wordt. Het elliptische intensiteitpatroon heeft niet langer dezelfde oriëntatie in de drie transversale vlakken. Bovendien wordt het golffront hyperbolisch in het vlak tussen de spiegels in. De resonatormode waarvan het intensiteitspatroon bestaat uit één ellipsvormige druppel noemen we de fundamentele mode. Andere (zogenaamde hogere-orde-modes) hebben een complexere structuur. Het effect van het verdraaien van een van de spiegels op zo'n mode is te zien in de figuren 2.7 en 2.8 op pagina 33. De elliptische vorm van de spiegels is nog steeds terug te zien in de vorm van het golffront, maar zowel het golffront als het intensiteitspatroon hebben nu een rijkere structuur. In het golffront zien we zogenaamde lijndislocaties. Dat zijn lijnen waarlangs de top van een golf met een oneindig scherpe overgang overgaat in een dal. Wanneer één van de spiegels verdraaid wordt (figuur 2.8), worden de lijndislocaties in de transversale vlakken tussen de spiegels in vervormd in optische vortices. Deze zijn zichtbaar als punten waar alle kleuren bij elkaar komen. Merk op dat dat alleen gebeurt in de vlakken tussen de spiegels. Vlakbij de spiegels blijven de lijndislocaties intact, maar verliezen hun loodrechte oriëntatie. Ook dat is een gevolg van de verdraaide modestructuur.

De wiskundige methode die we ontwikkelen om de structuur van deze modes te beschrijven maakt gebruik van ladderoperatoren. Vergelijkbare technieken worden toegepast in de quantummechanica en wij breiden ze uit zodat ze toepasbaar zijn op de optische systemen die we bestuderen. In het eenvoudigere geval van een tweedimensionale resonator (dus met één transversale dimensie) vormen de modes een ladder waarop ieder trede met een andere mode correspondeert. De onderste trede correspondeert met de fundamentele mode. De hogere orde modes kunnen worden gevonden door gebruikmaking van ladderoperatoren. Er zijn twee verschillende ladderoperatoren: één die het effect van een stap omhoog beschrijft en één die het (tegengestelde) effect van een stap naar beneden beschrijft. Vanaf de onderste trede is het niet mogelijk verder naar beneden te gaan en dus moet de daaloperator werkend op de fundamentele mode 0 geven. Op deze manier kunnen alle modes op de ladder gevonden worden. In het geval van driedimensionale modes vormen de modes geen ladder, maar een tweedimensionaal rooster waarop ieder punt met een mode correspondeert. We hebben nu dus twee paren van twee ladderoperatoren (of eigenlijk roosteroperatoren) nodig, één paar voor de horizontale richting en één paar voor de verticale richting. Ieder van deze operatoren beschrijft een stap in de bijbehorende richting en voor de tegengestelde richtingen (naar

boven en naar beneden dan wel naar links en naar rechts) worden wederom verschillende operatoren gebruikt. Net als een ladder heeft het rooster van modes een punt van waaruit men niet verder naar beneden en niet verder naar links kan. Dit punt correspondeert met de fundamentele mode van de resonator. Het bijzondere aan de ladderoperatoren is dat ze thuishoren in het golfoptische domein, maar dat hun eigenschappen direct samenhangen met het gedrag van lichtstralen in de resonator. In die zin slaat deze methode een brug tussen het straaloptische gedrag van de resonator en de structuur van zijn golfoptische modes. Dat maakt deze methode erg inzichtelijk en elegant. Daarnaast is de ladderoperatormethode wiskundig exact onder de (realistische) aanname dat de afstand tussen de spiegels groter is dan de diameter van de mode patronen.

Hoofdstuk 3: Verdraaid licht tussen roterende spiegels

In hoofdstuk 3 bespreken we een beschrijving van het gedrag van licht in optische systemen met bewegende elementen en passen deze toe om de modes van een roterende resonator te vinden. Opnieuw geldt dat we alleen een effect verwachten als ten minste één van de spiegels asferisch is en we beschouwen een resonator met roterende astigmatische spiegels. Omdat modes normaal gesproken gedefinieerd worden als tijdonafhankelijke golfpatronen, behoeft het modeconcept in een roterende resonator enige aandacht. We laten zien dat meeroterende oplossingen een zinvolle generalisatie van het modeconcept vormen en, bovendien, dat ze bestaan. Dat wil zeggen dat de wiskundige vergelijkingen waaraan zulke patronen moeten voldoen roterende oplossingen hebben. We breiden de ladderoperatormethode uit naar dit, tijdafhankelijke, geval en bespreken enkele fysische eigenschappen van de roterende resonatormodes. De intensiteitspatronen van een aantal van zulke modes zijn te zien in de figuren 3.3 en 3.5 respectievelijk op pagina 58 en pagina 62. De plaatjes in figuur 3.3 betreffen een resonator met een stilstaande sferische en een draaiende astigmatische spiegel terwijl figuur 3.5 een resonator met twee draaiende astigmatische spiegels betreft. In beide figuren tonen de plaatjes in de linker kolom de modestructuur op de linker spiegel en de plaatjes in de rechter kolom de modestructuur op de rechter spiegel. De plaatjes zijn steeds gegroepeerd in groepjes van vier die de intensiteitspatronen van verschillende modes bij dezelfde rotatiesnelheid tonen. In beide figuren betreft de bovenste rij een stilstaande resonator en neemt de draaisnelheid van boven naar onder toe. De plaatjes laten zien dat de modepatronen aanzienlijk vervormd worden door rotatie en dat fysieke rotatie van de spiegels een wezenlijk ander effect heeft dan het algemeen astigmatisme dat we in hoofdstuk 2 besproken hebben. We laten zien dat zowel de rotationele vervorming van de modes als het feit dat ze roteren bijdragen aan het impulsmoment in deze modes. De bijdrage als gevolg van de rotatie van de modepatronen is, in het algemeen, verwaarloosbaar klein ten opzichte van de bijdrage door de modestructuur. Omdat de roterende modepatronen tijdafhankelijk zijn, hebben de modes ook spectrale structuur. Ze zijn wat we noemen polychromatisch en bevatten licht van verschillende kleuren. De spectrale structuur van de modepatronen uit de onderste rij in figuur 3.5 is te zien in figuur 3.4 op pagina 59. In de praktijk zullen de kleurverschillen tussen de

verschillende componenten erg klein zijn.

Hoewel relatief eenvoudig, is een draaiende resonator met astigmatische spiegels een verrassend rijk fysisch systeem. Om die reden gaan we in de hoofdstukken 4 en 5 verder in op een aantal optische en optodynamische eigenschappen van zo'n opstelling.

Hoofdstuk 4: Rotationele stabilisatie en destabilisatie van een optische resonator

Tot nu toe hebben we steeds aangenomen dat het licht oneindig lang heen en weer blijft stuiteren tussen de twee spiegels waaruit een optische trilholte bestaat. In het algemeen hoeft dit niet het geval te zijn, zelfs niet wanneer men gebruik maakt van ideale (dat wil zeggen perfect reflecterende) spiegeloppervlakken. Omdat de spiegels gekromd zijn, verandert de richting van een lichtstraal wanneer deze weerkaatst wordt. Aangezien de resonator open is, gebeurt het in veel gevallen dat een lichtstraal vroeg of laat uit de resonator gekaatst wordt. In dat geval is de resonator niet in staat licht lang vast te houden en wordt deze geometrisch instabiel genoemd. Hoewel stabiliteit primair een straaloptische eigenschap van een resonator is, is het een voorwaarde voor het bestaan van (golfoptische) modes. In hoofdstuk 4 bestuderen we effecten van rotatie op de stabiliteit van een optische resonator. We laten zien dat stabiele resonatoren in het algemeen tenminste gedeeltelijk instabiel worden (dat wil zeggen instabiel in één richting) als ze in voldoende snelle rotatie worden gebracht. Het licht vliegt dan, als het ware, uit de bocht. Daarnaast tonen we ook aan dat sommige instabiele resonatoren juist stabiel worden als gevolg van rotatie. In dat geval helpt rotatie juist om het licht in te vangen. Dit verrassende effect heeft een mechanisch analogon in de zogeheten paulval (Paul trap). De paulval lijkt op het opsluiten van een knikker in een roterend zadelpunt. Een zadelpunt is een punt op een oppervlak waar de kromming in de ene richting hol en in de andere richting bol is. Een knikker die op een stilstaand zadelpunt gelegd wordt, valt langs de bolle flank naar beneden. Wanneer het zadelpunt echter voldoende snel ronddraait, wordt de knikker ingevangen door de holle flank van het zadelpunt voordat deze langs de bolle flank naar beneden kan vallen. De knikker wordt door de rotatie gevangen net als het licht in een resonator die door rotatie gestabiliseerd wordt. We bestuderen de effecten van stabilisatie en destabilisatie op de structuur van de resonatormodes en laten zien dat het licht inderdaad uit dan wel in de bocht vliegt. Dat is te zien in de plaatjes in figuur 4.2 op pagina 67. De bovenste rij toont de modestructuur in een resonator die gedestabiliseerd wordt terwijl de onderste rij een resonator betreft die gestabiliseerd wordt door rotatie. In beide gevallen neemt de draaisnelheid van links naar rechts toe. Tenslotte kijken we ook naar het impulsmoment in de resonatormodes en laten zien dat dat oneindig groot wordt op de grens van stabiliteit en (gedeeltelijke) instabiliteit. Dat is te zien in de grafieken in figuur 4.3 op pagina 70. De linker grafiek toont het geval van een resonator die gedestabiliseerd wordt, terwijl de rechter een resonator betreft die gestabiliseerd wordt door rotatie. In beide grafieken staat het impulsmoment op de verticale en de draaisnelheid op de horizontale as.

Hoofdstuk 5: Optische vortices geïnduceerd door rotatie van een resonator

Fysieke rotatie en het verschijnen van vortices hangen in het algemeen nauw met elkaar samen. In hoofdstuk 5 bestuderen we het door rotatie geïnduceerde vortexpatroon in de modes van een optische resonator. Omdat we alleen naar het effect van rotatie willen kijken, nemen we een resonator die niet verdraaid is. We beschouwen een resonator die bestaat uit een sferische en een astigmatische spiegel. We vatten de wiskundige aanpak uit het derde hoofdstuk kort samen en bespreken enkele algemene eigenschappen van de vortices in roterende resonatormodes. We laten onder andere zien dat even modes in het algemeen een vortex in het midden van het modepatroon hebben en dat dat niet zo kan zijn voor oneven modes. In figuur 5.4 op pagina 82 tonen we resultaten voor een specifiek geval. De linker kolom toont de modestructuur in geval van een stilstaande resonator. De rechterkolom toont dezelfde modes maar dan wanneer de resonator roteert. De resultaten laten opnieuw zien dat rotatie opvallende effecten heeft op de modestructuur en, bovendien, dat de lijndislocaties in de golffronten vervormd worden tot optische vortices. Anders dan in het geval van een verdraaide resonator (hoofdstuk 2) gebeurt dat nu in alle transversale vlakken, ook in die bij de spiegels.

Onder typische experimentele omstandigheden vereisen de effecten die we in de hoofdstukken 3, 4 en 5 besproken hebben rotatiesnelheden van tienduizenden tot miljoenen omwentelingen per seconde. Hoewel in principe niet onmogelijk, is het niet eenvoudig zulke hoge rotatiesnelheden te realiseren. Om die reden bespreken we in paragraaf 5.5 enkele andere mogelijkheden om de een opstelling te realiseren die de essentiële eigenschappen van een draaiende astigmatische resonator nabootst.

Hoofdstuk 6: Geometrische fasen voor astigmatische optische modes van willekeurige orde

De laatste decennia is er in de natuurkunde veel aandacht besteed aan het vinden van geometrische interpretaties van fysische verschijnselen. Het bekendste voorbeeld is Einsteins algemene relativiteitstheorie die een geometrische verklaring geeft voor de zwaartekracht. In vergelijking met analytische en algebraïsche beschrijvingen, zijn geometrische interpretaties meestal eenvoudig en elegant. Bovendien geven ze vaak een dieper inzicht in de oorsprong van fysische verschijnselen. In geometrische beschrijvingen van fysische verschijnselen spelen geometrische fasen een cruciale rol. In het algemeen treden geometrische fasen op wanneer de parameters die een fysisch systeem karakteriseren via een gesloten pad door de parameterruimte terugkomen op hun oorspronkelijke waarden. Een eenvoudig voorbeeld van een geometrische fase treedt op wanneer iemand met een pijl in zijn handen over een boloppervlak (laten we zeggen de aardbol) wandelt en de richting van zijn pijl onveranderd laat als hij zelf van richting verandert. Stel dat deze persoon vanaf de evenaar via de noordpool naar de andere kant van de evenaar loopt en vervolgens over de evenaar terugloopt naar zijn beginpositie. Dan is zijn pijl bij terugkomst precies 180 graden gedraaid ten opzichte van zijn oorspronkelijke richting. Als hij op de noordpool niet rechtdoor loopt maar rechtsaf slaat, is

zijn pijl precies 90 graden verdraaid ten opzichte van de oorspronkelijke positie. In het algemeen wordt de hoek waarover de pijl verdraaid is na het bewandelen van een gesloten pad op de aardbol bepaald door het ingesloten oppervlak (ten opzichte van het totale oppervlak van de bol). Dit effect hangt samen met de kromming van het boloppervlak en treedt niet op in een (plat) vlak. Bovendien is de hoek waarover de pijl bij terugkomst verdraaid is onafhankelijk van de snelheid waarmee het pad doorlopen is. De hoek wordt dus uitsluitend bepaald door de geometrische eigenschappen van het boloppervlak (de kromming) en door die van het pad (het ingesloten oppervlak).

In hoofdstuk 6 bespreken we soortgelijke effecten voor optische modes die zich voortplanten door een optische opstelling dan wel door de vrije ruimte. We introduceren een speciale klasse optische modes met transversale structuur en laten zien dat deze gesloten is onder een groep optische transformaties die onder andere vrije voorplanting van het licht, de effecten van gekromde spiegels en lenzen en effecten door breking op de modestructuur bevat. We karakteriseren de parameters die samenhangen met de transversale structuur van de modes en laten zien dat een gesloten pad door de bijbehorende parameterruimte aanleiding geeft tot een faseverschuiving die een geometrische interpretatie heeft in termen van de parameterruimte en het afgelegde pad. In het geval van optische modes correspondeert deze niet met een verdraaiing maar met een (kleine) verschuiving van de pieken en dalen van de golf. Zulke verschuivingen zijn te meten door het originele patroon te laten interfereren met het patroon dat een gesloten cyclus heeft afgelegd door de parameterruimte. Als speciale gevallen vinden we de gouyfase en de geometrische fase die optreedt als gevolg van een reeks modeconversies en rotaties van niet-astigmatische modes. In het laatste geval reduceert de parameterruimte weer tot een bol. Voorbeelden van zulke bollen en de bijbehorende modepatronen zijn te zien in de figuren 6.1 en 6.2 respectievelijk op pagina 111 en op pagina 114 en 115.

Hoofdstuk 7: Een exacte quantumtheorie voor draaiend licht

Het laatste hoofdstuk besluit de discussie over draaiend licht in dit proefschrift. Hoewel draaiende lichtbundels gedurende de laatste decennia door verschillende onderzoeksgroepen vanuit verschillende invalshoeken zowel theoretisch als experimenteel bestudeerd werden, werd de eerste quantumtheorie voor draaiend licht pas in 2006 gepubliceerd. Deze theorie beschrijft quantumtoestanden van licht met draaiende polarisaties en draaiende voortplantingsrichtingen. Ze beschrijft ook quantumtoestanden waarin beide draaien. Hoewel deze theorie in veel praktische situaties uitstekend toepasbaar is, is zij niet exact. De belangrijkste beperking is dat deze theorie alleen van toepassing is op lichtbundels waarvan de polarisatiestructuur onafhankelijk is van de ruimtelijke variatie van de voortplantingsrichting. Daarnaast beperkt zij zich tot (relatief) kleine draaisnelheden.

In hoofdstuk 7 presenteren we de eerste exacte quantumtheorie voor draaiend licht. We laten zien dat de vergelijkingen die licht in de vrije ruimte beschrijven exacte draaiende oplossingen hebben en dat zulke oplossingen alleen bestaan als het gehele veld, inclusief

zijn polarisatie, uniform draait. We bestuderen zulke oplossingen en formuleren een quantumtheorie voor dit type draaiend licht. Ook bespreken we het verband met de draaiende resonatormodes die we bestudeerd hebben in de hoofdstukken 3, 4, 5 en laten zien dat de quantumtheorie ook in dat geval van toepassing is.

Curriculum Vitae

Steven Habraken werd op 25 augustus 1980 geboren te Eindhoven. Nadat hij in 1999 het Atheneum-β diploma behaalde aan het Lorentz Casimir Lyceum in zijn geboorteplaats, schreef hij zich in voor de opleiding Natuurkunde aan de Universiteit Leiden. Zijn eerste onderzoeksstage verrichte hij onder begeleiding van Prof. dr. J. Aarts in de vakgroep 'Supergeleidende en magnetische materialen' van het Kamerlingh Onnes Laboratorium. Het betrof een experimenteel onderzoek naar de effecten van magnetisatie op de transporteigenschappen van nanostructuren in hybriden van supergeleidende en ferromagnetische materialen. Daarnaast vervulde hij drie studentassistentschappen binnen de Natuur- en Sterrenkunde opleidingen alsook binnen de Scheikunde en Life Science and Technology opleidingen. Zijn theoretische afstudeeronderzoek verrichtte hij onder begeleiding van Prof. dr. G. Nienhuis in de 'Quantum optica en quantum informatie' groep van het Huygens Laboratorium. Het onderzoek betrof een uitbreiding van de paraxiale benadering naar optische systemen waarin licht zich voortplant langs meerdere, welgedefinieerde, bundelassen en toepassing daarvan op quantumverstengeling in ruimtelijke vrijheidsgraden, in het bijzonder het baanimpulsmoment. Op 29 november 2005 slaagde hij voor het doctoraalexamen. Per 1 februari 2006 trad hij als assistent in opleiding in dienst van het Leids Instituut voor Onderzoek in de Natuurkunde (LION). Als promovendus van Prof. dr. G. Nienhuis bestudeerde hij fysische eigenschappen en geometrische aspecten van lichtbundels en quantumtoestanden van het stralingsveld met een rijke ruimtelijke en spectrale structuur, in het bijzonder draaiende velden, astigmatische modes en vortexbundels. De resultaten van dit onderzoek zijn te vinden in dit proefschrift. Hij presenteerde onderzoeksresultaten op Physics@FOM (Veldhoven 2007 en 2008), de NNV AMO bijeenkomst (Lunteren 2007 en 2008), de Casimir Research Day (Eindhoven 2007), IQEC/CLEO Europe (München (DE) 2007), the Fourth International Conference on Singular Optics (Alushta (UA) 2008), Trends in Theory (Dalfsen 2009), ABB 50/25 (Bristol (UK) 2009) en SPIE Photonics West (San Francisco (US) 2010). Tijdens zijn promotie nam hij deel aan de 'Spring School of the Casimir Research School' (Heeg 2006), de 'OptETH Winter School' (Zürich (CH) 2007), de '25th Jerusalem Winter School in Theoretical Physics' (Jerusalem (IL) 2007-2008) en de 'AIO/OIO school on SP/TCM of the DRSTP' (Driebergen 2009). Tijdens zijn aanstelling als promovendus, verzorgde hij vier maal het werkcollege 'Atoom- en Molecuulfysica' voor derdejaars Bachelor studenten. In 2006 en 2007 was hij groepsleider tijdens de eerstejaars boekdag. Daarnaast jureerde hij in 2008 bij de Interuniversitaire Natuurkunde Olympiade (PION). Van medio 2007 tot eind

2009 was hij lid van de instituutsraad van het LION. Ook nam hij in 2007 en 2009 zitting in de pepernotencommissie welke belast is met de organisatie van het Sinterklaasfeest op het instituut.

List of publications

Peer-reviewed journal articles

1. Steven J. M. Habraken and Gerard Nienhuis, *Quantum interference of rotating photons*, based on material contained in chapter 7, in preparation for Physical Review A.

2. Steven J. M. Habraken and Gerard Nienhuis, *Geometric phases for higher-order optical modes bearing orbital angular momentum*, partly based on material contained in chapter 6, in preparation.

3. Steven J. M. Habraken and Gerard Nienhuis, *Geometric phases for astigmatic optical modes of arbitrary order*, material is contained in chapter 6, in preparation for J. Phys. A: Math. Theor.

4. Steven J. M. Habraken and Gerard Nienhuis, *Rotationally induced vortices in optical cavity modes*, material is contained chapter 5, J. Opt. A: Pure Appl. Opt. **11**, 094006 (2009).

5. Steven J. M. Habraken and Gerard Nienhuis, *Rotational stabilization and destabilization of an optical cavity*, material is contained in chapter 4, Phys. Rev. A **79**, 011805(R) (2009).

6. Steven J. M. Habraken and Gerard Nienhuis, *Modes of a rotating astigmatic optical cavity*, material is contained in chapter 3, Phys. Rev. A **77**, 053803 (2008).

7. Steven J. M. Habraken and Gerard Nienhuis, *Modes of a twisted optical cavity*, material is contained in chapter 2, Phys. Rev. A **75**, 033819 (2007).

8. A. Yu. Rusanov, S. Habraken and J. Aarts, *Inverse spin switch effect in ferromagnet/ superconductor/ ferromagnet hybrids with strong ferromagnet*, Phys. Rev. B **73**, 060505(R) (2006).

9. A. Rusanov, M. Hesselberth, S. Habraken and J. Aarts, *Depairing currents in superconductor/ ferromaget Nb/CuNi trilayers close to T_C*, Physica C **404**, 322 (2004).

Published conference contributions

1. Steven J. M. Habraken and Gerard Nienhuis, *Stability properties of a rotating astigmatic optical cavity*, partly contained in chapter 4, Proc. SPIE **7227**, 72270H-1 (2009).

2. Gerard Nienhuis and Steven J. M. Habraken, *The structure of twisted cavity modes*, material is contained in chapter 2, Coherence and Quantum Optics IX, N. P. Bigelow, J. H. Eberly and C. R. Stroud, Jr, (Eds.), OSA, 358-359 (2008).

3. Steven J. M. Habraken and Gerard Nienhuis, *Orbital angular momentum in twisted and rotating cavity modes*, partly contained in chapter 2 and 3, Proc. SPIE **6905**, 690504-1 (2008).

4. Gerard Nienhuis and Steven J. M. Habraken, *Structure of cavity modes with general astigmatism*, partly contained in chapter 2, Proc. SPIE **6483**, 64830J (2007).

Nawoord

In weerwil van het hardnekkige beeld dat een theoretisch fysicus zich vier jaar in een stoffig kamertje opsluit om een proefschrift te schrijven, was de voltooiing van dit proefschrift onmogelijk geweest zonder de betrokkenheid van collega's en de liefde en steun van familie en vrienden. Hoewel het onmogelijk is iedereen die op zijn of haar manier bijgedragen heeft aan de totstandkoming van dit proefschrift te noemen, wil ik op deze plaats toch een aantal mensen bedanken voor hun bijdrage daaraan.

Allereerst is daar natuurlijk mijn promotor Gerard Nienhuis. Zijn enthousiasme en ideeën hebben zeer veel bijgedragen aan de resultaten die in dit proefschrift beschreven worden. Daarnaast wil ik hem bedanken voor zijn betrokkenheid, inzicht en wijsheid op velerlei gebied. De vele werkbesprekingen en informele discussies binnen de opticagroep zijn erg leerzaam en nuttig geweest. In het bijzonder wil ik Eric Eliel en Michiel de Dood bedanken voor stimulerende discussies en interessante suggesties. Naast inhoudelijke gedachtewisselingen is collegialiteit uiteraard ook een belangrijke factor tijdens het proces dat tot een proefschrift leidt. Ik heb de sfeer in groep altijd als erg prettig ervaren. De samenwerking en interactie met studenten, collega-promovendi en post-docs was vaak een verrijking. In de begindagen van mijn promotie heb ik de interesse en betrokkenheid van Thijs Klaassen en Graciana Puentes erg gewaardeerd. Het gezelschap van Eduard Driessen, Bart-Jan Pors en Joris Berkhout maakte het bezoeken van internationale conferenties en scholen leuker, interessanter en gemakkelijker. Jörg Götte wil ik graag bedanken voor zijn gezelschap en gastvrijheid voor en tijdens de 'ABB anniversary conference' in Bristol. Wouter Peeters, met wie ik ruim anderhalf jaar een kamer deelde, dank ik voor onze vele gesprekken en voor zijn, vaak verrassend andere, kijk op de natuurkunde die mij meer dan eens van inzicht heeft doen veranderen. Philip Chimento en Eyse van Terwisga wil ik bedanken voor hun taalkundige adviezen.

Bekenden, vrienden en familie waren vaak bereid onbegrijpelijke verhalen over mijn nieuwste inzichten aan te horen maar zorgden in de eerste plaats toch vooral voor de nodige afleiding: koffie op zaterdagmiddagen, biertjes in Leiden en Haarlem, avondjes/weekendjes Eindhoven, Best, Utrecht en Tilburg, platenbeurs- en familieweekenden, muziek op zondagavonden... veel dank daarvoor.

Het doen van onderzoek en het schrijven van een proefschrift is een creatief proces dat een andere werkhouding vergt dan een negen-tot-vijf-mentaliteit. Het gevolg was soms dat vrije uurtjes in gedachten dan wel feitelijk aan werk werden besteed. Niet zelden heb ik mijn

geliefde Astrid daarmee belast. Astrid, op deze plek wil ik je bedanken voor je flexibiliteit, energie en optimisme. Bovenal dank ik je voor je onvoorwaardelijke liefde, steun en interesse. Zonder jou was mijn leven de laatste tien jaar heel wat minder aangenaam geweest.

De allerlaatste woorden tenslotte zijn voor mijn ouders. Zonder hen was ik er immers überhaupt niet geweest. Bovendien hebben ze de nieuwsgierigheid waar ik als klein kind al mee behept was altijd aangemoedigd en hebben waarden als ontwikkeling en ontplooiing thuis altijd erg hoog in het vaandel gestaan. Dat heb ik vaak als een voorrecht beschouwd.

Leiden, 23 december 2009